

University of Warwick institutional repository: <http://go.warwick.ac.uk/wrap>

A Thesis Submitted for the Degree of PhD at the University of Warwick

<http://go.warwick.ac.uk/wrap/62732>

This thesis is made available online and is protected by original copyright.

Please scroll down to view the document itself.

Please refer to the repository record for this item for information to help you to cite it. Our policy information is available from the repository home page.

**A Generalised Powertrain Component Size
Optimisation Methodology to Reduce Fuel Economy
Variability in Hybrid Electric Vehicles**

by

Hillol Kumar Roy

A thesis submitted in partial fulfilment of the requirements for the
degree of

Doctor of Philosophy in Engineering

University of Warwick, WMG

April 2014

TABLE OF CONTENTS

LIST OF FIGURES.....	ix
LIST OF TABLES.....	xvi
ACKNOWLEDGEMENTS.....	xx
DECLARATION.....	xxi
LIST OF PUBLICATIONS.....	xxii
ABSTRACT.....	xxiii
LIST OF ABBREVIATIONS.....	xxiv
LIST OF SYMBOLS AND VARIABLES.....	xxv
CHAPTER 1: INTRODUCTION.....	1
1.1 Motivation and research question	1
1.2 Knowledge contributions	7
1.3 Organisation of the thesis.....	8
CHAPTER 2: OVERVIEW: HYBRID ELECTRIC VEHICLES AND OPTIMISATION METHODS.....	10
2.1 Hybrid electric vehicle (HEV)	10
2.1.1 Powertrain components.....	11
2.1.1.1 Internal combustion engine (ICE).....	11
2.1.1.2 Electric motor	15
2.1.1.3 Battery.....	18
2.1.2 Vehicle supervisory control (VSC).....	22
2.1.2.1 Major operations of HEV	23
2.1.3 Hybrid electric vehicle architecture.....	26
2.1.3.1 Series HEV	27
2.1.3.2 Parallel HEV	29
2.1.3.3 Series-parallel HEV	30
2.1.3.4 Plug-in HEV	34

2.1.3.5	Non-plug-in HEV	34
2.2	Driving patterns.....	35
2.3	Optimisation problems and methods.....	37
2.3.1	Derivative-based optimisation method	38
2.3.2	Derivative-free optimisation method.....	39
2.3.2.1	Genetic algorithm (GA).....	40
2.3.2.1.1	Initialisation	41
2.3.2.1.2	Selection.....	42
2.3.2.1.3	Crossover	42
2.3.2.1.4	Mutation.....	43
2.3.2.2	Particle swarm optimisation (PSO).....	44
2.3.3	Optimisation termination criterion.....	45
2.4	Summary	45
CHAPTER 3: REVIEW: FUEL ECONOMY IN HYBRID ELECTRIC		
VEHICLES.....		
3.1	Fuel economy (FE) improvement in HEVs	47
3.1.1	Simulation-based optimisation of powertrain component sizes	50
3.1.1.1	Powertrain components.....	51
3.1.1.2	Design limits	52
3.1.1.3	Vehicle supervisory control (VSC) strategy.....	54
3.1.1.4	Constraints	55
3.1.1.5	Driving patterns and optimum design.....	57
3.1.1.6	Optimisation method.....	60
3.1.1.7	Simulation approach	63
3.1.1.8	Generalisation of the traditional methodology of powertrain component size optimisation.....	63
3.2	FE variability in HEVs.....	66
3.2.1	FE variability factors	68
3.2.2	FE variability due to driving patterns: HEV and conventional vehicle.....	71

3.2.3 Reduction of FE variability due to driving patterns	74
3.3 Research question.....	78
3.4 Summary	80
CHAPTER 4: RESEARCH METHODOLOGY	82
4.1 Research methodology	82
4.1.1 Literature review	84
4.1.2 Formulation of research question	85
4.1.3 Proposal of a new methodology.....	85
4.1.4 Simulation setup	86
4.1.5 Investigation over standard conditions	86
4.1.6 Validation in real-world conditions	87
4.1.7 Interpretation and generalisation	88
4.2 Summary	88
CHAPTER 5: PROPOSAL OF A NEW METHODOLOGY	89
5.1 Proposal of new methodology.....	90
5.2 Summary	95
CHAPTER 6: SIMULATION SETUP.....	96
6.1 Simulation tool.....	97
6.2 Vehicle simulation model	97
6.2.1 Vehicle architecture	97
6.2.2 Powertrain components.....	98
6.2.2.1 Internal combustion engine (ICE).....	98
6.2.2.2 Motor	99
6.2.2.3 Generator	99
6.2.2.4 Battery.....	99
6.3 Design parameters.....	101
6.3.1 Design variables.....	101

6.3.2 Design limits	101
6.3.3 Design constraints.....	102
6.4 Vehicle supervisory control strategy.....	104
6.5 Optimisation problem formulation.....	107
6.6 Optimisation method.....	107
6.6.1 Integration of optimisation method with vehicle simulation model.....	108
6.7 Optimum design	109
6.7.1 Proposed methodology: classification of driving patterns.....	110
6.7.2 Proposed methodology: consideration of driving patterns	112
6.7.2.1 Proposed methodology: sequence of driving patterns	112
6.7.3 Traditional methodology: consideration of driving patterns	113
6.8 Driving patterns.....	114
6.8.1 Standard driving patterns	114
6.8.2 Real-world driving patterns	114
6.9 FE evaluation	117
6.10 Summary	118
CHAPTER 7: EVALUATION OF TRADITIONAL METHODOLOGY	120
7.1 Optimum designs of traditional methodology.....	120
7.2 Performance of optimum designs.....	124
7.3 Reason for failure to achieve an optimum design over HWFET	125
7.4 FE evaluation over standard driving patterns: Toyota Prius and M1.....	126
7.4.1 Battery SOC during FE evaluation: Toyota Prius and M1	127
7.5 FE over standard driving patterns: Toyota Prius and M1	129
7.6 Summary	131
CHAPTER 8: EVALUATION OF TRADITIONAL METHODOLOGY: WITH VARIABLE CONTROL STRATEGY PARAMETER.....	133
8.1 Optimum designs of traditional methodology.....	133

8.2	Performance of optimum designs: Toyota Prius and M1.....	141
8.3	FE evaluation over standard driving patterns: Toyota Prius and M1.....	143
8.3.1	Battery SOC during FE evaluation: Toyota Prius and M1	143
8.4	FE over standard driving patterns: Toyota Prius and M1	150
8.5	Summary	155
CHAPTER 9: EVALUATION OF PROPOSED METHODOLOGY		157
9.1	Optimum designs of proposed methodology with first approach	157
9.2	Performance of optimum designs: Toyota Prius and M2A1.....	164
9.3	Battery SOC during optimisation: optimum designs of M2A1 approach....	166
9.4	FE evaluation over standard driving patterns: optimum designs of M2A1 .	167
9.4.1	Battery SOC during FE evaluation: optimum designs of M2A1.....	167
9.5	FE over standard driving patterns: Toyota Prius and M2A1	171
9.6	FE variability over standard driving patterns: Toyota Prius and M2A1	173
9.7	Summary	176
CHAPTER 10: EVALUATION OF PROPOSED METHODOLOGY: CONTROL OF BATTERY STATE OF CHARGE OVER EACH DRIVING PATTERN.....		177
10.1	The proposed methodology with second approach	178
10.2	Optimum designs of M2A2 approach	179
10.3	Performance of optimum designs: Toyota Prius and M2A2 approach	183
10.4	Battery SOC during optimisation: optimum designs of M2A2 approach .	184
10.5	FE evaluation over standard driving patterns: optimum designs of M2A2 approach	185
10.5.1	Battery SOC during FE evaluation: optimum designs of M2A2 approach	186
10.6	FE over standard driving patterns: optimum designs of M2A2 approach	187
10.7	Optimum designs: Toyota Prius, M1, and M2A2	189

10.8	Performance of optimum designs: Toyota Prius, M1, and M2A2	192
10.9	FE evaluation over standard driving patterns: Toyota Prius, M1, and M2A2.....	194
10.9.1	Battery SOC during FE evaluation: Toyota Prius, M1, and M2A2.....	194
10.9.2	Battery system efficiency over standard driving patterns: Toyota Prius, M1, and M2A2.....	199
10.10	FE over standard driving patterns: Toyota Prius, M1, and M2A2	201
10.11	Analysis of FE over US06: Toyota Prius, M1, and M2A2.....	203
10.11.1	Comparison over US06: M2A2 and M1-NEDC	203
10.11.2	Comparison over US06: M2A2 and M1-US06	209
10.11.3	Comparison over US06: M2A2 and Toyota Prius.....	213
10.12	FE variability over standard driving patterns: Toyota Prius, M1, and M2A2.....	217
10.13	Summary.....	220
CHAPTER 11: REAL-WORLD INVESTIGATION OF PROPOSED METHODOLOGY.....		222
11.1	FE evaluation over real-world driving patterns: Toyota Prius, M1, and M2A2.....	223
11.1.1	Battery SOC during FE evaluation: Toyota Prius, M1, and M2A2.....	223
11.1.2	Battery system efficiency over real-world driving patterns: Toyota Prius, M1, and M2A2.....	230
11.2	FE over real-world driving patterns: Toyota Prius, M1, and M2A2	232
11.2.1	Comparison of FE: M2A2 and Toyota Prius	236
11.2.2	Comparison of FE: M2A2 and M1	239
11.3	Analysis of FE over D1: Toyota Prius, M1, and M2A2.....	240
11.3.1	Comparison over D1: M2A2 and M1-NEDC.....	240
11.3.2	Comparison over D1: M2A2 and M1-US06	246
11.3.3	Comparison over D1: M2A2 and Toyota Prius	251

11.4	Distribution of FE: Toyota Prius, M1, and M2A2	256
11.5	FE variability over real-world driving patterns: Toyota Prius, M1, and M2A2.....	259
11.6	Summary	262
CHAPTER 12: DISCUSSION AND FUTURE WORK.....		264
12.1	Proposed methodology	265
12.2	Effect of optimisation variable and design constraint on optimum components.....	266
12.3	Preferred design for FE	267
12.4	Suitability in real-world.....	269
12.5	Solution to the research question.....	271
12.6	Reduction of customer concerns	272
12.7	Elimination of decision making process	274
12.8	Component life and cost.....	275
12.9	Limitation related to the proposed methodology.....	277
12.10	Applications	278
12.11	Future work.....	280
CHAPTER 13: CONCLUSIONS		283
REFERENCES.....		287
APPENDIX A.....		298
A.1	Calculation of acceleration and maximum speed.....	298
A.2	Calculation of gradeability.....	300
APPENDIX B.....		301
B.1	Standard driving patterns.....	301
B.2	Real-world driving patterns.....	302

APPENDIX C	305
C.1 Variation in optimum component sizes for different optimisation trials: Traditional methodology.....	305
C.2 Variation in optimum component sizes for different optimisation trials: Proposed methodology with second approach.....	308
APPENDIX D	311
D.1 MATLAB script to find optimum design with the combination of optimisation algorithm and vehicle simulation software.....	311

LIST OF FIGURES

Figure 1.1: Factors responsible for FE variability in HEVs in the real-world.....	5
Figure 2.1: Typical torque-speed characteristic of ICE [23].....	12
Figure 2.2: Typical fuel consumption and efficiency characteristics of ICE w.r.t. ICE torque [23].....	12
Figure 2.3: Typical fuel consumption and efficiency characteristics of ICE w.r.t. ICE power [23].....	13
Figure 2.4: Typical characteristics of electric motor [23].....	15
Figure 2.5: Typical efficiency map of electric motor [23].....	16
Figure 2.6: Typical characteristic of open circuit voltage w.r.t. SOC of a battery [64]	19
Figure 2.7: Caloric energy density of batteries and liquid fuels [18].....	20
Figure 2.8: Optimum operating line of an ICE [24]	24
Figure 2.9: Series hybrid electric drive train [28], [75]	27
Figure 2.10: Parallel hybrid electric vehicle [28], [75].....	29
Figure 2.11: Series-parallel hybrid drivetrain using a planetary gear unit [28], [75]	31
Figure 2.12: Planetary gear unit [28]	31
Figure 2.13: Relationship of component speeds of Toyota Prius [77].....	33
Figure 2.14: Optimisation problem.....	37
Figure 2.15: Global and local optimum	39
Figure 2.16: Standard procedure of GA [84]	40
Figure 2.17: Single-point crossover	43
Figure 2.18: Mutation	44
Figure 3.1: Traditional methodology of powertrain component size optimisation (M1)	65
Figure 3.2: FE variability over the years for Toyota Prius HEV	67
Figure 3.3: FE variability over 100 real-world driving patterns [46]	73
Figure 3.4: FE versus FE variability	76
Figure 3.5: Existing scenario of FE variability in HEVs and research question.....	78
Figure 4.1: Flow diagram of research methodology	83

Figure 5.1: Concept of optimisation decision in the new methodology	91
Figure 5.2: Concept of optimisation decision in the traditional methodology.....	92
Figure 5.3: Proposed methodology of powertrain component size optimisation (M2)	94
Figure 6.1: ICE characteristics of Toyota Prius HEV	98
Figure 6.2: Motor torque and efficiency map of Toyota Prius HEV	99
Figure 6.3: Generator torque and efficiency map of Toyota Prius HEV	100
Figure 6.4: Battery characteristics of Toyota Prius HEV	100
Figure 6.5: Battery SOC for the proposed methodology with first approach (M2A1)	104
Figure 6.6: Model-in-loop approach: integration of optimisation method with vehicle simulation model.....	109
Figure 6.7: Sequence of driving patterns for C1 combination.....	113
Figure 6.8: Route for real-world driving.....	115
Figure 7.1: Average FE versus FE variability over standard driving patterns: Toyota Prius and M1	131
Figure 8.1: Comparison of ICE power: Toyota Prius and M1	135
Figure 8.2: Comparison of generator power: Toyota Prius and M1	136
Figure 8.3: Comparison of motor power: Toyota Prius and M1	137
Figure 8.4: Comparison of battery capacity: Toyota Prius and M1	137
Figure 8.5: Optimum target SOC values: M1 methodology	139
Figure 8.6: Battery SOC of M1-HWFET over HWFET.....	140
Figure 8.7: Battery SOC of the Toyota Prius over US06.....	145
Figure 8.8: Battery SOC of the M1-HWFET design over US06.....	145
Figure 8.9: Comparison of engine torque and battery SOC over US06: M1-HWFET and Toyota Prius	146
Figure 8.10: Comparison of motor torque and battery SOC over US06: M1-HWFET and Toyota Prius	147
Figure 8.11: Comparison of generator torque and battery SOC over US06: M1- HWFET and Toyota Prius.....	147
Figure 8.12: Battery SOC of the M1-HWFET design over 3 consecutive US06	148
Figure 8.13: Average FE versus FE variability over standard driving patterns: Toyota Prius and M1	154

Figure 9.1: Comparison of ICE power: Toyota Prius, M1, and M2A1	160
Figure 9.2: Comparison of generator power: Toyota Prius, M1, and M2A1	161
Figure 9.3: Comparison of motor power: Toyota Prius, M1, and M2A1	162
Figure 9.4: Comparison of battery capacity: Toyota Prius, M1, and M2A1	163
Figure 9.5: Battery SOC of the M2A1-C4 over US06.....	169
Figure 9.6: Battery SOC of the M2A1-C4 over 3 consecutive US06.....	170
Figure 9.7: Comparison of average FE: M2A1 versus M1	172
Figure 9.8: Average FE versus FE variability over standard driving patterns: Toyota Prius and M2A1	174
Figure 10.1: Battery SOC for the proposed methodology with second approach (M2A2).....	178
Figure 10.2: Battery SOC swing and battery capacity over NEDC and FTP: Toyota Prius, M1, and M2A2.....	198
Figure 10.3: Battery SOC swing and battery capacity over LA92 and HWFET: Toyota Prius, M1, and M2A2	198
Figure 10.4: Battery SOC swing and battery capacity over US06: Toyota Prius, M1, and M2A2	199
Figure 10.5: Battery system efficiency over NEDC, FTP, and HWFET: Toyota Prius, M1, and M2A2	200
Figure 10.6: Battery system efficiency over LA92 and US06: Toyota Prius, M1, and M2A2	200
Figure 10.7: Comparison of fuel consumption over US06: M2A2 and M1-NEDC designs.....	204
Figure 10.8: Comparison of ICE torque over US06: M2A2 and M1-NEDC designs	205
Figure 10.9: Comparison of ICE speed over US06: M2A2 and M1-NEDC designs	205
Figure 10.10: Distribution of fuel consumption w.r.t. ICE torque over US06: M2A2 and M1-NEDC designs	205
Figure 10.11: Distribution of fuel consumption w.r.t. ICE speed over US06: M2A2 and M1-NEDC designs	206
Figure 10.12: Distribution of ICE torque over US06: M2A2 and M1-NEDC designs	207

Figure 10.13: Distribution of ICE speed over US06: M2A2 and M1-NEDC designs	207
Figure 10.14: Comparison of ICE torque and battery SOC over US06: M2A2 and M1-NEDC designs	208
Figure 10.15: Comparison of fuel consumption over US06: M2A2 and M1-US06 designs.....	209
Figure 10.16: Comparison of ICE torque over US06: M2A2 and M1-US06 designs	210
Figure 10.17: Comparison of ICE speed over US06: M2A2 and M1-US06 designs	210
Figure 10.18: Distribution of fuel consumption w.r.t. ICE torque over US06: M2A2 and M1-US06 designs	210
Figure 10.19: Distribution of fuel consumption w.r.t. ICE speed over US06: M2A2 and M1-US06 designs	211
Figure 10.20: Distribution of ICE torque over US06: M2A2 and M1-US06 designs	212
Figure 10.21: Distribution of ICE speed over US06: M2A2 and M1-US06 designs	212
Figure 10.22: Comparison of ICE torque and battery SOC over US06: M2A2 and M1-US06 designs.....	213
Figure 10.23: Comparison of fuel consumption over US06: M2A2 design and Toyota Prius	213
Figure 10.24: Comparison of ICE torque over US06: M2A2 design and Toyota Prius	214
Figure 10.25: Comparison of ICE speed over US06: M2A2 design and Toyota Prius	214
Figure 10.26: Distribution of fuel consumption w.r.t. ICE torque over US06: M2A2 design and Toyota Prius	215
Figure 10.27: Distribution of fuel consumption w.r.t. ICE speed over US06: M2A2 design and Toyota Prius	215
Figure 10.28: Distribution of ICE torque over US06: M2A2 design and Toyota Prius	216

Figure 10.29: Distribution of ICE speed over US06: M2A2 design and Toyota Prius	216
Figure 10.30: Comparison of ICE torque and battery SOC over US06: M2A2 design and Toyota Prius	217
Figure 10.31: Average FE versus FE variability over standard driving patterns: Toyota Prius, M1, and M2A2	219
Figure 11.1: Battery system efficiency over D1, D2, D3, and D4: Toyota Prius, M1, and M2A2	230
Figure 11.2: Battery system efficiency over D5, D6, and D7: Toyota Prius, M1, and M2A2	230
Figure 11.3: Battery system efficiency over D8, D9, and D10: Toyota Prius, M1, and M2A2	231
Figure 11.4: Minimum FE versus minimum FE w.r.t. Prius over D1 to D10	234
Figure 11.5: Maximum speed: D1 to D10 driving patterns	235
Figure 11.6: Maximum acceleration: D1 to D10 driving patterns	236
Figure 11.7: Time for acceleration and deceleration: D1 to D10 driving patterns ..	236
Figure 11.8: Comparison of maximum speeds for the comparison of FE: M2A2 design and Toyota Prius	237
Figure 11.9: Comparison of maximum acceleration for the comparison of FE: M2A2 design and Toyota Prius	237
Figure 11.10: Comparison of driving time for acceleration for the comparison of FE: M2A2 design and Toyota Prius	238
Figure 11.11: Comparison of driving time for deceleration for the comparison of FE: M2A2 design and Toyota Prius	238
Figure 11.12: Comparison of fuel consumption over D1: M2A2 and M1-NEDC designs.....	241
Figure 11.13: Comparison of ICE torque over D1: M2A2 and M1-NEDC designs	242
Figure 11.14: Comparison of ICE speed over D1: M2A2 and M-NEDC designs...	242
Figure 11.15: Distribution of fuel consumption w.r.t. ICE torque over D1: M2A2 and M1-NEDC designs	243
Figure 11.16: Distribution of fuel consumption w.r.t. ICE speed over D1: M2A2 and M1-NEDC designs	243
Figure 11.17: Distribution of ICE torque over D1: M2A2 and M1-NEDC designs	244

Figure 11.18: Distribution of ICE speed over D1: M2A2 and M1-NEDC designs.	245
Figure 11.19: Comparison of fuel consumption over D1: M2A2 and M1-US06 designs.....	246
Figure 11.20: Comparison of ICE torque over D1: M2A2 and M1-US06 designs .	247
Figure 11.21: Comparison of ICE speed over D1: M2A2 and M1-US06 designs ..	247
Figure 11.22: Distribution of fuel consumption w.r.t. ICE torque over D1: M2A2 and M1-US06 designs.....	248
Figure 11.23: Distribution of fuel consumption w.r.t. ICE speed over D1: M2A2 and M1-US06 designs.....	248
Figure 11.24: Distribution of ICE torque over D1: M2A2 and M1-US06 designs .	249
Figure 11.25: Distribution of ICE speed over D1: M2A2 and M1-US06 designs...	250
Figure 11.26: Comparison of fuel consumption over D1: M2A2 design and Toyota Prius	251
Figure 11.27: Comparison of ICE torque over D1: M2A2 design and Toyota Prius	252
Figure 11.28: Comparison of ICE speed over D1: M2A2 design and Toyota Prius	252
Figure 11.29: Distribution of fuel consumption w.r.t. ICE torque over D1: M2A2 design and Toyota Prius	253
Figure 11.30: Distribution of fuel consumption w.r.t. ICE speed over D1: M2A2 design and Toyota Prius	253
Figure 11.31: Distribution of ICE torque over D1: M2A2 design and Toyota Prius	255
Figure 11.32: Distribution of ICE speed over D1: M2A2 design and Toyota Prius	255
Figure 11.33: Distribution of FE of Toyota Prius over D1 to D10.....	256
Figure 11.34: Distribution of FE of M1-NEDC design over D1 to D10	257
Figure 11.35: Distribution of FE of M1-FTP design over D1 to D10	257
Figure 11.36: Distribution of FE of M1-LA92 design over D1 to D10.....	257
Figure 11.37: Distribution of FE of M1-HWFET design over D1 to D10	257
Figure 11.38: Distribution of FE of M1-US06 design over D1 to D10	258
Figure 11.39: Distribution of FE of M2A2 design over D1 to D10.....	258
Figure 11.40: Average FE versus FE variability over real-world driving patterns: Toyota Prius, M1, and M2A2	260
Figure 12.1: Probable distribution of FE: M2A2 and Toyota Prius.....	273

Figure B.1: NEDC.....	301
Figure B.2: FTP.....	301
Figure B.3: LA92.....	301
Figure B.4: HWFET.....	301
Figure B.5: US06.....	302
Figure B.6: D1.....	302
Figure B.7: D2.....	302
Figure B.8: D3.....	303
Figure B.9: D4.....	303
Figure B.10: D5.....	303
Figure B.11: D6.....	303
Figure B.12: D7.....	303
Figure B.13: D8.....	303
Figure B.14: D9.....	304
Figure B.15: D10.....	304

LIST OF TABLES

Table 2.1: Standard legislative driving patterns.....	36
Table 3.1: Powertrain components and optimisation variables considered for powertrain components	51
Table 3.2: Design limits considered in literature	53
Table 3.3: Constraints considered in literature	55
Table 3.4: Driving patterns considered in literature.....	57
Table 3.5: Optimum component sizes over different driving patterns.....	59
Table 3.6: Optimisation methods used in literature	61
Table 3.7: Comparison of customer reported FE and manufacturers declared FE for Toyota Prius HEV [41]	66
Table 3.8: FE variability over standard driving patterns [38].....	69
Table 3.9: FE variability over 6 driving patterns [39]	70
Table 3.10: FE variability over driving patterns: CV and HEVs [44]	71
Table 3.11: FE variability over real-world driving patterns: CV and HEVs	73
Table 6.1: Range of variations in design variables	102
Table 6.2: Rules of VSC strategy of Toyota Prius HEV	105
Table 6.3: Major parameters of VSC strategy of Toyota Prius.....	106
Table 6.4: Classifications of standard driving patterns	111
Table 6.5: Combinations of driving patterns for proposed methodology	113
Table 6.6: Driving parameters of real-world driving patterns	116
Table 7.1: Component sizes for optimum designs of M1 methodology	121
Table 7.2: Variation in optimum component sizes for 10 optimisation trials: M1 methodology.....	123
Table 7.3: Performance of optimum designs: Toyota Prius and M1 methodology .	124
Table 7.4: Combined power of ICE and motor: Toyota Prius and M1 methodology	125
Table 7.5: Target SOC over driving patterns during FE evaluation: Toyota Prius and M1	127
Table 7.6: Final battery SOC over driving patterns during FE evaluation: Toyota Prius and M1	128

Table 7.7: FE over standard driving patterns: Toyota Prius and M1	129
Table 8.1: Optimum parameters of M1 methodology.....	134
Table 8.2: Variation in component sizes for M1 methodology: fixed and variable target SOC.....	138
Table 8.3: Performance of optimum designs: Toyota Prius and M1	141
Table 8.4: Combined power: Toyota Prius and M1	142
Table 8.5: Target SOC over driving patterns during FE evaluation: Toyota Prius and M1	143
Table 8.6: Final battery SOC over driving patterns during FE evaluation: Toyota Prius and M1	144
Table 8.7: Battery SOC swing over standard driving patterns: Toyota Prius and M1	149
Table 8.8: FE over standard driving patterns: Toyota Prius and M1	151
Table 9.1: Combinations of driving patterns and name of optimum designs for M2A1 approach	159
Table 9.2: Optimum parameters of optimum designs of M2A1 approach	159
Table 9.3: Comparison of optimum target SOC during optimisation: M1 and M2A1	163
Table 9.4: Variations in component sizes: M1 and M2A1	164
Table 9.5: Performance of optimum designs: Toyota Prius and M2A1	165
Table 9.6: Combined power: Toyota Prius and M2A1	165
Table 9.7: Battery SOC after each driving pattern during optimisation: optimum designs of M2A1 approach	166
Table 9.8: Target SOC over driving patterns during FE evaluation: M2A1.....	168
Table 9.9: Final battery SOC over driving patterns during FE evaluation: M2A1 ..	169
Table 9.10: FE over standard driving patterns: Toyota Prius and M2A1	171
Table 9.11: FE variation among designs over a driving pattern: M1 and M2A1	173
Table 10.1: Combinations of driving patterns and name of optimum designs for M2A2 approach.....	179
Table 10.2: Component sizes of optimum designs of M2A2 approach.....	180
Table 10.3: Variations in component sizes: M1, M2A1, and M2A2.....	181
Table 10.4: Variation in optimum component sizes for 10 optimisation trials.....	181

Table 10.5: Optimum target SOC during optimisation: optimum designs of M2A2 approach	182
Table 10.6: Performances of optimum designs: Toyota Prius and M2A2 approach	183
Table 10.7: Combined power: Toyota Prius and M2A2 approach	184
Table 10.8: Battery SOC after each driving pattern during optimisation: optimum designs of M2A2 approach	185
Table 10.9: Target SOC over driving patterns during FE evaluation: M2A2 approach	186
Table 10.10: Final battery SOC over driving patterns during FE evaluation: M2A2 approach	186
Table 10.11: FE over standard driving patterns: optimum designs of M2A2 approach	187
Table 10.12: FE variation among designs over a driving pattern: M1, M2A1, and M2A2	188
Table 10.13: M2A2 design.....	189
Table 10.14: Component sizes of optimum designs: Toyota Prius, M1, and M2A2	190
Table 10.15: Combined power: Toyota Prius, M1, and M2A2	191
Table 10.16: Performances of optimum designs: Toyota Prius, M1, and M2A2	192
Table 10.17: Target SOC and final battery SOC during FE evaluation: Toyota Prius and M2A2 design	194
Table 10.18: Comparison of battery SOC swing: Toyota Prius, M1, and M2A2....	196
Table 10.19: FE over standard driving patterns: Toyota Prius, M1, and M2A2.....	202
Table 11.1: Target SOC during FE evaluation over real-world driving patterns: Toyota Prius, M1, and M2A2	224
Table 11.2: Final battery SOC during FE evaluation over real-world driving patterns: Toyota Prius, M1, and M2A2	226
Table 11.3: Battery SOC swing during FE evaluation over real world driving patterns (D1 to D5): Toyota Prius, M1, and M2A2	227
Table 11.4: Battery SOC swing during FE evaluation over real world driving patterns (D6 to D10): Toyota Prius, M1, and M2A2	228
Table 11.5: FE over real world driving patterns: Toyota Prius, M1, and M2A2.....	233

Table C.1: Variation in optimum component sizes of the M1-NEDC design for 10 optimisation trials.....	305
Table C.2: Variation in optimum component sizes of the M1-FTP design for 10 optimisation trials.....	306
Table C.3: Variation in optimum component sizes of the M1-LA92 design for 10 optimisation trials.....	306
Table C.4: Variation in optimum component sizes of the M1-US06 design for 10 optimisation trials.....	307
Table C.5: Variation in optimum component sizes of the M2A2-C1 design for 10 optimisation trials.....	308
Table C.6: Variation in optimum component sizes of the M2A2-C2 design for 10 optimisation trials.....	309
Table C.7: Variation in optimum component sizes of the M2A2-C3 design for 10 optimisation trials.....	309
Table C.8: Variation in optimum component sizes of the M2A2-C4 design for 10 optimisation trials.....	310
Table C.9: Variation in optimum component sizes of the M2A2-C5 design for 10 optimisation trials.....	310

ACKNOWLEDGEMENTS

I would like to extend my deepest gratitude to my supervisors, Professor Paul A. Jennings and Dr. Andrew McGordon for the opportunities and support they have provided throughout my research. Their academic guidance on my research and the completion of the thesis is very much appreciated and remembered. I feel incredibly fortunate to work with them.

I am thankful to Professor Kevin Neailey, Dr. Dawei Lu, Dr. James Harte, and Dr. Jeffrey Jones for providing critical feedback and suggestions during various stages of my research.

I am also thankful to Dr. R. Peter Jones and Professor Keith Robert Pullen for their valuable suggestions to improve my thesis.

I would like to thank to the members of the Energy and Electrical Systems Group and Experiential Engineering Group, WMG for providing the state-of-the-art facilities. I would like to thank to Dr. John Poxon for his support and sharing real-world driving data from Sustainable Action on Vehicle Energy (SAVE) project, WMG. I am thankful to Experiential Engineering PhD/EngD group meeting members, Dr. Sarah Payne, Dr. James Mackrill, Brahmadevan Padmarajan, Anup Barai, Kieu Anh Vuong, Sneha Singh, and Mahdad Sadeghi for their helpful discussions and suggestions. I would also like to thank to Dr. James Mackrill, Dr. M. Ahtamad, and Dr. Mazuir Shah for sharing their PhD experiences.

My sincere thanks go to Mr. Gunwant Dhadyalla and Mr. Mark Amor-Segan for their valuable feedback and time during various stages of my research.

I am thankful to the past and present colleagues of the International Digital Laboratory, WMG, Brahmadevan Padmarajan, Girish Kurup, Saurin Badiyani, Nagesh Shukla, Prakash, Vibhor Agarwal, Arnab Palit, Abhishek Das, Chris Golby, Mitan Solanki, Selim Yilmazer, and Dr. Pasquale Franciosa for making my stay at Warwick delightful.

I would like to acknowledge my employer TVS Motor Company Limited, India for providing opportunity for the doctoral research and financial support. I would like to thank to Mr. Vinay Harne, Mr. N. Jayaram, Mr. Y. Ramachandra Babu, and Mr. V. J. Johnson for their continuous support and encouragement. I would also like to acknowledge the support from Mr. K. Vengadasubramanian, Mr. M. N. Sivaprasad, and Mr. C. Subash.

Finally, I am grateful to my parents, Mr. Bimal Chandra Roy and Mrs. Basumati Roy and my brother, Dr. Kallol Kumar Roy for their endless love, support and encouragement throughout my life. I am also grateful to my wife, Tanushree Roy and son, Ankush Roy for their continuous love, support, and understanding through the difficult and challenging times.

DECLARATION

I hereby declare that this thesis contains my own research. No part of this thesis was previously published or submitted for a degree at any other university. This thesis is presented in accordance with the regulations of the university.

LIST OF PUBLICATIONS

1. **Hillol Kumar Roy**, Andrew McGordon, Paul A. Jennings, “A generalized powertrain design optimization methodology to reduce fuel economy variability in hybrid electric vehicles”, *IEEE Transactions on Vehicular Technology*, vol. 63 (3), pp. 1055-1070, 2014. (Peer reviewed).
2. **Hillol Kumar Roy**, Andrew McGordon, Paul A. Jennings, “Real-world investigation of a methodology for powertrain component sizing of hybrid electric vehicles”, *Proceedings of the 27th International Battery, Hybrid and Fuel Cell Electric Vehicle Symposium, EVS27*, Barcelona, Spain, November 17-20, 2013. (Peer reviewed).
3. **Hillol Kumar Roy**, Andrew McGordon, Paul A. Jennings, “Component sizing of a power-split hybrid electric vehicle using hybrid genetic algorithm”, *Proceedings of the 34th FISITA World Automotive Congress*, Beijing, China, November 27-30, 2012. (Peer reviewed).
4. **Hillol Kumar Roy**, Andrew McGordon, Paul A. Jennings, “A methodology for component sizing of hybrid electric vehicles based on a range of driving patterns”, *Proceedings of the 26th International Battery, Hybrid and Fuel Cell Electric Vehicle Symposium, EVS26*, Los Angeles, California, USA, May 6-9, 2012. (Peer reviewed).

ABSTRACT

Although hybrid electric vehicles (HEVs) generally improve fuel economy (FE) compared to conventional vehicles, evidence of higher FE variability in HEVs compared to conventional vehicles indicates that apart from the improvement in FE, the reduction of FE variability is also of significant importance for HEVs. Over the years research on how to optimise powertrain component sizes of HEVs has generally focused on improving FE over a given driving pattern; FE variability over a realistic range of driving patterns has generally been overlooked, and this can lead to FE benefits of HEVs not being fully realised in real-world usage.

How to reduce the FE variability in HEVs due to variation in driving patterns through the optimisation of powertrain component sizes is considered as the research question. This research proposes a new methodology in which powertrain components are optimised over a range of driving patterns representing different traffic conditions and driving styles simultaneously. This improves upon the traditional methodology followed in the reviewed literature, where an optimisation is performed for each individual driving pattern. An analysis shows that the traditional methodology could produce around 20% FE variability due to variation in driving patterns.

This study considers a computer simulation model of a series-parallel Toyota Prius HEV for the investigation. Four powertrain components, namely, internal combustion engine, generator, motor, and battery of the Toyota Prius are optimised for FE using a genetic algorithm. For both the proposed and traditional methodologies, the powertrain components are optimised based on 5 standard driving patterns representing different traffic conditions and driving styles. During the optimisation, the proposed methodology considers all the 5 driving patterns simultaneously, whereas the traditional methodology considers each driving pattern separately. The optimum designs of both the methodologies and the simulation model of the Toyota Prius which is the benchmark vehicle for this study are evaluated for FE over the aforementioned 5 standard driving patterns and also 10 real-world driving patterns of a predefined route consisting of urban and highway driving patterns.

The proposed methodology provides a single optimum design over the 5 standard driving patterns, whereas the traditional methodology provides 5 different optimum designs, one for each driving pattern. The single optimum design produced by the proposed methodology is independent of the sequence of driving patterns. The proposed methodology reduces FE variability by 5.3% and up to 48.9% with comparable average FE compared to the Toyota Prius and traditional methodology, respectively over the 10 real-world driving patterns, whereas none of the optimum designs of the traditional methodology is able to reduce FE variability compared to the Toyota Prius.

This research provides a promising direction to address customer concerns related to FE in the real-world and improves understanding of the effect of driving patterns on the design of powertrain components.

LIST OF ABBREVIATIONS

CV	Conventional Vehicle
DC	Direct Current
DP	Driving Pattern
EV	Electric Vehicle
FE	Fuel Economy
FC	Fuel Consumption
GA	Genetic Algorithm
HEV	Hybrid Electric Vehicle
ICE	Internal Combustion Engine
PSO	Particle Swarm Optimisation
SA	Simulated Annealing
SQP	Sequential Quadratic Programming
VSC	Vehicle Supervisory Control

LIST OF SYMBOLS AND VARIABLES

Ah	Ampere hour
g	gram
kg	kilogram
kW	kilo Watt
km	kilometer
l	litre
s	second
g/s	gram per second
m ²	meter squared
m/s	meter per second
m/s ²	meter per second squared
mpg	miles per gallon
mph	miles per hour
Nm	Newton meter
\$	United States Dollar
P_{ICE}	Power of ICE
η_f	Fuel conversion efficiency
\dot{m}_{air}	Mass flow rate of air
LHV	Lower heating value of fuel
m_f	Mass of fuel
m_a	Mass of air
n_r	Number of power stroke per crank rotation
N	Engine speed
P_M	Electrical power of electric motor
V	Voltage
I	Current
η_{bat}	Battery system efficiency
t_i	Start time

t_f	End time
$V_{terminal}$	Cell terminal voltage
I_{chg}	Charging current
I_{dischg}	Discharging current
ω_{ICE}	Rotational speed of ICE
ω_G	Rotational speed of generator
ω_M	Rotational speed of motor
v	Vehicle speed
T_{ICE}	Torque of ICE
T_G	Torque of generator
T_{RING}	Torque of ring gear
v_i^k	Current velocity of particle i
v_i^{k+1}	Modified velocity of particle i
r_1	Random number [0, 1]
r_2	Random number [0, 1]
ω	Inertia
c_1	Social parameter
c_2	Social parameter
x_i^k	Current position of particle i
x_i^{k+1}	Modified position of particle i
$pbest_i$	Local best of particle i
$gbest$	Global best of the population

CHAPTER 1

INTRODUCTION

1.1 Motivation and research question

Transportation is one of the major reasons behind the development of civilisation [1]. Automotive is one of the major forms of transportation. The automotive sector heavily depends on fossil fuels [2]. It has been predicted that there will be a scarcity of fossil fuels reserves by the middle of the 21st century [3]. The fossil fuel price is going up steadily over the years and it is projected that it will continue to increase into the future [4]. The decline in fossil fuel reserves and rise in fuel prices has motivated the automotive industry to search for alternative technologies to reduce the fossil fuel dependency. Apart from the dependency on the fossil fuels, the automotive sector also contributes largely to global emissions [5]. To reduce the harmful effect of the global emissions, strict emission norms for automotive vehicles are in place and the emission norms will become stricter in coming years [6]. To reduce the dependency on the fossil fuels and emissions, several approaches could be followed, such as more efficient internal combustion engines (ICEs) [7-9], use of alternate fuels [10], electric vehicles (EVs), and hybrid electric vehicles (HEVs) [11].

More efficient ICEs have the potential to reduce the fuel dependency of conventional vehicles (CVs) i.e., ICE powered vehicles by improving fuel economy (FE) [7-9]. The improvement of FE will be required more in future due to shortage of fuels and

increase in number of vehicles [12]. Therefore, the improvement in the efficiency of ICEs to match the requirement of the improvement of FE will become increasingly difficult in future [9]. Although more efficient ICEs have the potential to reduce the local emissions, they cannot eliminate the emissions completely.

Use of alternate fuels such as hydrogen can reduce the dependency of fossil fuels and local emissions [13], [14]. Due to lower energy density of hydrogen by volume compared to other fossil fuels (gasoline, diesel etc.), finding a compact, inexpensive, and safe hydrogen storage system in the limited space of a vehicle is challenging [15]. The lack of mature technologies for on-board hydrogen storage and infrastructure for hydrogen filling station limit the use of hydrogen.

EVs can eliminate on-board fuel dependency and are free from local emissions [16]. But EVs indirectly depend on fossil fuel as fuel is used for generation of electricity. Similarly, EVs also indirectly contribute to global emissions because emissions occur during the generation of electricity [17]. A major concern of EVs is limited driving range (i.e., distance traveled before recharging the battery) compared to CVs [16]. The limitation in driving range is due to lower energy density of the battery (by around 50 times) compared to fossil fuels such as gasoline or diesel [18]. Lack of battery charging infrastructure also limits the mass usage of EVs [19], [20]. An EV also has higher initial cost compared to a CV [21]. With an improvement in energy density of the battery with cost-effective technologies and charging infrastructure, EVs have the potential for mass usage by 2030 [22].

Until the development of the battery with equivalent energy density of fossil fuels and charging infrastructure, HEVs are potential technologies to reduce the fuel dependency and emissions [23]. As per the proposal of Technical Committee 69

(Electric Road Vehicles) of the International Electrotechnical Commission, a HEV is a vehicle in which propulsion energy is available from two or more kinds or types of energy stores, sources, or converters and at least one of them can deliver electrical energy [24]. As per this general definition, there are many types of HEVs, such as the gasoline ICE and battery, diesel ICE and battery, battery and fuel cell (FC), battery and capacitor, battery and flywheel, and battery and battery hybrids. But in common practice, a HEV is simply a vehicle having both an ICE and electric motor [24].

Although the idea of HEVs dates back to 1905 [25], HEVs have since been overlooked mainly due to the significant developments in ICE technologies and the availability of fossil fuels at a reasonable cost. Although HEVs are expensive compared to CVs and reliability is still not up to the mark [26], today, the situation is changing rapidly as the cost of fossil fuels continues to increase and the growing global population continues to take its toll on supply and also cheap computers for controlling the power electronics. As a result, HEVs are rapidly entering the mainstream and are now produced in a variety of powertrain configurations to meet the requirements of automobile consumers [27] and the demanding requirements of government regulations related to emissions.

HEVs are classified generally into three major architectures, namely, series, parallel, and series-parallel HEVs [28-33]. The schematic diagrams of all the architectures are shown in chapter 2. In a series HEV, an electric motor provides drive torque by connecting it to the wheel and an ICE is used only to charge the battery when required. As the ICE is used only to charge the battery and the electric motor is used majority of times to drive the vehicle, the FE of a series HEV is generally higher

compared to a CV [32]. In parallel HEV, both the ICE and electric motor are connected to the wheel to provide drive torque. The electric motor operates at lower speed and the ICE operates at mid-speed range. At higher speeds both the ICE and electric motor provide drive torque in combination. Although the ICE operates more time in a parallel HEV compared to a series HEV, the ICE operates majority of time at its most efficient region (mid-speed range) and therefore, the FE of a parallel HEV is also generally higher compared to a CV [32]. A series-parallel HEV has the ability of both the series and parallel HEV i.e., it could act as the series as well as parallel HEV. Therefore, a series-parallel HEV also generally provides higher FE compared to a CV [32].

HEVs generally have higher FE compared to CVs as the ICE operates always at its most efficient region and the electric motor operates its efficient region at lower speed range which is less efficient region for the ICE. HEVs also have higher driving range compared to EVs due to the presence of ICE.

Although irrespective of architectures, HEVs generally have higher FE than CVs, FE variability i.e., the variation in FE under different conditions exists in HEVs [34-39], like it does in CVs [40]. Considerable variation exists between customers reported real-world FE and declared FE data by the manufacturers and the variation was around 34% for Toyota Prius HEVs in 2013 [41]. The FE varies with the variation in factors such as operation of air-conditioning [34], atmospheric temperature [36], [37], and variation in driving patterns [38], [39], as shown in Figure 1.1. The variation in FE could also be due to other factors such as variation in the gradient of road and time of operation.

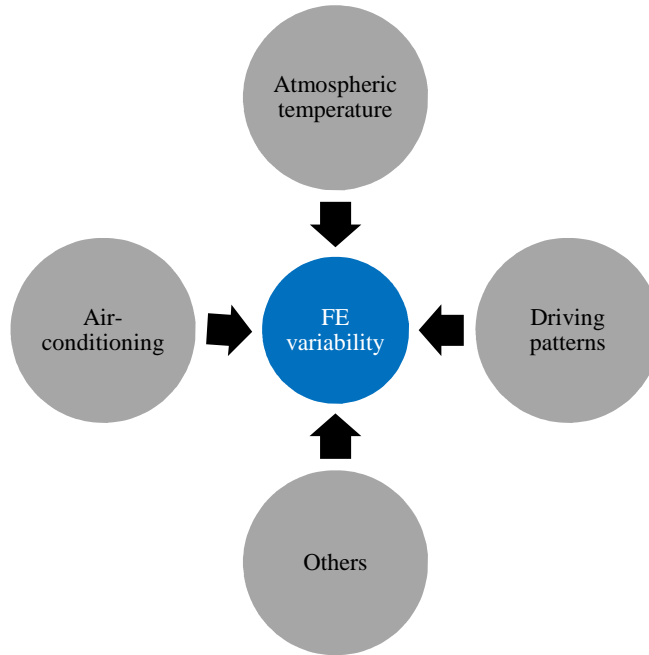


Figure 1.1: Factors responsible for FE variability in HEVs in the real-world

Driving patterns are generally considered as speed-time profiles of a vehicle [42]. Among all the factors, the variation in driving patterns not only depends on driving styles but also external factors such as traffic conditions [43]. As a result, driving patterns vary from person to person, vehicle to vehicle, and even time to time. The importance of driving patterns is even higher in HEVs as the supportive evidence of higher FE variability of HEVs compared to its conventional counterpart are found [44-46]. The FE variability of a HEV could be as high as around 100% compared to the FE variability of a CV [46]. The evidences of higher FE variability of HEVs compared to CVs and the variation between reported FE of customers and declared FE of manufacturers indicate that without the reduction of FE variability in HEVs, actual improvements of FE could not be perceived fully by all customers in the real-world. So, apart from the improvement in FE, the reduction of FE variability due to variation in driving patterns is also of significant importance for HEVs.

FE variability could be reduced by making HEVs less sensitive to variations in driving patterns. In other words, FE of a HEV should vary as little as possible with the variation in driving patterns. A HEV is a complex electromechanical system involving hundreds of design parameters [23]. Each of the parameters must be optimally chosen for the best performance of the HEV. The FE of a HEV is affected by the combination of powertrain components and optimum function of those components according to the strategy of the vehicle supervisory control. Regardless of the selected HEV architecture, finding the optimum combination of powertrain components is important for FE performance. Among several components, the ICE, electric machine, and energy storage device are major contributors to the performance of HEVs. Development and testing of each design combination to find the optimum combination of powertrain components is time consuming and expensive [47]. Simulation-based optimisation where an optimisation method works with a computer simulation model is a preferred time saving and cost-effective method to find an optimum combination of powertrain components of HEVs [47], [48].

Various research studies have been conducted over the years on the simulation-based optimisation of powertrain component sizes of HEVs [49-60]. In all previous studies [49-60], irrespective of the architecture, the optimisation of powertrain components was mainly focused on the improvement of FE. All studies followed a similar methodology for the optimisation of powertrain component sizes. The traditional methodology followed in those studies generally found an optimum design over a given driving pattern by the optimisation of powertrain components over that driving pattern. In other words, powertrain components were only optimum over a given

driving pattern. As a result, those studies found different sets of optimum components, one for each driving pattern, and concluded that optimum design over a driving pattern was not optimum over other driving patterns [52], [55], [57]. No study has investigated FE performance of different optimum designs over different driving patterns i.e., FE variability of optimum designs due to variation in driving patterns. Although no study was found investigating the details of FE variability of different optimum designs, around 20% FE variability of an optimum design was found by analysing a simulation study of a parallel HEV [49]. This indicated that there is a scope for improvement in the traditional methodology for the optimisation of powertrain component sizes. No systematic methodology was found in the reviewed literature to reduce FE variability through the optimisation of powertrain component sizes.

Due to the importance of powertrain components for FE improvement and the lack of knowledge for the reduction of FE variability, how to reduce FE variability in HEVs due to variation in driving patterns through the optimisation of powertrain component sizes was considered as the research question.

1.2 Knowledge contributions

This thesis discusses a new methodology for the optimisation of powertrain component sizes of HEVs to reduce FE variability due to variation in driving patterns. In the new methodology, powertrain components of HEVs are optimised over a range of driving patterns representing different traffic conditions and driving styles simultaneously. This improves upon the traditional methodology followed in the reviewed literature where powertrain components are generally optimised over a single driving pattern.

Apart from the proposal of a new methodology, this research study also does, for the first time, an investigation of the potential of the traditional methodology in terms of FE variability. This study helps to improve the understanding of the effect of optimum powertrain component sizes on the FE variability in real-world driving.

1.3 Organisation of the thesis

The thesis is structured into 13 chapters of which this introduction is the first. Chapter 2 provides background knowledge about the major terminologies used in the study.

Chapter 3 reviews the related literature of FE in HEVs and discusses how reviewed literature directed towards the formulation of the research question.

Chapter 4 presents the research methodology. It provides an overview of the major steps followed in this study from the start to end.

Chapter 5 discusses the proposal of a new methodology to address the research question. This chapter explains the new methodology and describes the concept.

Chapter 6 describes the simulation setup used for the evaluation of the traditional and new methodologies for the optimisation of powertrain component sizes.

Chapters 7 and 8 discuss the evaluation of the traditional methodology in standard conditions. These chapters present the investigation of the traditional methodology over 5 standard driving patterns. The objective of this work was to understand the traditional methodology in terms of FE variability when a Toyota Prius HEV was used as a case study.

Chapters 9 and 10 discuss the evaluation of the new methodology for the optimisation of powertrain component sizes over the same standard conditions used in chapters 7 and 8.

Chapter 11 discusses the validation of the new methodology in real-world conditions. This chapter presents the investigation of the new methodology for 10 real-world driving patterns over a predefined route.

Chapter 12 discusses the major outcomes of the research study along with the learning, applications, limitations, and suggested future directions of the work and finally, chapter 13 summarises the main conclusions.

CHAPTER 2

OVERVIEW: HYBRID ELECTRIC VEHICLES AND OPTIMISATION METHODS

The main objective of this chapter is to introduce the basics of hybrid electric vehicles (HEVs) and associated terminologies to be used in subsequent chapters. This chapter discusses the architectures, major powertrain components, and vehicle supervisory control strategies of HEVs. Like any other automotive vehicles, HEVs are also evaluated over different speed-time profiles of vehicles known as driving patterns to predict performance in real-world conditions. This chapter provides an overview of driving patterns. As HEVs consist of more components and complex strategies to control those components, optimisation is required to determine the component sizes and control strategies. This chapter also provides a brief overview of different methods for optimisation.

2.1 Hybrid electric vehicle (HEV)

A vehicle powered only by internal combustion engine (ICE) is known as conventional vehicle (CV) and a vehicle powered only by electric motor is called electric vehicle (EV) [23]. A vehicle in which propulsion energy is available from more than one types of energy stores, sources, or converters and at least one of them can deliver electrical energy, is called hybrid electric vehicle (HEV) [24]. The most popular form of HEV is the combination of an ICE with an electric motor.

As HEVs consist of more powertrain components (ICE, electric motor, and battery) compared to CVs (ICE) and EVs (Electric motor and battery), the interaction of powertrain components is also important. The optimal interaction of powertrain components is done through energy management, also known as vehicle supervisory control (VSC). Therefore, powertrain components and VSC are two main systems of significant importance for a HEV. A basic overview of powertrain components are discussed next followed by the VSC.

2.1.1 Powertrain components

Three main powertrain components, namely, ICE, electric motor, and battery are considered for discussion. The definition, characteristics, advantages, and disadvantages of each component are discussed next.

2.1.1.1 Internal combustion engine (ICE)

Internal combustion engine (ICE) is a device that produces mechanical energy by the combustion of fuels (generally fossil fuels) internally [61]. A typical characteristic of an ICE are shown from Figure 2.1 to Figure 2.3.

The ICE is not able to generate torque from zero speed. It is able to generate torque and power after reaching a certain speed (Idling), around 750 rpm in case of Figure 2.1 to Figure 2.3. Therefore, a separate external source such as electric motor is required to raise the speed of the ICE up to the idling speed in the ICE powered vehicle. Although the ICE starts to generate torque after the idling speed, the torque is very low at lower throttle opening, as shown in Figure 2.1 and not sufficient to move the vehicle from rest. To overcome the problem of low torque at very low speed, a transmission is associated with the ICE to regulate the torque of the ICE as

per the requirement of the vehicle. Transmission is a system which can transmit torque and speed of a rotating source to another, generally using gears.

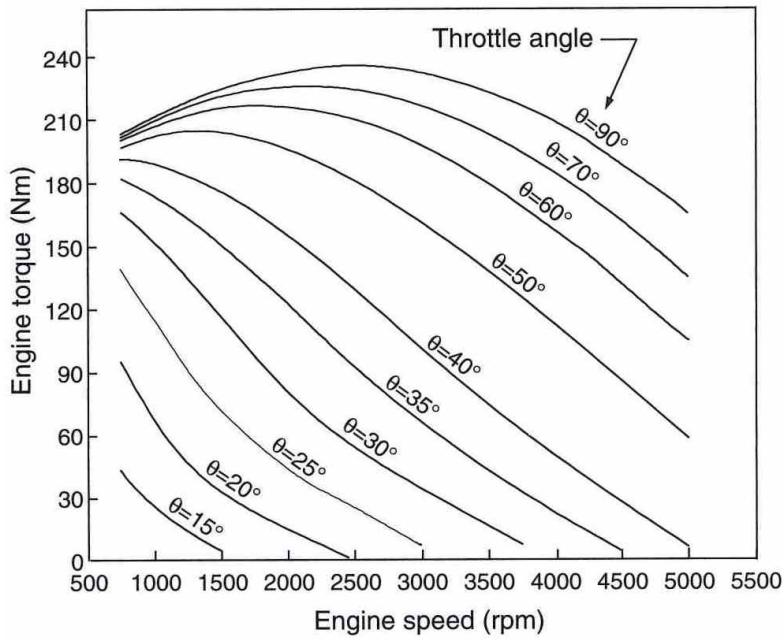


Figure 2.1: Typical torque-speed characteristic of ICE [23]

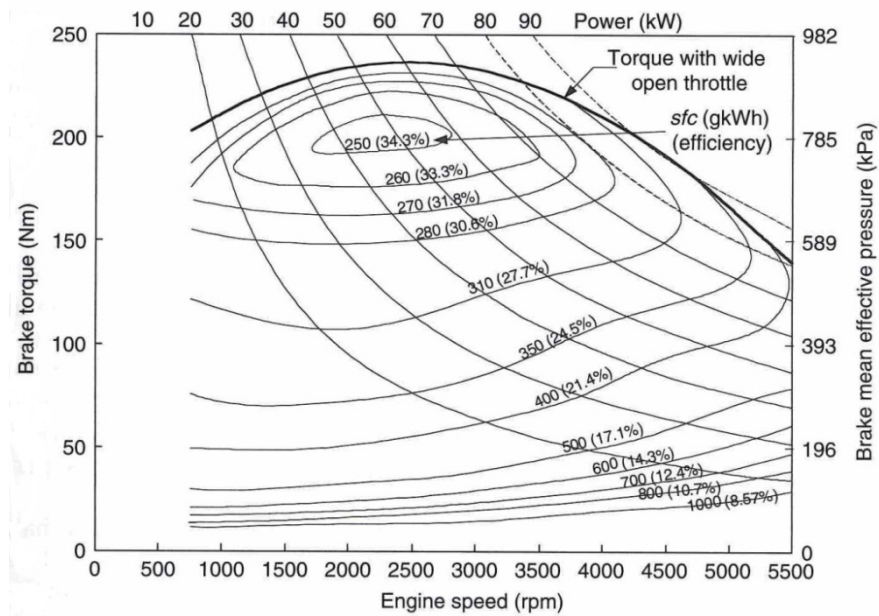


Figure 2.2: Typical fuel consumption and efficiency characteristics of ICE w.r.t. ICE torque [23]

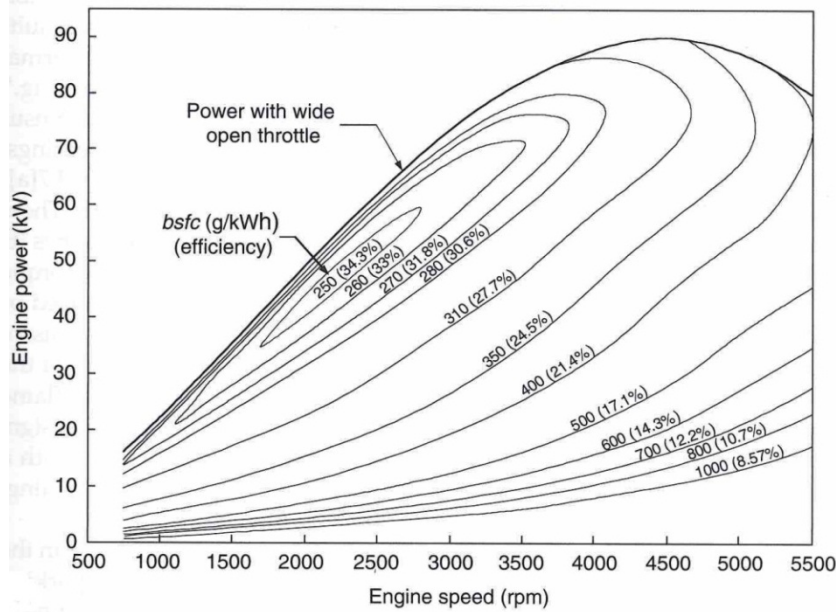


Figure 2.3: Typical fuel consumption and efficiency characteristics of ICE w.r.t. ICE power [23]

The efficiency and fuel consumption (FC) of the ICE varies with torque, power, and speed, as shown in Figure 2.2 and Figure 2.3. Generally, fuel consumption (FC) of the ICE is lower in mid-speed range near the region of maximum torque compared to lower or higher speed. Therefore, the ICE powered vehicle provides lower FC if it operates more time in mid-speed range. The maximum efficiency of the ICE is typically around 34%, as shown in Figure 2.2 and Figure 2.3.

The relationship between power and FC of the ICE is shown in Equation 2.1 [61].

$$P_{ICE} = \eta_f * \dot{m}_{air} * N * LHV * \frac{m_f}{m_a} * \frac{1}{n_r} \dots \dots \dots Eq. 2.1$$

Where,

P_{ICE} = Power of ICE

η_f = fuel conversion efficiency

\dot{m}_{air} = mass flow rate of air

LHV = Lower heating value of fuel

$m_f = \text{mass of fuel}$

$m_a = \text{mass of air}$

$n_r = \text{number of power stroke per crank rotation}$

$N = \text{engine speed}$

Equation 2.1 shows that the FC of the ICE increases with the increase of the power of the ICE when all other parameters of Equation 2.1 remain constant. The increase in the power increases performance (such as acceleration and maximum speed) of the ICE powered vehicle. Therefore, a trade-off exists between FE and performance of the ICE. The cost of the ICE also increases with the maximum power of the ICE, as shown in Equation 2.2 found from studies by Electric Power Research Institute (EPRI), USA [52], [62], [63]. Hence, the selection of the maximum power of the ICE is of critical importance. It is even more important for a HEV as a HEV consists of more components compared to a CV and an EV, and a HEV is much more focused at high FE.

$$\text{Cost of ICE} = \$12.0 * (\text{Maximum power of ICE in kW}) + \$424 \dots \dots \dots \text{Eq. 2.2}$$

The ICEs can be classified into two major groups, spark ignition (SI) and compression ignition (CI) engines [61]. Among the two groups, the SI engines are generally used in HEVs, probably due to lower FE of the SI engines compared to the CI engines. As this study considers same type of ICE for all investigations i.e., study is independent of the type of ICE, the details discussion of each type of ICE is of little significance.

2.1.1.2 Electric motor

Electric motor is an electric machine that converts electric energy to mechanical energy [23]. The electric motor can be powered by direct current (DC) sources such as battery or alternating current (AC) sources such as generator. The electric motor can operate both in motoring mode and generating mode. In generating mode electric energy is generated from mechanical energy.

A typical torque and power characteristics of an electric motor are shown in Figure 2.4.

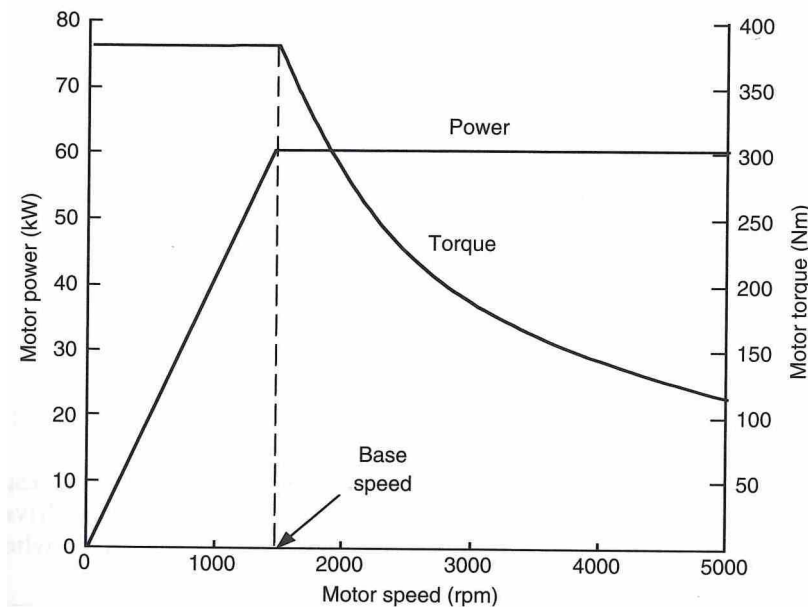


Figure 2.4: Typical characteristics of electric motor [23]

Figure 2.4 shows that the electric motor generates the maximum torque from zero speed and the torque remains constant up to a certain speed known as base speed and torque decreases with the increase in speed after the base speed. The power of the electric motor is zero at zero speed and the maximum at the base speed, as shown in Figure 2.4. The power remains constant after the base speed. Therefore, the electric

motor generates constant torque up to the base speed and after the base speed, it generates constant power.

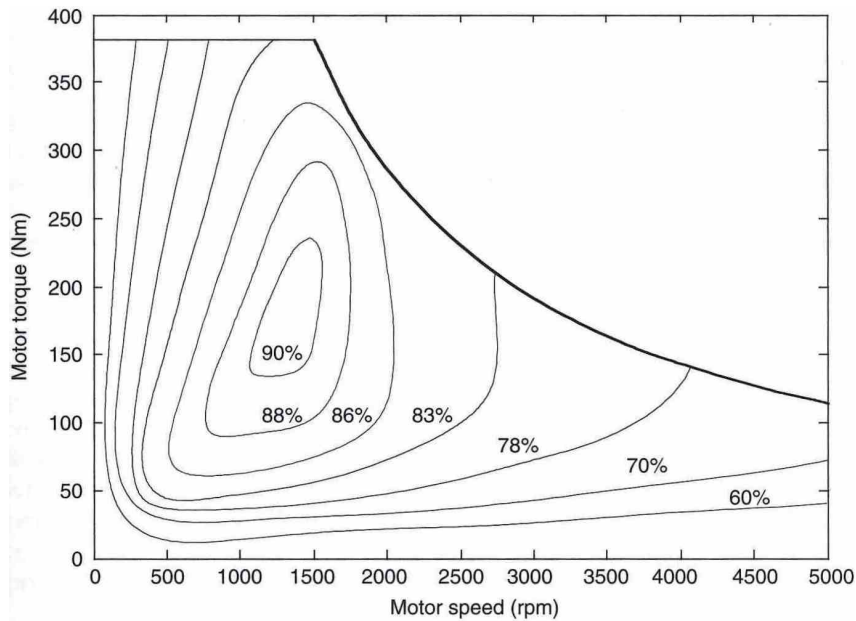


Figure 2.5: Typical efficiency map of electric motor [23]

A typical efficiency map of an electric motor is shown in Figure 2.5. The efficiency map generally does not consider the efficiency of power converter which is used to supply voltage and current to the electric motor. The maximum efficiency of the electric motor is typically around 90% i.e., approximately 2.5 times that of an ICE. The higher efficiency region of the electric motor is at lower speed. The region of 90% efficiency is between 1000 and 1500 rpm and region of 88% efficiency is between 750 to 1750 rpm, as shown in Figure 2.5. The ability to produce higher torque and efficiency at lower speed makes the electric motor suitable to combine with an ICE which suffers from low torque at lower speed.

is even more important for a HEV as a HEV consists of more components compared to a CV and an EV.

Cost of electric motor

$$= \$21.775 * (\text{Maximum power of electric motor in kW}) + \$425 \dots \dots \dots \text{Eq. 2.4}$$

The electric motors generally used in HEVs can be classified into three groups, permanent magnet brushless (PMBL) DC motor, induction motor (IM), and switched reluctance (SR) motor [24], [28]. Although the three groups of motors have different advantage and disadvantages, the research study performed in this thesis used the same type of electric motor for all investigations and therefore, the details of each type of electric motor is of little significance for this thesis.

2.1.1.3 Battery

Battery is a storage device which consists of one or more electrochemical cells that convert the stored chemical energy into electrical energy [64]. One of the important characteristics of the battery is battery capacity, which is measured in ampere-hours (Ah). It is defined as the amount of current that a battery can deliver for one hour before the battery reaches zero capacity.

The state-of-charge (SOC) of the battery which is represented in percentage terms or normalised forms is equally important as it indicates the instantaneous status of charge available in the battery. The battery SOC is represented in percentage terms or normalised form in terms of full charge. In percentage terms, 100% SOC means that the battery is fully charged and 0% SOC means that the battery is fully discharged. In normalised form, battery SOC of 1.0 means fully charged and battery SOC of 0.0 means fully discharged.

A typical characteristic of open circuit voltage of a battery w.r.t. battery SOC is shown in Figure 2.6. The battery voltage decreases with the decrease in battery SOC, as shown in Figure 2.6. Below 10% and above 90% of battery SOC, battery open circuit voltage gradients (i.e., increase of voltage w.r.t. to SOC) are high compared to battery SOC between 10 to 90%. Therefore, operating at lower battery SOC could affect the power delivery as battery voltage directly related to battery power output.

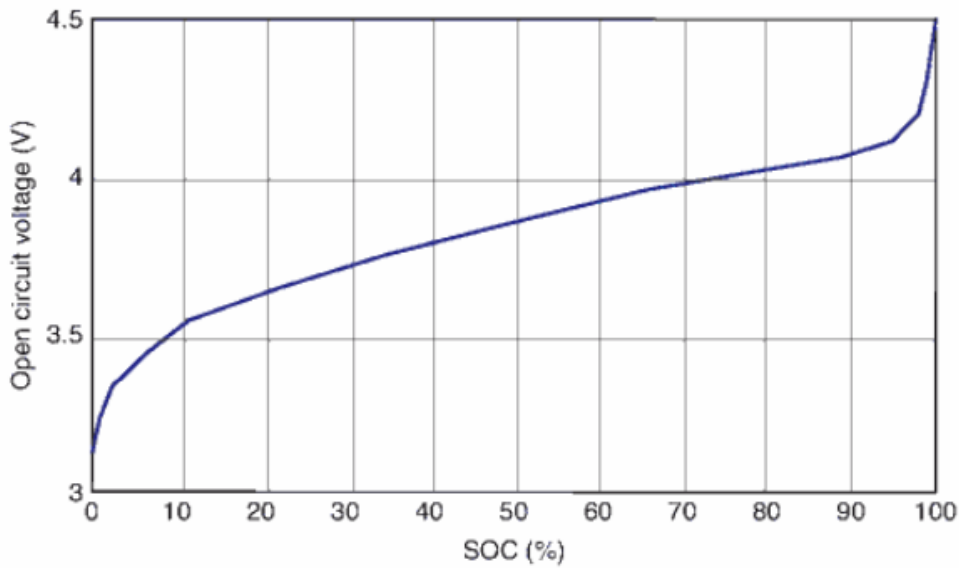


Figure 2.6: Typical characteristic of open circuit voltage w.r.t. SOC of a battery [64]

In HEV applications, battery system efficiency has a significant influence on FE and electric range [64]. To maximise FE, it is necessary to know the battery system efficiency. The efficiency of a battery system is defined as a ratio of energy out to energy in during a round charging-discharging trip subjected to charging balance during the cycle, in other words, the SOC at the end needs to be exactly the same as the SOC at the beginning. The battery system efficiency can be calculated, as shown in Equation 2.5 [64].

$$\eta_{bat}(T, SOC) = \frac{\int_{t_i}^{t_f} V_{terminal}(t) I_{dischg}(t) dt}{\int_{t_i}^{t_f} V_{terminal}(t) I_{chg}(t) dt} * 100\% \dots \dots \dots Eq. 2.5$$

Where,

η_{bat} is the battery system efficiency at the given temperature (T) and SOC

t_i is the start time and t_f is the end time

$V_{terminal}$ is cell terminal voltage

I_{chg} is the charging current and I_{dischg} is the discharging current

Depending on the chemistry and system configuration, the efficiency of a battery system is normally between 75 and 98% in the operable temperature and SOC range [64].

Energy densities of batteries per kg are around 50 times lower than conventional fossil fuels such as gasoline or diesel [18], as shown in Figure 2.7.

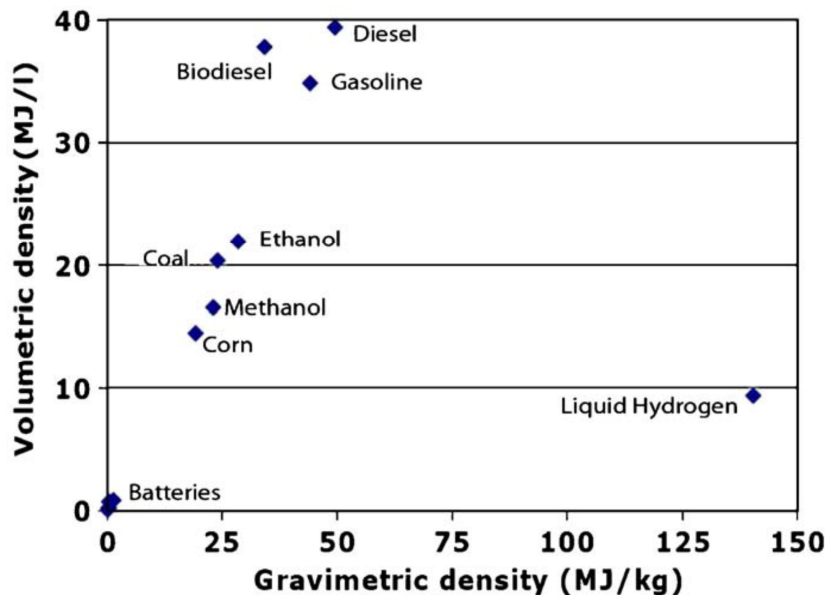


Figure 2.7: Caloric energy density of batteries and liquid fuels [18]

With existing battery technologies, to supply the same amount of energy of gasoline or diesel, weight of the battery would be around 50 times higher than gasoline or diesel powered vehicles and therefore, overall weight of the vehicle would increase accordingly. This limits the battery size which limits the total energy availability in the vehicle. The limitation in the available energy limits range of a battery powered electric vehicle.

In terms of conversion of energy, gasoline (or diesel) requires an ICE to use the energy of gasoline (or diesel), but the battery does not requires any such convertor. Therefore, the total weight of the components that is required to convert the energy of gasoline (or diesel) is equal to the weight of gasoline (or diesel) and the ICE, whereas in case of the battery it is only weight of the battery. Hence, in terms of the weight for conversion of energy, the battery and gasoline (or diesel) does not differ as much as it seems from Figure 2.7.

The cost of battery increases with the maximum capacity of the battery, as shown in Equation 2.6 found from studies by Electric Power Research Institute (EPRI), USA [52], [62], [63].

Cost of battery

$$= \$321.2 * (\text{Maximum energy of battery in kWh}) + \$680 \dots \dots \dots \text{Eq. 2.6}$$

As the weight and cost of the battery increase with the increase in the maximum energy of the battery, the selection of the maximum energy of the battery is of critical importance. It is even more important for a HEV as a HEV consists of more components compared to a CV and an EV.

Five groups of batteries are available in the market suitable for road transportation applications. These groups are lead-acid, nickel, ZEBRA (zero emissions batteries research activity), lithium, and zinc-air [20], [65]. The research study in this thesis is considered a particular type of battery and the study is independent of the type of battery chemistry, therefore, detailed discussions of each type of battery is of little significance for this thesis.

2.1.2 Vehicle supervisory control (VSC)

Typically HEVs consist of an internal combustion engine (ICE), electric motor, single or multiple energy storage systems (ESS), power electronic converters, and controllers. Regardless of the HEV architecture, critical tasks in the control of an HEV include optimal power distribution between an ICE and electric motor as well as smart and efficient co-ordination between multiple energy sources and converters. Vehicle supervisory control (VSC) helps to achieve these goals. Vehicle supervisory control (VSC) strategies for HEVs are sets of algorithms, implemented in the vehicle master controller, which optimally controls the flow of power between drivetrain components. Moreover, the VSC strategies also decide turn-off or turn-on of the powertrain components, as well as the transition of their operating points, by commanding subsystem controllers to achieve best performance and overall system efficiency [66].

The objective of the VSC strategy is to satisfy the power demand, while minimising fuel consumption and emissions, without compromising vehicle performance constraints, such as acceleration, gradeability, and regulation of ESS state of charge (SOC) [66].

2.1.2.1 Major operations of HEV

The major operations of a HEV could be classified into the operation of ICE at efficient regions, electric only, regenerative braking, ICE stop-start, and charge sustaining. Each classification is discussed next.

- **Operation of ICE at efficient regions**

The ICE of a HEV always tries to operate its most efficient region (in terms of efficiency and FC). This is in contrast to a CV where the ICE cannot operate always at its most efficient region as the ICE is the only energy source that meets the vehicle demand. Two major strategies associated with the operation of the ICE at its most efficient region are known as load levelling [67] and electric assist [66].

- **Load levelling**

In load levelling strategy [67], the ICE always operates as close as possible to some predetermined value known as optimal operating point for every instant in time during the vehicle operation. All the optimum operating points constitute an optimum operating line, as shown in Figure 2.8. Generally, the optimum operating line is the minimum FC curve which connects the minimum FC speed-torque operating points at different ICE speeds [68]. In actual practice it is difficult to operate on the optimum operating line, rather the ICE operates in the optimum operating region near the optimum operating line. The resulting power difference between the ICE and vehicle demand is used or contributed by an electric motor.

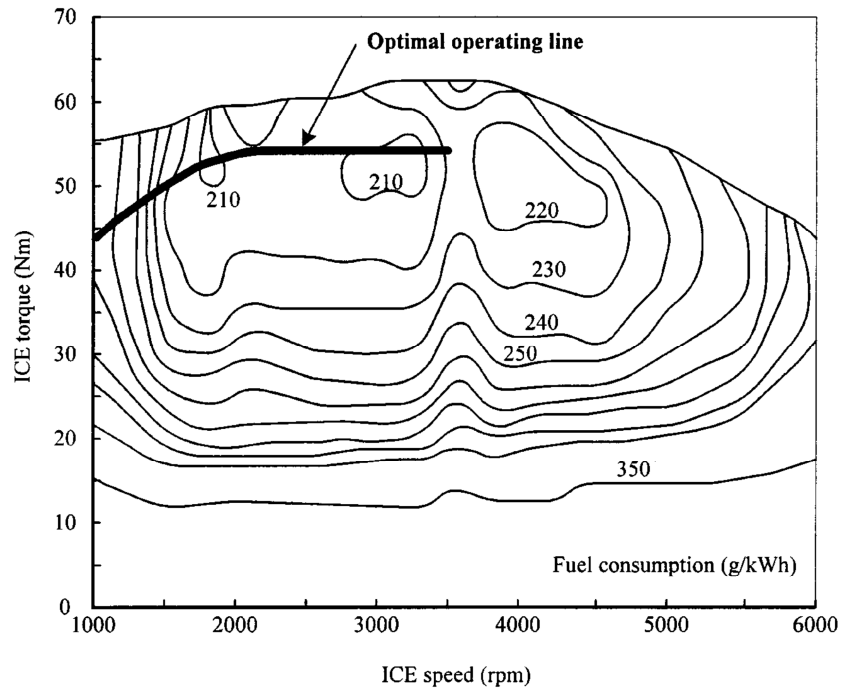


Figure 2.8: Optimum operating line of an ICE [24]

- **Electric assist**

In electric assist strategy [66], also known as power follower [69], the ICE does not operate at lower speed. At lower speed, an electric motor supplies drive torque to meet the vehicle demand. At higher speeds, the ICE always operates as close as possible to the points of its best efficiency region. The resulting power difference is used or contributed by an electric motor.

- **ICE stop-start**

In this strategy, the ICE is switched off when vehicle is at stationary [70] to reduce idling fuel consumption [71], [72].

- **Electric only**

In this operation, only electric motor provides drive torque to meet vehicle power demand at lower speed where operation of the ICE is not efficient.

- **Regenerative braking**

An important operation of HEVs is to recapture the kinetic energy during braking and convert it to electrical energy to recharge the battery, known as regenerative braking [73]. To realise it, the electric motor is controlled to operate as a generator converting vehicle's kinetic energy into electricity.

- **Charge sustaining**

In this operation, the ICE is operated to maintain battery SOC as close as possible to its initial battery SOC over the driving range [27]. This strategy is generally applied to non-plug-in HEVs where the battery needs to be recharged during operation.

The VSC strategies that are used in HEVs can be classified into rule-based and optimisation-based strategies [20], [66], [74]. Although the optimisation-based VSC strategies have the potential to perform optimally under varied conditions in the real world, high computational time and complexity in implementation limit their usage in production HEVs. The rule-based VSC strategies use predefined fixed rules for operation and therefore, the rule-based strategies might not be able to perform optimally under all conditions in the real world. However, the rule-based strategies are generally used in production HEVs as these are straightforward to implement.

The major parameters of a rule-based VSC strategy are as follows.

- SOC_H : battery SOC above which no regenerative braking
- SOC_L : battery SOC below which battery is recharged by ICE
- Target SOC: desired battery SOC during operation
- V_{EV} : vehicle speed below which vehicle operates as electric vehicle
- V_{REGEN} : vehicle speed below which no regenerative braking occurs

2.1.3 Hybrid electric vehicle architecture

As HEVs incorporate multiple powertrain and energy storage components, different vehicle architectures are evolved by integrating these components. The major architectures of HEVs based on the combinations of powertrain components are as follows [20], [24], [28-33].

- Series HEV
- Parallel HEV
- Series-parallel HEV

Based on the charging of battery, HEVs can also be classified as follows.

- Plug-in HEV
- Non-plug-in HEV

The architecture, operating principle, advantage and disadvantages of series, parallel and series-parallel HEVs are discussed next followed by plug-in and non-plug-in HEVs.

2.1.3.1 Series HEV

Series HEV can be considered as an extension of EV with the addition of an ICE to charge the battery whenever required [28]. Series HEV consists of ICE, generator, electric motor, and battery as shown in Figure 2.9. Series HEV has no mechanical connections between ICE and transmissions [28], [29].

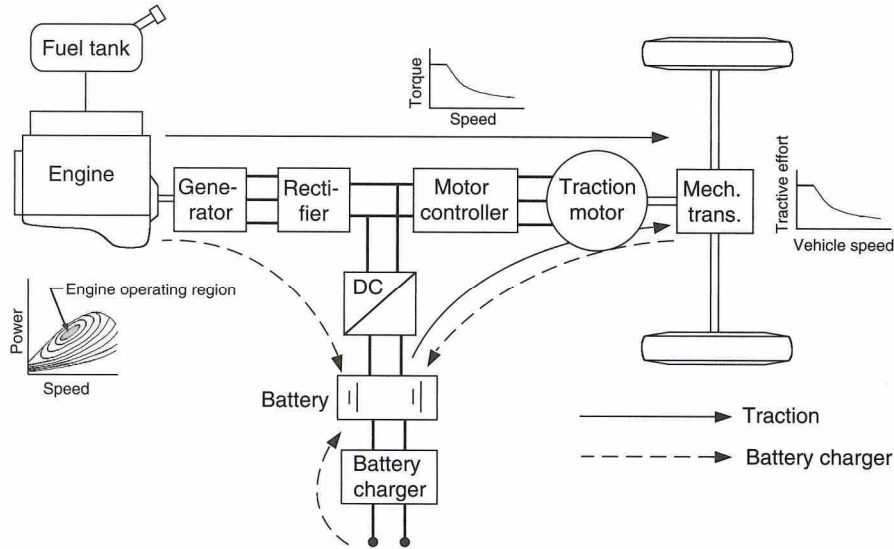


Figure 2.9: Series hybrid electric drive train [28], [75]

The ICE is generally turned off in urban driving to avoid inefficient operation of ICE in frequent start-stop low speed operation [29], [32]. During this time, the power to the electric motor is supplied from battery and battery charges through regenerative braking. The ICE is turned on only when the battery SOC is low or in highway driving [29], [32]. If power demand of the electric motor is less than the output power of the generator, the remaining power is used to charge the battery. If power demand of electric motor is higher than the output power of the generator, additional power is supplied from the battery. Therefore, the ICE is either off or operates at its

highest efficiency region and hence, the FE is improved and exhaust emissions is reduced for series HEV compared to CV [29], [32]. As the ICE is required to operate only to charge the battery, the ICE can operate in a very narrow operating region.

Single torque source (electric motor) simplifies the speed control of series HEV. Packaging is easy for series HEV as ICE, generator, motor, and battery are connected by electrical cables only [28].

Although series HEV offers several advantages, series HEV bears some disadvantages as follows [28], [29].

- High energy loss due to conversion of energy twice i.e., first from mechanical to electrical (generator) and second from electrical to mechanical (motor).
- Two electric machines (generator and motor) are required
- Big motor since it is the only torque source for the wheel

Series HEV usually used in large heavy-duty vehicles such as buses and locomotives due to large space requirement for bulky engine-generator-motor system [28], [76]. Chevrolet Volt is a commercially available series HEV [20], [32].

2.1.3.2 Parallel HEV

In a parallel HEV, both the ICE and electric motor can directly supply torque to the driven wheels through a mechanical coupling [28], [29], [32], as shown in Figure 2.10.

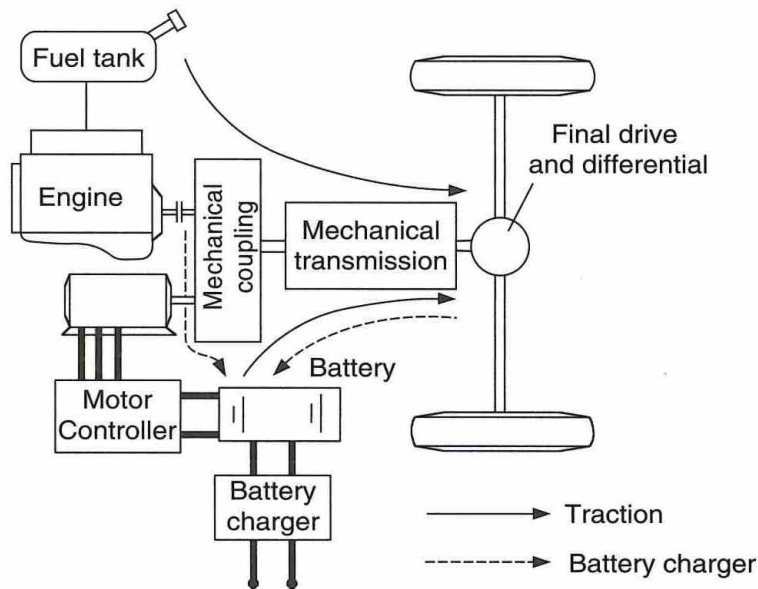


Figure 2.10: Parallel hybrid electric vehicle [28], [75]

As both the ICE and electric motor can deliver torque in parallel, one of the most common strategies for the operation of parallel HEV is known as electric assist charge sustaining (EACS) [55]. In this strategy, the ICE operates at almost maximum efficiency region. If power requested from transmission is higher than the output from the ICE, the electric motor turns on and the ICE and electric motor supply power to the transmission. If power requested from transmission is less than the output of the ICE, electric motor behaves as generator and the remaining power is used to charge the battery [32]. At low speed region, only electric motor supply power to transmission. In this configuration power conversion by regeneration

during braking and on a downslope is used to charge the battery. As ICE operates at maximum efficiency region and electric motor helps to prevent the ICE from operating in its low-efficiency region, FE is improved and emissions is reduced for parallel HEV compared to CV [29], [32].

As both the ICE and electric motor supply torques to the driven wheels and no energy conversion is occurred, energy conversion loss is less compared to series HEV [28]. Parallel HEV is compact due to no need of generator and smaller electric motor compared to series HEV [28].

The major disadvantages of parallel HEV are as follows [28], [29].

- The operating regions of ICE are wider compared to series HEV because of the direct torque supply of the ICE to the driven wheels.
- Complex structure and control.

Due to compact characteristics, parallel configuration is used for small vehicles, such as passenger cars [28]. Honda Insight, Honda Civic hybrid and Ford Escape are commercially available parallel HEV [20], [29] .

2.1.3.3 Series-parallel HEV

By adding a generator and connections between ICE and battery in a parallel HEV allow both series and parallel operation of ICE and electric motor and hence results in series-parallel HEV [28], [29], [32].

The most commonly used configuration of series-parallel architecture uses a planetary gear unit. Figure 2.11 shows a typical configuration of the series-parallel HEV drivetrain consists of a planetary gear unit [28], [75].

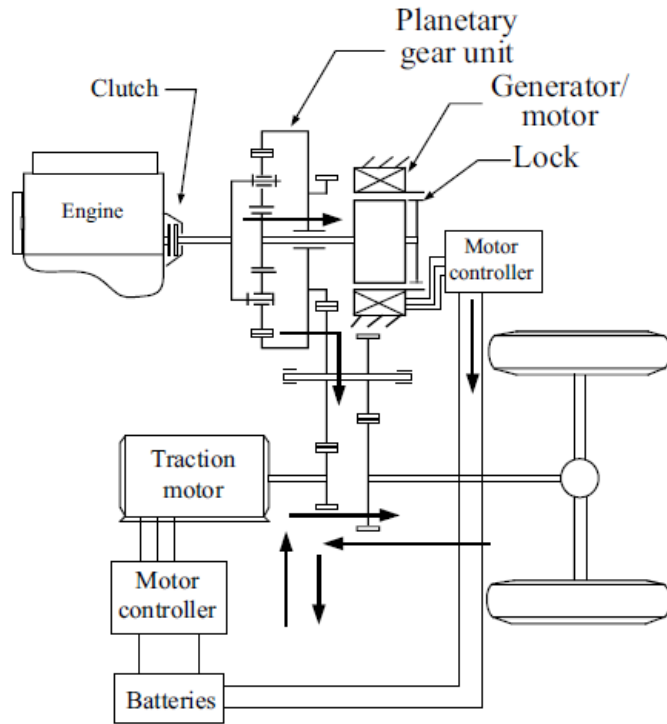


Figure 2.11: Series-parallel hybrid drivetrain using a planetary gear unit [28], [75]

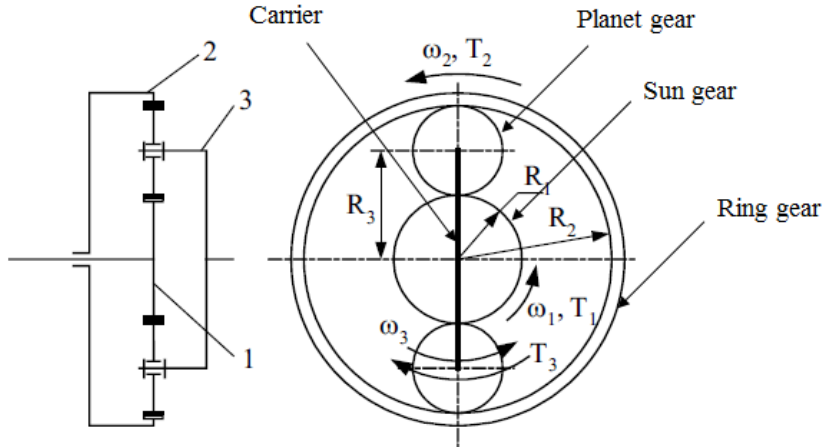


Figure 2.12: Planetary gear unit [28]

Planetary gear unit is a combination of gear set, as shown in Figure 2.12. In a planetary gear unit, some gears (planet gears) rotate around a central gear (sun gear)

and a bigger gear (ring gear) also rotates in mesh with the planet gears. All the planet gears are also connected by a movable plate (carrier).

The series-parallel configuration in Toyota Prius HEV combines an ICE, generator, and motor using a planetary gear unit. This configuration is also known as power-split. The ICE is connected with the carrier; the generator is connected with the sun gear and the motor is connected with the ring gear.

The rotational speed of the ICE, generator, and motor are interrelated, as shown in Equation 2.7. The motor rotates at a fixed ratio to the wheel speed, as shown in Equation 2.8. The torques of the ICE, generator and ring gear are shown in Equations 2.9 and 2.10.

$$\left(\frac{1}{R}\right) * \omega_G + \omega_M = \left(1 + \frac{1}{R}\right) * \omega_{ICE} \dots\dots\dots Eq. 2.7$$

$$\omega_M = 36.75 * v \dots\dots\dots Eq. 2.8$$

$$T_G = \frac{T_{ICE}}{(1 + R)} \dots\dots\dots Eq. 2.9$$

$$T_{RING} = R * T_G \dots\dots\dots Eq. 2.10$$

Where,

$$R = \frac{Ring\ gear\ teeth}{Sun\ gear\ teeth}$$

ω_{ICE} , ω_G , and ω_M are rotational speeds of the ICE, generator, and motor respectively

v is the vehicle speed in km/h.

T_{ICE} , T_G , T_{RING} are torques of the ICE, generator, and ring gear, respectively.

The above equations show that the vehicle speed determines the relationship between the ICE and generator speed. This complex relationship can be understood by Figure 2.13 [77]. When the ICE is started and the vehicle is at rest, the generator speed is increased. When the vehicle speed increases, the ICE speed can increase at the same generator speed. Under low-load driving, to reduce the ICE power, the speed is reduced by controlling the generator to rotate in the opposite direction.

Owing to the connection of the sun gear and planet gears, the speed of the ICE can be adjusted by varying the speed of the generator [29]. Therefore, the ICE speed is independent of the wheel speed.

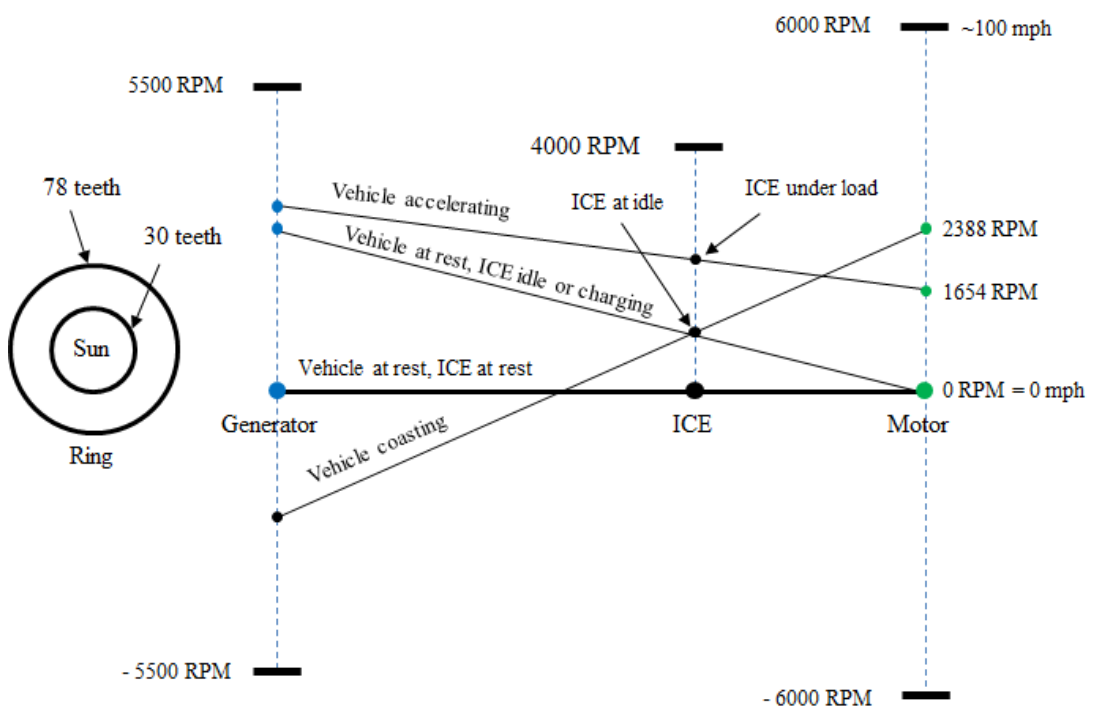


Figure 2.13: Relationship of component speeds of Toyota Prius [77]

Changes in the generator operation affects the ICE operation yielding total control over the ICE at all driving conditions. As the generator controls the operation of the ICE, the ICE potentially can operate at the most efficient region at each speed of operation. Therefore, FE is improved and emission is reduced for series-parallel HEV compared to CV. Apart from that, as in this configuration no gear change is involved, the ICE operation is less transient compared to parallel HEV, but not as steady as series HEV [29].

Toyota Prius, Toyota Auris, Lexus LS 600h, Lexus CT 200h and Nissan Tino are commercially available series-parallel HEVs [20].

2.1.3.4 Plug-in HEV

A HEV capable of recharging the battery from an external electrical source is known as plug-in HEV [32]. It usually has an on-board charger to allow charging from an electric socket. Plug-in configuration can be applied to any architecture. The main advantages are further improving FE and reducing emissions. While the main disadvantage is that, it needs the vehicle user to take care of the battery charging procedure, which one may easily forget. In addition, usually a large battery set is used in order to ensure a longer driving range in all-electric mode. This implies a higher initial cost of plug-in HEVs.

2.1.3.5 Non-plug-in HEV

A HEV where external charging is not possible and the battery is recharged by ICE and regenerative braking is known as non-plug-in HEV [32]. Non-plug-in configuration can be applied to any architecture. As the battery is recharged during normal vehicle operation, the user is not required to take care of battery charging.

Non-plug-in configuration expected to provide lower FE compared to plug-in configuration as the ICE has to operate more time to recharge the battery.

2.2 Driving patterns

A driving pattern is generally defined as speed-time profiles of a vehicle [42]. Drive cycles or driving cycles have been developed over the years to represent real-world driving conditions. Therefore, driving cycles are standardised driving patterns [42]. The standard driving patterns are used to predict vehicle performance such as fuel consumption and emissions in laboratories. The standard driving patterns could be classified into two groups, legislative and real-world. The standard legislative driving patterns are used to verify the compliance of a vehicle to legislative norms. Several standard real-world driving patterns have been developed to predict actual real-world driving conditions but those are specific to particular locations.

The standard legislative driving patterns for passenger cars [20], [78] are shown in Table 2.1. Three categories of standard legislative driving patterns are available, namely, European Union, United States, and Japan, as shown in Table 2.1. The standard legislative driving patterns for the European Union are ECE15, EUDC, and NEDC. The standard legislative driving patterns for the United States are UDDS, FTP-75, US06, and LA92. The standard legislative driving pattern for Japan is JP 10-15. The standard legislative driving patterns are generally based on two types of traffic conditions, namely, urban and highway. ECE15, UDDS, FTP-75, and LA92 are urban driving patterns. EUDC, HWFET, and US06 are highway driving patterns. NEDC and JP 10-15 are combinations of urban and highway driving patterns.

Table 2.1: Standard legislative driving patterns

Category	Driving patterns	Additional information
European union	ECE15	
	EUDC (Extra Urban Driving Cycle)	
	ECE15 + EUDC	Includes initial 40 seconds idle period at start
	NEDC (New European Driving Cycle)	Excludes initial 40 seconds idle period at start in ECE15 + EUDC
United States	UDDS (Urban Dynamometer Driving Schedule)	
	FTP-75	
	HWFET (Highway Fuel Economy Test)	
	US06	Supplement to the FTP-75 – high speeds and acceleration
	LA92 (California Dynamometer Driving Schedule)	
Japanese	JP 10-15 Mode	

Several standard real-world driving patterns have also been developed for passenger cars such as ARTEMIS, OSCAR, and MODEM to name a few [78]. ARTEMIS and OSCAR driving patterns were developed within the European 5th Framework project ARTEMIS-cars and OSCAR-cars respectively. MODEM driving patterns were developed within MODEM project, based on data from 60 cars in normal use in 6 towns in the UK, France, and Germany.

2.3 Optimisation problems and methods

An optimisation problem is the problem of finding the best solution from all feasible solutions [79]. If it is assumed that $f(x)$ is a function and the value of $f(x)$ is the minimum for x_m , as shown in Figure 2.14, then finding x_m from all possible values of x is known as optimisation problem.

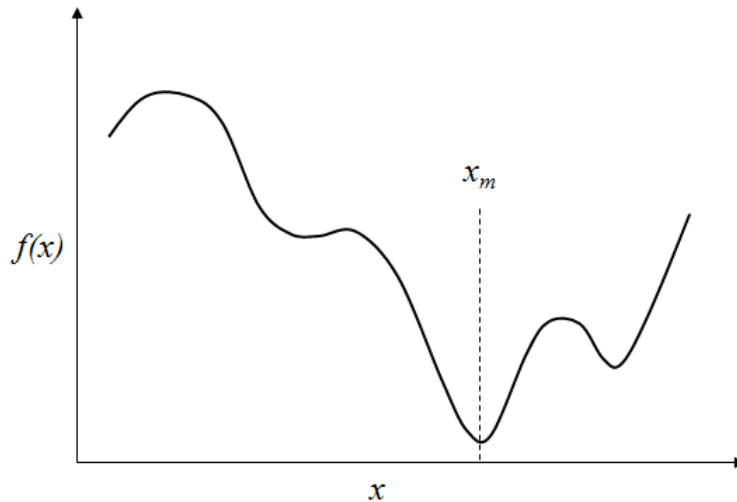


Figure 2.14: Optimisation problem

Each optimisation problem consists of the following basic ingredients [79]:

- An **objective function** which represents the quantity to be optimised, that is, the quantity to be minimised or maximised. Let f denote the objective function. Then the maximum of f is the minimum of $-f$. Some problems, specifically constraint satisfaction problems, do not define an explicit objective function. Instead, the objective is to find a solution which satisfies all of a set of constraints.
- A set of **unknowns** or **variables** which affects the value of the objective function. If x represents the unknowns, also referred to as the independent variables, then $f(x)$ quantifies the quality of the candidate solution x .

- A set of *constraints* that restricts the values that can be assigned to the unknowns. Most problems define at least a set of boundary constraints, which defines the domain of values for each variable. Constraints can, however, be more complex, excluding certain candidate solutions from being considered as solutions.

Optimisation methods are search methods, where the aim is to find a solution to an optimisation problem, such that a given quantity is optimised, possibly subject to a set of constraints. This type of optimisation problem where constraints need to be satisfied during optimisation is known as constraint optimisation problem. The aim of an optimisation method is to assign values, from the allowed domain, to the unknowns such that the objective function is optimised and all constraints are satisfied.

The optimisation methods can be classified in many ways, depending on the focus and can be classified as derivative-based and derivative-free optimisation methods [80].

2.3.1 Derivative-based optimisation method

Derivative-based or gradient-based optimisation methods use the information of derivatives [80]. The derivative-based methods are applicable if the first and second derivatives of an objective function exist. They have the disadvantage of being trapped in a local optimum if the problem is multi-modal (involving large number of local optima) in nature, as shown in Figure 2.15. It can be seen in Figure 2.15 that function $f(x)$ has two local optimums (at x_{L1} and x_{L2}) and a global optimum (at x_G). As the derivative-based methods require first and second derivative of an objective function, it is difficult to apply the derivative-based methods to complex problems

where finding the first and second derivatives of an objective function are challenging. Sequential quadratic programming (SQP) is a derivative-based optimisation method.

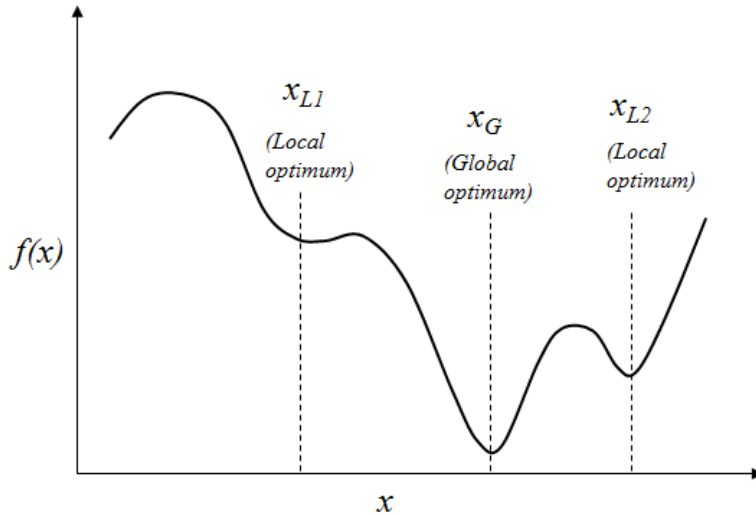


Figure 2.15: Global and local optimum

2.3.2 Derivative-free optimisation method

The derivative-based optimisation methods are efficient but may pose certain strict requirements on the objective functions. Like other engineering designs, due to the highly non-linear and non-smooth characteristics of the drivetrain system, the component size optimisation problem of HEV is typically multi-modal [47]. It is also difficult to find an objective function for a HEV due to its highly complex drivetrain systems with hundreds of design parameters. In such problems with multi-modal functions and difficulty in formulating objective functions, derivative-free optimisation methods are more suitable than the derivative-based optimisation methods [80]. The derivative-free methods use the values of the objective, not any derivatives. The derivative-free methods are good at finding global optimum, as shown Figure 2.15, and can be applied without domain specific knowledge. The

derivative-free methods are often the best algorithms for global optimum because they often sample a large portion of the design space to be successful.

Evolutionary algorithms are one group of derivative-free optimisation methods [80]. The evolutionary algorithms are nature-inspired and non-deterministic [81]. Although the evolutionary algorithms have the potential to find global optimum, it is not always guaranteed that the algorithms would find global optimum; the algorithms usually find near-optimal solutions. Genetic algorithms (GAs) and particle swarm optimisations (PSOs) are widely used evolutionary algorithms in the field of HEVs, and these are discussed next.

2.3.2.1 Genetic algorithm (GA)

Among several genetic algorithms, this section introduces a simple version known as canonical genetic algorithm [82-84]. The GA is a stochastic global search and optimisation method that mimics natural biological evolution. The standard procedure of the GA is outlined in Figure 2.16.

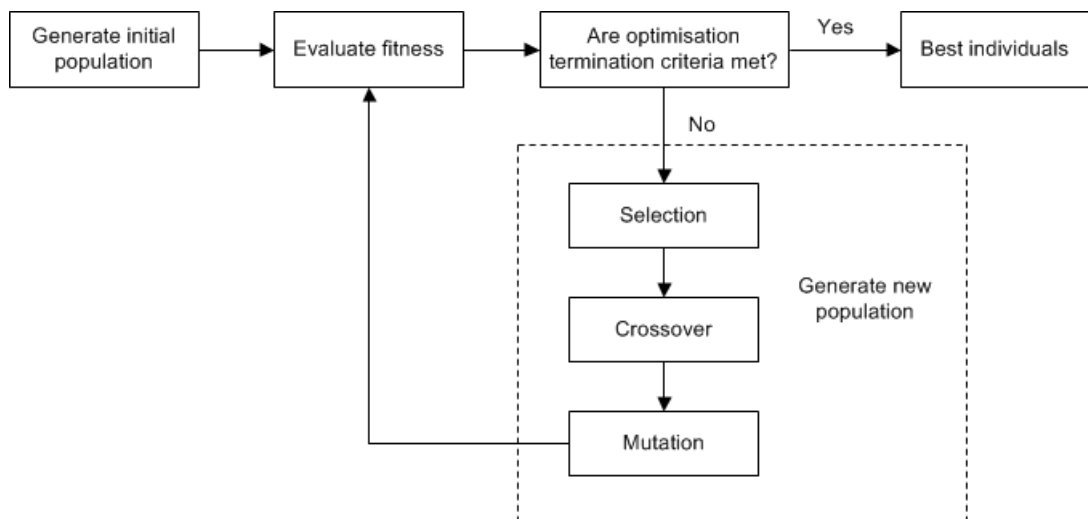


Figure 2.16: Standard procedure of GA [84]

The process starts with the generation of an initial population. After the generation of an initial population, the fitness of each chromosome is evaluated i.e., the value of the objective function for each chromosome is evaluated. After the evaluation of fitness, optimisation termination criteria need to be checked. If the optimisation termination criteria are not satisfied, a new population is generated. The new population is generated through three operations, namely, selection, crossover, and mutation. The new population is again evaluated for fitness and checked for the optimisation termination criteria. The process is continued until the optimisation termination criteria are met. Once the optimisation termination criteria are satisfied it gets the best individual i.e., the optimum solution. Therefore, the GA consists of four major operations, namely, initialisation, selection, crossover, and mutation operation, which are discussed next.

2.3.2.1.1 Initialisation

The initialisation is the process to generate random initial population. A population is the sets of individuals which are probable solutions. Each individual is an encoded structure known as chromosome that contains optimisation variables known as genes. Each gene is a string of binary numbers i.e., 0 and 1. The number of bits that must be used to describe a gene is problem dependent.

If 3 bits are used to describe a gene (optimisation variable) and the problem contains 3 optimisation variables, then total length of a chromosome (individual) is 3 times 3 bits i.e., 9 bits.

Gene 1 (Variable 1): 0 1 0

Gene 2 (Variable 2): 1 1 0

Gene 3 (Variable 3): 0 0 1

first generated. The first child chromosome is formed by appending the last $l - c$ elements of the first parent chromosome to the first c elements of the second parent chromosome. The second child chromosome is formed by appending the last $l - c$ elements of the second parent chromosome to the first c elements of the first parent chromosome.

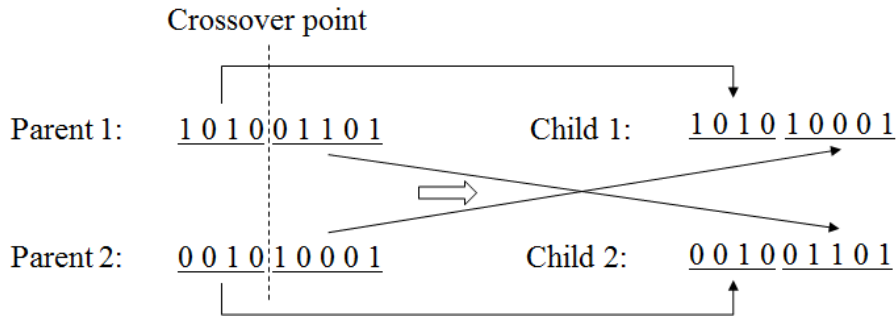


Figure 2.17: Single-point crossover

The crossover probability (P_c) is the probability that decides whether crossover will occur at a particular mating. A usual way for crossover is to generate a random number R_c (between 0 and 1) for each mating and if $R_c \leq P_c$ then allow crossover for that mating.

2.3.2.1.4 Mutation

The mutation is a probabilistic random deformation of the genetic information for an individual. It operates independently on each individual by probabilistically changing each bit of a string. The probability which decides mutation is known as mutation probability (P_m). A usual way to mutate is to generate a random number R_m between 0 and 1 for each bit and if $R_m \leq P_m$ then make a change in the bit of the string, as shown in Figure 2.18.



Figure 2.18: Mutation

2.3.2.2 Particle swarm optimisation (PSO)

Particle swarm optimisation (PSO) is also a population based method for global optimisation [85]. It is inspired by the behaviour of bird flocking. Every individual in the population is called particle. During each generation, each particle's movement depends on its previous best position and the global best position. At each generation, a new velocity value for each particle is calculated based on its current velocity and the distance from the global best position. The next position of the particle is calculated using the new velocity value. This process is then continued until the optimisation termination criterion is achieved. The calculation of the velocity and position are shown in Equations 2.12 and 2.13, respectively.

$$v_i^{k+1} = \omega v_i^k + c_1 r_1 (pbest_i - x_i^k) + c_2 r_2 (gbest - x_i^k) \dots\dots\dots Eq. 2.12$$

$$x_i^{k+1} = x_i^k + v_i^{k+1} \dots\dots\dots Eq. 2.13$$

Where,

v_i^k = current velocity of particle i

v_i^{k+1} = modified velocity of particle i

r_1, r_2 = random numbers [0,1]

ω = inertia

c_1, c_2 = social parameters

x_i^k = current position of particle i

x_i^{k+1} = modified position of particle i

$pbest_i$ = local best of particle i

gbest = global best of the population

2.3.3 Optimisation termination criterion

The derivative-free optimisation methods are iterative. A stopping criterion is necessary to terminate the search process. The search can be terminated when a specified number of iteration, known as generation has been exceeded. Alternatively, conditions can be used to measure progress at each iteration, and if progress is not satisfactory, the search is terminated [79].

2.4 Summary

- Powertrain components and vehicle supervisory control are major systems of a HEV.
- The ICE, electric motor, and battery are major powertrain components of a HEV.
- An ICE cannot produce torque from zero speed, it produces torque after idling speed, and it is most efficient in a narrow region in medium speed range.
- The maximum efficiency of an ICE is around 34%.
- An electric motor can produce maximum torque from zero speed and is more efficient in lower speed region
- The maximum efficiency of an electric motor is around 90%.
- The battery has nearly 50 times lower energy density compared to gasoline and diesel.
- Three major architectures of HEVs are series, parallel, and series-parallel.

- All the HEV architectures have the potential for higher FE and lower emissions due to the operation of ICE and electric motor at their efficient regions.
- The vehicle supervisory control strategy decides the operation of the ICE, electric motor, and battery.
- Driving patterns are speed-time profiles of vehicles.
- The derivative-free evolutionary optimisation algorithms such as GA and PSO are good at finding global optima.

CHAPTER 3

REVIEW: FUEL ECONOMY IN HYBRID ELECTRIC VEHICLES

Hybrid electric vehicles (HEVs), irrespective of the architectures are promising technologies for the improvement of fuel economy (FE), as discussed in chapter 2. Chapter 2 has highlighted that HEVs generally have higher FE compared to conventional vehicles (CVs) due to the operation of the internal combustion engine (ICE) and electric motor at their respective efficient regions. This chapter reviews the FE in HEVs and is subdivided into three sections. The first section focuses on the details of the approaches followed for the improvement in FE. The second section discusses the variation in FE of HEVs in real-world. The third section describes the research question for this thesis.

3.1 Fuel economy (FE) improvement in HEVs

HEVs are a complex combination of various components involving a large number of design parameters which must be selected optimally to get optimum performance [86]. The major systems responsible for the improvement of FE in a HEV are powertrain components and vehicle supervisory control (VSC), as discussed in the previous chapter. Therefore, optimum selections of the parameters of the VSC strategy and powertrain components are important for better FE. Development and testing of each design combination to find an optimum combination of powertrain components and parameters of VSC strategy is time consuming and expensive [47]. The use of an optimisation method along with a computer simulation model is a

preferred time saving and cost effective method to find an optimum combination of components and parameters of a VSC strategy for HEVs [47], [53], [54]. This will be called simulation-based optimisation in subsequent discussions.

The simulation-based optimisation of parameters of a VSC strategy for a given set of powertrain components of HEVs could improve FE [87-89]. The optimisation of parameters of a rule-based VSC strategy for a given set of powertrain components was used to improve FE by 9.4% over NEDC, 25.7% over US06, and 12.4% over Manhattan driving patterns for a series HEV when compared with the base data [87]. Even for a parallel HEV, the optimisation of parameters of a rule-based VSC strategy could improve FE by 50% over UDDS and 21% over HWFET driving patterns [88]. But the optimisation of six parameters of a rule-based VSC strategy for a given set of powertrain components using a genetic algorithm (GA) made no improvement in FE over NEDC and reduced FE by 1.4% over an urban driving pattern for a parallel HEV when compared to the base data of a vehicle simulation software, ADVISOR [89]. This indicated that considering parameters of a VSC strategy only for optimisation might not always improve FE, and powertrain components might need to be considered also for the optimisation.

Although optimum selection of parameters of a VSC strategy could improve FE, their potential could not be fully utilised unless the powertrain components are also optimised. In other words, powertrain components need to be optimum for the full utilisation of an optimised VSC strategy. Among both the factors, powertrain components not only directly influence the FE but also contribute to the weight and configuration of a vehicle. The importance of optimum selection of powertrain components is even higher for a HEV as a HEV consists of more powertrain

components compared to CVs and EVs [16]. Among several components, powertrain components such as ICE, electric machine, and energy storage device such as battery are major contributors to the FE performance of HEVs, as discussed in chapter 2. The details of the powertrain components are discussed in section 3.1.1.1. The improvement of FE in HEVs through the simulation-based optimisation of powertrain components can be classified into two approaches as follows.

- 1) The optimisation of powertrain components keeping all parameters of a VSC strategy along with other parameters of the vehicle fixed [49-52].
- 2) The optimisation of powertrain components along with the parameters of a VSC strategy [53-60].

As the parameters of the VSC strategy are prefixed in the 1st approach, the parameters of the VSC strategy might not be optimum for the condition under consideration. Therefore, these studies might not be able to utilise the benefits of the VSC strategy completely. But optimum parameters of the VSC strategy could be found for an already optimised set of powertrain components by further study.

As the 2nd approach considers both the powertrain and parameters of VSC strategy, this approach has the potential to obtain better optimum value compared to the 1st approach. In the 2nd approach, though the parameters of a VSC strategy are considered for the optimisation, the logic of the VSC strategy is kept same. Although the 2nd approach has the potential for better optimum value, the approach is unable to distinguish between the benefits of powertrain components and VSC strategy. The quantification of benefits is useful for future study to develop powertrain components and VSC strategy. The quantification would help to understand the effect of any modification in powertrain components or VSC strategy individually.

The details of the simulation-based optimisation of powertrain components for the improvement of FE are reviewed next.

3.1.1 Simulation-based optimisation of powertrain component sizes

The simulation-based optimisation of powertrain components has been applied for optimum FE over the years for all major architectures of HEVs, namely, series [50], [56], parallel [49], [52-55], [57-60], and series-parallel [51] HEVs. It was applied to non-plug-in as well as plug-in [51] architectures. The investigation over all major architectures shows the importance of the optimisation of powertrain component sizes for the improvement of FE in HEVs. The optimisation of powertrain component sizes could improve FE by up to 15.0, 30.9, and 30.0% for series [56], parallel [54], and series-parallel [51] HEVs, respectively.

To understand the process of the optimisation of powertrain component sizes, the details of powertrain components, VSC strategies, design constraints, optimisation method, and driving patterns are important and discussed in turn. Section 3.1.1.8 summarises the approaches followed in the literature.

3.1.1.1 Powertrain components

The ICE, electric motor, and battery were the major powertrain components considered for the optimisation to improve FE [49-60], as shown in Table 3.1.

Table 3.1: Powertrain components and optimisation variables considered for powertrain components

Reference	Powertrain components				Optimisation variables of powertrain components				
	ICE	M	G	B	ICE	Motor (M)	Generator (G)	Battery (B)	
					Max. power	Max. power	Max. power	Module	Max. Capacity
[49]	✓	✓		✓	✓	✓		✓	
[50]	✓	✓	✓	✓	✓	✓	✓	✓	✓
[51]	✓	✓		✓	✓	✓		✓	
[52]	✓	✓		✓	✓	✓		✓	✓
[53]	✓	✓		✓	✓	✓		✓	
[54]	✓	✓		✓	✓	✓			✓
[55]	✓	✓		✓	✓	✓		✓	
[56]	✓	✓		✓	✓	✓			✓
[57]	✓	✓		✓	✓	✓		✓	
[58]	✓	✓		✓	✓	✓		✓	
[59]	✓	✓		✓	✓	✓		✓	
[60]	✓	✓		✓	✓	✓		✓	

For the ICE and electric motor, the maximum power was considered as the optimisation variable for all the reviewed literature [49-60], as shown in Table 3.1. For the battery, total number of modules [49-53], [55], [57-60] and the maximum capacity [50], [52], [54], [56] were considered as the optimisation variables. The maximum power alone is not sufficient to design the ICE or electric motor. Similarly, the battery also requires more parameters to design. Even though one or two parameters are not sufficient to design the ICE, electric motor, and battery

completely, it could be used to validate a concept through comparative study [53], [57], [60]. In a study [60], four optimisation algorithms were compared over a parallel HEV and all the optimisation variables were kept same for all the optimisation algorithms. Therefore, consideration of one parameter for each of the three components, ICE, motor, and battery were sufficient to compare the four algorithms [60]. Similarly, another study compared two optimisation algorithms over a parallel HEV [57].

During the optimisation, optimisation methods generated powertrain components of different sizes. Therefore, to evaluate the performance of those components over different driving patterns, the performance characteristics of those components were required. This was done through linear interpolation of the performance of the base components [50], [52], [55]. The base components generally were the components of the simulation model of the HEV on which the investigation was carried out [55]. But the powertrain component sizes and their performance are not always linear. For example, the relationship between the power and fuel consumption (FC) of the ICE are not linear [61]. Although the power and FC of the ICE are not linear and there is possibility of variation of FC value with experimental result, the variation in the FC value is of little significance for any comparative study.

3.1.1.2 Design limits

To find optimum powertrain component sizes, an optimisation method searches within the upper and lower limits decided by the designer. Therefore, the limits affect the optimum component sizes. The upper and lower limits of each powertrain component were often found different in the reviewed literature, as shown in Table 3.2.

Table 3.2: Design limits considered in literature

Reference	ICE			Motor			Battery			
	Base size, kW	Lower limit w.r.t. base, %	Upper limit w.r.t. base, %	Base size, kW	Lower limit w.r.t. base, %	Upper limit w.r.t. base, %	Base size		Lower limit w.r.t. base, %	Upper limit w.r.t. base, %
							Unit	Ah		
[49]	41	-44	0	75	-80	-20	11		-18	82
[50]	38	-40	200	125	0	200	28		-29	29
[51]	57	-30	49	50	-40	50				
[53]	86	-53	16	65.9	-85	21	240		-38	46
[54]	208	-44	0	150	-34	200		90	-80	300
[55]	41	-30	30	75	-90	30				
[56]	41	-39	29	75	-49	49		26	-50	50
[57]	41	-30	30	75	-90	-50				
[58]	41			75			25			
[60]	84	-52	19	33	-70	142	240		-38	46

For the ICE, the lower limit found up to -53% [53] and the upper limit up to 200% [50], as shown in Table 3.2. For the motor, the lower limit found up to -90% [55] and the upper limit up to 200% [50], [54], as shown in Table 3.2. For the battery, the lower limit found up to -80% [54] and the upper limit up to 300% [54], as shown in Table 3.2. Although the ICE and motor sizes of four studies [49], [55-57] were the same, the lower and upper limits were not the same, as shown in Table 3.2. Some studies [49], [50], [54] kept the upper or lower limits equal to the base size. This indicates the intention of the designer. For example, for both the studies [49], [54] the upper limits of the ICE were equal to the base size. Therefore, the designer wanted the optimum ICE size to be smaller than the base size. Even though a smaller ICE size is expected to be helpful in improving FE, the restriction in the upper limits might not be helpful to find the optimum design. Therefore, Table 3.2 indicates that

there was no consistency for the consideration of design limits in the literature. The reasons for choosing the upper and lower limits were not explained in majority of the literature shown in Table 3.2. One study did not mention the design limits [58]. Two studies [55], [57] mentioned the reason as the performance requirement, but what the performance requirement was, and how the performance requirement leads to the upper and lower limits were not explained. The possible reason for not explaining the designs limits might be the comparative nature of all studies. Although the upper and lower limit might affect the optimum design, it is of little significance for a comparative study where the upper and lower limits are same for all studies.

3.1.1.3 Vehicle supervisory control (VSC) strategy

The rule-based vehicle supervisory control strategies were generally used as the energy management technique for the optimisation of powertrain component sizes [52-60]. The electric assist charge sustaining (EACS) was the preferred rule-based VSC strategy for energy management of HEVs [52], [54], [55], [57-59], but use of a rule-based thermostat control strategy was also found [56]. Some studies did not discuss the details of VSC strategies [49-51].

Although rule-based VSC strategies are not always able to operate optimally in unpredictable real-world conditions, the possible reason for the wider use of the rule-based VSC strategies might be due to easy implementation in practical applications.

3.1.1.4 Constraints

The optimisation of powertrain component sizes were generally formulated as a constraint optimisation problem [49-60]. The constraints were considered to avoid deterioration of the performance of an optimum design when compared to the benchmark vehicle.

Acceleration, maximum acceleration, maximum speed, gradeability (ability to move on a slope), delta SOC (difference between initial and final battery SOC), all electric range (AER) and distance travelled in a particular time were considered in the reviewed literature [49-60] as constraints, as shown in Table 3.3.

Table 3.3: Constraints considered in literature

Reference	Constraints						
	Acceleration	Maximum acceleration	Maximum speed	Gradeability	Delta SOC	Distance in 5s	All electric range
[49]	✓		✓	✓			
[50]	✓		✓	✓	✓		
[51]	✓		✓	✓			
[52]	✓		✓	✓			✓
[53]	✓	✓					
[54]	✓		✓	✓			
[55]	✓	✓	✓	✓		✓	
[56]	✓			✓			
[57]	✓	✓	✓	✓		✓	
[58]	✓			✓	✓		
[59]	✓		✓	✓			
[60]	✓	✓					

Among all the constraints, the acceleration, maximum speed, and gradeability were used by most of the reviewed literature. For acceleration, stand-still (acceleration

from zero to a certain speed e.g., 0~60 mph) as well as pass-by acceleration (acceleration from certain non-zero speed to another speed e.g., 40~60 mph) were considered. Delta SOC was considered to ensure that the optimum design should operate as charge sustaining [50], [58]. AER is an important parameter for EV or plug-in HEV, which indicates the distance travelled before recharging the battery. For a HEV also AER has significance but not as critical as for an EV as a HEV has an ICE which is capable to charge the battery while driving. Although the consideration of AER could influence the size of the battery, only one study considered AER as a constraint [52].

The values of constraints for the acceleration, maximum speed, and gradeability were decided based on the US Consortium for Automotive Research for the PNGV (Partnership for a New Generation of Vehicles) requirements [55], [58], [90], [91] as well as based on the performance of a benchmark vehicle [51]. The consideration of PNGV requirements as constraints ensures that the performance of an optimum design would be at least equal to the PNGV requirements. However the benchmark vehicle performance might be higher than the PNGV requirements. Therefore, constraint values based on the PNGV requirements could be used if the main objective is not to compare with the benchmark vehicle. But if an optimum design needs to be compared with a benchmark vehicle then it is logical to consider performance values of the benchmark vehicle as values of constraints instead of the PNGV requirements. For both the studies [50], [58], delta SOC was considered less than 0.5%.

3.1.1.5 Driving patterns and optimum design

The standard legislative driving patterns were the preferred driving patterns for the optimisation of powertrain component sizes to get optimum FE. Generally seven standard driving patterns, namely, UDDS, HWFET, US06, FTP, NEDC, ECE-EUDC, and LA92 were considered in the reviewed literature [49-60], as shown in Table 3.4. The usage of these standard driving patterns in the reviewed literature indicates their importance in the design of powertrain components of HEVs. The probable reason for choosing the standard driving patterns is due to wider acceptability of those driving patterns and therefore easy to understand the improvements of designs based on those standard driving patterns. Real-world driving patterns specific to a location such as TEH-Car based on Tehran city [55] was also considered for the selection of optimum combination of powertrain components.

Table 3.4: Driving patterns considered in literature

Reference	Driving patterns							
	UDDS	HWFET	US06	FTP	ECE-EUDC	NEDC	LA92	Real-world
[49]	✓	✓	✓	✓				
[51]	✓							
[52]	✓	✓	✓				✓	
[54]	✓							
[55]				✓	✓			TEH-Car
[57]				✓	✓			
[58]	✓							
[59]	✓			✓		✓		
[50]	Combination of Urban and Highway (names were not mentioned)							
[53]	Combination of FTP and HWFET							
[56]	Combination of UDDS and HWFET							
[60]	Combination of FTP and HWFET							

Although standard legislative driving patterns were commonly used by researchers, the standard legislative driving patterns are not sufficient to predict the entire variations in the real-world driving patterns. The standard legislative driving patterns are useful for comparative studies of vehicles. However to predict actual performance on road, it is more logical to evaluate the optimum designs over real-world driving patterns.

It could be seen from Table 3.4 that some literature [51], [54], [58] limited their study to one driving pattern only, whereas, some others [49], [52], [55], [57], [59] considered more than one driving pattern. The majority of studies, [49], [51], [52], [54], [55], [57-59] considered one driving pattern at a time to find an optimum combination of powertrain components over that driving pattern only. The studies which considered one driving pattern obviously found only a single optimum design. The reason behind the selection of any particular driving pattern was not explained in those literatures. It might be due to the objective of those literatures where the main objective was to compare a particular optimisation method as compared to another optimisation method in terms of optimum FE and/or emissions and therefore, the selection of driving pattern was of little significance. However the studies [49], [52], [55], [57], [59] which investigated more than one driving pattern, also considered only one driving pattern at a time for the optimisation of powertrain component sizes; found different sets of optimum powertrain components, one for each driving pattern. In other words, powertrain components were optimum only over a given driving pattern. It was found that a set of optimum powertrain components over a driving pattern was not optimum over other driving patterns [52], [55], [57], as shown in Table 3.5.

Table 3.5: Optimum component sizes over different driving patterns

Reference	Components	Optimum sizes over driving patterns	Variation in sizes, %
[52]	ICE power, kW	UDDS: 46, HWFET: 44, LA92: 50, US06: 54	18.5
	Motor power, kW	UDDS: 48, HWFET: 51, LA92: 52, US06: 82	41.5
	Battery power, kWh	UDDS: 4.8, HWFET: 4.6, LA92: 5.2, US06: 6	23.3
[55]	ICE power, kW	FTP: 42.6, ECE-EUDC: 36.9, TEH-Car: 41.4	13.4
	Motor power, kW	FTP: 12.8, ECE-EUDC: 15.8, TEH-Car: 13.5	19.0
	Battery module	FTP: 13, ECE-EUDC: 17, TEH-Car: 14	23.5
[57]	ICE power, kW	FTP: 40.7, ECE-EUDC: 36.9	9.3
	Motor power, kW	FTP: 12.2, ECE-EUDC: 14.9	18.1
	Battery module	FTP: 13, ECE-EUDC: 15	13.3

Where,

$$\text{Variation in sizes, \%} = \frac{(\text{Maximum}_{parameter} - \text{Minimum}_{parameter})}{\text{Maximum}_{parameter}} * 100$$

The first study [52] found 18.5, 41.5, and 23.3% variation in the maximum power of the ICE, motor, and battery, respectively among the UDDS, HWFET, LA92, and US06 driving patterns, as shown in Table 3.5. The second study [55] found 13.4, 19.0, and 23.5% variation in the maximum power of the ICE, the maximum power the motor, and number of the battery modules, respectively among the FTP, ECE-EUDC and TEH-Car driving patterns, as shown in Table 3.5. The third study [57] found 9.3, 18.1, and 13.3% variation in the maximum power of the ICE, the maximum power of the motor, and number of the battery modules, respectively between the FTP and ECE-EUDC driving patterns, as shown in Table 3.5.

Although FE is generally evaluated over a single driving pattern during the optimisation of powertrain components, four studies were found that used a

combination of two driving patterns for the evaluation of FE [50], [53], [56], [60], as shown in Table 3.4. Two studies [53], [60] considered a combination of urban driving pattern (FTP-75) and highway driving pattern (HWFET) for the evaluation of FE. Similarly, another study considered a combination of urban driving pattern, UDDS and highway driving pattern, HWFET [56]. Another study also considered a combination of urban and highway driving patterns [50], though the names of those driving patterns were not discussed. Although those studies [50], [53], [56], [60] considered a combination of two driving patterns for the evaluation of FE, the usage of the combined driving patterns for the optimisation was not explained. It is logically better to consider urban and highway driving patterns together to represent the actual driving patterns of the real-world, but it is also required to consider different driving styles of urban and highway to represent real-world driving conditions more realistically. When there is a combination of driving patterns, different sequence of driving patterns are possible and each sequence might affect the optimum component sizes. Even though a combination of urban and highway driving patterns were considered for study, the effect of sequence of driving patterns on optimum component sizes was not studied.

As different optimum designs of powertrain components are available for different driving patterns, the natural question would be which design to choose from the available designs for real-world application. Therefore, a designer's decision is required to select a design from available designs.

3.1.1.6 Optimisation method

Derivative-free optimisation algorithms such as genetic algorithms (GAs) [49], [50], [53-58], [60] particle swarm optimisation (PSO) [51], [59], [60], simulated annealing

(SA) [53], [60], DIRECT [53], [60], multi-objective self-adaptive differential evolution (MOSADE) [57], and parallel chaos optimisation algorithm (PCOA) [52] have been used in the reviewed literature for the optimisation of powertrain component sizes of HEVs, as shown in Table 3.6.

Table 3.6: Optimisation methods used in literature

Reference	Optimisation method					
	GA	PSO	SA	DIRECT	MOSADE	PCOA
[49]	✓					
[50]	✓					
[53]	✓		✓	✓		
[54]	✓					
[55]	✓					
[56]	✓					
[57]	✓				✓	
[58]	✓					
[60]	✓	✓	✓	✓		
[51]		✓				
[59]		✓				
[52]						✓

Among several derivative-free optimisation algorithms, GAs [49], [50], [53-58], [60] and PSO [51], [59], [60] were mostly used for the selection of an optimum combinations of powertrain components of HEVs.

A simple GA was found to reduce CO (carbon monoxide) emission by the optimisation of powertrain component sizes of a parallel HEV by 17% compared to a derivative-based optimisation method used in a vehicle simulation software, ADVISOR [49]. A multi-objective GA was able to reduce the fuel consumption (FC)

value of a series HEV by 15% compared to the sequential quadratic programming (SQP) which is a derivative-based optimisation method used in ADVISOR [56]. For another study on a parallel HEV, a GA was able to find an optimum design that reduced FC compared to that of the SQP used in ADVISOR [55]. Therefore, it could be concluded that GA performed better in finding optimum combinations of powertrain components compared to derivative-based optimisation methods irrespective of architectures and objectives.

The application of PSO was found in series-parallel HEV as well as parallel HEV. The PSO improved FE of a series-parallel HEV by 30% over UDDS compared to the FE value generated by a vehicle simulation software, PSAT [51] and improved FE of a parallel HEV compared to FE value of ADVISOR [59].

Although a study found that SA performed better compared to a simple GA and PSO in finding optimum powertrain components for a parallel HEV [60], but more investigations are required for a general conclusion.

The usage of a hybrid of derivative-free and derivative-based methods, combining a GA and SQP also found its potential in finding an optimum combination of powertrain components for a series HEV [50]. However more investigations are needed to establish the hybrid algorithm for wider applications.

Although there was insufficient evidence regarding the best derivative-free optimisation method for the selection of optimum combination of powertrain components in HEVs, one conclusion came out from the reviewed literature; derivative-free optimisation methods are better at finding an optimum compared to derivative-based optimisation methods. The reviewed literature also showed that

GAs are better at finding the optimum combination of powertrain components compared to derivative-based optimisation methods considering its wider application in all major types of architectures and ability to find optimum FE and emissions.

3.1.1.7 Simulation approach

Model-in-loop approach was used for the simulation-based optimisation of powertrain component sizes of HEVs [49-60]. In the model-in-loop approach, a vehicle simulation model works along with an optimisation algorithm. As the name suggests, an optimisation method and a vehicle simulation model work in a loop i.e., the output of the optimisation algorithm works as the input for the vehicle simulation model and the output of the vehicle simulation model works as the input for the optimisation algorithm. The optimisation objectives such as FE, emissions etc. are calculated through the vehicle simulation model and an objective value is fed into the optimisation algorithm that generates different combinations of components that are fed into the vehicle simulation model for the evaluation of an objective.

3.1.1.8 Generalisation of the traditional methodology of powertrain component size optimisation

It has been found in the discussions from sections 3.1.1.1 to 3.1.1.7 that the literature [50] and [52] considered more number of optimisation variables compared to others (section 3.1.1.1), the literature [55] and [57] were considered more number of design constraints compared to others (section 3.1.1.4), the literature [49] and [52] considered more number of driving patterns compared to others, and the literature [60] studied more number of optimisation methods compared to others (section 3.1.1.6). Therefore, it can be conferred that no literature was comprehensive overall. Even though all previous studies were conducted over the years on different

architectures considering different optimisation methods, interestingly all studies followed the same methodology, but this was difficult to obtain explicitly from the literature. The methodology for the optimisation of powertrain component sizes followed in the reviewed literature can be generalised as follows.

- 1) Assumption of initial sizes of powertrain components.
- 2) The characteristics of those components are decided based on the base components. The base components are the components whose performance characteristics are used to determine the characteristics of new components during the optimisation process.
- 3) The components are evaluated according to a vehicle supervisory control (VSC) strategy for an objective or objectives (e.g., FE, emissions etc.) over a single driving pattern.
- 4) The components are checked against design constraints to ensure the minimum performance requirements.
- 5) The optimisation process is checked against a termination criterion which might be a fixed number of iterations or until a stable objective value is achieved.
- 6) If the optimisation termination criterion is not met, the current component sizes are fed into an optimisation method.
- 7) The optimisation method generates new sizes of the powertrain component.
- 8) If a parameter of the VSC strategy is also needs to be optimised, the optimisation method also generates a new value of the parameter.
- 9) Repeat 2 to 7, if only the powertrain components need to be optimised or repeat 2 to 8, if both the powertrain components and parameters of the VSC

strategy need to be optimised, until the optimisation termination criterion is achieved.

10) If the optimisation termination criterion is met, the optimisation process reaches the optimum sizes of the powertrain components.

The above methodology of the optimisation of powertrain component sizes in the reviewed literature is shown in Figure 3.1 and will be called the traditional methodology (M1) in the subsequent discussion.

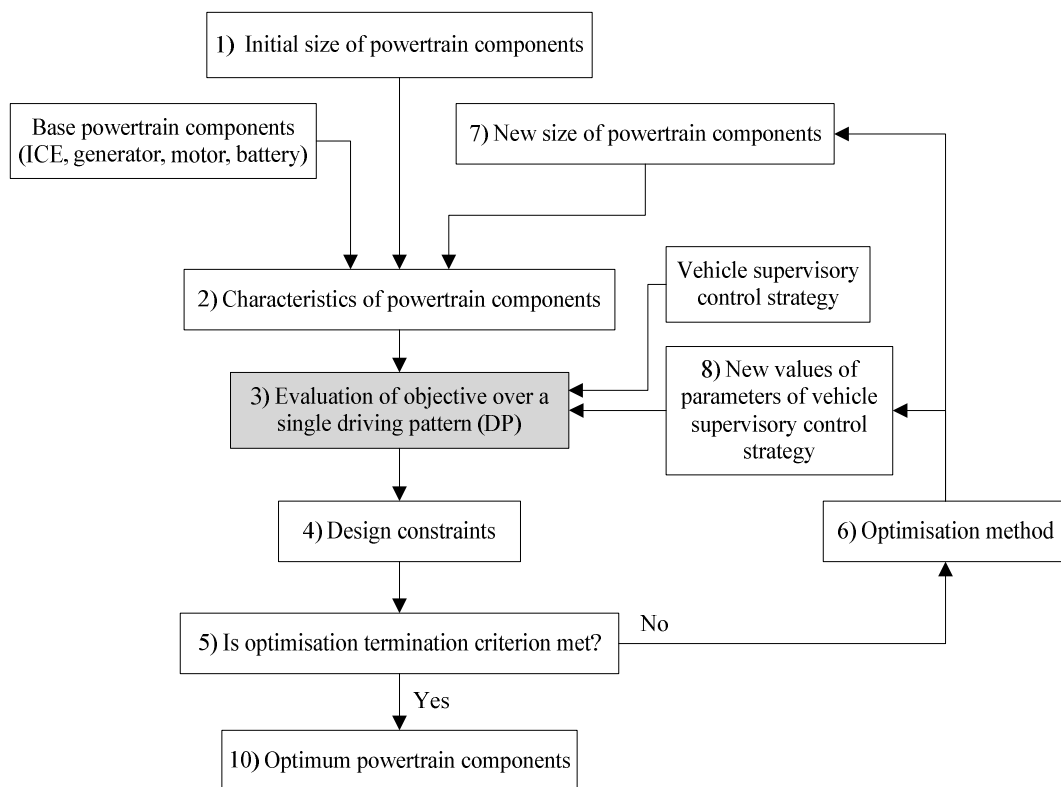


Figure 3.1: Traditional methodology of powertrain component size optimisation (M1)

3.2 FE variability in HEVs

As HEVs generally improve FE compared to CVs, it is expected that customers of HEVs would get better FE. But in the real-world, there are variations between manufacturer’s declared data and their real-world FE [41], [45]. The FE data shared by customers of Toyota Prius HEVs revealed that FE was varied from 12.2% in 2001 to 34.0% in 2013 compared to the declared FE values of its manufacturer [41], as shown in Table 3.7.

Table 3.7: Comparison of customer reported FE and manufacturers declared FE for Toyota Prius HEV [41]

Year	Customer reported FE, mpg (miles per gallon)			Manufacturer declared FE (US EPA certified), mpg			FE variability, %
	Average	Range	Number of vehicles	Combined	City	Highway	
2001	45.1	36-50	24	41	42	41	12.2
2002	44.2	36-58	29	41	42	41	12.2
2003	45.8	36-59	26	41	42	41	12.2
2004	47.4	34-67	90	46	48	45	26.1
2005	47.6	32-65	200	46	48	45	30.4
2006	47.6	37-63	151	46	48	45	19.6
2007	46.5	34-75	186	46	48	45	26.1
2008	46.2	32-62	145	46	48	45	30.4
2009	48.0	36-82	38	46	48	45	21.7
2010	49.4	35-74	187	50	51	48	30.0
2011	48.5	37-62	46	50	51	48	26.0
2012	49.8	38-62	32	50	51	48	24.0
2013	46.6	33-58	23	50	51	48	34.0

Where,

$$FE \text{ variability, \%} = \frac{(\text{Declared } FE_{\text{Combined}} - \text{Reported } FE_{\text{Minimum}})}{\text{Declared } FE_{\text{Combined}}} * 100$$

In 2001, the declared FE value of the manufacturer of Toyota Prius certified by US EPA (United States Environment Protection Agency) was 41 mpg over combined city and highway conditions, but the customer reported FE values ranged from 36 to 50 mpg. Therefore, FE values for some customers were below the declared FE value and it was as low as 36 mpg. Similarly in 2013, the declared FE value was 51 mpg over combined city and highway driving patterns but the customers reported FE was as low as 33 mpg. Therefore, even though all the customers had the same model of the car, the variation in FE i.e., FE variability existed among customers. It is obvious that the customers who got FE less than the declared FE were less satisfied.

The customer reported FE data in Table 3.7 indicated that even though the manufacturer's declared FE values have been improved over the years, the FE variability has not been reduced, rather it has been increased, as shown in Figure 3.2 by the trend line of the FE variability.

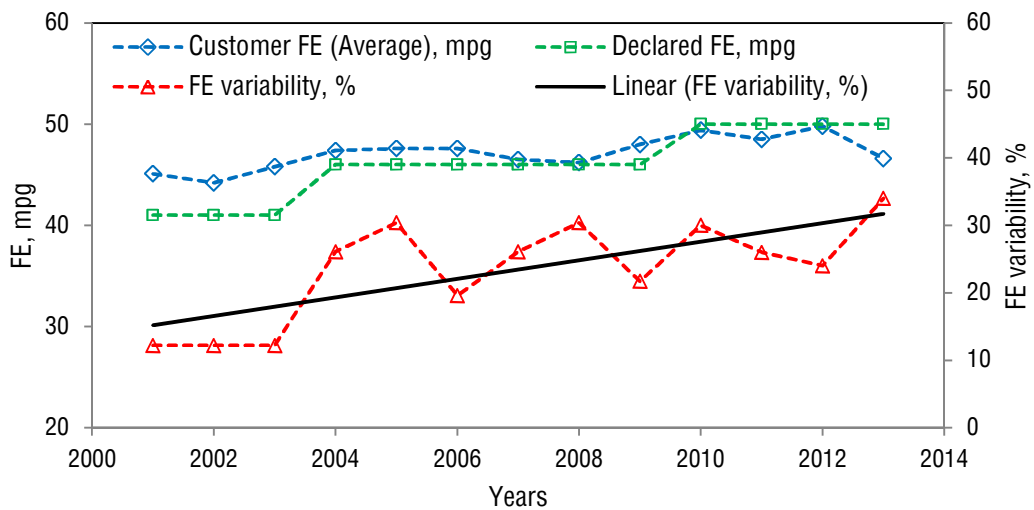


Figure 3.2: FE variability over the years for Toyota Prius HEV

The evidence of registering higher FE variability between the real-world and declared FE by the customers of HEVs compared to the customers of CVs was also found by Sharer et al. [45]. This is probably due to higher complexity in control of HEVs compared to CVs. The FE variability in the real-world indicates that there are certain factors that influenced the FE variability and without reducing the FE variability the actual improvement of FE of HEVs could not be perceived fully by everyone in real-world usage.

3.2.1 FE variability factors

The FE variability in HEVs occurs due to factors such as operation of air conditioning [34], variation in atmospheric temperature [34-37], and variation in driving patterns [38], [39].

The operation of air conditioning could reduce FE of HEVs by 18% to 27% compared to when it was not in operation [34]. The variation in atmospheric temperature of 37°F between summer and winter could affect the FE variability by up to 11% between summer and winter in HEVs [34]. Similarly another study [35] over three HEV models (Honda Civic, Honda Insight, and Toyota Prius) also showed that the FE variability were on average 10% and could be as high as 11.5% when the atmospheric temperature varied from 66°F to 103°F. A recent study also supported the FE variability with the variation of atmospheric temperature between -7°C to 23°C in HEVs [36]. Another research using a Toyota Camry HEV and a Ford Escape HEV over a predefined route showed a decrease in FE by more than 2 times at an atmospheric temperature of -14°C compared to that of the atmospheric temperature of 25°C [37]. The FE variability due to the operation of air-conditioning and variation in atmospheric temperature could be inter-related as more air-

conditioning are required during higher atmospheric temperatures compared to lower atmospheric temperatures.

The variation in driving patterns could affect the FE variability in HEVs by up to 20.5% [38], [39]. An experimental study in a laboratory showed 14.9 and 20.5% FE variability for a Toyota Prius and a Honda Civic HEVs, respectively over 6 different real-world simulated driving cycles [38], as shown in Table 3.8. The testing was conducted on a chassis dynamometer and the test data closely matched with the officially reported data of the same car manufacturer. Therefore, the test data could be considered as an indication that the HEV might have as high as 20.5% FE variability on road due to the variation in driving patterns.

Table 3.8: FE variability over standard driving patterns [38]

Driving patterns	Fuel consumption (FC), litre/100 km	
	Toyota Prius HEV	Honda Civic HEV
UDC cold	4.8	5.9
EUDC	3.6	4.0
NEDC	4.2	4.6
Artemis urban	3.7	7.2
Artemis road	3.2	4.4
Artemis highway	4.8	5.6
<i>Average FC, litre/100 km</i>	4.1	5.3
<i>Standard deviation, litre/100 km</i>	0.6	1.1
<i>FE variability, % (Standard deviation/Average)</i>	14.9	20.5

Another evidence of FE variability of 18.4% over 6 driving patterns was found due to variation in driving patterns in a Toyota Prius HEV [39], as shown in Table 3.9. The study considered UDDS and US06 driving patterns. The remaining 4 driving

patterns were generated by increasing the speed profile of UDDS by 10, 20, 30, and 40%.

Table 3.9: FE variability over 6 driving patterns [39]

Driving patterns	Fuel consumption (FC), litre/100 km
	Toyota Prius HEV
UDDS	3.6
UDDS x 1.1	4.2
UDDS x 1.2	5.3
UDDS x 1.3	5.7
UDDS x 1.4	6.7
US06	5.8
<i>Average FC, litre/100 km</i>	5.2
<i>Standard deviation, litre/100 km</i>	1.0
<i>FE variability, % (Standard deviation/Average)</i>	18.4

Among all the factors, the variation in driving patterns not only depends on driving styles but also external factors such as traffic conditions [43]. As a result, driving patterns vary from person to person, vehicle to vehicle, and even time to time. As driving patterns vary with every person, the FE variability due to driving patterns is a concern not only between different vehicle models but also for every vehicle of every model. Even for a certain atmospheric temperature with the air conditioning off, the variation in driving patterns cannot be avoided. As driving patterns are affected by external factors like traffic which could not be controlled, the variations due to this are less predictable. The importance of driving patterns is even higher in HEVs as the supportive evidence of higher FE variability of HEVs compared to its conventional counterpart have been found [44-46].

3.2.2 FE variability due to driving patterns: HEV and conventional vehicle

The variation in driving patterns causes FE variability in HEVs and the FE variability can be higher compared to CVs. A study showed that a CV had 9.5% FE variability over 8 driving patterns, whereas FE variability of a Toyota Prius HEV, series HEV, and power-split HEV had FE variability of 9.1, 54.9, and 27.0%, respectively over the same driving patterns [44], as shown in Table 3.10. Therefore, although all the HEVs had higher average FE compared to the CV, the FE variability of a HEV could be around 6 times higher compared to the CV, as shown in Table 3.10. The study considered 8 driving patterns which included urban as well as highway traffic. Although real-world consists of more than 8 types of driving patterns, the 8 different driving patterns studied represent a portion of real-world driving and results indicated that the variation in driving patterns is one of the major reasons for FE variability in the real-world.

Table 3.10: FE variability over driving patterns: CV and HEVs [44]

Driving patterns	Fuel consumption (FC), litre/100km			
	CV	Toyota Prius HEV	Series HEV	Plug-in Power-split HEV
C1	10.0	6.0	1.0	2.4
C2	9.7	6.9	1.5	3.2
C3	9.8	7.2	1.8	3.6
SU1	9.3	7.0	2.1	4.0
SU2	8.9	7.1	3.2	4.0
SU3	10.4	8.5	5.5	6.1
HWY1	7.9	7.3	5.0	5.0
HWY2	7.9	7.6	5.5	5.4
<i>Average FC, litre/100 km</i>	9.2	7.2	3.2	4.2
<i>Standard deviation, litre/100 km</i>	0.9	0.7	1.8	1.1
<i>FE variability, % (Standard deviation/Average)</i>	9.5	9.1	54.9	27.0

Another study also supported the evidence that the FE of a HEV was more sensitive than a CV with the increase in aggressiveness of driving patterns by comparing a Toyota Prius HEV and conventional Ford Focus [45]. The study used the term aggressiveness for higher vehicle speed and greater rates of acceleration. The study used driving patterns of different aggressiveness by scaling the speed of UDDS and HWFET. Although the study did not use completely different driving patterns, it could be considered a valid experiment to justify the effect of driving patterns on FE of HEVs. The similar conclusion of higher increase in FC of HEVs compared to CVs with the increase in aggressiveness of driving patterns was found through testing on a dynamometer at Argonne's Advanced Powertrain Research Facility [92].

Higher FE variability of HEVs compared to a CV was found in another study conducted in the real-world by testing over 100 different drivers in Kansas City conducted by the United States Environment Protection Agency (US EPA) [46]. The study showed that average FE of a Toyota Camry HEV was higher by 29%, whereas average FE values of plug-in HEVs were higher by up to 81% compared to a CV, as shown in Figure 3.3 and Table 3.11. But FE variability of the HEV was higher by 111%, whereas FE variability of the plug-in HEVs were higher by up to 1369% compared to the CV, as shown in Table 3.11. Figure 3.3 and Table 3.11 showed that though HEVs had better average FE compared to the CV, HEVs had higher FE variability compared to the CV.

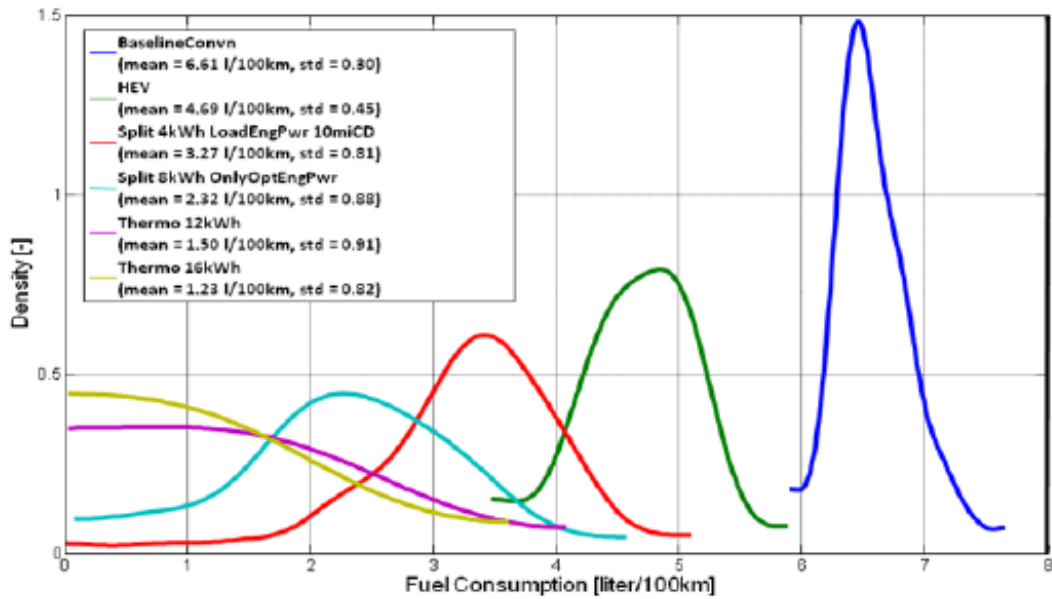


Figure 3.3: FE variability over 100 real-world driving patterns [46]

Table 3.11: FE variability over real-world driving patterns: CV and HEVs

Parameters	Fuel consumption, litre/100 km					
	CV	HEV (Toyota Camry)	Plug-in HEV 1 (4 kWh battery)	Plug-in HEV 2 (8 kWh battery)	Plug-in HEV 3 (12 kWh battery)	Plug-in HEV 4 (16 kWh battery)
<i>Average FC, litre/100 km</i>	6.61	4.69	3.27	2.32	1.50	1.23
<i>Standard deviation, litre/100 km</i>	0.30	0.45	0.81	0.88	0.91	0.82
<i>FE variability, % (Standard deviation/Average)</i>	4.5	9.6	24.8	37.9	60.7	66.7

Each driver’s driving data can be considered as a driving pattern because each driver’s driving profile would be different. As the study was conducted in the real-world over a large number of driving patterns, the study can be considered as a strong indication for the higher FE variability of HEVs due to variation in driving

patterns compared to CVs in real-world. The study also showed that the FE variability due to variation in driving patterns in HEVs could be higher in real-world as compared to FE variability over standard driving patterns.

Although three studies [44-46] suggested higher FE variability of HEVs compared to CVs, one study concluded the opposite i.e., HEVs had lower FE variability compared to a CV [93]. The analysis of the results of the study showed that the CV had higher FE variability than parallel and series-parallel HEVs and almost same as a series HEV when compared over two standard driving patterns, namely, UDDS and HWFET. Although in this case the FE variability values of HEVs were lower than the CV, but the FE variability values of the HEVs were ranged from 7.1 to 16.2% which were quite high considering the reviewed literature [44-46] and therefore, worth of further investigation.

It is quite clear from the reviewed literature that FE variability due to variation in driving patterns is present in CVs as well as in HEVs. It is more critical for HEVs as more number of components in HEVs makes the control of components of HEVs more complex, and therefore HEVs are more susceptible to variation. So, apart from the improvement in FE, the reduction of FE variability due to variation in driving patterns is also of significant importance for HEVs.

3.2.3 Reduction of FE variability due to driving patterns

Although much research has been done to improve FE of HEVs using the traditional methodology for the optimisation of powertrain component sizes [49-60], no study has been found to address the FE variability. The study [55] found 3 optimum designs, one for each of the 3 driving patterns, namely, FTP, ECE-EUDC, and TEH-Car. The results showed FE value of each optimum design over the respective

driving pattern. But the research did not study the effect on FE value of each optimum design over other driving patterns i.e., the FE value of the design optimised over FTP when evaluated over ECE-EUDC and TEH-Car, and similarly for other designs. This study is important to know the FE variability of each optimum design over different driving patterns. Similarly other studies [51], [54], [58] also restricted their study up to getting optimum design over a single driving pattern. Those researches overlooked the study to evaluate the performance of an optimum design over different driving patterns, which is important to determine the FE variability of each optimum design. Another study optimised powertrain components over FTP-75 only and the optimum design was evaluated for FE over UDDS, HWFET, and US06 [49]. The study concluded that GA was better at finding optimum components compared to conventional approach by comparing average FE over UDDS, HWFET, and US06. But an analysis of FE data of the study showed around 50% variation in FE among the three driving patterns. The study overlooked the FE variability of the optimum design due to variation in driving patterns and did not make any investigation for the reduction of FE variability. The studies [50], [53], [56], [60] which considered a combination of two different traffic conditions (city and highway) also focussed on the improvement of FE; FE variability was not addressed.

FE values of vehicles have been improved over the years, but FE variability has not been reduced [41]. This indicates a lack of attention towards FE variability due to variation in driving patterns.

Due to the importance of FE variability, it could be said that the improvement of FE and FE variability need to be considered simultaneously for optimum design of

powertrain components. The relationship between FE improvement and FE variability could be represented, as shown in Figure 3.4.

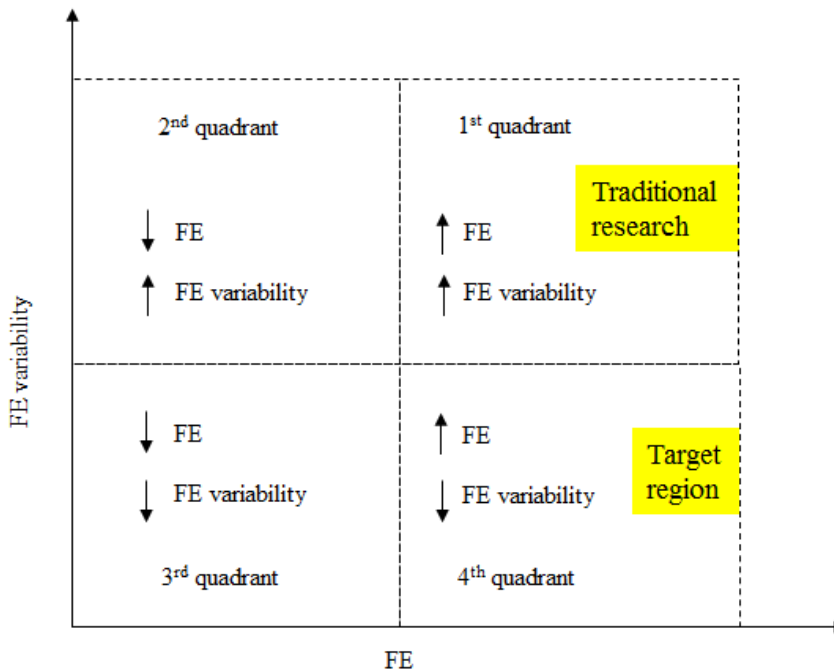


Figure 3.4: FE versus FE variability

Figure 3.4 is divided into four quadrants and each quadrant shows a relationship between the FE and FE variability. In the 1st quadrant, both the FE and FE variability increase. In the 2nd quadrant, the FE decreases but the FE variability increases. In the 3rd quadrant, both the FE and FE variability decrease. In the 4th quadrant, the FE increases but the FE variability decreases. As traditional research has been more focused on the improvement of FE and evidence of high FE variability exists, traditional research is more likely situated in the 1st quadrant. Table 3.7 also supports this assumption related to traditional research as the FE variability of HEVs have been increased over the years along with the declared FE values. It is easy to predict from Figure 3.4 that the target region for any HEV should be in the 4th quadrant, i.e.,

the design of powertrain components should increase the FE and reduce the FE variability in real-world driving.

One of the probable reasons for the lack of attention towards the analysis of the FE variability could be that the main purpose many studies were more inclined towards comparison of optimisation methods [53], [60]. The improvement of FE over a given driving pattern for an optimum combination of components produced by an optimisation method compared to the FE value of the optimum combination of components produced by another optimisation method was sufficient to validate the first optimisation method. Another possible reason might be the competition between vehicle manufacturers to show better FE over competitors to attract customer. Although higher FE is an attractive feature for customers, without reducing FE variability the actual FE improvement could not be perceived fully by all customers.

As different optimum designs are available, the natural question would be which design is best in terms of FE variability. The answer is unknown. The question, whether the design with the highest FE would produce the least FE variability, needs to be answered. Even though one design among the various optimum designs would be better over other optimum designs in terms of FE variability, the design with least FE variability actually is not optimum over all the driving patterns but over a single driving pattern.

As driving patterns depend on driver behaviour and external factors such as traffic conditions, the FE variability due to driving patterns could be reduced if vehicle performance is less sensitive to driving variations. The performance of HEV depends on optimum selection of powertrain components and the proper function of those components as per VSC strategies. The potential of the optimisation of powertrain

component sizes for the improvement of FE has already been established, so FE variability may also be reduced through the optimisation of powertrain component sizes. Therefore, optimum selection of powertrain components might be a possible way to reduce FE variability due to driving patterns. It has been found in the reviewed literature that optimum design of powertrain components has been focussed on the improvement of FE, and FE variability has not been addressed. No investigation was found in the literature regarding an optimum powertrain design for reduced FE variability. By considering the importance of the FE variability due to variations in driving patterns, it is important to investigate how to reduce the FE variability due to driving variations through the optimisation of powertrain component sizes.

3.3 Research question

The discussions of the previous sections related to the FE variability in HEVs are shown in Figure 3.5.

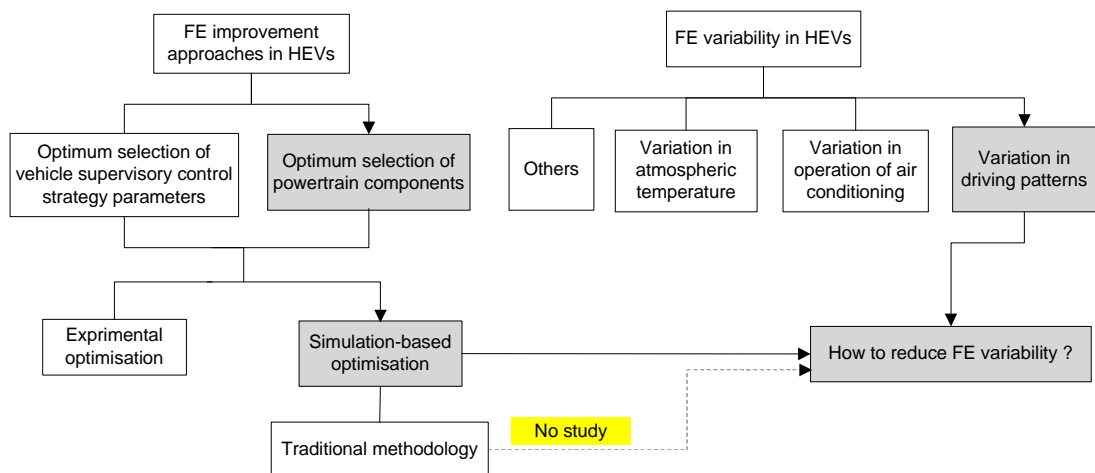


Figure 3.5: Existing scenario of FE variability in HEVs and research question

Although optimum selection of parameters of a vehicle supervisory control (VSC) strategy influences FE [87], [88], only consideration of VSC strategy is not always sufficient for the improvement of FE of HEVs [89]. The optimum selection of powertrain components is important because it not only helps to improve FE but also affects overall weight and configuration of HEVs. Higher number of components of HEVs compared to CVs also makes the optimum selection of powertrain components important. Simulation-based optimisation of powertrain components is a preferred approach over experiment because development and testing of each combination of powertrain components are time consuming and expensive [47], [53], [54].

The operation of air-conditioning [34], variation in atmospheric temperature [34-37], and variation in driving patterns [38], [39] are responsible for FE variability in HEVs. Other factors such as variation in the gradient of road and time of operation could also affect the FE variability. Among the factors, the variation in driving patterns is important due to more unpredictability and the effect of the variation in driving patterns cannot be avoided even for a certain atmospheric temperature with air-conditioning off. Therefore, how to reduce FE variability due to variation in driving patterns is a major problem in HEVs.

The traditional methodology for the simulation-based optimisation of powertrain components followed in the reviewed literature [49-60] has generally been more focused on the improvement of FE; FE variability due to variation in driving patterns has been overlooked. The traditional methodology might not be suitable to address the problem of FE variability in HEVs due to the conceptual weakness in representing real-world driving conditions realistically.

Therefore, due to the importance of FE variability in HEVs due to variation in driving patterns, lack of research for the reduction of the FE variability, and the influence of the powertrain components for the improvement of FE, the research question was as follows.

- How to reduce FE variability in HEVs due to variation in driving patterns through the optimisation of powertrain component sizes?

3.4 Summary

- The optimisation of powertrain component sizes through simulation model is a preferred method for the improvement of FE in HEVs.
- All the reviewed literature followed the same methodology for the optimisation of powertrain component sizes, which was termed as the traditional methodology (M1).
- The ICE, motor, and battery were major powertrain components considered for the optimisation of powertrain component sizes in the reviewed literature.
- The rule-based vehicle supervisory control (VSC) strategies were considered for the optimisation of powertrain component sizes in the reviewed literature.
- The standard driving patterns, namely, NEDC, FTP, LA92, HWFET, and US06 were used in majority of the reviewed literature.
- The evolutionary algorithms, GA and PSO were used as optimisation methods in majority of the reviewed literature for the optimisation of powertrain component sizes.
- The variation in FE i.e., FE variability exists in HEVs between the customer reported FE and manufacturer declared FE.

- The variation in atmospheric temperature, operation of air-conditioning, and variation in driving patterns are major factors responsible for the FE variability in HEVs.
- The FE variability due to variation in driving patterns is of significant importance due to unpredictability of the driving patterns.
- The FE variability in HEVs due to variation in driving patterns could be higher than that of CVs.
- Over the years, research has generally been focused on the improvement of FE in HEVs; FE variability has been overlooked.
- The traditional methodology followed in the reviewed literature has not been investigated for the FE variability in HEVs and is conceptually not suitable for the reduction of the FE variability.
- The research question of this thesis was how to reduce the FE variability in HEVs due to variation in driving patterns through the optimisation of powertrain component sizes.

CHAPTER 4

RESEARCH METHODOLOGY

Chapter 3 has discussed the research question which was how to reduce FE variability due to variation in driving patterns. This chapter discusses the overall research methodology followed to address the research question. The main objective of this chapter is to explain the major stages of this study. This chapter briefly discusses each stage and indicates the position of each stage in the thesis chapter-wise to get an overview of the thesis.

4.1 Research methodology

The research methodology can be divided into 7 major stages. These stages are as follows and outlined in Figure 4.1.

- 1) Literature review
- 2) Formulation of research question
- 3) Proposal of a new methodology to solve the research question
- 4) Simulation setup
- 5) Investigation over standard conditions
- 6) Validation in real-world conditions
- 7) Interpretation and generalisation

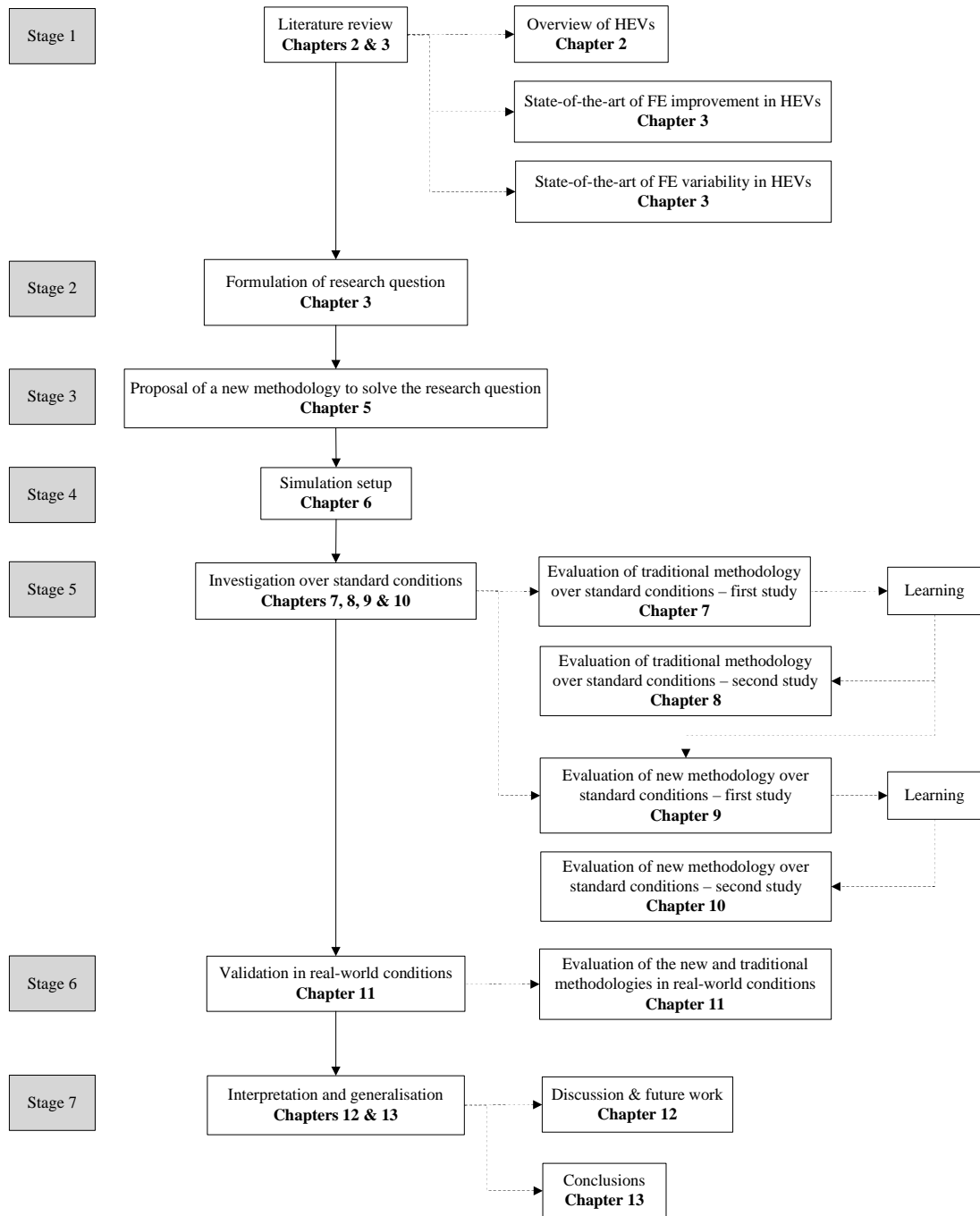


Figure 4.1: Flow diagram of research methodology

4.1.1 Literature review

The first and one of the most important stages of research is literature review. Literature review helps to understand the state-of-the-art and clarify the research question.

The review of related literature was discussed in two chapters, chapters 2 and 3. Chapter 2 provided an overview of HEVs and associated terminologies used throughout the thesis. This chapter also discussed the reasons for higher FE in HEVs compared to conventional vehicles.

Chapter 3 provided a review of current state-of-the-art of FE in HEVs. The importance of powertrain components for FE in HEVs and the approaches followed for the optimum selection of powertrain components of HEVs were discussed. This chapter generalised the approach followed in the reviewed literature for the optimum selection of powertrain components of HEVs and termed as traditional methodology. The reviewed literature indicates that variation in FE under different conditions i.e., FE variability is a problem in HEVs. The variation in atmospheric temperature, operation of air-conditioning, and variation in driving patterns are responsible for the problem. Among the three factors, driving patterns are affected by external factors like traffic which could not be controlled and therefore, the variations in driving patterns are less predictable. Even for a certain atmospheric temperature with the air conditioning off, the variation in driving patterns cannot be avoided. The FE variability due to the variation in driving patterns was chosen for study due to the relative importance of the factor compared to the other factors. The reviewed literature indicates that no study has yet addressed the problem and the traditional

methodology for the selection of powertrain components is insufficient to address the problem of FE variability.

4.1.2 Formulation of research question

Due to the importance of FE variability in HEVs due to variation in driving patterns and the inability of the traditional methodology to address the FE variability, how to reduce the FE variability due to variation in driving patterns through the optimum selection of powertrain components was considered as the research question. The research question was discussed in chapter 3.

4.1.3 Proposal of a new methodology

Due to the limitations of the traditional methodology to address the research question, a new methodology was required. The new methodology is conceptually improves upon the traditional methodology. In the traditional methodology, powertrain components of HEVs are generally optimised over a single driving pattern. The reason for considering a single driving pattern probably because the research was more focused on the development of better optimisation methods to improve FE and for that purpose the optimisation over a single driving pattern was sufficient. This indicates a conceptual flaw in the traditional methodology as real-world consists of different driving patterns. On the other hand, in the new methodology, powertrain components are optimised over a range of driving patterns representing different traffic conditions and driving styles simultaneously. Consideration of different driving patterns makes the concept of the new methodology potentially more applicable in the real-world. The proposal of the new methodology is discussed in chapter 5.

4.1.4 Simulation setup

The research question was related to the optimisation of powertrain component sizes. Development and testing of each combination of powertrain component sizes is time consuming as well as expensive. The reviewed literature suggests that computer simulation is a preferred approach over the experimental study for the optimisation of powertrain component sizes. Based on the suggestion of the reviewed literature, computer simulation was considered to address the research question. A computer simulation model of a Toyota Prius HEV, pre-built in a vehicle-simulation-software was considered for the investigation. The simulation model of the Toyota Prius was considered as the benchmark vehicle for comparison. The design parameters, design constraints, optimisation method, and driving patterns were selected based on their usage in the reviewed literature. The performance of the simulation model of the Toyota Prius was considered as the design constraints for an optimum design to ensure that the performance of the optimum design should not be inferior compared to the Toyota Prius. The simulation set up of all the investigations is discussed in chapter 6.

4.1.5 Investigation over standard conditions

Investigation over standard conditions is useful to establish any new concept, before investigation in more complex real-world conditions. The standard driving patterns, namely, NEDC, FTP, LA92, HWFET, and US06, generally used in the reviewed literature for studies related to FE, were considered as the standard conditions.

The traditional methodology was evaluated over standard conditions for FE variability, which has not been investigated in the reviewed literature. The study also provides insight into the reasons of higher FE variability due to variation in driving

patterns. As the study has not been investigated before, first a preliminary study was conducted. As the preliminary study failed to provide desired results, another study was conducted by incorporating the learning from the analysis of the first study. The preliminary investigations of the traditional methodology over the standard conditions are discussed in chapter 7. Chapter 8 discusses the second study of the traditional methodology over the same standard conditions.

The new methodology was also investigated over the same standard conditions. As the new methodology considers a range of different driving patterns, two different approaches are possible to maintain charge sustaining after the end of the last driving pattern. As the first study which investigated the first approach failed to provide the desired results, learning from the first study was incorporated in the second approach which was investigated in the second study to improve the new methodology. The new methodology was compared with the traditional methodology as well as with the simulation model of the benchmark vehicle (Toyota Prius). The first study of the new methodology over the standard conditions is discussed in chapter 9. Chapter 10 discusses the second study of the new methodology over the standard conditions.

4.1.6 Validation in real-world conditions

After the establishment over standard conditions, the optimum design produced by the new methodology over standard driving patterns was needed to be validated over driving patterns that were not used for the optimisation. For complete generality these driving patterns were selected to be real-world driving patterns. The new methodology was investigated over real-world driving patterns to validate the applicability of the new methodology in real-world conditions.

Speed-time data logged for a conventional vehicle driven by 10 drivers over a predefined route consisting of urban and highway driving patterns were considered as real-world driving conditions.

The optimum designs produced by the traditional methodology over standard conditions and the simulation model of the benchmark vehicle (Toyota Prius) were also evaluated over the same real-world driving patterns to understand the improvement of the new methodology in real-world conditions. The investigation over the real-world conditions are discussed in chapter 11.

4.1.7 Interpretation and generalisation

This discussion is divided into two chapters, chapters 12 and 13. Chapter 12 interprets the results individually and comparatively in the context of the research question and discusses the potential of the new methodology to address the research question. The learning, limitations, and applications of the traditional and new methodologies are also discussed in chapter 12. The future direction of work related to this research is suggested in chapter 12. The major conclusions of the thesis are summarised in chapter 13.

4.2 Summary

- The approach followed for the research in this thesis has been discussed. The research methodology consisted of 7 major stages, namely, literature review; formulation of research question; proposal of a new methodology; simulation setup; investigation over standard conditions; validation in real-world conditions; and interpretation and generalisation.

CHAPTER 5

PROPOSAL OF A NEW METHODOLOGY

Chapter 3 has indicated that research has generally been more focused on the improvement of FE in HEVs; FE variability has not been addressed. The reduction of FE variability through the optimisation of powertrain component sizes is considered as research question for this thesis. The traditional methodology for the optimisation of powertrain component sizes followed in the reviewed literature, as discussed in chapter 3, generally considers a single standard driving pattern to find optimum powertrain component sizes. Therefore, powertrain components are only optimum over that given driving pattern. As different driving patterns exist in real-world, selecting a single driving pattern for optimisation is far from real-world conditions and that makes the traditional methodology conceptually weak for practical application. This conceptual weakness might lead to higher FE variability in real-world. As real-world driving patterns vary due to traffic conditions and driving styles, the powertrain components need to be optimum over different traffic conditions and driving styles simultaneously for the reduction of FE variability in real-world. Systematic consideration of different driving patterns for the optimisation of powertrain component sizes are not found in the reviewed literature, important for the reduction of FE variability.

This chapter proposes a new methodology for the optimisation of powertrain component sizes based on the shortcomings of the traditional methodology to

address the research question. The details of the proposal of the new methodology are discussed next.

5.1 Proposal of new methodology

As vehicles are subjected to different driving conditions in the real-world, powertrain component sizes need to be optimum over different driving patterns simultaneously to perform optimally in the real-world. With this hypothesis, a new methodology is proposed for the optimisation of powertrain components through computer simulation model, so that powertrain components are optimum over a range of different driving patterns simultaneously. The main concept of the new methodology is that no ideal driving pattern is possible and no single driving pattern can represent the real-world and for that reason different driving patterns need to be considered during the optimisation of powertrain component sizes to represent the real-world in a realistic way. The new methodology improves the conceptual weakness of the traditional methodology by considering a range of driving patterns representing different traffic conditions and driving styles simultaneously to make the new methodology more applicable for real-world application, and for this reason the new methodology can be considered conceptually original. In the new methodology, driving patterns are categorised into different traffic conditions and each traffic condition is further classified into different driving styles. For example, traffic conditions could be categorised into urban and highway and each traffic condition could be further classified into different driving styles e.g., conservative, normal, and aggressive. After categorisation, all the driving patterns are considered during the evaluation of an objective (e.g., FE, emissions etc.). During optimisation, the objective (e.g., FE, emissions etc.) needs to be evaluated over all the categorised

driving patterns. The optimisation needs to be decided based on the cumulative value of the objective over all the categorised driving patterns.

For example, it is assumed that driving patterns are classified into four different driving patterns and the objective of optimisation is the minimisation of FE, as shown in Figure 5.1. If the FE values over the four driving patterns are FE1, FE2, FE3, and FE4 respectively, then the optimisation decision needs to be done based on the summation of the FE1 to FE4 for the new methodology, as shown in Figure 5.1. This improves upon the traditional methodology which considers FE over only one driving pattern and therefore, provides different optimum designs over different driving patterns, as shown in Figure 5.2.

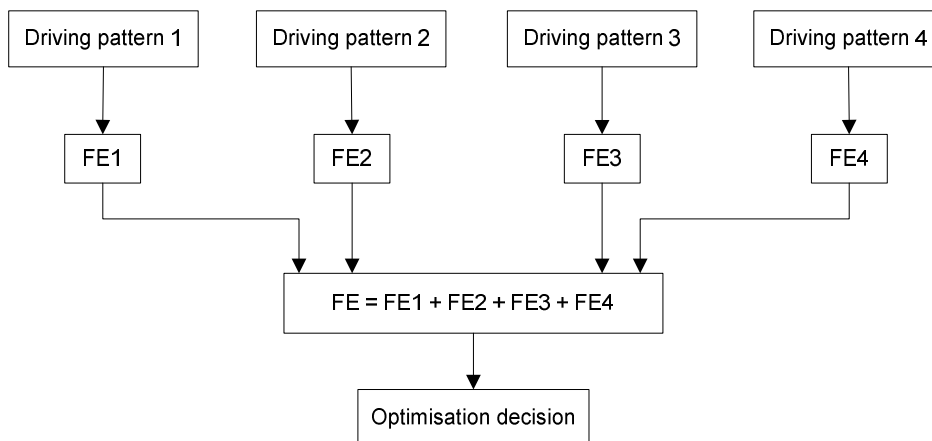


Figure 5.1: Concept of optimisation decision in the new methodology

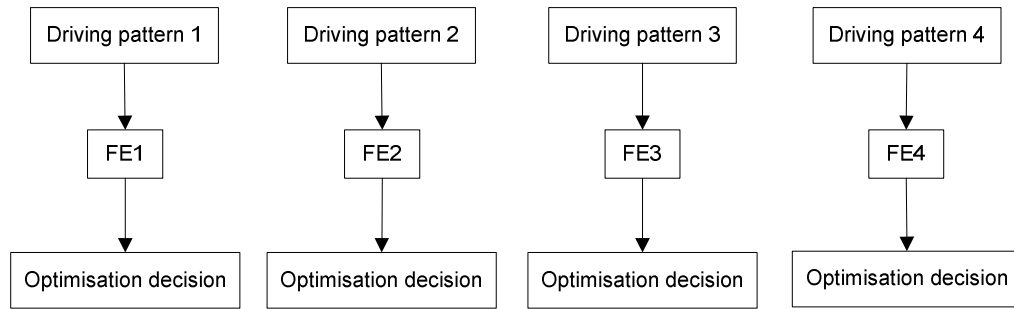


Figure 5.2: Concept of optimisation decision in the traditional methodology

As the optimisation in the new methodology is done based on the objective value over a range of different driving patterns representing different traffic conditions and driving styles, the powertrain components are actually optimum over a range of driving patterns representing different traffic conditions and driving styles. As the optimum design produced by the new methodology is optimum over a range of different driving patterns, it is expected that FE variability of the optimum design will be reduced. The new methodology will be called as proposed methodology and termed as M2 in the remaining discussion.

The proposed methodology is as follows and shown in Figure 5.3.

- 1) Assumption of initial sizes of powertrain components.
- 2) The characteristics of those components are decided based on the base components. The base components are the components whose performance characteristics are used to determine the characteristics of new components during the optimisation process.
- 3) Driving patterns are categorised into different traffic conditions (e.g., urban, highway etc.) and driving styles (e.g., conservative, normal, aggressive etc.).
- 4) All the categorised driving patterns are combined in series.

- 5) The components are evaluated according to a vehicle supervisory control (VSC) strategy for an objective or objectives (e.g., FE, emissions etc.) over the combination of categorised driving patterns.
- 6) The components are checked against design constraints to ensure the minimum performance requirements.
- 7) The optimisation process is checked against a termination criterion which might be a fixed number of iterations or until a stable objective value is achieved.
- 8) If the optimisation termination criterion is not met, the current component sizes are fed into an optimisation method.
- 9) The optimisation method generates new sizes of the powertrain component.
- 10) If a parameter of the VSC strategy also needs to be optimised, the optimisation method generates a new value of the parameter.
- 11) Repeat 2 and 5 to 9, if only the powertrain components need to be optimised or repeat 2 and 5 to 10, if both the powertrain components and parameters of the VSC strategy need to be optimised, until the optimisation termination criterion is achieved.
- 12) If the optimisation termination criterion is met, the optimisation process reaches the optimum sizes of the powertrain components.

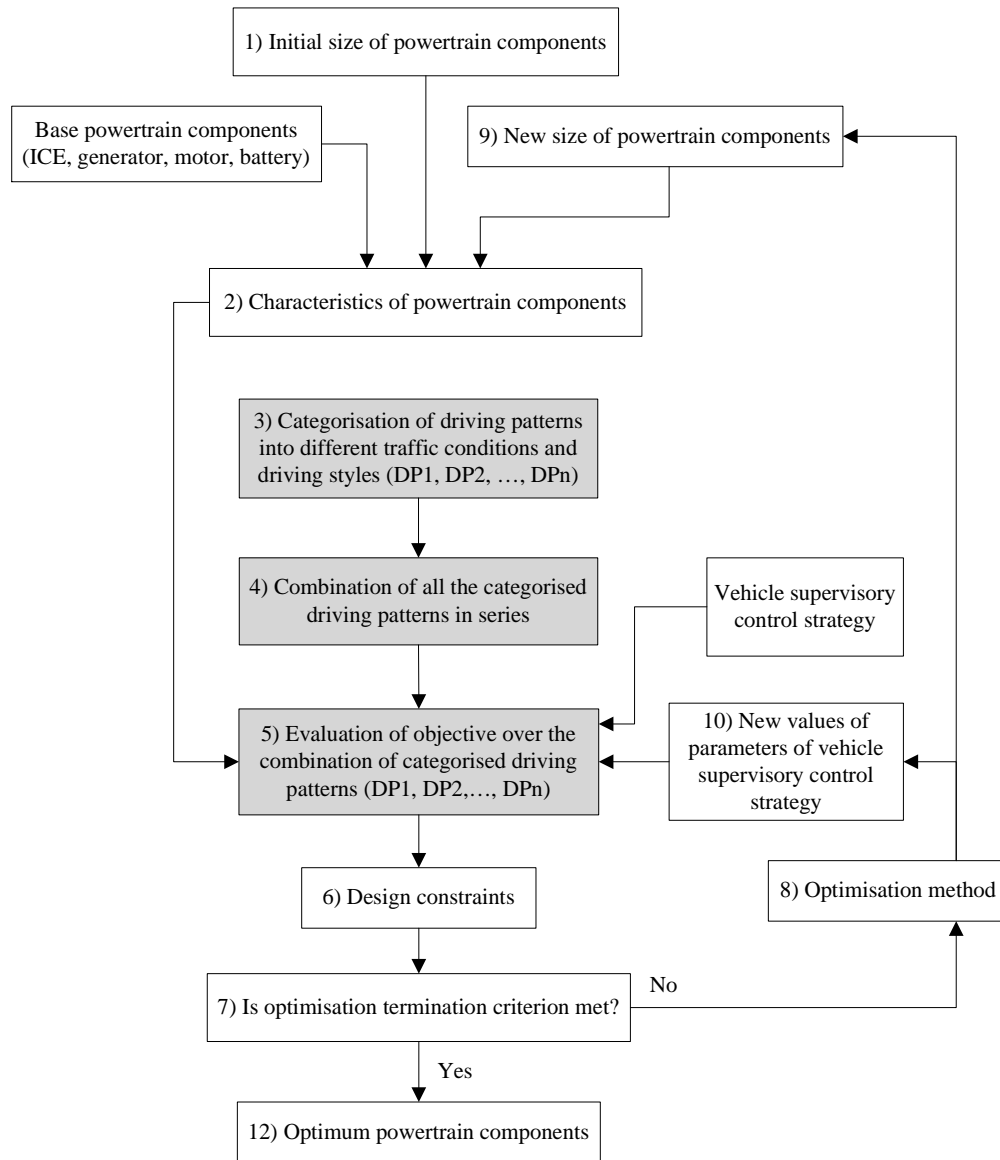


Figure 5.3: Proposed methodology of powertrain component size optimisation (M2)

The conceptual difference between the proposed and traditional methodologies is that the proposed methodology considers a range of driving patterns representing different traffic conditions and driving styles simultaneously, as shown in Figure 5.3, whereas the traditional methodology generally considers a single standard driving pattern for the optimisation of powertrain component sizes, as discussed in chapter 3 and shown in Figure 3.1 (repeated on next page).

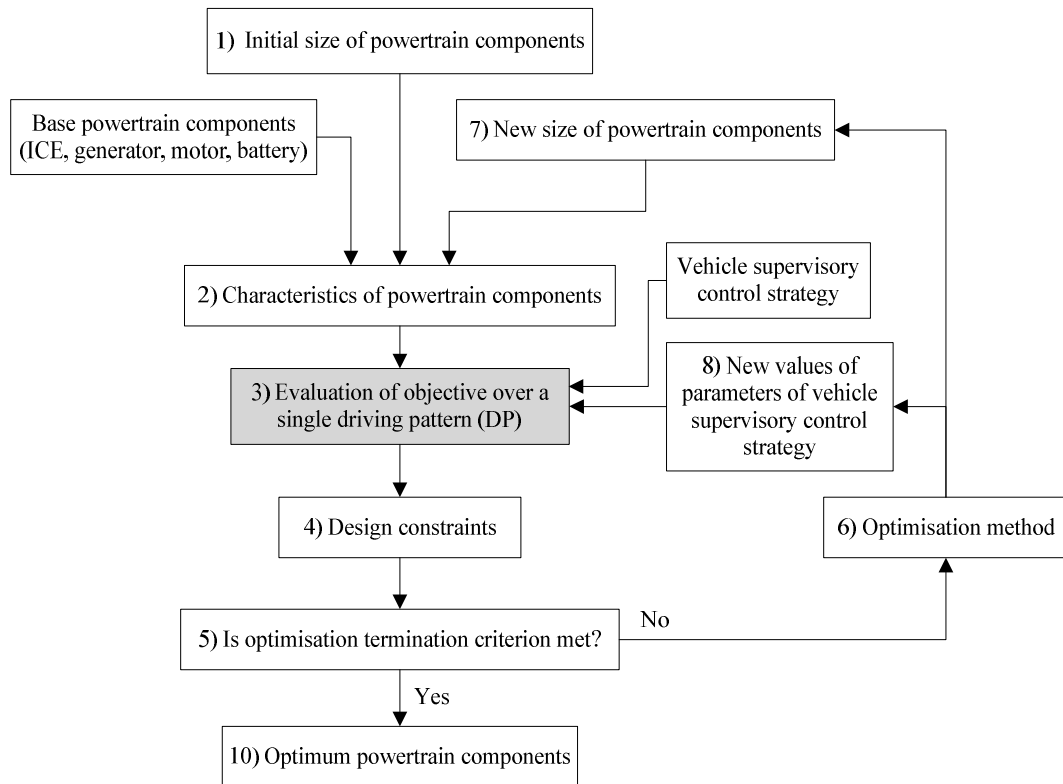


Figure 3.1 (Repeated): Traditional methodology of powertrain component size optimisation (M1)

5.2 Summary

- A new methodology has been proposed for the optimisation of powertrain component sizes to address FE variability due to variation in driving patterns in HEVs.
- The proposed methodology considers a range of driving patterns representing different traffic conditions and driving styles simultaneously instead of a single standard driving pattern used in the traditional methodology followed in the reviewed literature.

CHAPTER 6

SIMULATION SETUP

The proposal of a new methodology (M2) for the optimisation of powertrain component sizes to address the research question has been discussed in chapter 5. The potential of the proposed methodology (M2) in solving the research question is evaluated through simulation studies because the optimisation of powertrain component sizes through the simulation is a preferred method found in the reviewed literature in chapter 3. The purpose of this chapter is to present details of the parameters chosen for the simulation studies including the reasons for choosing them. This chapter is divided into 10 sections. The 1st section discusses the simulation tool used for the study. The 2nd section briefly describes the vehicle simulation model on which all the investigations were carried out. The 3rd section details the design parameters of the study. The 4th section discusses the vehicle supervisory control strategy. The 5th section shows the formulation of the optimisation problem. The 6th section discusses the optimisation method used and the approach followed to integrate the optimisation method with the vehicle simulation model. The 7th section discusses about the classification and consideration of driving patterns for optimum designs. The 8th section describes the driving patterns used for the evaluation of the proposed methodology in standard and real-world conditions. The 9th section describes the approach followed to evaluate fuel economy (FE) of a design over a driving pattern. The last section summarises this chapter.

6.1 Simulation tool

An in-house vehicle simulation software Warwick Powertrain Simulation Tool for Architectures (WARPSTAR) [94] was used for this research. WARPSTAR is developed based on MATLAB-Simulink. WARPSTAR consists of several prebuilt models of all known architectures of HEVs and a component model library to build new architectures. Although other software for vehicle simulation such as ADVISOR [55] and PSAT [60] exist, WARPSTAR was chosen because of its easy availability and on-site support.

As this research study was mainly focused on FE and WARPSTAR was found suitable to predict FE for conventional vehicles (CVs) as well as HEVs [94], WARPSTAR was considered as a simulation tool for this research study.

6.2 Vehicle simulation model

6.2.1 Vehicle architecture

A vehicle simulation model of a non-plug-in series-parallel Toyota Prius HEV was considered for this study. The optimisation of powertrain component sizes is important for series-parallel architecture due to its relatively complicated architecture compared to series and parallel architecture. The simulation model of the Toyota Prius was considered as benchmark vehicle for comparison.

The major parameters of the simulation model of the Toyota Prius HEV were as follows.

- Vehicle mass: 1368 kg
- Rolling resistance coefficient: 0.01
- Body aerodynamic drag coefficient: 0.29
- Vehicle frontal area: 2.0 m²

- Transmission: Power-split

6.2.2 Powertrain components

The internal combustion engine (ICE), motor, generator, and battery were the major powertrain components of the Toyota Prius HEV, as discussed in chapter 2. The characteristics and major parameters of the ICE, generator, motor, and battery of the Toyota Prius are discussed next.

6.2.2.1 Internal combustion engine (ICE)

The Toyota Prius HEV had a 1.5 litre spark ignition (SI) engine. The torque-speed characteristic and fuel consumption map are shown in Figure 6.1. The maximum power and torque of the ICE of the Toyota Prius were 43 kW and 101.9 Nm, respectively.

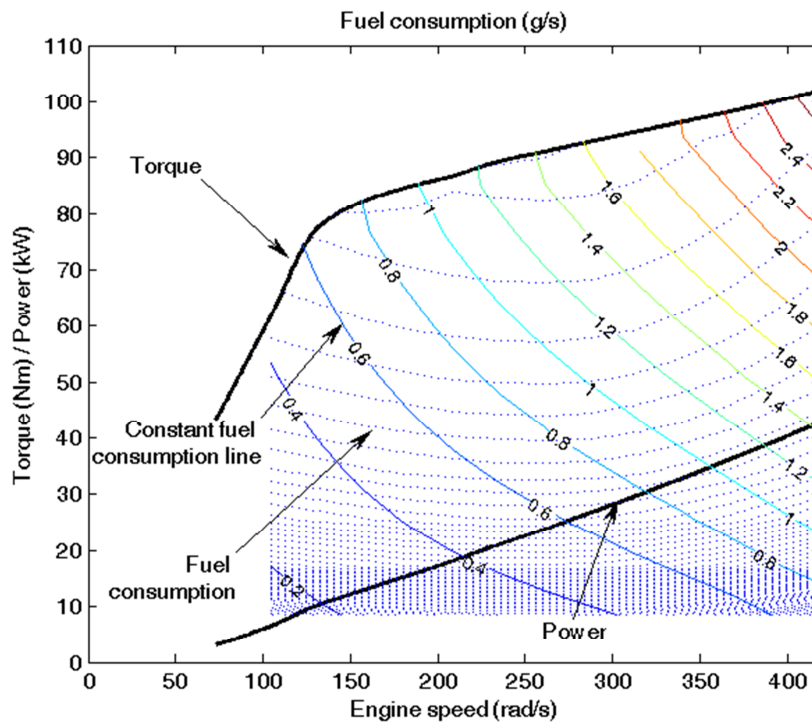


Figure 6.1: ICE characteristics of Toyota Prius HEV

6.2.2.2 Motor

The Toyota Prius HEV had a 30kW permanent magnet brushless DC motor. The speed-torque characteristic and efficiency of the motor are shown in Figure 6.2. The maximum torque was 305 Nm and maximum efficiency was 90%.

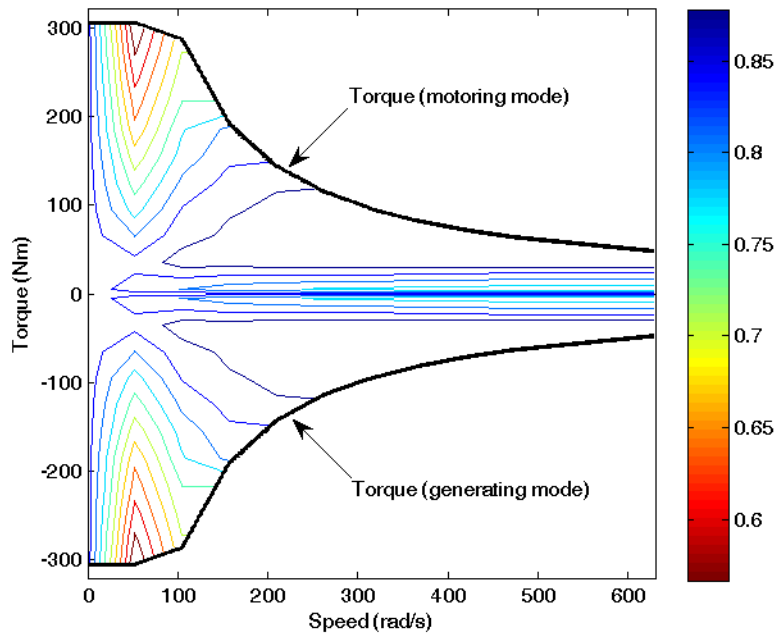


Figure 6.2: Motor torque and efficiency map of Toyota Prius HEV

6.2.2.3 Generator

The Toyota Prius HEV had a 15kW permanent magnet brushless DC generator. The speed-torque characteristic and efficiency of the generator is shown in Figure 6.3. The maximum torque was 55 Nm and maximum efficiency was 85%.

6.2.2.4 Battery

The Toyota Prius HEV consisted of a 6Ah NiMH battery. The battery had 40 modules and 6 cells in a module for a total of 240 cells. Each cell was of 1.5V. The battery characteristics are shown in Figure 6.4.

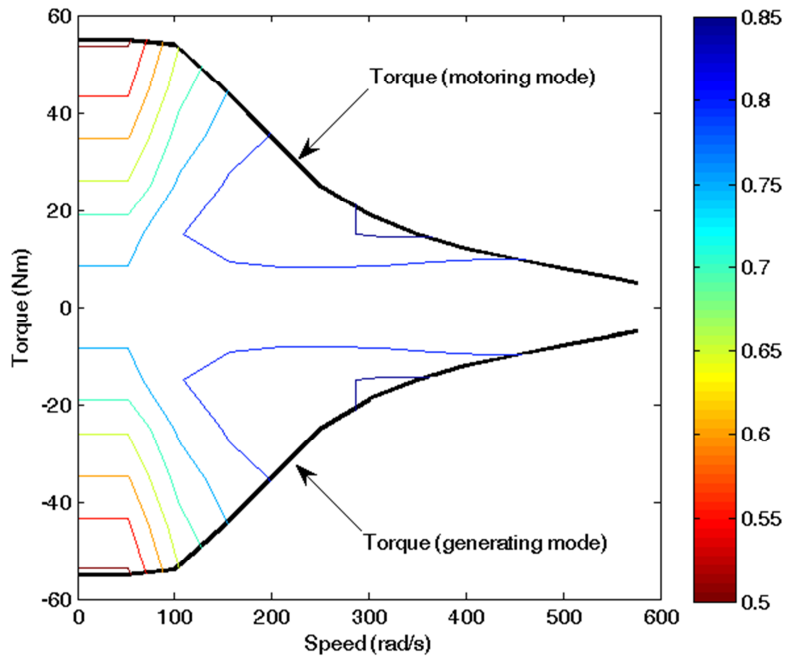


Figure 6.3: Generator torque and efficiency map of Toyota Prius HEV

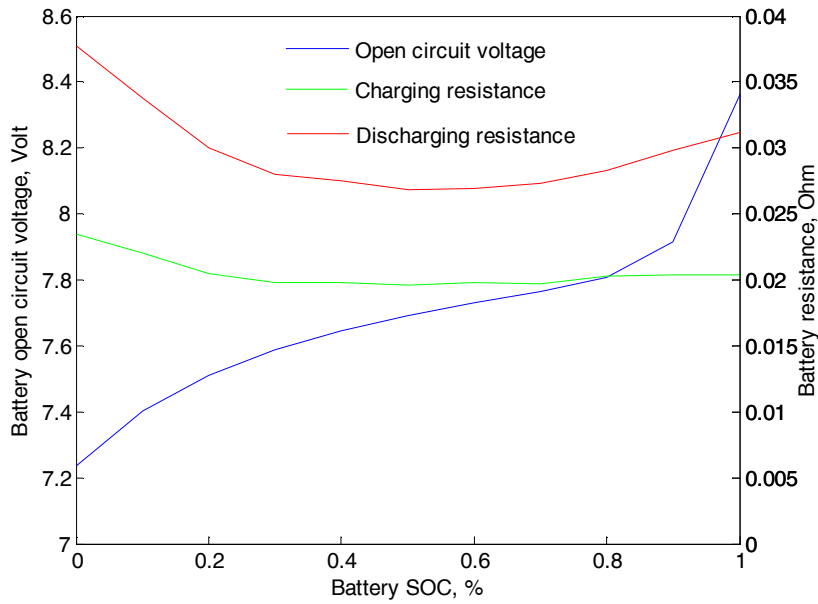


Figure 6.4: Battery characteristics of Toyota Prius HEV

6.3 Design parameters

6.3.1 Design variables

Four major powertrain components, namely, ICE, generator, motor, and battery of the Toyota Prius HEV were considered for the optimisation due to their direct influence on the FE performance. The design variables considered for this study are as follows.

- Maximum power of ICE (P_{ICE})
- Maximum power of generator (P_G)
- Maximum power of motor (P_M)
- Maximum capacity of battery (C_B)

The design variables were considered for the optimisation following their use in the reviewed literature in chapter 3.

6.3.2 Design limits

The components of the Toyota Prius HEV were considered as the base components for this study. The range of the variations in each design variable of the powertrain components was kept within $\pm 70\%$ of the base components, as listed in Table 6.1 to allow sufficient design limits for the optimisation method to find optimum values. With very restricted design limits, the search for optimum components also becomes restricted. With infinite design limits, the optimisation method would take higher computational time to find optimum components and also not necessarily realistic. As the ranges were constant for all investigations and the study was of comparative in nature, the effect of the ranges on the comparative results was of little significance.

Table 6.1: Range of variations in design variables

Design variable	Lower limit	Upper limit
P_{ICE}, kW	12.9	73.1
P_G, kW	4.5	25.5
P_M, kW	9.0	51.0
C_B, Ah	1.8	10.2

Different power ratings of the components during optimisation were achieved by linear scaling of the performance of the base components, as seen in the reviewed literature. The study also assumed a linear relationship between power and fuel consumption of the ICE. In actual case it might not vary linearly and might affect the final FE values. However the effect is expected to be the same for the traditional and proposed methodologies.

A linear relationship between torque and power of the ICE, generator, and motor was assumed. The efficiencies of the ICE, generator, and motor were assumed constant.

For the battery, a linear relationship between battery capacity and current was assumed. The charging and discharging resistance of the battery were assumed constant. The number of modules in a battery and number of cell in a module were also assumed constant.

6.3.3 Design constraints

As the simulation model of the Toyota Prius HEV was considered as the benchmark vehicle, the acceleration, maximum speed, and gradeability values of the Toyota Prius were considered as constraints for optimum designs. These constraints were

needed during the optimisation process to ensure that the performance of the optimum designs should not be inferior when compared to the Toyota Prius. These performance constraints were calculated based on the suggestions in [95], [96] and the calculations are shown in Appendix A. The design constraints for this study were as follows.

- Acceleration (0 to 60 mph): < 13.4 seconds
- Maximum speed: > 113.3 mph
- Gradeability: >13.8% at 55 mph
- Delta SOC (i.e., difference between the initial and final battery SOC): < 0.5%

The Delta SOC was considered in order to eliminate the effect of battery SOC on FE while comparing different designs for FE performance. In order to eliminate the influence of battery SOC on FE, the initial and final battery SOC on all driving patterns needed to be same [50], [58], [97].

As the proposed methodology considered different driving patterns simultaneously, the final battery SOC was maintained after the end of the last driving pattern. For example, if 5 driving patterns were considered and the initial battery SOC at the start of the 1st driving pattern was 0.7, then the final battery SOC was needed to be maintained within <0.5% of the initial battery SOC only after the end of the 5th driving pattern irrespective of the battery SOC at the end of the 1st, 2nd, 3rd, and 4th driving patterns, as shown in Figure 6.5. This was the proposed methodology with first approach (M2A1).

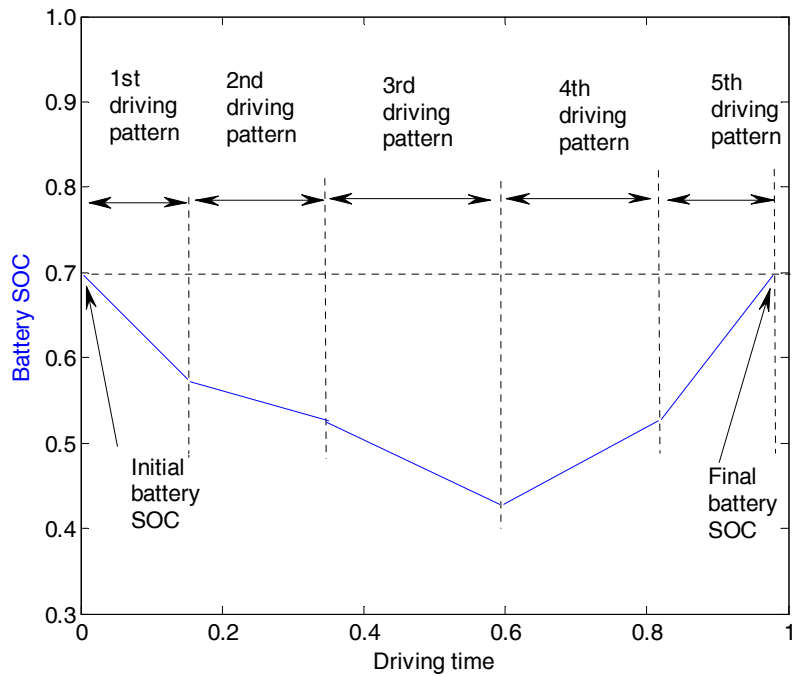


Figure 6.5: Battery SOC for the proposed methodology with first approach (M2A1)

6.4 Vehicle supervisory control strategy

The vehicle supervisory control (VSC) strategy of the Toyota Prius HEV was a rule-based electric-assist charge sustaining control strategy. The control strategy consisted of 4 major operations. These operations were stationary-mode, EV-mode, ICE-mode, and regeneration-mode. These operations consisted of 10 major states, as shown in Table 6.2.

Table 6.2: Rules of VSC strategy of Toyota Prius HEV

Operation	State	Battery	Other conditions	ICE	G	M	Descriptions
Stationary-mode	Stationary	$SOC > SOC_{ICE-ON}$	$V=0$	Off	Off	Off	Vehicle off
	Stationary	$SOC < SOC_{ICE-ON}$	$V=0$	On and at idle speed	On	Off	Charging of battery
EV-mode	Motor only	$SOC \Rightarrow SOC_{EV}$	$0 < V < EV_{MAX}$, $T_D > 0$ and $P_D < P_M$	Off	On	On	Motor provided drive torque
ICE-mode	Charging	$SOC \leq SOC_L$	$T_D > 0$	On	On	Off	ICE supported battery charging
	High demand	$SOC > SOC_L$	$T_D > 0$ and $P_D > P_{HYBRID}$	On	On	On	Both ICE and motor provided drive torque
	ICE only	$SOC \Rightarrow SOC_L$	$T_D > 0$ and $P_D < P_{HYBRID}$	On	On	Off	ICE operated on optimum operating torque and supported battery charging
Regeneration-mode	Regeneration at low speed	$SOC \leq SOC_H$	$V_{REGEN} < V < EV_{MAX}$	Off	On	On	Regenerative braking
	Regeneration at high speed	$SOC \leq SOC_H$	$V \Rightarrow EV_{MAX}$	Off and at idle speed	On	On	Regenerative braking
	Regeneration at high SOC	$SOC > SOC_H$	$T_D < 0$				No regenerative braking
	Regeneration at very low speed		$T_D < 0$ and $V < V_{REGEN}$				No regenerative braking

Where,

- ICE: Internal combustion engine
- G: Generator
- M: Motor
- SOC_L : Low battery SOC below which motor did not operate

- SOC_{EV} : Minimum battery SOC above which motor-only operation (i.e., only motor provided torque for propulsion) permitted
- SOC_{ICE-ON} : Battery SOC below which the battery was charged while vehicle was at stationary
- SOC_H : Battery SOC above which no regeneration
- V : Speed of vehicle
- EV_{MAX} : Maximum vehicle speed below which motor-only operation permitted
- V_{REGEN} : Velocity below which no regeneration
- P_D : Power demand of vehicle
- T_D : Torque demand of vehicle
- P_M : Maximum power of motor
- P_{HYBRID} : Power demand above which ICE and motor operated together

The default values of all the major parameters of the VSC strategy of the Toyota Prius are shown in Table 6.3.

Table 6.3: Major parameters of VSC strategy of Toyota Prius

Parameters	Value
SOC_L	0.30
SOC_{EV}	0.45
SOC_{ICE-ON}	0.50
SOC_H	0.75
EV_{MAX}	12.5 m/s
V_{REGEN}	4.47 m/s
P_{HYBRID}	25 kW
Initial battery SOC	0.70

As the final battery SOC needed to be maintained within <0.5% of the initial battery SOC (0.7) and the target SOC needed to be maintained close to the minimum charging resistance [57], [98] which was minimum at battery SOC of 0.55 and almost constant after 0.55, the target SOC was fixed at 0.7.

6.5 Optimisation problem formulation

The problem was defined as a constraint optimisation problem where four powertrain components were optimised with the objective of minimum FE without sacrificing vehicle performance. The problem was formulated as follows.

Minimise, $f(x)$, $x \in X$

Satisfy, $h_i(x) \leq 0$, $i = 1, 2, \dots, N$

Where,

x is the solution to the problem within the design limits X

X is the upper and lower limits of the design variables

$f(x)$ is the objective function

$h_i(x)$ are constraints

N is the number of constraints

6.6 Optimisation method

A simple genetic algorithm (GA) known as canonical GA, as discussed in chapter 2 was used as the optimisation method for this study due to the potential of GA in solving optimisation problems related to powertrain component sizes of HEVs, as found in the reviewed literature in chapter 3. Each optimisation variable was consisted of 8 bits. Single point crossover was used and the crossover probability was considered as 0.9. The mutation probability was considered as 0.15. The roulette wheel method was used as the selection method. The population size was considered

50. The number of generation was considered 250 as there was little improvement of results after 200 generations. The total number of generations was considered as optimisation termination criterion i.e., optimisation terminated after 250 generations.

Since the GA is stochastic in nature, each optimisation trial does not show the same result and there is no simple method to verify for a component size optimisation problem whether the solution reaches a global optimum. Therefore, the optimisation trial for each design was carried out 10 times and the optimum design with the minimum FE value was presented as the result.

6.6.1 Integration of optimisation method with vehicle simulation model

This study used model-in-loop approach for the integration of the vehicle simulation model and optimisation method due to its use in similar type of application found in the reviewed literature. The model-in-loop approach is shown in Figure 6.6. The optimisation method (GA) was coupled with the vehicle simulation model of the Toyota Prius. In each optimisation run, the optimisation method produced new sizes of powertrain components and FE of that combination of components was evaluated through the vehicle simulation model. After the evaluation of FE, the optimisation termination criterion was checked. If the termination criterion was not satisfied, the optimisation method produced new sizes of components and the procedure continued until the termination criterion was satisfied. Once the termination criterion was satisfied, the procedure reached the optimum sizes of powertrain components.

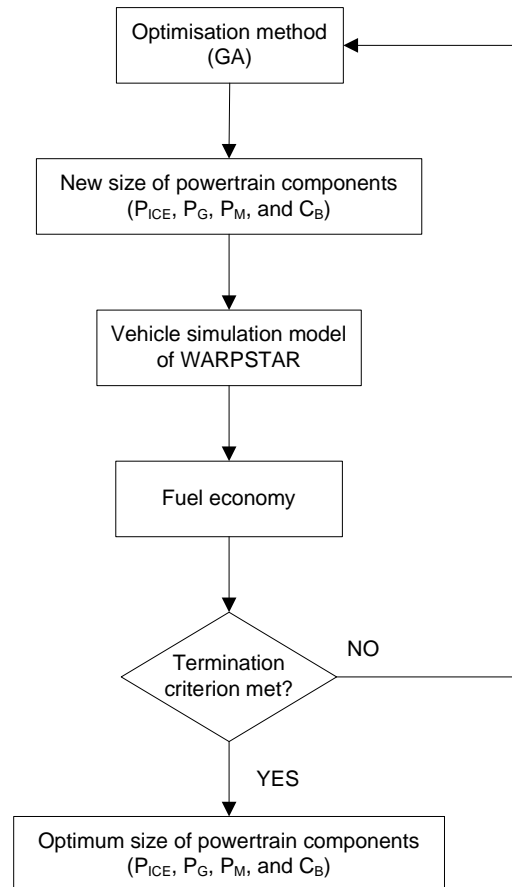


Figure 6.6: Model-in-loop approach: integration of optimisation method with vehicle simulation model

The computer code for the optimisation method (GA) as well as the integration of the optimisation method with WARPSTAR was written in MATLAB scripts. As WARPSTAR was based on MATLAB, it was convenient to use the same environment for the optimisation method also.

6.7 Optimum design

The discussion in the previous chapters shows that the traditional methodology (M1) considers a single driving pattern, whereas the proposed methodology (M2) considers a range of driving patterns representing different traffic conditions and

driving styles simultaneously to represent real-world driving more realistically for the optimisation of powertrain component sizes. Therefore, classification of driving patterns into different traffic conditions and driving styles were required for the proposed methodology.

6.7.1 Proposed methodology: classification of driving patterns

The standard driving patterns were categorised into different traffic conditions and driving styles. For this study, the traffic conditions were categorised into urban and highway. Each traffic condition was further classified into three driving styles, namely, conservative, normal, and aggressive driving. The study considered one normal urban driving pattern – FTP-75, one aggressive urban driving pattern – LA92, one normal highway driving pattern – HWFET, one aggressive highway driving pattern – US06 and one conservative driving pattern – NEDC which consisted of urban (ECE15) as well as highway (EUDC) driving. These driving patterns were chosen following the reviewed literature [49-60] in similar type of application discussed in chapter 3. The driving patterns were classified as per driving parameters [52], [78], [99], [100]. The driving time spent for acceleration and deceleration, the maximum acceleration, and the maximum speed were considered as the parameters for the categorisation of driving patterns as acceleration and the maximum speed could affect FE [42], [101]. The categorised driving patterns are shown in Table 6.4 and figures are shown in Appendix B.

Table 6.4: Classifications of standard driving patterns

Driving parameters	Standard driving patterns				
	Conservative	Normal		Aggressive	
	Urban + Highway	Urban	Highway	Urban	Highway
	NEDC	FTP-75	HWFET	LA92	US06
Total distance, miles	6.8	11.1	10.3	9.8	8.0
Total time, seconds	1180	1874	765	1435	596
Driving time, seconds	939	1633	764	1258	583
Drive time spent accelerating, seconds	278	683	264	587	216
Drive time spent decelerating, seconds	204	574	210	509	214
Driving time accelerating, %	29.6	41.8	34.6	46.7	37.1
Driving time decelerating, %	21.7	35.2	27.5	40.5	36.7
Maximum acceleration, m/s ²	1.07	1.48	1.43	3.08	3.76
Maximum speed, mph	74.6	56.6	59.9	66.7	80.1

Where,

$$\text{Driving time accelerating, \%} = \frac{\text{Drive time spent accelerating}}{\text{Driving time}} * 100$$

$$\text{Driving time decelerating, \%} = \frac{\text{Drive time spent decelerating}}{\text{Driving time}} * 100$$

Although real-world driving consists of more types of driving patterns, in order to evaluate the potential of both the proposed and traditional methodologies the above-mentioned 5 different driving patterns which include different traffic conditions (urban and highway) and driving styles (conservative, normal, and aggressive) could be considered as a representation of real-world driving for an initial study. As the main purpose of this study was to investigate the potential of the proposed methodology compared to the traditional methodology, the above mentioned five

driving patterns which were considered systematically can be considered as sufficient for this initial study. As the proposed methodology is not restricted to any number of driving patterns, if the methodology works for five driving patterns of different traffic conditions and driving styles, it should work for any number of driving patterns as well.

6.7.2 Proposed methodology: consideration of driving patterns

The proposed methodology (M2) considered all the categorised driving patterns, namely, NEDC, FTP, HWFET, LA92, and US06, simultaneously for the optimisation of powertrain component sizes. As the M2 methodology considered a range of different driving patterns simultaneously, the effect of different sequence of the driving patterns needed to be investigated.

6.7.2.1 Proposed methodology: sequence of driving patterns

In order to evaluate the effect of the sequence of driving patterns on the proposed methodology (M2), different sequences of the 5 standard driving patterns (NEDC, FTP, HWFET, LA92, and US06) were considered. The 5 driving patterns could be arranged in 120 different combinations. Among them, 5 combinations were selected where the last driving patterns were the NEDC, FTP, LA92, HWFET, and US06, respectively. The chosen combinations of driving patterns were termed as C1 to C5. The sequence of driving patterns in each combination is as per the order shown in Table 6.5. For example, in case of the C1 combination, the 1st driving pattern was HWFET, the 2nd driving pattern was FTP, the 3rd driving pattern was LA92, the 4th pattern was US06, and the 5th driving pattern was NEDC, as shown in Table 6.5 and Figure 6.7.

Table 6.5: Combinations of driving patterns for proposed methodology

Combination of driving patterns	Sequence of driving patterns				
	First	Second	Third	Fourth	Fifth
C1	HWFET	FTP	LA92	US06	NEDC
C2	NEDC	HWFET	LA92	US06	FTP
C3	NEDC	HWFET	FTP	US06	LA92
C4	NEDC	FTP	LA92	US06	HWFET
C5	NEDC	HWFET	FTP	LA92	US06

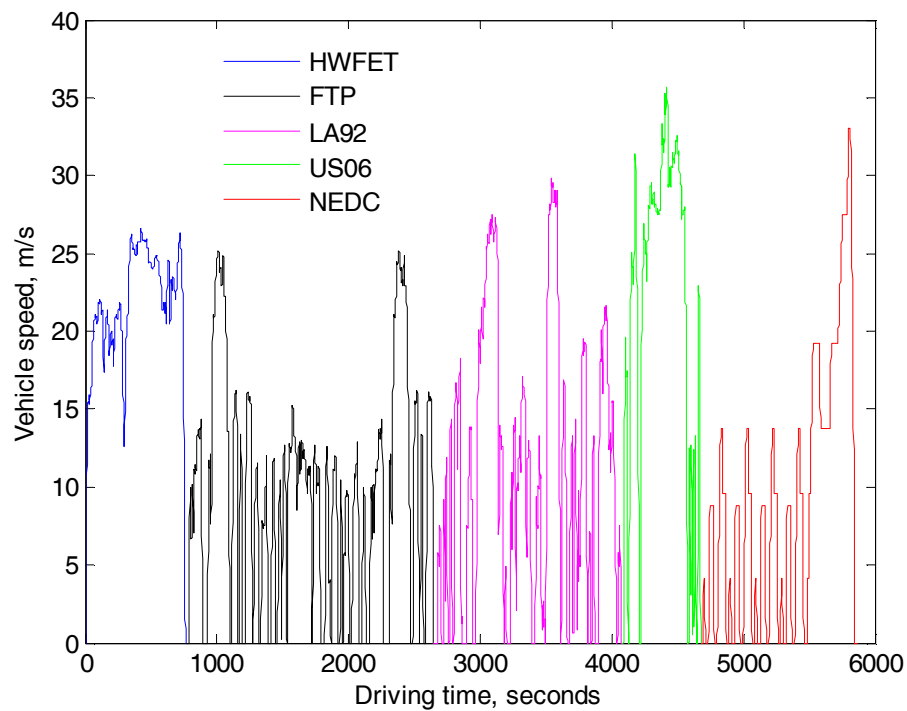


Figure 6.7: Sequence of driving patterns for C1 combination

6.7.3 Traditional methodology: consideration of driving patterns

The traditional methodology (M1) considered each of the 5 driving patterns (NEDC, FTP, HWFET, LA92, and US06) separately for the optimisation of powertrain

component sizes. The M1 methodology considered the same driving patterns separately to understand the difference in the performance between considering a single driving pattern against considering a range of driving patterns simultaneously.

6.8 Driving patterns

For the investigation of the traditional (M1) and proposed (M2) methodologies over standard and real-world conditions, the standard and real-world driving patterns considered for this study are discussed next.

6.8.1 Standard driving patterns

For the investigation over standard conditions, NEDC, FTP, LA92, HWFET, and US06 driving patterns discussed in Table 6.4 were considered.

6.8.2 Real-world driving patterns

For the investigation over standard conditions, the proposed methodology (M2) considered the same driving patterns that were used for the optimisation. Therefore, the M2 methodology needed to be validated over driving patterns that were not used in the optimisation. For complete generality these driving patterns were selected to be real-world driving patterns. The optimum design produced by the M2 methodology needed to be validated in real-world driving for more applicability in practical application.

Speed-time data of a conventional vehicle for 10 drivers was considered as data for real-world driving patterns. Data was logged for a previously completed project conducted by WMG, the University of Warwick, UK over a predefined route consisting of urban and highway driving [102-104]. The route started from the

University of Warwick, then passed through Kenilworth, Leamington Spa, and Coventry, and finally finished at the University of Warwick, as shown in Figure 6.8.

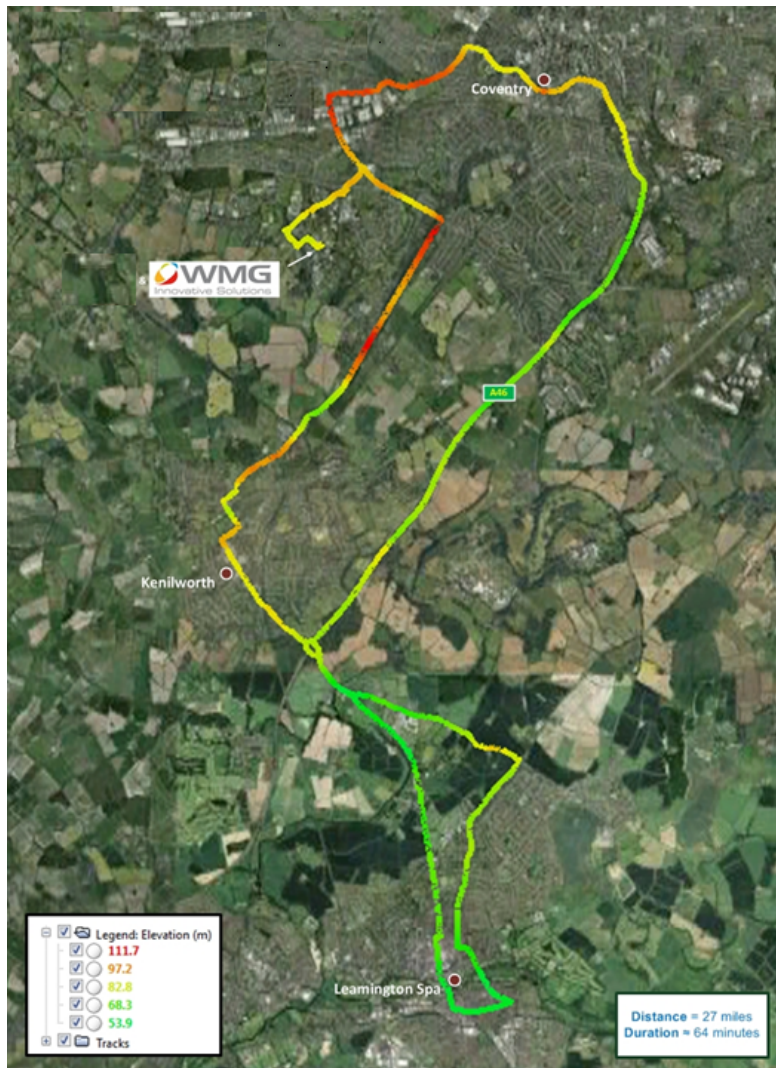


Figure 6.8: Route for real-world driving

Although the data was collected for a conventional vehicle, the data was valid for a HEV also with the assumption that driving patterns were independent of the type of vehicles. The assumption was quite valid with the perspective that standard legislative driving patterns were also used for all type of vehicles i.e., standard legislative driving patterns (NEDC, FTP etc.) are also independent of the type of

vehicles. Although real-world driving may consist of different type of driving, the 10 different driving patterns could be considered for an initial study to establish the potential of the proposed methodology for the application in real-world driving conditions. The parameters of the 10 driving patterns are shown in Table 6.6 and figures of the driving patterns are shown in Appendix B.

Table 6.6: Driving parameters of real-world driving patterns

Driving parameters	Real-world driving patterns									
	D1	D2	D3	D4	D5	D6	D7	D8	D9	D10
Total distance, miles	27.4	27.4	27.5	27.2	27.4	27.4	27.4	27.4	27.4	27.4
Total time, seconds	3560	4059	3862	3763	3644	4065	3826	3799	3898	4053
Driving time, seconds	3062	3571	3417	3407	3303	3526	3373	3423	3349	3590
Drive time spent accelerating, seconds	1369	1490	1546	1601	1400	1494	1589	1540	1500	1601
Drive time spent decelerating, seconds	1371	1668	1639	1498	1523	1823	1482	1506	1558	1714
Driving time accelerating, %	44.7	41.7	45.2	47.0	42.4	42.4	47.1	45.0	44.8	44.6
Driving time decelerating, %	44.8	46.7	48.0	44.0	46.1	51.7	43.9	44.0	46.5	47.7
Maximum acceleration, m/s ²	3.31	2.85	3.34	2.45	3.40	3.37	2.68	2.39	2.39	2.38
Maximum speed, mph	79.1	77.6	86.9	75.3	83.0	85.6	74.8	74.1	74.2	73.9

6.9 FE evaluation

To compare different optimum designs for FE, the initial and final battery SOC of all the designs were kept same in order to eliminate the effect of battery SOC on FE. The battery SOC is closely related to the operation of ICE which can influence the FE. In this study, the final battery SOC after the evaluation of FE over each driving pattern was maintained within $<0.5\%$ of the initial battery SOC i.e., $\Delta \text{SOC} < 0.5\%$. During the evaluation of FE, the final battery SOC was achieved by controlling the target SOC value of the vehicle supervisory control (VSC) strategy using a separate optimisation.

For the evaluation of FE over standard driving conditions, each optimum design of the traditional (M1) and proposed (M2) methodologies were evaluated over 5 standard driving patterns, namely, NEDC, FTP, LA92, HWFET, and US06. The simulation model of the Toyota Prius HEV (the benchmark vehicle for this study) was also evaluated for FE over the same driving patterns for comparison. The coefficient of variation of FE over the 5 driving patterns was considered as the FE variability. The coefficient of variation was the ratio of the standard deviation to the average.

For the evaluation of FE over real-world driving conditions, each optimum design of the M1 and M2 methodologies were evaluated over 10 real-world driving patterns, as mentioned in Table 6.6. The simulation model of the Toyota Prius HEV (the benchmark vehicle for this study) was also evaluated for FE over the same driving patterns for comparison. The coefficient of variation of FE over the 10 driving patterns was considered as the FE variability.

The evaluation of FE over different driving patterns was helpful to answer whether both the methodologies are applicable under different driving situations. The FE variability data of each optimum design was beneficial to answer whether any FE variability existed among the optimum designs and which design provided the minimum FE variability. The comparative data of the FE variability was helpful in demonstrating the potential improvement of the proposed methodology over the traditional methodology.

6.10 Summary

- A simulation model of a series-parallel Toyota Prius HEV was considered for investigations.
- The Toyota Prius was considered as the benchmark vehicle for comparison.
- The Toyota Prius used a rule-based electric assist charge sustaining control strategy.
- Four powertrain components, namely, ICE, generator, motor, and battery were considered for the optimisation.
- The maximum power of the ICE, generator, and motor, and the maximum capacity of the battery were considered as the optimisation variables and the minimisation of FE was the objective of the optimisation.
- The acceleration (0~60 mph), maximum speed, gradeability, and delta SOC were considered as design constraints.
- GA was considered as the optimisation method.
- The standard driving patterns were categorised into two traffic conditions (urban and highway) and each traffic condition was further categorised into three driving styles (conservative, normal, and aggressive).

- One normal urban driving pattern – FTP-75, one aggressive urban driving pattern – LA92, one normal highway driving pattern – HWFET, one aggressive highway driving pattern – US06 and one conservative driving pattern – NEDC which consists of urban (ECE15) as well as highway (EUDC) were considered.
- The traditional methodology considered each aforementioned 5 standard driving pattern separately and the proposed methodology considered all the driving patterns simultaneously for the optimisation.
- For the investigation over standard conditions, NEDC, FTP, LA92, HWFET, and US06 driving patterns were considered.
- For the validation of the proposed methodology over real-world driving conditions, 10 real-world driving patterns over a predefined route consisting of urban and highway driving patterns were considered. The Toyota Prius and optimum designs of the traditional methodology were also evaluated over the same real-world driving patterns for comparison.
- During the optimisation of powertrain component sizes over each driving pattern, the target SOC value was fixed at 0.7.
- During FE evaluation of an optimum design over driving patterns other than the driving pattern over which the design was optimised, the target SOC was varied to achieve the desired final battery SOC (<0.5% of the initial battery SOC).

CHAPTER 7

EVALUATION OF TRADITIONAL METHODOLOGY

This chapter discusses the evaluation of the traditional methodology for its potential to reduce FE variability due to the variation in driving patterns. The traditional methodology was investigated over 5 standard driving patterns discussed in chapter 6 for the optimisation of powertrain component sizes considering each driving pattern separately. The optimum designs produced by the traditional methodology and the simulation model of the Toyota Prius HEV (benchmark vehicle) were evaluated for FE over the same standard driving patterns to compare the FE variability of each optimum design. This chapter first discusses the optimum designs produced by the traditional methodology followed by the performance of the optimum designs in comparison to the benchmark vehicle. Next the battery SOC, FE, and FE variability of the optimum designs over the standard driving patterns are discussed in comparison to the benchmark vehicle.

7.1 Optimum designs of traditional methodology

The traditional methodology (M1) considered NEDC, FTP, LA92, HWFET, and US06 driving patterns separately for the optimisation of four powertrain components, namely, the ICE, generator, motor, and battery.

The optimisation variables for this study were as follows.

- Maximum power of ICE (P_{ICE})
- Maximum power of generator (P_G)
- Maximum power of motor (P_M)
- Maximum capacity of battery (C_B)

The optimum component sizes over each of the 5 driving patterns are shown in Table 7.1. The M1 methodology failed to obtain an optimum design over HWFET. The optimum designs over NEDC, FTP, LA92, and US06 are termed as M1-NEDC, M1-FTP, M1-LA92, and M1-US06, respectively.

Table 7.1: Component sizes for optimum designs of M1 methodology

Driving pattern	Design	Optimum component sizes			
		P_{ICE}	P_G	P_M	C_B
NEDC	M1-NEDC	29.91 kW	12.12 kW	43.91 kW	6.98 Ah
FTP	M1-FTP	37.92 kW	14.13 kW	39.53 kW	8.88 Ah
LA92	M1-LA92	35.31 kW	15.22 kW	42.73 kW	8.79 Ah
US06	M1-US06	38.53 kW	17.34 kW	39.81 kW	7.89 Ah
HWFET		Failed to obtain optimum component sizes			
	<i>Variation in optimum sizes, %</i>	22.37	30.10	9.97	21.40
	Toyota Prius (Benchmark)	43.0 kW	15.0 kW	30.0 kW	6.0 Ah

Where,

Variation in optimum sizes, %

$$= \frac{\text{Max size}(M1 - NEDC \text{ to } M1 - US06) - \text{Min size}(M1 - NEDC \text{ to } M1 - US06)}{\text{Max size}(M1 - NEDC \text{ to } M1 - US06)} * 100$$

The optimum power of the ICE of the M1-NEDC, M1-FTP, M1-LA92, and M1-US06 designs were lower by 30.4, 11.8, 17.9, and 10.4%, respectively compared to that of the Toyota Prius. The optimum ICE power of the 4 designs ranged from 29.91 kW to 38.53 kW, and hence, the variation in the optimum ICE power over the 4 driving patterns (NEDC, FTP, LA92, and US06) was 22.37%, as shown in Table 7.1. Among all the optimum designs of the M1 methodology, the M1-US06 design had the highest and the M1-NEDC design had the lowest power of the ICE.

The optimum power of the generator of the M1-NEDC and M1-FTP designs were 19.2 and 5.8% lower, but the optimum power of the generator of the M1-LA92 and M1-US06 designs were 1.5 and 15.6% higher compared to that of the Toyota Prius. The optimum generator power of the 4 designs ranged from 12.12 kW to 17.34 kW and hence, the variation in the optimum generator power over the 4 driving patterns was 30.1%, as shown in Table 7.1. Among all the optimum designs of the M1 methodology, the M1-US06 design had the highest and the M1-NEDC design had the lowest power of the generator.

The optimum power of the motor of the M1-NEDC, M1-FTP, M1-LA92, and M1-US06 designs were 46.4, 31.8, 42.4, and 32.7%, respectively higher compared to that of the Toyota Prius. The optimum motor power of the 4 designs ranged from 39.53 kW to 43.91 kW and hence, the variation in the optimum motor power over the 4 driving patterns was 9.97%, as shown in Table 7.1. Among all the optimum designs of the M1 methodology, the M1-NEDC design had the highest and the M1-FTP design had the lowest power of the motor.

The optimum capacity of the battery of the M1-NEDC, M1-FTP, M1-LA92, and M1-US06 designs were 16.3, 48.0, 46.5, and 31.5%, respectively higher compared to

that of the Toyota Prius. The optimum battery capacity of the 4 designs ranged from 6.98 Ah to 8.88 Ah and hence, the variation in the optimum battery capacity over the 4 driving patterns was 21.4%, as shown in Table 7.1. Among all the optimum designs of the M1 methodology, the M1-FTP design had the highest and the M1-NEDC design had the lowest capacity of the battery.

Due to the stochastic nature of the genetic algorithm (GA), each optimisation trial was conducted 10 times and the optimum component sizes with the minimum FE was presented as the result, as discussed in chapter 6. The variations in the optimum component sizes of each design of the M1 methodology for 10 optimisation trials were within 1.0%, as shown in Table 7.2. The optimum component sizes of each design of the M1 methodology for 10 optimisation trials are shown in Appendix C. The variations in the optimum component sizes over different optimisation trials were due to the stochastic nature of the GA.

Table 7.2: Variation in optimum component sizes for 10 optimisation trials: M1 methodology

Design	Variation in optimum sizes for 10 optimisation trials, %			
	P_{ICE}	P_G	P_M	C_B
M1-NEDC	0.30	0.82	0.75	0.99
M1-FTP	0.47	0.77	0.80	0.90
M1-LA92	0.54	0.91	0.70	0.80
M1-US06	0.13	0.80	0.70	0.89

As the variations in the ICE, generator, motor, and battery sizes for the M1-NEDC, M1-FTP, M1-LA92, and M1-US06 designs were 22.37, 30.1, 9.97, and 21.4%, respectively, as shown in Table 7.1, it can be concluded that each design of the M1 methodology was a completely different design, as found in the reviewed literature

in chapter 3. Hence, the M1 methodology provided 4 different optimum designs, namely, M1-NEDC, M1-FTP, M1-LA92, and M1-US06 over NEDC, FTP, LA92, and US06, respectively.

7.2 Performance of optimum designs

The performance of the M1-NEDC, M1-FTP, M1-LA92, and M1-US06 designs are shown in Table 7.3. The M1-NEDC, M1-FTP, M1-LA92, and M1-US06 designs reduced the time of acceleration (0~60 mph) by 13.4, 13.4, 16.4, and 14.2%, respectively compared to the Toyota Prius, as shown in Table 7.3. The M1-NEDC, M1-FTP, M1-LA92, and M1-US06 designs improved the maximum speed by 0.4, 2.1, 2.4, and 2.6%, respectively compared to the Toyota Prius. The M1-NEDC, M1-FTP, M1-LA92, and M1-US06 designs improved the gradeability by 1.4, 7.2, 8.0, and 8.7%, respectively compared to the Toyota Prius.

Table 7.3: Performance of optimum designs: Toyota Prius and M1 methodology

Performance	Toyota Prius	M1 methodology			
		M1-NEDC	M1-FTP	M1-LA92	M1-US06
Acceleration (0~60 mph), seconds	13.4	11.6	11.6	11.2	11.5
Acceleration (0~60 mph) w.r.t. Prius, %		-13.4	-13.4	-16.4	-14.2
Maximum speed, mph	113.3	113.7	115.7	116.0	116.2
Maximum speed w.r.t. Prius, %		0.4	2.1	2.4	2.6
Gradeability, %	13.8	14.0	14.8	14.9	15.0
Gradeability w.r.t. Prius, %		1.4	7.2	8.0	8.7

Where,

$$w.r.t. Prius, \% = \frac{Parameter_{Design} - Parameter_{Prius}}{Parameter_{Prius}} * 100$$

The improvement of the performances were due to 1.1, 6.1, 6.9, and 7.3% higher combined power of the ICE and motor of the M1-NEDC, M1-FTP, M1-LA92, and M1-US06 designs compared to the Toyota Prius, as shown in Table 7.4. The M1-US06 design showed the highest improvement in the maximum speed and gradeability among all the optimum designs of the M1 methodology compared to the Toyota Prius due to its highest combined power of the ICE and motor among all the designs of the M1 methodology, as shown in Table 7.4. The M1-LA92 design had the lowest time of acceleration. Although the M1-LA92 design had 0.4% lower combined power of the ICE and motor compared to the M1-US06 design, the M1-LA92 design had 2.6% lower time of acceleration compared to the M1-US06 design. This was due to 7.3% higher motor power of the M1-LA92 design compared to the M1-US06 design.

Table 7.4: Combined power of ICE and motor: Toyota Prius and M1 methodology

Combined power	Toyota Prius	M1 methodology			
		M1-NEDC	M1-FTP	M1-LA92	M1-US06
(ICE + Motor), kW	73.0	73.82	77.45	78.04	78.34
(ICE + Motor) w.r.t. Prius, %		1.1	6.1	6.9	7.3

7.3 Reason for failure to achieve an optimum design over HWFET

The probable reason for the failure to obtain an optimum design over HWFET could be insufficient design limits ($\pm 70\%$ of base components) of powertrain components or failure to satisfy design constraints. The first reason of the insufficient design limits could be ruled out as the optimisation method was able to find optimum

designs over more aggressive driving patterns (LA92 and US06) compared to HWFET, as shown in Table 7.1.

Regarding the failure due to the second reason related to constraints, it was required to analyse the constraints used for the study. The study considered four constraints, namely, acceleration, maximum speed, gradeability, and delta SOC. The first three constraints were related to the combined power of the ICE and motor. As the optimisation method was able to find optimum designs over other 4 driving patterns (NEDC, FTP, LA92, and US06), satisfying the first three constraints (acceleration, maximum speed, and gradeability) should not be a problem for HWFET also.

Therefore, there was a possibility that the 4th constraint (delta SOC < 0.5%) was not satisfied over HWFET during the optimisation of powertrain component sizes. As target SOC was a parameter which could influence the battery SOC apart from the ICE, motor, and battery, the value of the target SOC (fixed at 0.7) might influenced the delta SOC.

7.4 FE evaluation over standard driving patterns: Toyota Prius and M1

Each of the 4 designs, namely, M1-NEDC, M1-FTP, M1-LA92, and M1-US06 were evaluated for FE over NEDC, FTP, LA92, HWFET, and US06 driving patterns. Similarly the simulation model of the Toyota Prius was also evaluated over NEDC, FTP, LA92, HWFET, and US06 driving patterns.

During the FE evaluation of an optimum design over the driving patterns other than the driving pattern over which the design was optimised, the target SOC was varied to achieve the desired final battery SOC (within <0.5% of the initial battery SOC i.e., delta SOC < 0.5%), as discussed in section 6.9 of chapter 6.

7.4.1 Battery SOC during FE evaluation: Toyota Prius and M1

The target SOC values of each optimum design to achieve the desired final battery SOC value during the FE evaluation over each driving pattern are shown in Table 7.5.

Table 7.5: Target SOC over driving patterns during FE evaluation: Toyota Prius and M1

Driving pattern	Target SOC				
	Toyota Prius	M1 methodology			
		M1-NEDC	M1-FTP	M1-LA92	M1-US06
NEDC	0.5401	0.7000	0.6001	0.6216	0.5804
FTP	0.6803	0.8235	0.7000	0.7235	0.6961
LA92	0.6604	0.8118	0.6686	0.7000	0.6628
HWFET	0.5502	0.5567	0.5490	0.5549	0.5529
US06	0.6204	0.9900 (x)	0.6843	0.8157	0.7000
(x): Failed to operate charge sustaining					

The minimum and maximum target SOC values of the Toyota Prius were 0.5401 and 0.6803 respectively when compared for all the 5 driving patterns. The minimum target SOC values of the M1-NEDC, M1-FTP, M1-LA92, and M1-US06 designs were 0.5567, 0.5490, 0.5549, and 0.5529, respectively. The maximum target SOC values of the M1-NEDC, M1-FTP, M1-LA92, and M1-US06 designs were 0.99, 0.7, 0.8157, and 0.7, respectively. Therefore, the minimum and maximum target SOC values of the Toyota Prius were lower compared to all the designs of the M1 methodology when compared for all the driving patterns, as shown in Table 7.5. This was probably due to the higher power of the ICE of the Toyota Prius compared to all the designs of the M1 methodology. Due to the higher ICE power, the ICE of the Toyota Prius was able to deliver more torque for charging the battery even after

providing the torque demand of the vehicle and therefore, the Toyota Prius was able to meet the desired final battery SOC with the lower target SOC values.

The final battery SOC values of each optimum design over each driving pattern during FE evaluation are shown in Table 7.6. Table 7.6 shows that all designs except the M1-NEDC design were able to maintain the desired final battery SOC (<0.5% of the initial battery SOC) over all the 5 driving patterns and therefore able to operate as charge sustaining. The final battery SOC of the M1-NEDC design over US06 was 0.6093 (12.9% lower compared to the initial battery SOC) and therefore, the M1-NEDC design failed to operate as charge sustaining over US06. The Toyota Prius was able to operate as charge sustaining over all the 5 driving patterns.

Table 7.6: Final battery SOC over driving patterns during FE evaluation: Toyota Prius and M1

Driving pattern	Final battery SOC				
	Toyota Prius	M1 methodology			
		M1-NEDC	M1-FTP	M1-LA92	M1-US06
NEDC	0.6978	0.6999	0.7008	0.6978	0.6979
FTP	0.6982	0.6986	0.6994	0.6975	0.7002
LA92	0.6985	0.6972	0.6994	0.7001	0.6971
HWFET	0.6995	0.6976	0.6982	0.6997	0.7018
US06	0.6989	0.6093 (x)	0.6995	0.7000	0.6992
(x): Failed to operate charge sustaining					

7.5 FE over standard driving patterns: Toyota Prius and M1

The FE values of the Toyota Prius, M1-NEDC, M1-FTP, M1-LA92, and M1-US06 designs are shown in Table 7.7. The average FE of the Toyota Prius, M1-NEDC, M1-FTP, M1-LA92, and M1-US06 designs were 76.9, 78.2, 80.4, 79.3, and 80.1 mpg, respectively. Therefore, the M1-NEDC, M1-FTP, M1-LA92, and M1-US06 designs had 1.7, 4.6, 3.1, and 4.2%, respectively higher average FE over NEDC, FTP, LA92, and US06, respectively compared to the Toyota Prius, as shown in Table 7.7. Therefore, the optimisation method was able to find better design in terms of average FE over NEDC, FTP, LA92, and US06 compared to the Toyota Prius, as expected considering the reviewed literature in chapter 3.

Table 7.7: FE over standard driving patterns: Toyota Prius and M1

Driving pattern	FE, mpg (miles per gallon)				
	Toyota Prius	M1 methodology			
		M1-NEDC	M1-FTP	M1-LA92	M1-US06
NEDC	83.1	84.2	86.2	85.4	85.1
FTP	68.0	69.1	72.4	72.4	71.0
LA92	57.5	57.1	61.4	60.8	61.3
HWFET	120.3	137.6	127.6	130.3	127.1
US06	55.4	43.0 (x)	54.2	47.7	55.8
<i>Average FE, mpg</i>	76.9	78.2	80.4	79.3	80.1
<i>Average FE w.r.t. Prius, %</i>		1.7	4.6	3.1	4.2
<i>Standard Deviation of FE, mpg</i>	23.8	32.7	26.0	28.4	25.5
<i>FE variability, %</i>	31.0	41.8	32.3	35.8	31.9
<i>FE variability w.r.t. Prius, %</i>		34.8	4.2	15.5	2.9
(x): Failed to operate charge sustaining					

Where,

$$FE \text{ variability, \%} = \frac{\text{Standard deviation of FE}}{\text{Average FE}} * 100$$

The standard deviation of FE of the Toyota Prius, M1-NEDC, M1-FTP, M1-LA92, and M1-US06 designs were 23.8, 32.7, 26.0, 28.4, and 25.5 mpg, respectively. Therefore, FE variability of the Toyota Prius, M1-NEDC, M1-FTP, M1-LA92, and M1-US06 designs were 31.0, 41.8, 32.3, 35.8, and 31.9%, respectively, as shown in Table 7.7. Hence, the M1-NEDC, M1-FTP, M1-LA92, and M1-US06 designs had 34.8, 4.2, 15.5, and 2.9%, respectively higher FE variability compared to the Toyota Prius, as expected considering the reviewed literature in chapter 3.

The M1-FTP, M1-LA92, and M1-US06 designs had 2.4, 1.4, and 1.2%, respectively higher FE compared to the M1-NEDC design over NEDC. The M1-FTP and M1-US06 had 1.0 and 0.8% higher FE compared to the M1-LA92 design over LA92. This clearly indicated that though the M1-NEDC and M1-LA92 designs were better in terms of average FE compared to the Toyota Prius, the M1-NEDC and M1-LA92 designs were not global optimum over NEDC and LA92 respectively.

The failure to obtain an optimum design over HWFET and inability to obtain global optimum over two driving patterns (NEDC and LA92) indicated that the value of the target SOC might had an influence on the optimum component sizes.

The average FE and FE variability of the M1-NEDC, M1-FTP, M1-LA92, and M1-US06 designs w.r.t. Toyota Prius are shown in Figure 7.1. The average FE and FE variability of the Toyota Prius are shown as the origin of Figure 7.1.

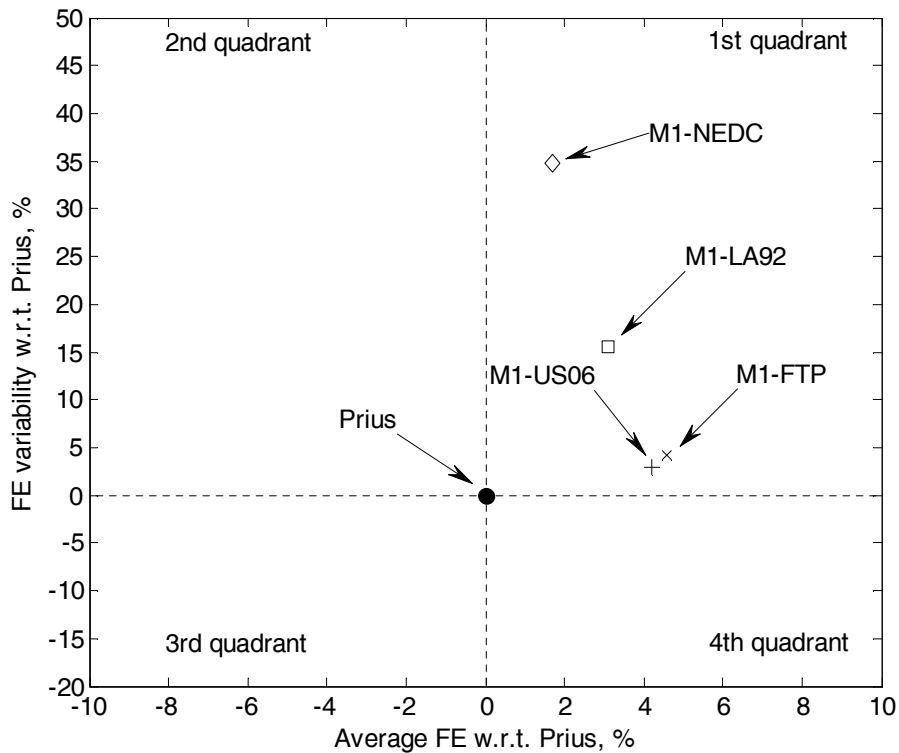


Figure 7.1: Average FE versus FE variability over standard driving patterns: Toyota Prius and M1

All the optimum designs situate in the 1st quadrant in Figure 7.1 as all the designs increased the average FE as well as the FE variability compared to the Toyota Prius. This indicates the same research trend as discussed in chapter 3 that the research in the reviewed literature are more focussed on improving average FE and overlooked the FE variability.

7.6 Summary

- The traditional methodology (M1) failed to provide an optimum design over HWFET.
- The traditional methodology provided 4 different optimum designs over NEDC, FTP, LA92, and US06.

- The optimum designs provided by the traditional methodology, namely, M1-NEDC, M1-FTP, M1-LA92, and M1-US06 designs had 1.7, 4.6, 3.1, and 4.2%, respectively higher average FE compared to the Toyota Prius (benchmark vehicle), as seen in the reviewed literature.
- The traditional methodology failed to provide global optimum designs over NEDC and LA92.
- The M1-NEDC, M1-FTP, M1-LA92, and M1-US06 designs had 34.8, 4.2, 15.5, and 2.9%, respectively higher FE variability compared to the Toyota Prius (benchmark vehicle).
- The traditional methodology failed to reduce FE variability when compared to the simulation model of the benchmark vehicle (Toyota Prius), as expected considering the reviewed literature.
- A reason for the failure to obtain an optimum design over HWFET driving pattern and the global optimum designs over NEDC and LA92 driving patterns might be the choice of the target SOC value which was fixed at 0.7 during the optimisation of powertrain component sizes.

CHAPTER 8

EVALUATION OF TRADITIONAL METHODOLOGY: WITH VARIABLE CONTROL STRATEGY PARAMETER

It has been seen in the previous chapter that the traditional methodology (M1) failed to provide an optimum design over a driving pattern (HWFET) and failed to obtain global optimum design over two driving patterns (NEDC and LA92). The reason for these might be the value of the target SOC which was fixed at 0.7 during the optimisation for all driving patterns. For this reason, this chapter discusses about the evaluation of the M1 methodology considering the target SOC as an optimisation variable along with the variables of the powertrain components. After the optimisation, the optimum designs produced by the M1 methodology and the simulation model of the Toyota Prius HEV (benchmark vehicle) were evaluated for FE over 5 standard driving patterns to compare FE variability of each optimum design. This chapter first discusses the optimum designs produced by the traditional methodology followed by the performance of the optimum designs in comparison to the benchmark vehicle. Next the battery SOC, FE, and FE variability of the optimum designs over the standard driving patterns are discussed in comparison to the benchmark vehicle.

8.1 Optimum designs of traditional methodology

In this study, the target SOC was considered as an optimisation variable along with the powertrain component sizes. All other parameters of the simulation setup described in chapter 6 remained the same.

The optimisation variables for this study were as follows.

- Maximum power of ICE (P_{ICE})
- Maximum power of generator (P_G)
- Maximum power of motor (P_M)
- Maximum capacity of battery (C_B)
- Target SOC

The lower and upper limits for the target SOC were considered as 0.0 and 1.0 respectively.

Four variables of the powertrain components and the target SOC were optimised over NEDC, FTP, LA92, HWFET, and US06 as per the traditional methodology (M1). The optimum designs over the NEDC, FTP, LA92, HWFET, and US06 are termed as M1-NEDC, M1-FTP, M1-LA92, M1-HWFET, and M1-US06, respectively. The optimum parameters of each optimum design of the M1 methodology are shown in Table 8.1.

Table 8.1: Optimum parameters of M1 methodology

Driving pattern	Design	Optimum parameters				
		Component size				Target SOC
		P_{ICE}	P_G	P_M	C_B	
NEDC	M1-NEDC	35.12 kW	13.21 kW	39.93 kW	6.21 Ah	0.5901
FTP	M1-FTP	37.91 kW	14.13 kW	39.52 kW	8.92 Ah	0.7003
LA92	M1-LA92	36.33 kW	13.72 kW	44.41 kW	8.71 Ah	0.6802
HWFET	M1-HWFET	29.32 kW	12.23 kW	44.32 kW	7.33 Ah	0.5701
US06	M1-US06	40.52 kW	18.33 kW	34.82 kW	8.74 Ah	0.6004
	<i>Variation in optimum sizes, %</i>	27.64	33.28	21.59	30.38	
	Toyota Prius (Benchmark)	43.0 kW	15.0 kW	30.0 kW	6.0 Ah	

Where,

Variation in optimum sizes, %

$$= \frac{\text{Max size}(M1 - NEDC \text{ to } M1 - US06) - \text{Min size}(M1 - NEDC \text{ to } M1 - US06)}{\text{Max size}(M1 - NEDC \text{ to } M1 - US06)} * 100$$

The optimum power of the ICE of the M1-NEDC, M1-FTP, M1-LA92, M1-HWFET, and M1-US06 designs were lower by 18.3, 11.8, 15.5, 31.8, and 5.8%, respectively compared to that of the Toyota Prius, as shown in Figure 8.1. The optimum ICE power over the 5 driving patterns ranged from 29.32 kW to 40.52 kW, and hence, the variation in the optimum ICE power over the 5 driving patterns was 27.64%. Among all the optimum designs of the M1 methodology, the M1-US06 design had the highest and the M1-HWFET design had the lowest power of the ICE.

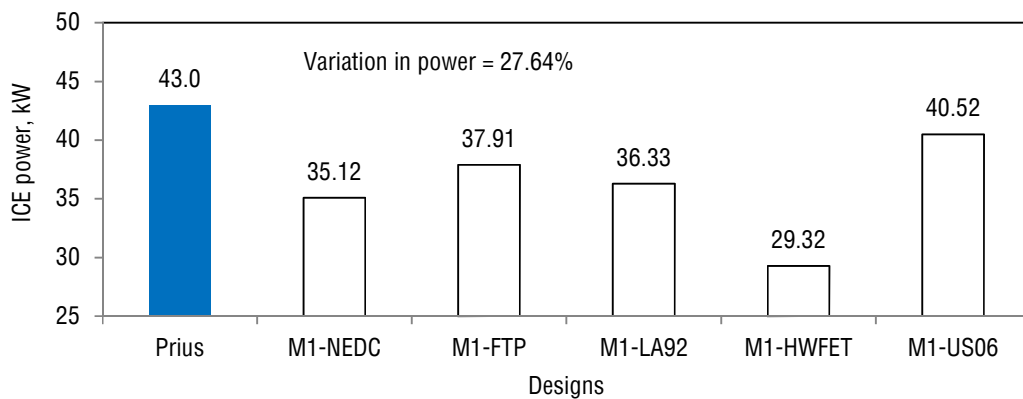


Figure 8.1: Comparison of ICE power: Toyota Prius and M1

The optimum power of the generator of the M1-NEDC, M1-FTP, M1-LA92, and M1-HWFET designs were 12.0, 6.0, 8.7, and 18.7% lower respectively, but the optimum power of the generator of the M1-US06 design was 22.0% higher compared to that of the Toyota Prius, as shown in Figure 8.2. The optimum

generator power over the 5 driving patterns ranged from 12.23 kW to 18.33 kW and hence, the variation in the optimum generator power over the 5 driving patterns was 33.28%. Among all the optimum designs of the M1 methodology, the M1-US06 design had the highest and the M1-HWFET design had the lowest power of the generator.

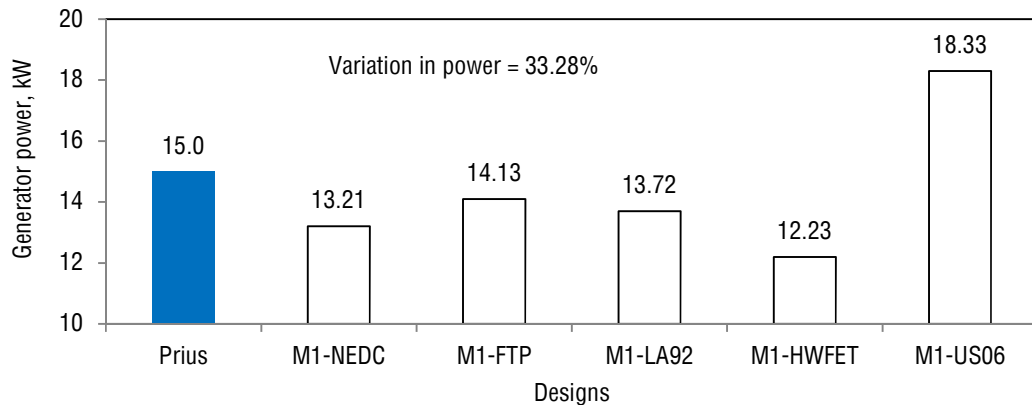


Figure 8.2: Comparison of generator power: Toyota Prius and M1

The optimum power of the motor of the M1-NEDC, M1-FTP, M1-LA92, M1-HWFET and M1-US06 designs were 33.0, 31.7, 48.0, 47.7, and 16.0%, respectively higher compared to that of the Toyota Prius, as shown in Figure 8.3. The optimum motor power over the 5 driving patterns ranged from 34.82 kW to 44.41 kW and hence, the variation in the optimum motor power over the 5 driving patterns was 21.59 %. Among all the optimum designs of the M1 methodology, the M1-LA92 design had the highest and the M1-US06 design had the lowest power of the motor.

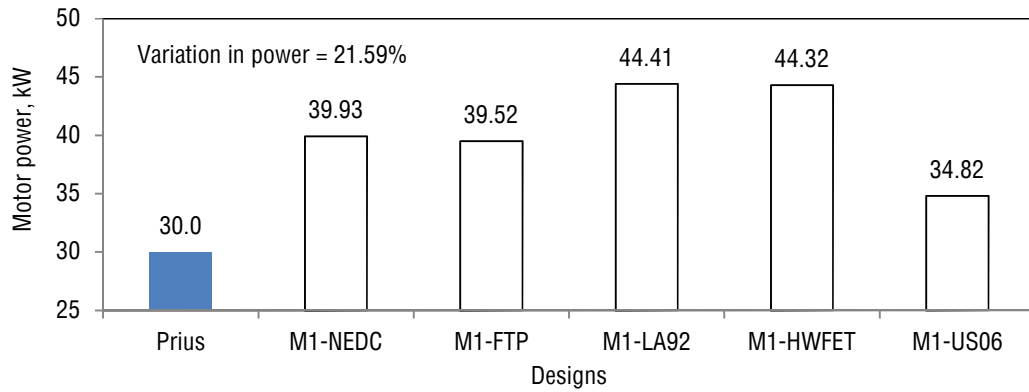


Figure 8.3: Comparison of motor power: Toyota Prius and M1

The optimum capacity of the battery of the M1-NEDC, M1-FTP, M1-LA92, M1-HWFET and M1-US06 designs were 3.3, 48.3, 45.0, 21.7, and 45.0%, respectively higher compared to that of the Toyota Prius, as shown in Figure 8.4. The optimum battery capacity over the 5 driving patterns ranged from 6.21 Ah to 8.92 Ah and hence, the variation in the optimum battery capacity over the 5 driving patterns was 30.38%. Among all the optimum designs of the M1 methodology, the M1-FTP design had the highest and the M1-NEDC design had the lowest capacity of the battery.

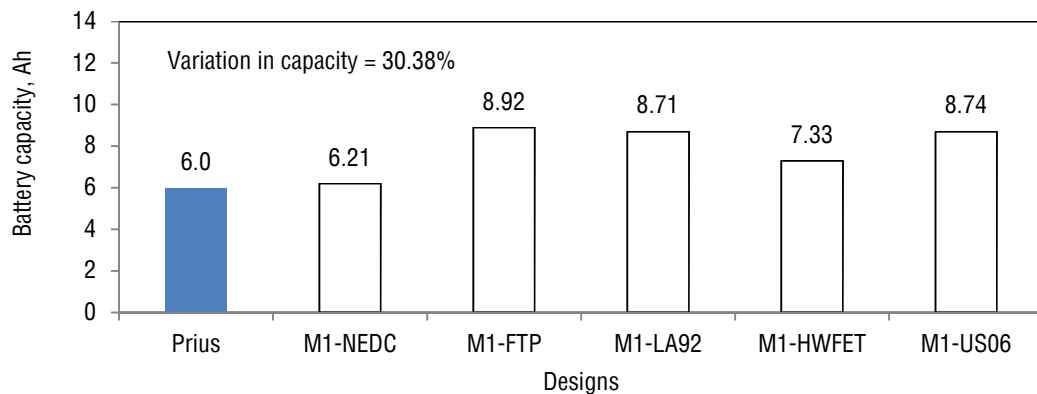


Figure 8.4: Comparison of battery capacity: Toyota Prius and M1

The variation in the ICE, generator, motor, and battery sizes among the 5 optimum designs were 27.64, 33.28, 21.59, and 30.38%, respectively. The variations were increased compared to the variations when the target SOC was fixed at a value 0.7 in chapter 7, as shown in Table 8.2. The variation in the optimum component sizes among the M1-NEDC, M1-FTP, M1-LA92, M1-HWFET, and M1-US06 designs showed that each design was a completely different design, as found in the reviewed literature in chapter 3. Therefore, the M1 methodology provided 5 different optimum designs over the 5 standard driving patterns.

Table 8.2: Variation in component sizes for M1 methodology: fixed and variable target SOC

Variation in component sizes, %	M1 methodology	
	Target SOC: Fixed	Target SOC: Variable
P_{ICE}	22.37	27.64
P_G	30.10	33.28
P_M	9.97	21.59
C_B	21.40	30.38

The optimum values of the target SOC for the M1-NEDC, M1-FTP, M1-LA92, M1-HWFET, and M1-US06 designs during the optimisation were 0.5901, 0.7003, 0.6802, 0.5701, and 0.6004, respectively, as shown in Figure 8.5. The different target SOC values for different optimum designs proved that the target SOC influenced the optimum component sizes, as suspected in chapter 7. The optimum value of the target SOC for the M1-HWFET design was 0.5701, which was lower than the target SOC value (0.7) considered in chapter 7.

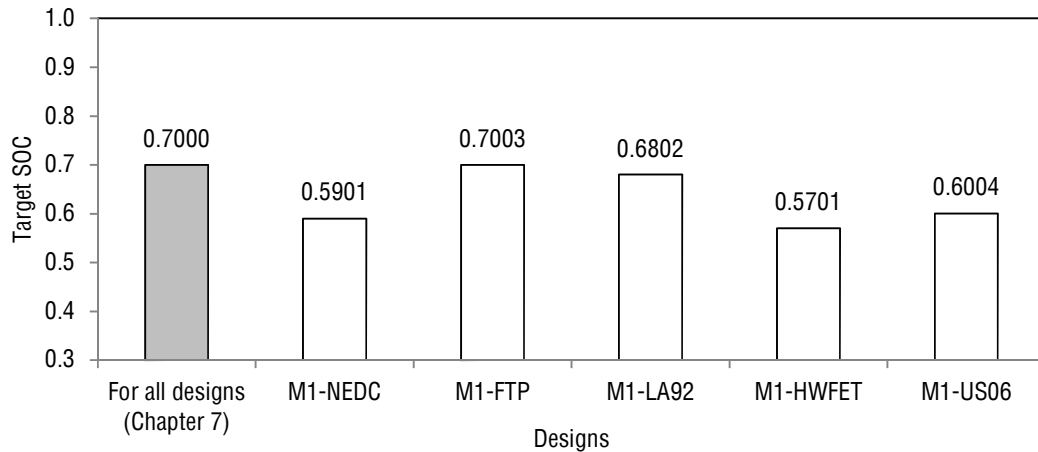


Figure 8.5: Optimum target SOC values: M1 methodology

With the target SOC value of 0.5701, the minimum and maximum battery SOC values of the M1-HWFET design over HWFET were 0.6587 and 0.7542 respectively, as shown in Figure 8.6. The battery SOC was always close to 0.7 as majority of driving time was required to operate at higher speed. The higher speed operation was up to 718 seconds and within remaining 60 seconds speed becomes zero. It showed that the M1-HWFET design got less time for discharge of battery. The final battery SOC value of the M1-HWFET design was 0.7923 with a target SOC value of 0.7, as shown in Figure 8.6. With target SOC value of 0.7, the battery SOC value near 718 seconds over HWFET was higher and during last 60 seconds it was failed to discharge the battery within the desired limits of the final battery SOC, which was <0.5% of the initial battery SOC (0.7). This indicated that a probable reason for the failure to obtain an optimum design over HWFET in chapter 7 was the value of the target SOC which was fixed at 0.7 during the optimisation of powertrain component sizes, as suspected in chapter 7.

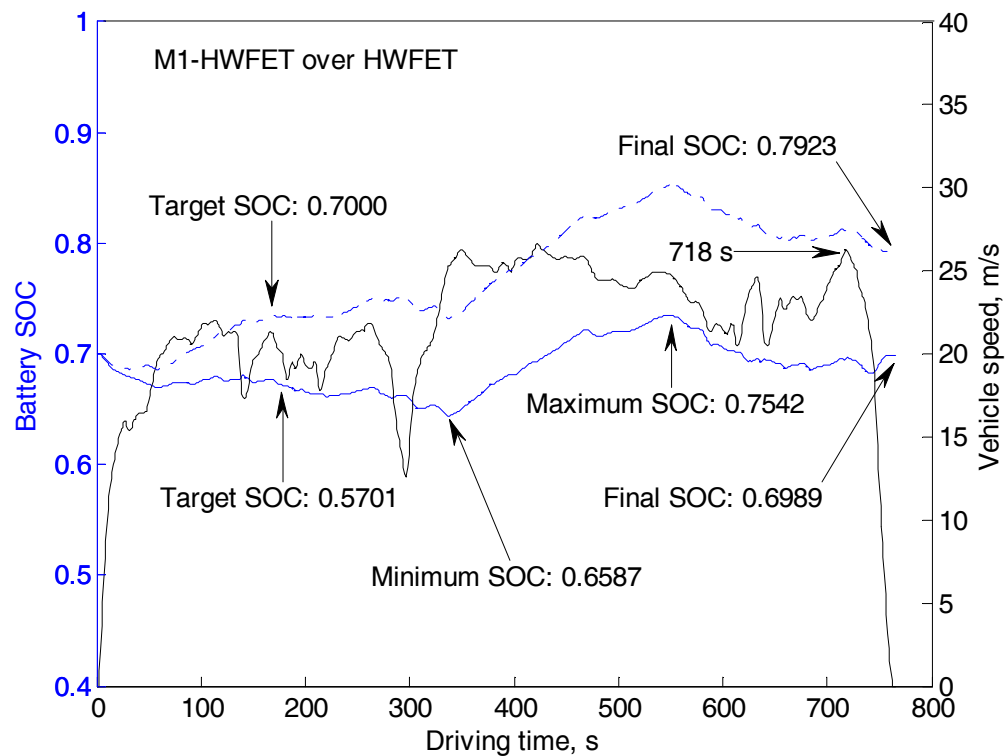


Figure 8.6: Battery SOC of M1-HWFET over HWFET

Although there were difference in the powertrain component sizes of the Toyota Prius compared to the optimum designs of the M1 methodology, the ICE, motor and battery sizes of the Toyota Prius were close to the maximum sizes of ICE, the minimum sizes of motor and the minimum sizes of battery among all the optimum designs of the M1 methodology. The generator size of the Toyota Prius was in between the sizes of the biggest and the smallest generator sizes of the optimum designs of the M1 methodology.

The variations in the ICE, generator, motor, and battery sizes among the five optimum designs produced by the traditional methodology were 27.64, 33.28, 21.59, and 30.38%, respectively. As five different sets of optimum components were found,

it was not clear at this point that which design was the best design for the minimum FE variability, and further FE evaluation of each individual optimum design was required to find the design with the minimum FE variability. Although one design would be the best among all the designs after evaluation, it is not clear whether it would be actually optimum over all the driving patterns rather than just one. As a result, there is a possibility that a design simultaneously optimum over a range of driving patterns might be different than the best design among the five optimum designs based on five separate driving patterns.

8.2 Performance of optimum designs: Toyota Prius and M1

The acceleration (0~60 mph), maximum speed, and gradeability of the simulation model of the Toyota Prius (benchmark vehicle) were considered as constraints for each optimum design. The acceleration, maximum speed, and gradeability of each optimum design compared with the Toyota Prius are shown in Table 8.3.

Table 8.3: Performance of optimum designs: Toyota Prius and M1

Performance	Toyota Prius	M1 methodology				
		M1-NEDC	M1-FTP	M1-LA92	M1-HWFET	M1-US06
Acceleration (0~60 mph), seconds	13.4	11.8	11.6	10.8	11.6	12.4
Acceleration (0~60 mph) w.r.t. Prius, %		-11.9	-13.4	-19.4	-13.4	-7.5
Maximum speed, mph	113.3	114.4	115.7	117.5	113.6	114.6
Maximum speed w.r.t. Prius, %		1.0	2.1	3.7	0.3	1.1
Gradeability, %	13.8	14.3	14.8	15.6	14.0	14.4
Gradeability w.r.t. Prius, %		3.6	7.2	13.0	1.4	4.3

The M1-NEDC, M1-FTP, M1-LA92, M1-HWFET, and M1-US06 designs reduced the time of acceleration (0~60 mph) by 11.9, 13.4, 19.4, 13.4, and 7.5%, respectively when compared to the acceleration of the Toyota Prius. The M1-NEDC, M1-FTP, M1-LA92, M1-HWFET, and M1-US06 designs increased the maximum speed by 1.0, 2.1, 3.7, 0.3, and 1.1%, respectively compared to that of the Toyota Prius. The M1-NEDC, M1-FTP, M1-LA92, M1-HWFET, and M1-US06 designs increased the gradeability by 3.6, 7.2, 13.0, 1.4, and 4.3%, respectively compared to that of the Toyota Prius.

The improvement of the performances were due to 2.8, 6.1, 10.6, 0.9, and 3.2% higher combined power of the ICE and motor of the M1-NEDC, M1-FTP, M1-LA92, M1-HWFET, and M1-US06 designs compared to the Toyota Prius, as shown in Table 8.4.

Table 8.4: Combined power: Toyota Prius and M1

Combined power	Toyota Prius	M1 methodology				
		M1-NEDC	M1-FTP	M1-LA92	M1-HWFET	M1-US06
(ICE + Motor), kW	73.0	75.05	77.43	80.74	73.64	75.34
(ICE + Motor) w.r.t. Prius, %		2.8	6.1	10.6	0.9	3.2

The M1-LA92 design showed the highest improvement in the acceleration, maximum speed and gradeability among all the optimum designs produced by the M1 methodology compared to the Toyota Prius, as shown in Table 8.3. This was due to the highest combined power of the ICE and motor (Table 8.4) and biggest motor power (Table 8.1) of the M1-LA92 design compared to all the designs of the M1 methodology.

8.3 FE evaluation over standard driving patterns: Toyota Prius and M1

Each of the five optimum designs produced by the M1 methodology and the Toyota Prius were evaluated for FE over the NEDC, FTP, LA92, HWFET, and US06 driving patterns separately. During the FE evaluation of an optimum design over the driving patterns other than the driving pattern over which the design was optimised, the target SOC was varied to achieve the desired final battery SOC (within <0.5% of the initial battery SOC i.e., $\Delta \text{SOC} < 0.5\%$), as discussed in section 6.9 of chapter 6.

8.3.1 Battery SOC during FE evaluation: Toyota Prius and M1

The values of the target SOC of each optimum design during the FE evaluation over the NEDC, FTP, LA92, HWFET, and US06 are shown in Table 8.5.

Table 8.5: Target SOC over driving patterns during FE evaluation: Toyota Prius and M1

Driving pattern	Target SOC					
	Toyota Prius	M1 methodology				
		M1-NEDC	M1-FTP	M1-LA92	M1-HWFET	M1-US06
NEDC	0.5401	0.5901	0.5941	0.6098	0.7254	0.5851
FTP	0.6803	0.7216	0.7003	0.7157	0.8471	0.6952
LA92	0.6604	0.7001	0.6686	0.6802	0.8431	0.6633
HWFET	0.5502	0.5529	0.5490	0.5549	0.5701	0.5524
US06	0.6204	0.8725	0.6823	0.7471	0.9900 (x)	0.6004
(x): Failed to operate charge sustaining						

The minimum and maximum target SOC values of the Toyota Prius were 0.5401 and 0.6803 respectively when compared for all the 5 driving patterns. The minimum target SOC values of the M1-NEDC, M1-FTP, M1-LA92, M1-HWFET, and M1-US06 designs were 0.5529, 0.5490, 0.5549, 0.5701, and 0.5524, respectively. The

maximum target SOC values of the M1-NEDC, M1-FTP, M1-LA92, M1-HWFET, and M1-US06 designs were 0.8725, 0.7003, 0.7471, 0.99, and 0.6952, respectively. Therefore, the minimum and maximum target SOC values of the Toyota Prius were lower compared to all the designs of the M1 methodology when compared for all the driving patterns, as shown in Table 7.5. This was probably due to the higher power of the ICE of the Toyota Prius compared to all the designs of the M1 methodology. Due to the higher ICE power, the ICE of the Toyota Prius was able to deliver more torque for charging the battery even after providing vehicle torque demand and therefore, the Toyota Prius was able to meet the desired final battery SOC with the lower target SOC values.

The final battery SOC values of the optimum designs of the M1 methodology and the Toyota Prius over the NEDC, FTP, LA92, HWFET, and US06 during the FE evaluation are shown in Table 8.6.

Table 8.6: Final battery SOC over driving patterns during FE evaluation: Toyota Prius and M1

Driving pattern	Final battery SOC					
	Toyota Prius	M1 methodology				
		M1-NEDC	M1-FTP	M1-LA92	M1-HWFET	M1-US06
NEDC	0.6978	0.6974	0.6968	0.6970	0.7013	0.6998
FTP	0.6982	0.7007	0.6976	0.7002	0.7002	0.7010
LA92	0.6985	0.6994	0.6994	0.6969	0.7020	0.7000
HWFET	0.6995	0.6982	0.6982	0.7016	0.6989	0.6989
US06	0.6989	0.7004	0.6984	0.6999	0.5846 (x)	0.6979
(x): Failed to operate charge sustaining						

It can be seen from Table 8.6 that all optimum designs except the M1-HWFET design were able to operate charge sustaining over the five standard driving patterns i.e., all designs, except the M1-HWFET design were able to achieve the final battery SOC within desired limits (within $<0.5\%$ of the initial battery SOC).

The M1-HWFET design failed to operate in charge sustaining over US06. The final battery SOC was 0.5846 i.e., 17.1% lower than the initial battery SOC even with the maximum possible target SOC (0.99), as shown in Table 8.6. The battery SOC traces of the Toyota Prius and M1-HWFET design over US06 are shown in Figure 8.7 and Figure 8.8 respectively.

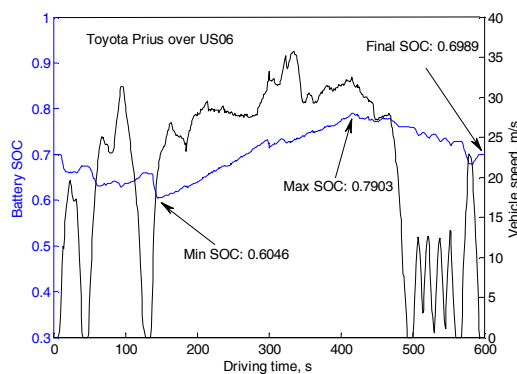


Figure 8.7: Battery SOC of the Toyota Prius over US06

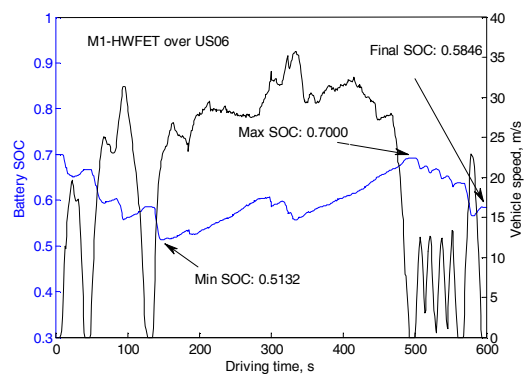


Figure 8.8: Battery SOC of the M1-HWFET design over US06

The probable reason for the failure of the M1-HWFET design to charge the battery was due to its 31.0% lower ICE power compared to the Toyota Prius. Due to low ICE power, the M1-HWFET design was not able to charge the battery up to the desired final battery SOC, whilst simultaneously driving the vehicle.

It can be seen from Figure 8.7 and Figure 8.8 that after 150 seconds over US06, the battery SOC of the Toyota Prius and M1-HWFET design were 0.6066 and 0.5132

respectively. Although after 150 seconds the battery was charged for the M1-HWFET design, it was not able to be charged sufficiently to achieve the desired final battery SOC.

The difference between the battery SOC of the M1-HWFET design and Toyota Prius started after 50 seconds over US06, as shown in Figure 8.9. Both the M1-HWFET design and Toyota Prius were operated at comparatively similar motor torques over US06, as shown in Figure 8.10.

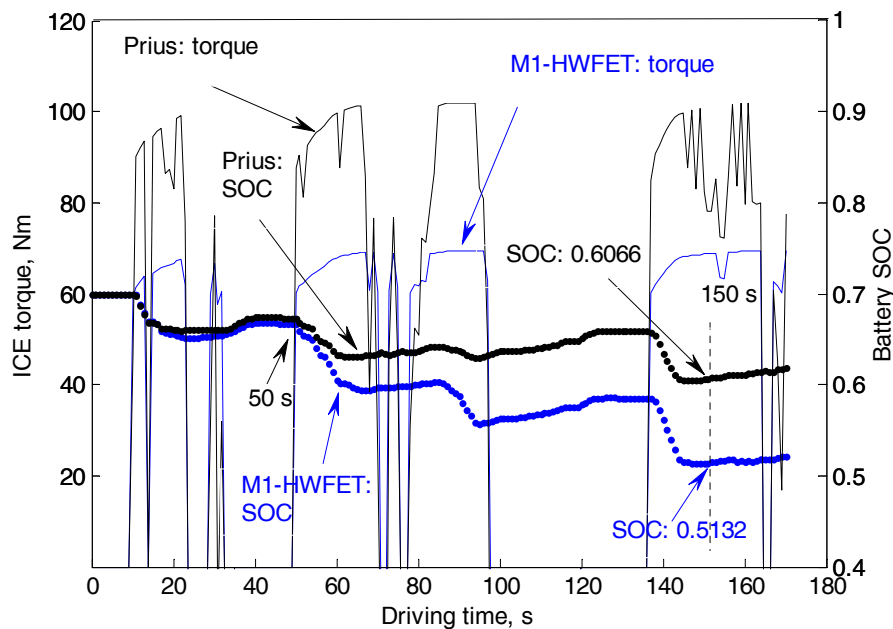


Figure 8.9: Comparison of engine torque and battery SOC over US06: M1-HWFET and Toyota Prius

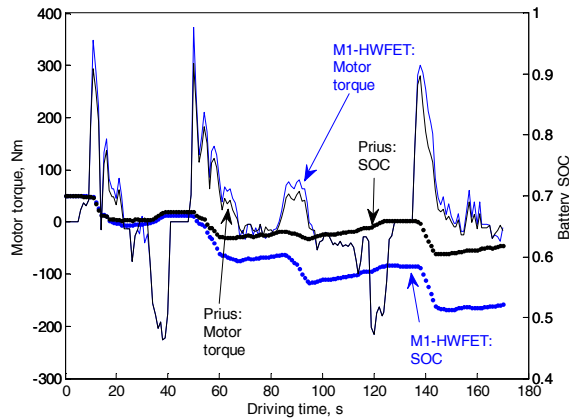


Figure 8.10: Comparison of motor torque and battery SOC over US06: M1-HWFET and Toyota Prius

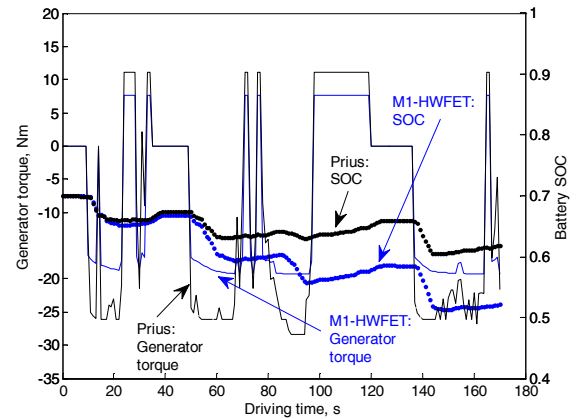


Figure 8.11: Comparison of generator torque and battery SOC over US06: M1-HWFET and Toyota Prius

Due to the ability of the Toyota Prius to operate at higher torque (ICE and generator) that assisted higher battery charging compared to the M1-HWFET design, as shown in Figure 8.9 and Figure 8.11, the Toyota Prius was able to maintain the battery SOC to 0.6046, whereas the battery SOC of the M1-HWFET design was decreased to 0.5132. The maximum battery SOC of the Toyota Prius increased up to 0.7903, whereas the maximum battery SOC of the M1-HWFET design increased up to 0.7, as shown in Figure 8.7 and Figure 8.8 respectively. This battery SOC difference of around 0.1 reflected at the end of US06, i.e., the final battery SOC of the Toyota Prius and M1-HWFET design were 0.6995 and 0.5846 respectively.

Figure 8.8 shows that the M1-HWFET design failed to charge the battery over one US06 driving pattern, but whether the design would be able to charge the battery in a subsequent time over the same driving pattern was unknown. And for that purpose the M1-HWFET design was evaluated over three consecutive US06 driving patterns, as shown in Figure 8.12.

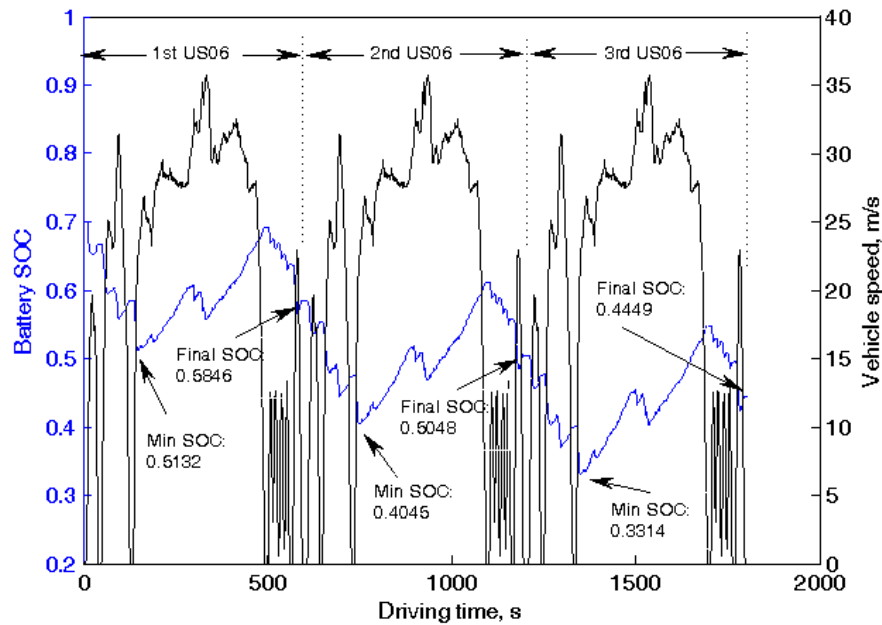


Figure 8.12: Battery SOC of the M1-HWFET design over 3 consecutive US06

The lowest battery SOC values over the 1st, 2nd, and 3rd US06 were 0.5132, 0.4045, and 0.3314, respectively. The final battery SOC values after the 1st, 2nd, and 3rd US06 were 0.5846, 0.5048, and 0.4449, respectively i.e., 17.1, 28.6, and 37.1%, respectively lower when compared to the initial battery SOC. Therefore it can be said that the M1-HWFET design failed to operate in charge sustaining over the driving range. The battery SOC of the design will reduce further by driving continuously over US06. Hence, the M1-HWFET design has higher probability of operating at lower battery SOC and could result in lack of power for acceleration [30] over aggressive highway driving when compared to the Toyota Prius.

The swing of the battery SOC i.e., the difference between the maximum and minimum battery SOC over a driving pattern of each design over the NEDC, FTP, LA92, HWFET, and US06 are shown in Table 8.7.

Table 8.7: Battery SOC swing over standard driving patterns: Toyota Prius and M1

Driving pattern	Parameters	Battery SOC					
		Toyota Prius	M1 methodology				
			M1-NEDC	M1-FTP	M1-LA92	M1-HWFET	M1-US06
NEDC	Maximum SOC	0.7016	0.7000	0.7000	0.7000	0.7030	0.7013
	Minimum SOC	0.5117	0.5315	0.5765	0.5788	0.5832	0.5718
	<i>SOC swing</i>	0.1899	0.1685	0.1235	0.1212	0.1198	0.1295
	<i>Swing w.r.t. Prius, %</i>		-11.3	-34.9	-36.2	-36.9	-31.8
FTP	Maximum SOC	0.7421	0.7458	0.7335	0.7355	0.7417	0.7355
	Minimum SOC	0.5738	0.5878	0.6187	0.6204	0.6190	0.6175
	<i>SOC swing</i>	0.1683	0.1580	0.1148	0.1151	0.1227	0.1180
	<i>Swing w.r.t. Prius, %</i>		-6.1	-31.8	-31.6	-27.1	-29.9
LA92	Maximum SOC	0.7320	0.7374	0.7286	0.7248	0.7185	0.7334
	Minimum SOC	0.6405	0.6281	0.6558	0.6502	0.6274	0.6595
	<i>SOC swing</i>	0.0915	0.1093	0.0728	0.0746	0.0911	0.0739
	<i>Swing w.r.t. Prius, %</i>		19.5	-20.4	-18.5	-0.4	-19.2
HWFET	Maximum SOC	0.7320	0.7298	0.7203	0.7253	0.7354	0.7212
	Minimum SOC	0.6405	0.6413	0.6491	0.6522	0.6430	0.6492
	<i>SOC swing</i>	0.0915	0.0885	0.0712	0.0731	0.0924	0.0720
	<i>Swing w.r.t. Prius, %</i>		-3.3	-22.2	-20.1	1.0	-21.3
US06	Maximum SOC	0.7903	0.8342	0.7643	0.7686	0.7000	0.7518
	Minimum SOC	0.6046	0.5408	0.6024	0.5954	0.5132	0.6067
	<i>SOC swing</i>	0.1857	0.2934	0.1619	0.1732	0.1868	0.1451
	<i>Swing w.r.t. Prius, %</i>		58.0	-12.8	-6.7	0.6	-21.9

The M1-FTP, M1-LA92, and M1-US06 designs always had lower battery SOC swing compared to the Toyota Prius over all the five driving patterns, as shown in Table 8.7. The lower swing of the battery SOC of the three designs might be helpful in terms of battery life [20], [105]. The lower swing of the battery SOC of the three

designs (M1-FTP, M1-LA92, and M1-US06) was probably due to 48.3, 45.0, and 45.0%, respectively higher battery capacity compared to the Toyota Prius.

The M1-NEDC design had 19.5 and 58.0% higher battery SOC swing over aggressive urban (LA92) and highway (US06) driving patterns, respectively compared to the Toyota Prius, as shown in Table 8.7. Although the M1-NEDC design had 3.3% higher battery capacity but 18.3% lower ICE power and 12.0% lower generator power compared to the Toyota Prius probably caused higher battery SOC swing which might reduce the battery life-cycle [20], [105] of the M1-NEDC design over aggressive driving patterns.

8.4 FE over standard driving patterns: Toyota Prius and M1

The FE values of the M1-NEDC, M1-FTP, M1-LA92, M1-HWFET, and M1-US06 designs over the NEDC, FTP, LA92, HWFET and US06 driving patterns are shown in Table 8.8.

All the optimum designs, namely, M1-NEDC, M1-FTP, M1-LA92, M1-HWFET, and M1-US06 showed the highest FE over NEDC, FTP, LA92, HWFET, and US06, respectively, as shown in Table 8.8. Therefore, it could be said that the optimum designs were global optimums over the respective driving patterns. This in contrast to the results found in chapter 7 where it was failed to found global optimums over NEDC and LA92. The FE values of the M1-NEDC design over NEDC, M1-LA92 design over LA92, and M1-US06 design over US06 were 84.2, 60.8, and 55.8 mpg respectively considering a fixed value (0.7) of target SOC, as shown in Table 7.7 of chapter 7. Considering the target SOC as an optimisation variable, the FE values of the M1-NEDC design over NEDC, M1-LA92 design over LA92, and M1-US06 design over US06 became 86.3, 61.5, and 57.1 mpg, respectively, as shown in Table

8.8. The improvement in FE values of the M1-NEDC, M1-LA92, and M1-US06 designs and the ability to find global optimums over NEDC, FTP, LA92, HWFET, and US06 proved that the target SOC influenced the optimum component sizes, as expected in chapter 7.

Table 8.8: FE over standard driving patterns: Toyota Prius and M1

Driving pattern	FE, mpg						FE variation among designs over a driving pattern, %
	Toyota Prius	M1 methodology					
		M1-NEDC	M1-FTP	M1-LA92	M1-HWFET	M1-US06	
NEDC	83.1	86.3	86.2	85.8	79.8	83.4	7.5
FTP	68.0	71.9	72.4	72.2	68.2	70.4	5.8
LA92	57.5	56.9	61.4	61.5	56.1	57.3	8.8
HWFET	120.3	130.5	127.6	129.0	138.4	123.9	10.5
US06	55.4	44.5	54.2	50.8	43.6 (x)	57.1	23.6
<i>Average FE, mpg</i>	76.9	78.0	80.4	79.9	77.2	78.4	4.0
<i>Average FE w.r.t. Prius, %</i>		1.4	4.6	3.9	0.4	2.0	
<i>Standard deviation of FE, mpg</i>	23.8	29.8	26.0	27.2	32.9	24.7	
<i>FE variability, %</i>	31.0	38.2	32.3	34.0	42.6	31.5	
<i>FE variability w.r.t. Prius, %</i>		23.2	4.2	9.7	37.4	1.6	
(x): Failed to operate charge sustaining							

Where,

FE variation among designs over a driving pattern, %

$$= \frac{\text{Max FE}(M1 - NEDC \text{ to } M1 - US06) - \text{Min FE}(M1 - NEDC \text{ to } M1 - US06)}{\text{Max FE}(M1 - NEDC \text{ to } M1 - US06)} * 100$$

The average FE values of the M1-NEDC, M1-FTP, M1-LA92, M1-HWFET, and M1-US06 designs over NEDC, FTP, LA92, HWFET, and US06 were 78.0, 80.4, 79.9, 77.2, and 78.4 mpg, respectively. The standard deviation of FE values of the M1-NEDC, M1-FTP, M1-LA92, M1-HWFET, and M1-US06 designs over the 5 driving patterns were 29.8, 26.0, 27.2, 32.9, and 24.7 mpg, respectively. Therefore, the FE variability values of the M1-NEDC, M1-FTP, M1-LA92, M1-HWFET, and M1-US06 designs over the 5 driving patterns were 38.2, 32.3, 34.0, 42.6 and 31.5%, respectively.

The average FE, standard deviation of FE and FE variability of the Toyota Prius over the 5 driving patterns were 76.9 mpg, 23.8 mpg, and 31.0%, respectively. The M1-NEDC, M1-FTP, M1-LA92, M1-HWFET and M1-US06 designs had 1.4, 4.6, 3.9, 0.4, and 2.0%, respectively higher average FE compared to the Toyota Prius, as shown in Table 8.8. The M1-NEDC, M1-FTP, M1-LA92, M1-HWFET, and M1-US06 designs had 23.2, 4.2, 9.7, 37.4, and 1.6%, respectively higher FE variability compared to the Toyota Prius, as shown in Table 8.8.

The results in Table 8.8 indicated that all the optimum designs based on the M1 methodology were able to improve average FE; however none of the designs were able to reduce FE variability compared to the Toyota Prius, as expected considering the reviewed literature in chapter 3.

The M1-NEDC design showed 3.9, 5.7, and 8.5% higher FE over NEDC, FTP, and HWFET, respectively compared to the Toyota Prius, however, the M1-NEDC design showed second lowest FE over aggressive urban (LA92) as well as highway (US06) driving patterns. The second highest FE variability and second lowest average FE

over aggressive driving patterns made the M1-NEDC design less suitable for aggressive driving patterns.

The M1-HWFET design provided lowest FE over all the driving patterns, except HWFET. The M1-HWFET design had 0.4% higher average FE compared to the Toyota Prius due to its 15.0% higher FE compared to Toyota Prius over HWFET. The M1-HWFET design also had the highest FE variability among all the designs. The highest FE variability, lowest FE over majority of driving patterns (4 out of 5 driving patterns) and failure to operate charge sustaining over aggressive highway driving (US06) indicated that the M1-HWFET design was less suitable for practical application.

The M1-FTP design provided the highest average FE and second lowest FE variability, The M1-LA92 design showed the second highest average FE and third lowest FE variability, and the M1-US06 design provided the third highest average FE and the lowest FE variability among the designs of the M1 methodology.

The average FE and FE variability of the M1-NEDC, M1-FTP, M1-LA92, M1-HWFET, and M1-US06 designs w.r.t. Toyota Prius are shown in Figure 8.13. The average FE and FE variability of the Toyota Prius are shown as the origin of Figure 8.13. All the optimum designs situate in the 1st quadrant in Figure 8.13 as all the designs increased the average FE as well as the FE variability compared to the Toyota Prius. This indicates the same research trend as discussed in chapter 3 that the research in the reviewed literature are more focussed on improving average FE and overlooked the FE variability.

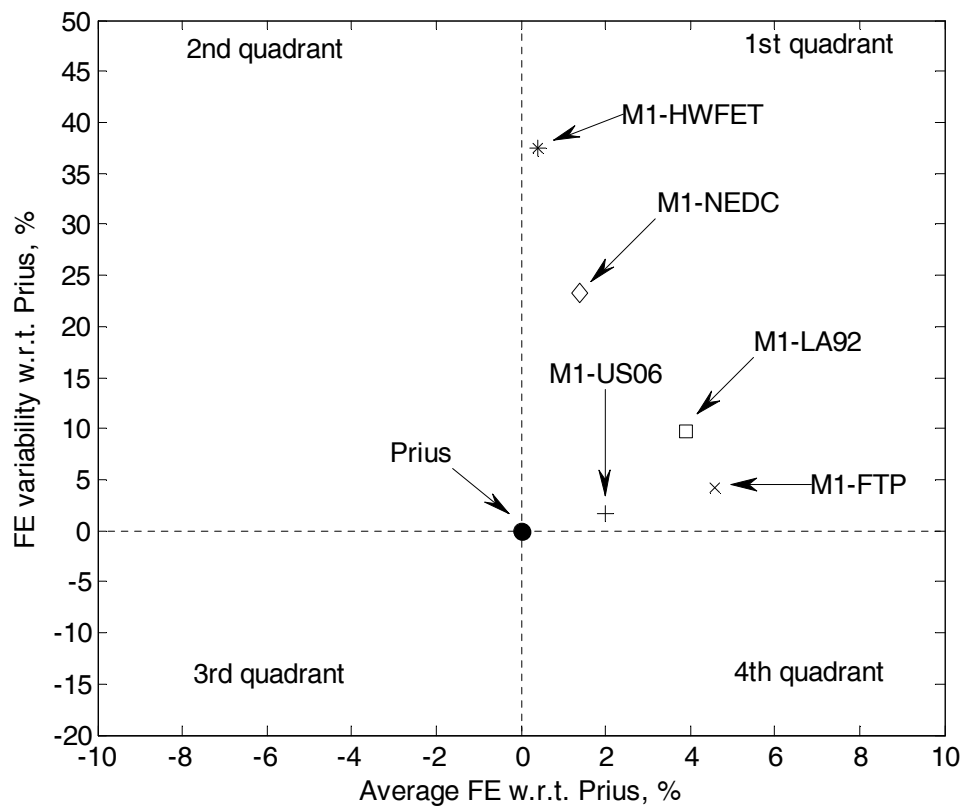


Figure 8.13: Average FE versus FE variability over standard driving patterns: Toyota Prius and M1

As all the five optimum designs of the M1 methodology show completely different FE performance and none of the designs is able to reduce FE variability compared to the Toyota Prius, a further decision making process is required to choose one design from the five designs. As the number of driving patterns increase (as the case in real world conditions), the decision making process would become more complex.

The M1 methodology failed to operate in charge sustaining mode when evaluated over aggressive driving pattern (US06), if the design was based on a normal highway driving (HWFET) and hence, increased the possibility of the lack of power during high demand. The FE variability values of the designs of the M1 methodology

ranged from 31.5 to 42.6%. Both the points indicate that the application of the M1 methodology is limited by the choice of driving patterns. Hence, the M1 methodology cannot be considered as a generalised methodology for the optimisation of powertrain component sizes of HEVs.

8.5 Summary

- The traditional methodology (M1) provided 5 different optimum designs, one for each driving pattern, as seen in the reviewed literature.
- The target SOC influenced the optimum component sizes and it was the reason for the failure to obtain an optimum design over HWFET in chapter 7.
- The consideration of the target SOC as an optimisation variable along with the powertrain components provided global optimum design over each of the 5 driving patterns, namely, NEDC, FTP, LA92, HWFET, and US06.
- A separate decision making process is required to choose a design from the 5 optimum designs for practical applications.
- The optimum designs of the traditional methodology, namely, M1-NEDC, M1-FTP, M1-LA92, M1-HWFET, and M1-US06 designs improved the average FE by 1.4, 4.6, 3.9, 0.4, and 2.0%, respectively compared to the simulation model of the Toyota Prius (benchmark vehicle), as seen in the reviewed literature.
- The M1-NEDC, M1-FTP, M1-LA92, M1-HWFET, and M1-US06 designs had 23.2, 4.2, 9.7, 37.4, and 1.6%, respectively higher FE variability compared to the Toyota Prius (benchmark vehicle).

- The traditional methodology failed to reduce FE variability when compared to the simulation model of the benchmark vehicle (Toyota Prius), as expected considering the reviewed literature.
- The traditional methodology failed to operate charge sustaining over aggressive highway driving pattern (US06) when design was based on normal highway driving pattern (HWFET).
- The applicability of the traditional methodology is limited by the choice of driving patterns and cannot be considered as a generalised methodology for the optimisation of powertrain component sizes of HEVs.

CHAPTER 9

EVALUATION OF PROPOSED METHODOLOGY

As the traditional methodology (M1) failed to reduce FE variability over 5 standard driving patterns in chapter 8, this chapter discusses the evaluation of the proposed methodology. The proposed methodology differed as against the traditional methodology in the way that the driving patterns are considered in the optimisation of powertrain component sizes, as discussed in chapter 5. This chapter compares the proposed methodology with the results of the traditional methodology and the simulation model of the Toyota Prius (benchmark vehicle) found in chapter 8. This chapter first discusses the optimum designs produced by the proposed methodology followed by the performance of the optimum designs over 5 standard driving patterns. Next the battery SOC, FE and FE variability of the optimum designs over the standard driving patterns are discussed.

9.1 Optimum designs of proposed methodology with first approach

The proposed methodology (M2) considered 5 categorised driving patterns (NEDC, FTP, LA92, HWFET, and US06) simultaneously for the optimisation of four powertrain components, namely, the ICE, generator, motor, and battery along with the target SOC.

The optimisation variables for this study were as follows.

- Maximum power of ICE (P_{ICE})
- Maximum power of generator (P_G)
- Maximum power of motor (P_M)
- Maximum capacity of battery (C_B)
- Target SOC

The proposed methodology needed to be checked for different sequence of driving patterns to evaluate the effect of the sequence of driving patterns, as discussed in chapter 6. All the variables were optimised according to the proposed methodology with first approach (M2A1 approach) for 5 different combinations of driving patterns as shown in Table 6.5. In the M2A1 approach, the delta SOC ($<0.5\%$) was controlled after end of the last driving pattern, as discussed in chapter 6 and shown in Figure 6.5 (Repeated below). In this study, the delta SOC was therefore controlled only after the 5th driving pattern.

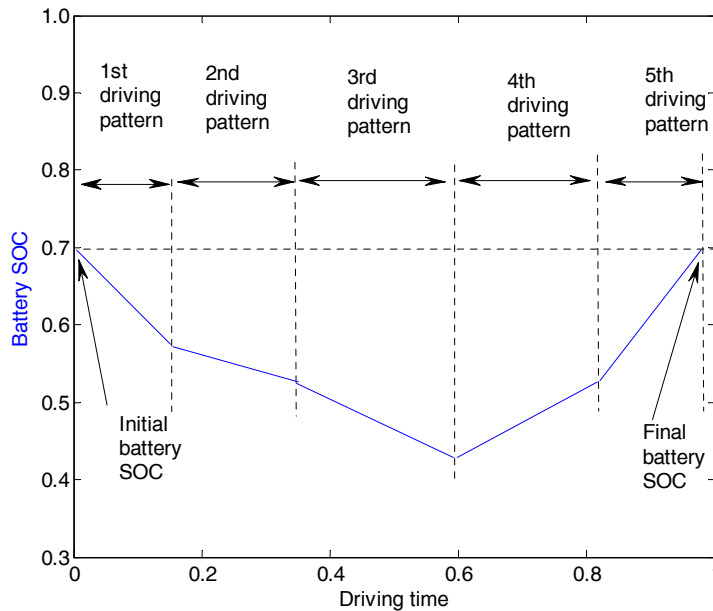


Figure 6.5 (Repeated): Battery SOC for the proposed methodology with first approach (M2A1)

The optimum designs over the C1 to C5 combinations are termed as M2A1-C1, M2A1-C2, M2A1-C3, M2A1-C4, and M2A1-C5, respectively, as shown in Table 9.1. The optimum parameters of the designs are shown in Table 9.2.

Table 9.1: Combinations of driving patterns and name of optimum designs for M2A1 approach

Combination of driving patterns	Design	Sequence of driving patterns				
		First	Second	Third	Fourth	Fifth
C1	M2A1-C1	HWFET	FTP	LA92	US06	NEDC
C2	M2A1-C2	NEDC	HWFET	LA92	US06	FTP
C3	M2A1-C3	NEDC	HWFET	FTP	US06	LA92
C4	M2A1-C4	NEDC	FTP	LA92	US06	HWFET
C5	M2A1-C5	NEDC	HWFET	FTP	LA92	US06

Table 9.2: Optimum parameters of optimum designs of M2A1 approach

Design	Optimum parameters				
	Component size				Target SOC
	P _{ICE}	P _G	P _M	C _B	
M2A1-C1	36.51 kW	14.91 kW	37.42 kW	6.01 Ah	0.5706
M2A1-C2	37.52 kW	14.52 kW	37.53 kW	8.51 Ah	0.7039
M2A1-C3	36.72 kW	13.13 kW	44.71 kW	8.22 Ah	0.6824
M2A1-C4	31.53 kW	10.91 kW	42.03 kW	8.34 Ah	0.5628
M2A1-C5	43.31 kW	16.71 kW	39.21 kW	8.23 Ah	0.5980
<i>Variation in optimum sizes, %</i>	27.20	34.71	16.31	29.38	

Where,

Variation in optimum sizes, %

$$= \frac{\text{Max size}(M2A1 - C1 \text{ to } M2A1 - C5) - \text{Min size}(M2A1 - C1 \text{ to } M2A1 - C5)}{\text{Max size}(M2A1 - C1 \text{ to } M2A1 - C5)} * 100$$

The M2A1-C5 design had 0.7% higher power of the ICE and the M2A1-C1, M2A1-C2, M2A1-C3, and M2A1-C4 designs had 15.1, 12.8, 14.7, and 26.7%, respectively lower power of the ICE compared to the Toyota Prius, as shown in Figure 9.1. The minimum and maximum powers of the ICEs among the 5 designs of the M1 methodology were 29.32 and 40.52 kW respectively, whereas the minimum and maximum powers of the ICEs among the 5 designs of the M2A1 approach were 31.53 and 43.31 kW respectively. Therefore, in case of the M2A1 approach both the minimum and maximum powers of the ICEs were increased. Although all the optimum designs of the M1 methodology had lower ICE power, one design (M2A1-C5) of the M2A1 approach had 0.7% higher ICE power compared to the Toyota Prius.

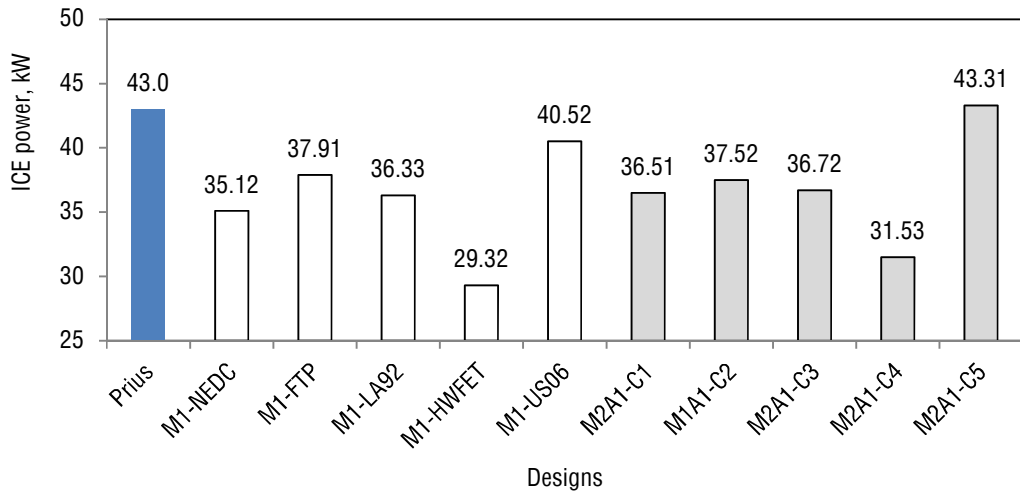


Figure 9.1: Comparison of ICE power: Toyota Prius, M1, and M2A1

The M2A1-C5 design had 11.3% higher power of the generator and the M2A1-C1, M2A1-C2, M2A1-C3, and M2A1-C4 designs had 0.7, 3.3, 12.7, and 27.3%, respectively lower power of the generator compared to the Toyota Prius, as shown in Figure 9.2. The minimum and maximum powers of the generators among the 5

designs of the M1 methodology were 12.23 and 18.33 kW respectively, whereas the minimum and maximum powers of the generators among the 5 designs of the M2A1 approach were 10.91 and 16.71 kW respectively. Therefore, in case of the M2A1 approach both the minimum and maximum powers of the generators were decreased. Only one design (M2A1-C5) of the M2A1 approach had higher power of the generator compared to the Toyota Prius, similar to the M1 methodology.

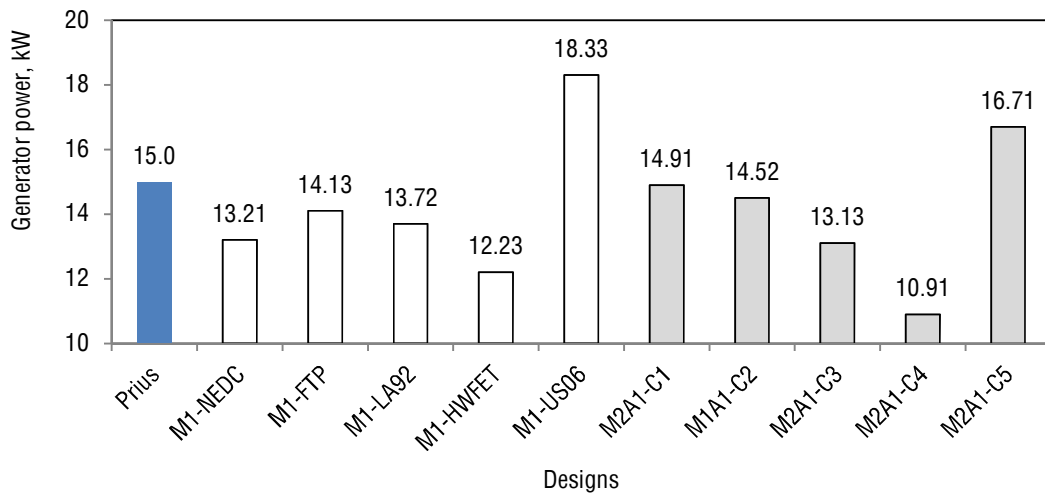


Figure 9.2: Comparison of generator power: Toyota Prius, M1, and M2A1

The M2A1-C1, M2A1-C2, M2A1-C3, M2A1-C4, and M2A1-C5 designs had 24.7, 25.0, 49.0, 40.0, and 30.7%, respectively higher power of the motor compared to the Toyota Prius, as shown in Figure 9.3. The minimum and maximum powers of the motors among the 5 designs of the M1 methodology were 34.82 and 44.41 kW respectively, whereas the minimum and maximum powers of the motors among the 5 designs of the M2A1 methodology were 37.42 and 44.71 kW respectively. Therefore, in case of the M2A1 approach both the minimum and maximum powers of the motors were increased. All the designs of the M2A1 approach had higher power of the motor compared to the Toyota Prius, similar to the M1 methodology.

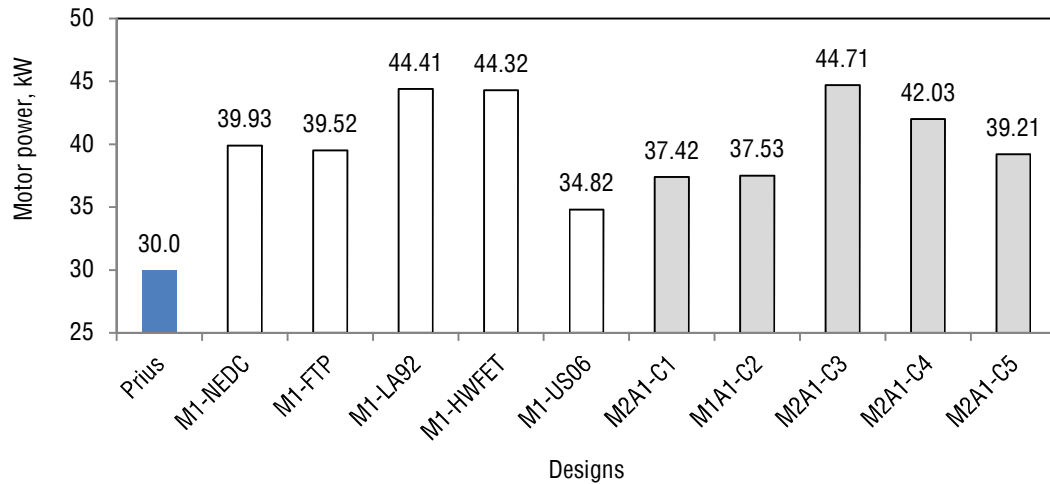


Figure 9.3: Comparison of motor power: Toyota Prius, M1, and M2A1

The M2A1-C1 design had same capacity of the battery and the M2A1-C2, M2A1-C3, M2A1-C4, and M2A1-C5 designs had 41.7, 36.7, 38.3, and 36.7%, respectively higher capacity of the battery compared to the Toyota Prius, as shown in Figure 9.4. The minimum and maximum battery capacities among the 5 designs of the M1 methodology were 6.21 and 8.92 Ah respectively, whereas the minimum and maximum battery capacities among the 5 designs of the M2A1 approach were 6.01 and 8.51 Ah respectively. Therefore, in case of the M2A1 approach both the minimum and maximum battery capacities were decreased. Except one design (M2A1-C1), all designs had higher battery capacity compared to the Toyota Prius.

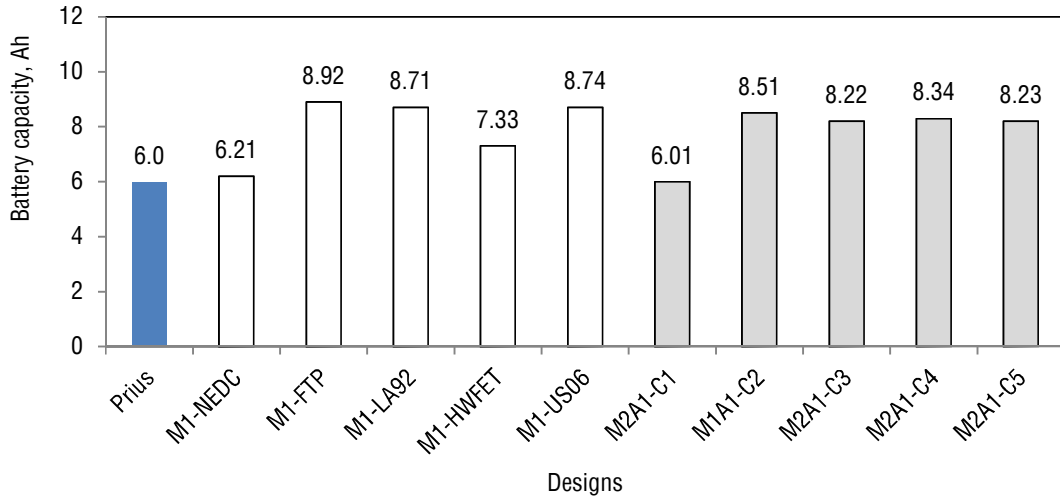


Figure 9.4: Comparison of battery capacity: Toyota Prius, M1, and M2A1

The optimum target SOC values of the M2A1-C2, M2A1-C3, M2A1-C4, and M2A1-C5 designs during the optimisation were 0.5706, 0.7039, 0.6824, 0.5628, and 0.5980, respectively, as shown in Table 9.2. The optimum target SOC values for the M2A1 approach ranged from 0.5628 to 0.7039, whereas the optimum target SOC values for the M1 methodology ranged from 0.5701 to 0.7003, as shown Table 9.3.

Table 9.3: Comparison of optimum target SOC during optimisation: M1 and M2A1

Optimum value	M1 methodology					M2 methodology: M2A1 approach				
	M1-NEDC	M1-FTP	M1-LA92	M1-HWFET	M1-US06	M2A1-C1	M2A1-C2	M2A1-C3	M2A1-C4	M2A1-C5
Target SOC	0.5901	0.7003	0.6802	0.5701	0.6004	0.5706	0.7039	0.6824	0.5628	0.5980

The variations in the ICE, generator, motor and battery sizes of the M2A1 approach over the C1 to C5 combinations were 27.2, 34.71, 16.31, and 29.38%, respectively, as shown in Table 9.2. The variations in the component sizes of the M2A1 approach were in the similar order that of the M1 methodology, as shown in Table 9.4.

Table 9.4: Variations in component sizes: M1 and M2A1

Variation in component sizes, %	M1 methodology	M2 methodology
		M2A1 approach
P_{ICE}	27.64	27.20
P_G	33.28	34.71
P_M	21.59	16.31
C_B	30.38	29.38

The variations in the component sizes in Table 9.4 indicated that the M2A1 approach provided five different optimum designs, one for each combination. It indicated the dependency of the optimum component sizes of the M2A1 approach on the sequence of driving pattern. Hence, similar to the M1 methodology, it is also required to evaluate each optimum design of the M2A1 approach separately to find the design for the minimum FE variability.

9.2 Performance of optimum designs: Toyota Prius and M2A1

The performances of all the optimum designs of the M2A1 approach are shown in Table 9.5. The time of acceleration of the M2A1-C1, M2A1-C2, M2A1-C3, M2A1-C4, and M2A1-C5 designs were reduced by 9.0, 20.1, 20.1, 11.9, and 17.2%, respectively compared the Toyota Prius, as shown in Table 9.5. The maximum speed of the M2A1-C1, M2A1-C2, M2A1-C3, M2A1-C4, and M2A1-C5 designs were increased by 0.4, 4.1, 4.0, 0.3, and 4.5%, respectively compared the Toyota Prius, as shown in Table 9.5. The gradeability of the M2A1-C1, M2A1-C2, M2A1-C3, M2A1-C4, and M2A1-C5 designs were increased by 1.4, 14.5, 14.5, 0.7, and 15.9%, respectively compared the Toyota Prius, as shown in Table 9.5.

Table 9.5: Performance of optimum designs: Toyota Prius and M2A1

Performance	Toyota Prius	M2 methodology: M2A1 approach				
		M2A1-C1	M2A1-C2	M2A1-C3	M2A1-C4	M2A1-C5
Acceleration (0~60 mph), seconds	13.4	12.2	10.7	10.7	11.8	11.1
<i>Acceleration (0~60 mph) w.r.t. Prius, %</i>		-9.0	-20.1	-20.1	-11.9	-17.2
Maximum speed, mph	113.3	113.7	117.9	117.8	113.6	118.4
<i>Maximum speed w.r.t. Prius, %</i>		0.4	4.1	4.0	0.3	4.5
Gradeability, %	13.8	14.0	15.8	15.8	13.9	16.0
<i>Gradeability w.r.t. Prius, %</i>		1.4	14.5	14.5	0.7	15.9

The improvement in performances was due to 1.3, 2.8, 11.5, 0.8, and 13.0% higher combined power of the ICE and motor of the M2A1-C1, M2A1-C2, M2A1-C3, M2A1-C4, and M2A1-C5 designs, respectively compared to the Toyota Prius, as shown in Table 9.6.

Table 9.6: Combined power: Toyota Prius and M2A1

Combined power	Toyota Prius	M2 methodology: M2A1 approach				
		M2A1-C1	M2A1-C2	M2A1-C3	M2A1-C4	M2A1-C5
(ICE + Motor), kW	73.0	73.93	75.05	81.43	73.56	82.52
<i>(ICE + Motor) w.r.t. Prius, %</i>		1.3	2.8	11.5	0.8	13.0

9.3 Battery SOC during optimisation: optimum designs of M2A1 approach

The battery SOC of the M2A1-C1, M2A1-C2, M2A1-C3, M2A1-C4, and M2A1-C5 designs during the optimisation over respective combination of driving patterns are shown in Table 9.7.

Table 9.7: Battery SOC after each driving pattern during optimisation: optimum designs of M2A1 approach

Design	Sequence of driving patterns	Battery SOC after each driving pattern	Delta SOC, %
M2A1-C1	1 st (HWFET)	0.7371	5.3
	2 nd (FTP)	0.5982	14.54
	3 rd (LA92)	0.6014	14.09
	4 th (US06)	0.6067	13.33
	5 th (NEDC)	0.6992	0.11
M2A1-C2	1 st (NEDC)	0.7490	7.00
	2 nd (HWFET)	0.8206	17.23
	3 rd (LA92)	0.7277	3.96
	4 th (US06)	0.7033	0.47
	5 th (FTP)	0.7006	0.09
M2A1-C3	1 st (NEDC)	0.7486	6.94
	2 nd (HWFET)	0.7996	14.23
	3 rd (FTP)	0.6774	3.23
	4 th (US06)	0.6868	1.89
	5 th (LA92)	0.6989	0.16
M2A1-C4	1 st (NEDC)	0.6322	9.69
	2 nd (FTP)	0.5397	22.90
	3 rd (LA92)	0.4959	29.16
	4 th (US06)	0.5000	28.57
	5 th (HWFET)	0.6992	0.11
M2A1-C5	1 st (NEDC)	0.7156	2.23
	2 nd (HWFET)	0.7476	6.80
	3 rd (FTP)	0.6189	11.59
	4 th (LA92)	0.6442	7.97
	5 th (US06)	0.7016	0.23

The delta SOC after the 5th driving pattern was within desired limits (<0.5%), but the delta SOC after each of the other driving patterns was not within limits for all the optimum designs, as shown in Table 9.7. For the M2A1-C1 design, the delta SOC after 1st (HWFET), 2nd (FTP), 3rd (LA92), 4th (US06), and 5th (NEDC) driving patterns were 5.3, 14.54, 14.09, 13.33, and 0.11%, respectively, as shown in Table 9.7.

9.4 FE evaluation over standard driving patterns: optimum designs of M2A1

The M2A1-C1, M2A1-C2, M2A1-C3, M2A1-C4, and M2A1-C5 designs were evaluated over NEDC, FTP, LA92, HWFET, and US06 individually to find FE performance of each optimum design. The target SOC was varied during the FE evaluation for each design to maintain the desired final battery SOC (within <0.5% of the initial battery SOC i.e., delta SOC < 0.5%) over individual driving pattern, as discussed in section 6.9 of chapter 6.

9.4.1 Battery SOC during FE evaluation: optimum designs of M2A1

The target SOC of each optimum design during the FE evaluation over the standard driving patterns are shown in Table 9.8. The minimum and maximum target SOC values of the Toyota Prius were 0.5401 and 0.6803 respectively when compared for all the 5 driving patterns. The minimum target SOC values of the M2A1-C1, M2A1-C2, M2A1-C3, M2A1-C4, and M2A1-C5 designs were 0.5549, 0.5490, 0.5529, 0.5628, and 0.5549, respectively. The maximum target SOC values of the M2A1-C1, M2A1-C2, M2A1-C3, M2A1-C4, and M2A1-C5 designs were 0.7922, 0.7039, 0.7471, 0.99, and 0.6922, respectively. Therefore, the minimum and maximum target SOC values of the Toyota Prius were lower compared to all the designs of the M2A1 approach when compared for all the driving patterns, as shown in Table 7.5. This

was probably due to the higher power of the ICE of the Toyota Prius compared to all the designs of the M2A1 approach. Due to the higher ICE power, the ICE of the Toyota Prius was able to deliver more torque for charging the battery even after providing vehicle torque demand and therefore, the Toyota Prius was able to meet the desired final battery SOC with the lower target SOC values.

Table 9.8: Target SOC over driving patterns during FE evaluation: M2A1

Driving pattern	Target SOC					
	Toyota Prius	M2A1-C1	M2A1-C2	M2A1-C3	M2A1-C4	M2A1-C5
NEDC	0.5401	0.5706	0.6039	0.6059	0.6765	0.5745
FTP	0.6803	0.7059	0.7039	0.7098	0.7863	0.6922
LA92	0.6604	0.6863	0.6726	0.6824	0.7706	0.6569
HWFET	0.5502	0.5549	0.5490	0.5529	0.5628	0.5549
US06	0.6204	0.7922	0.7000	0.7471	0.9900 (x)	0.5980
(x): Failed to operate charge sustaining						

The final battery SOC of each optimum design of the M2A1 approach during the FE evaluation over the standard driving patterns are shown in Table 9.9. Except the M2A1-C4 design, all the designs (M2A1-C1, M2A1-C2, M2A1-C3 and M2A1-C5) were able to operate in charge sustaining mode over all the driving patterns. The final battery SOC of the M2A1-C4 design was 0.665 i.e., 5.0% lower than the initial battery SOC, as shown in Table 9.9 and Figure 9.5 and therefore, failed to operate in charge sustaining mode over US06.

Table 9.9: Final battery SOC over driving patterns during FE evaluation: M2A1

Driving pattern	Final battery SOC					
	Toyota Prius	M2A1-C1	M2A1-C2	M2A1-C3	M2A1-C4	M2A1-C5
NEDC	0.6978	0.6992	0.7032	0.7007	0.7031	0.6968
FTP	0.6982	0.7011	0.7006	0.6995	0.6981	0.7020
LA92	0.6985	0.7025	0.7003	0.6989	0.6979	0.7025
HWFET	0.6995	0.7024	0.6973	0.7005	0.6992	0.7031
US06	0.6989	0.7001	0.6999	0.6999	0.6650 (x)	0.7016
(x): Failed to operate charge sustaining						

Interestingly, like the M1 methodology where the M1-HWFET design failed to operate in charge sustaining mode over US06, the M2A1 approach also failed to operate in charge sustaining mode for the C4 combination where the last driving pattern was the HWFET.

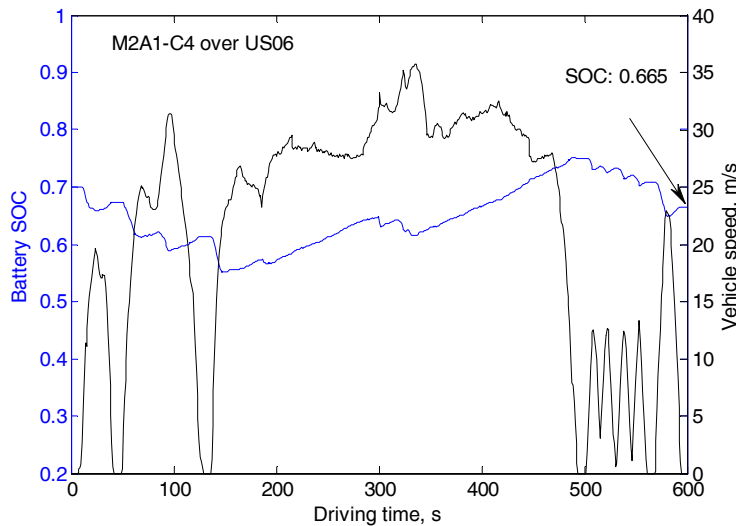


Figure 9.5: Battery SOC of the M2A1-C4 over US06

As the M2A1-C4 design was not able to charge the battery up to the desired final battery SOC (0.7) over the US06, the M2A1-C4 design was evaluated over 3 consecutive US06 to investigate its battery SOC, as shown in Figure 9.6. The final battery SOC values after the 1st, 2nd, and 3rd US06 were 0.665, 0.6439, and 0.6307, respectively i.e., 5.0, 8.0, and 9.5%, respectively lower compared to the initial battery SOC, as shown in Figure 9.6. Although the M2A1-C4 design behaved similarly to the M1-HWFET design, the final battery SOC of the M1-HWFET design after 3rd US06 was lower by 37.1%, whereas that of the M2A1-C4 design was lower by 9.5% compared to initial battery SOC. Therefore, the M2A1-C4 design could not operate charge sustaining but was better than the M1-HWFET design.

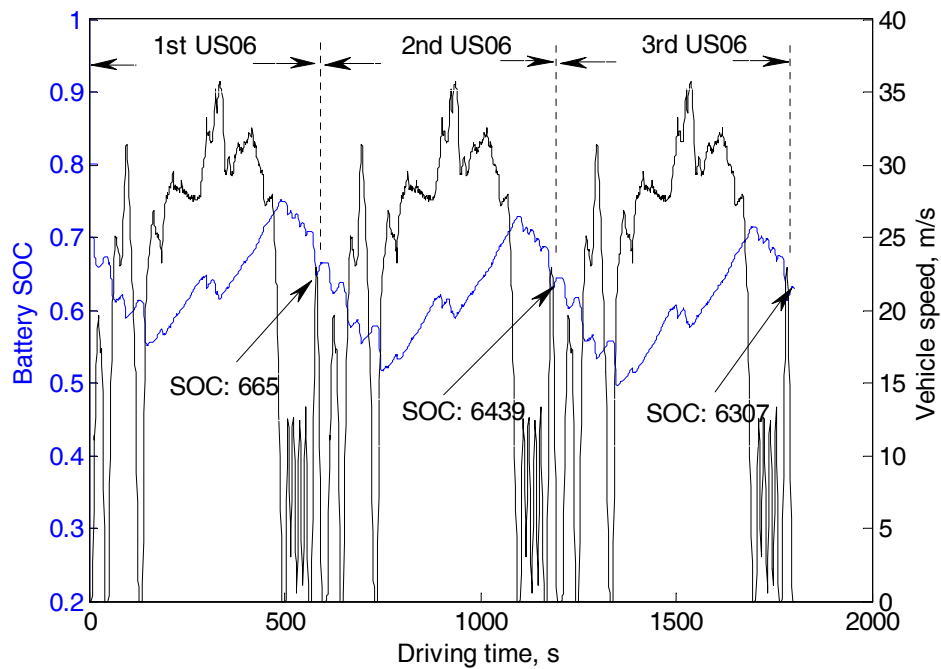


Figure 9.6: Battery SOC of the M2A1-C4 over 3 consecutive US06

9.5 FE over standard driving patterns: Toyota Prius and M2A1

The FE performance of all the optimum designs of the M2A1 approach over the NEDC, FTP, LA92, HWFET, and US06 are shown in Table 9.10.

Table 9.10: FE over standard driving patterns: Toyota Prius and M2A1

Driving pattern	FE, mpg						FE variation among designs over a driving pattern, %
	Toyota Prius	M2 methodology: M2A1 approach					
		M2A1-C1	M2A1-C2	M2A1-C3	M2A1-C4	M2A1-C5	
NEDC	83.1	86.6	85.0	85.4	82.9	82.3	5.0
FTP	68.0	71.7	72.1	72.2	70.7	68.3	5.4
LA92	57.5	60.9	61.5	61.1	58.6	58.5	4.9
HWFET	120.3	128.2	127.9	128.7	135.6	119.7	11.7
US06	55.4	48.2	53.4	50.7	42.0 (x)	55.5	24.3
<i>Average FE, mpg</i>	76.9	79.1	80.0	79.6	78.0	76.9	3.9
<i>Average FE w.r.t. Prius, %</i>		2.9	5.1	3.5	1.4	0.0	
<i>Standard Deviation of FE, mpg</i>	23.8	27.6	26.2	27.1	31.8	23.4	
<i>FE variability, %</i>	31.0	34.9	32.8	34.1	40.8	30.4	
<i>FE variability w.r.t. Prius, %</i>		12.6	5.8	10.0	31.6	-1.9	
(x): Failed to operate charge sustaining							

Where,

FE variation among designs over a driving pattern, %

$$= \frac{\text{Max FE}(M1 - \text{NEDC to } M1 - \text{US06}) - \text{Min FE}(M1 - \text{NEDC to } M1 - \text{US06})}{\text{Max FE}(M1 - \text{NEDC to } M1 - \text{US06})} * 100$$

The average FE of the M2A1-C1, M2A1-C2, M2A1-C3, M2A1-C4, and M2A1-C5 designs were 79.1, 80.0, 79.6, 78.0, and 76.9 mpg, respectively. Therefore, the M2A1-C1, M2A1-C2, M2A1-C3, and M2A1-C4 designs had 2.9, 5.1, 3.5, and 1.4%, respectively higher average FE over NEDC, FTP, LA92, HWFET, and US06 respectively compared to the Toyota Prius, as shown in Table 9.10. However, the M2A1-C5 design had same average FE as that of the Toyota Prius.

The minimum and maximum average FE values among the 5 designs of the M2A1 approach were 76.9 and 80.8 mpg respectively. On the other hand, the minimum and maximum average FE values among the 5 designs of the M1 methodology, which were 78.0 and 80.4 mpg respectively, as shown in Figure 9.7. The M1-HWFET design was not considered as it was failed to operate in charge sustaining over US06. Therefore, the maximum and minimum average FE values of the M2A1 approach was improved by 0.7% and reduced by 1.4% respectively compared to the M1 methodology.

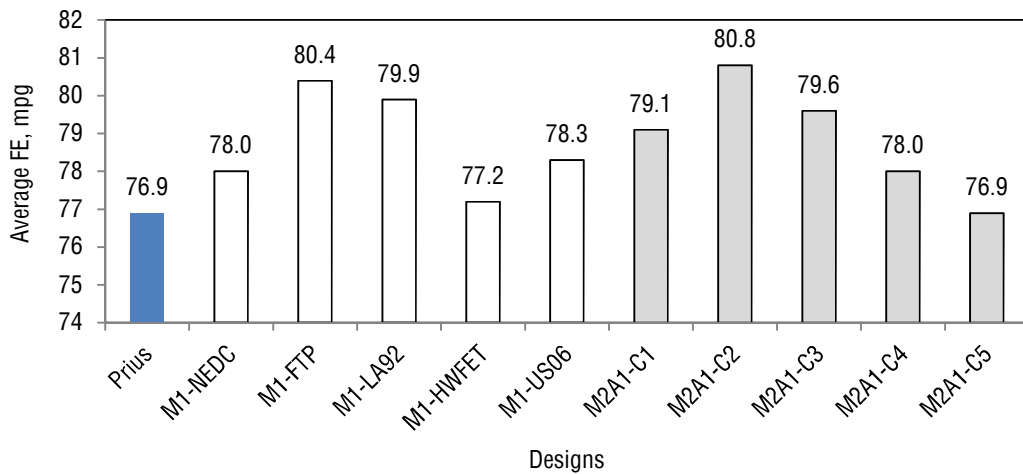


Figure 9.7: Comparison of average FE: M2A1 versus M1

The variation in the average FE among all the designs of the M2A1 approach was 3.9%, whereas the variation in FE among all the designs over NEDC, FTP, LA92, HWFET, and US06 were 5.0, 5.4, 4.9, 11.7, and 24.3%, respectively, as shown in Table 9.10. The variation in FE among the designs of M2A1 approach and M1 methodology are compared in Table 9.11.

Table 9.11: FE variation among designs over a driving pattern: M1 and M2A1

Driving pattern	FE variation among designs over a driving pattern, %	
	M1 methodology	M2 methodology
		M2A1 approach
NEDC	7.5	5.0
FTP	5.8	5.4
LA92	8.8	4.9
HWFET	10.5	11.7
US06	23.6	24.3
Average FE	4.0	3.9

This variations among the designs of the M2A1 approach clearly indicated that each combination of driving patterns provided different optimum design, as seen with the M1 methodology. It means the M2A1 approach depends on the sequence of driving patterns.

9.6 FE variability over standard driving patterns: Toyota Prius and M2A1

The FE variability values of the M2A1-C1, M2A1-C2, M2A1-C3, M2A1-C4, and M2A1-C5 designs were 34.9, 32.8, 34.1 40.8, and 30.4%, respectively, as shown in Table 9.10. Therefore, only the M2A1-C5 design was able to reduce FE variability by 1.9% with comparable average FE compared to the Toyota Prius, whereas the FE

variability of the M2A1-C1, M2A1-C2, M2A1-C3, and M2A1-C4 designs were 12.6, 5.8, 10.0, and 31.6%, respectively higher compared to the Toyota Prius, as shown in Table 9.10.

The average FE and FE variability of the M2A1-C1, M2A1-C2, M2A1-C3, M2A1-C4, and M2A1-C5 designs w.r.t. Toyota Prius are shown in Figure 9.8. The average FE and FE variability of the Toyota Prius are shown as the origin of Figure 9.8. Except the M2A1-C5 design, all the optimum designs situate in the 1st quadrant in Figure 9.8, as all the designs increase the average FE as well as the FE variability w.r.t. the Toyota Prius.

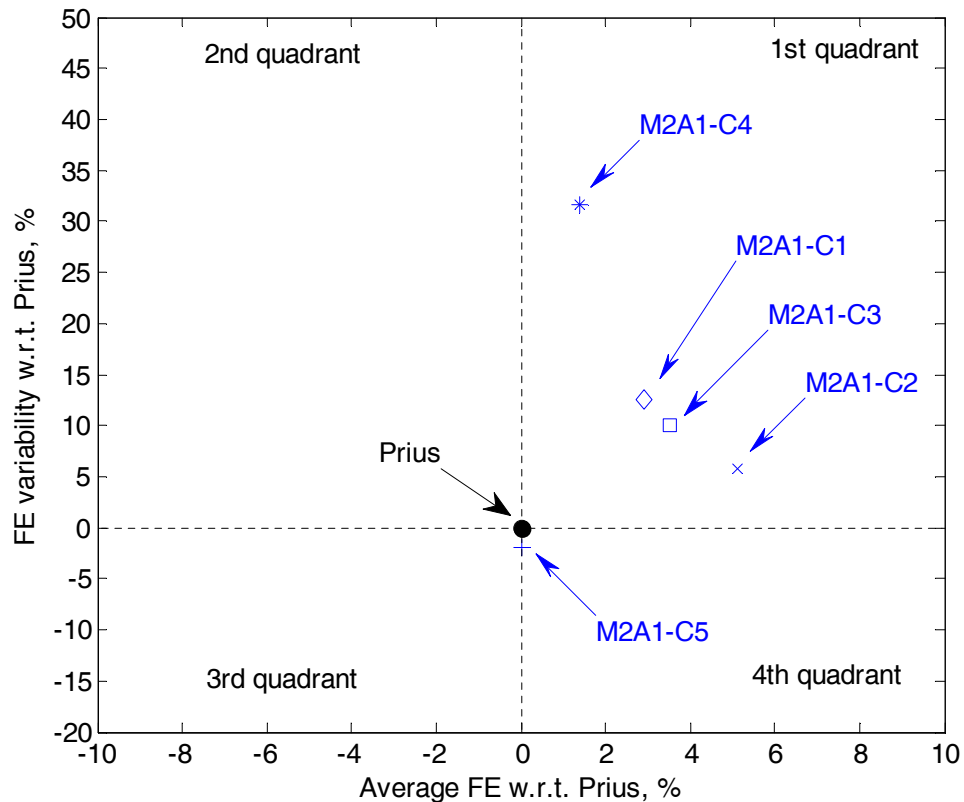


Figure 9.8: Average FE versus FE variability over standard driving patterns: Toyota Prius and M2A1

The M2A1 approach provided different optimum designs with the change in sequence of driving patterns. This made the M2A1 approach dependent on the designer's decision (of which is the last driving pattern) similar to the M1 methodology. One design (M2A1-C5) of the M2A1 approach was able to reduce FE variability, whereas none of the M1 methodology was able to reduce FE variability when compared to the Toyota Prius. The lower FE variability of the M2A1-C5 design when compared to the Toyota Prius shows the potential of considering a range of different driving patterns simultaneously during the optimisation.

In the M2A1 approach, the 4th constraint (delta SOC <0.5%) was satisfied overall but not for each individual driving pattern in a combination. The philosophy of the proposed methodology to get an optimum design over different driving patterns simultaneously with the satisfaction of all the constraints over each driving pattern was not achieved, as the 4th constraint was not satisfied over each driving pattern in the combination.

Although one (M2A1-C5) of the designs of the M2A1 approach was able to reduce FE variability by 1.9%, the FE variability of other optimum designs were up to 31.6% higher compared to the Toyota Prius. One design (M2A1-C4) of the M2A1 approach failed to operate charge sustaining over an aggressive driving pattern (US06). Therefore, it could be said that the M2A1 approach depends on the sequence of driving patterns and could not be considered as a generalised methodology for the optimisation of powertrain component sizes over driving patterns of different traffic conditions and driving styles.

9.7 Summary

- The proposed methodology with first approach (M2A1 approach) was dependent on the sequence of driving patterns.
- The M2A1 approach provided 5 different optimum designs one for each combination of driving pattern.
- A separate decision making process is required to choose a design from the 5 optimum designs for practical applications, similar to the traditional methodology.
- One optimum design (M2A1-C5) had equal average FE and other four optimum designs, namely, M2A1-C1, M2A1-C2, M2A1-C3, and M2A1-C4 designs had 2.9, 5.1, 3.5, and 1.4%, respectively higher average FE compared to the Toyota Prius (benchmark vehicle) over 5 standard driving patterns.
- Only one design (M2A1-C5) reduced FE variability by 1.9% compared to the Toyota Prius (benchmark vehicle), whereas other four designs (M2A1-C1, M2A1-C2, M2A1-C3 and M2A1-C4) had 12.6, 5.8, 10.0, and 31.6%, respectively higher FE variability compared to the Toyota Prius.
- One design (M2A1-C4) of the M2A1 approach failed to operate charge sustaining over an aggressive highway driving pattern (US06), similar to the traditional methodology.
- The M2A1 approach could not be considered as a generalised methodology for the optimisation of powertrain component sizes of HEVs, similar to the traditional methodology.

CHAPTER 10

EVALUATION OF PROPOSED METHODOLOGY: CONTROL OF BATTERY STATE OF CHARGE OVER EACH DRIVING PATTERN

It has been found in chapter 9 that the proposed methodology with the first approach (M2A1 approach) i.e., the control of delta SOC after the end of the last driving pattern of a range of driving patterns failed to provide a generalised methodology. Four optimum designs out of the five optimum designs of the M2A1 approach failed to reduce FE variability over 5 standard driving patterns compared to the simulation model of the Toyota Prius (benchmark vehicle). As both the traditional methodology and M2A1 approach failed to reduce the FE variability, there was a need for an alternate approach. The control of the delta SOC after the end of the last driving pattern failed to satisfy the 4th constraint (delta SOC) for each driving pattern. Therefore, to satisfy the delta SOC for each driving pattern, an alternate approach of the proposed methodology was to constrain the design such that the delta SOC was maintained within the desired limits (<0.5%) over each driving pattern in a sequence. The evaluation of the proposed methodology with this second approach over 5 standard driving patterns is discussed in this chapter. The proposed methodology is compared with the results of the traditional methodology and the simulation model of the Toyota Prius (benchmark vehicle) found in chapter 8. This chapter first discusses the optimum designs produced by the proposed methodology followed by the performance of the optimum designs. Next the battery SOC and FE of the proposed methodology over the standard driving patterns are discussed. After that,

the discussion is focused on the analysis to understand the reason for a particular FE over a driving pattern. Finally the FE variability of the proposed methodology over the standard driving patterns is discussed.

10.1 The proposed methodology with second approach

In the second approach, the battery SOC after each driving pattern was maintained within the desired delta SOC ($<0.5\%$). For example, if 5 driving patterns were considered simultaneously and the initial battery SOC was 0.7, then the battery SOC needed to be maintained within the desired limits ($<0.5\%$ of the initial battery SOC) after each driving pattern i.e., 2nd, 3rd, 4th, and 5th driving patterns, as shown in Figure 10.1. The proposed methodology (M2) with the second approach is called as M2A2 approach in the subsequent discussion.

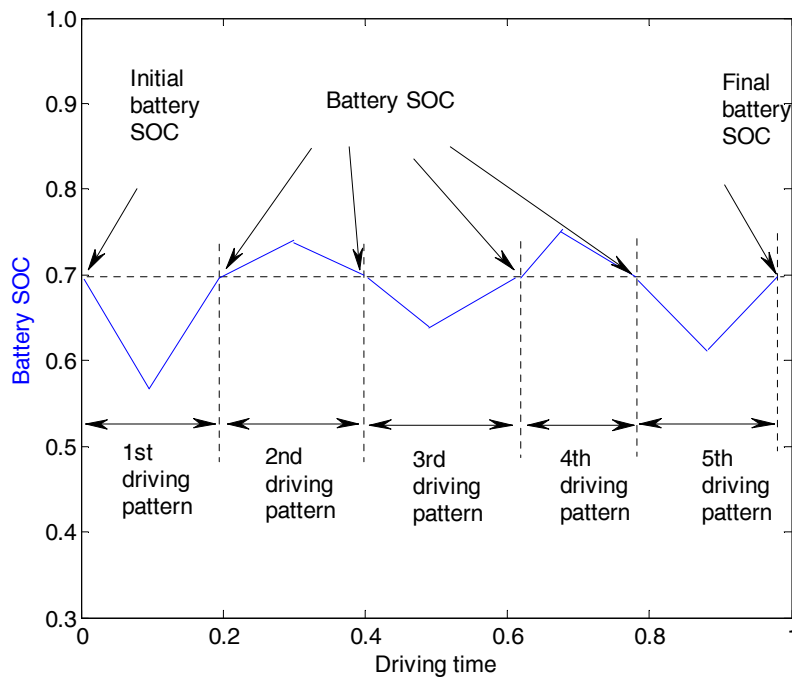


Figure 10.1: Battery SOC for the proposed methodology with second approach (M2A2)

10.2 Optimum designs of M2A2 approach

The M2A2 approach considered 5 categorised driving patterns, NEDC, FTP, LA92, HWFET, and US06 simultaneously for the optimisation of four powertrain components, namely, the ICE, generator, motor, and battery along with target SOC. Therefore, the optimisation variables for this study were as follows.

- Maximum power of ICE (P_{ICE})
- Maximum power of generator (P_G)
- Maximum power of motor (P_M)
- Maximum capacity of battery (C_B)
- Target SOC

To evaluate the effect of the sequence of driving patterns, the same 5 combinations, C1 to C5 as tested in the case of the M2A1 approach, were considered, as shown in Table 10.1. The optimum component sizes for the C1 to C5 combinations are termed as M2A2-C1, M2A2-C2, M2A2-C3, M2A2-C4, and M2A2-C5 respectively, as shown in Table 10.1.

Table 10.1: Combinations of driving patterns and name of optimum designs for M2A2 approach

Combination of driving patterns	Design	Sequence of driving patterns				
		First	Second	Third	Fourth	Fifth
C1	M2A2-C1	HWFET	FTP	LA92	US06	NEDC
C2	M2A2-C2	NEDC	HWFET	LA92	US06	FTP
C3	M2A2-C3	NEDC	HWFET	FTP	US06	LA92
C4	M2A2-C4	NEDC	FTP	LA92	US06	HWFET
C5	M2A2-C5	NEDC	HWFET	FTP	LA92	US06

The optimum component sizes obtained through the optimisation are shown in Table 10.2.

Table 10.2: Component sizes of optimum designs of M2A2 approach

Design	Optimum size			
	P_{ICE}	P_G	P_M	C_B
M2A2-C1	44.83 kW	16.51 kW	30.46 kW	7.65 Ah
M2A2-C2	44.92 kW	16.53 kW	30.49 kW	7.71 Ah
M2A2-C3	44.95 kW	16.44 kW	30.44 kW	7.66 Ah
M2A2-C4	44.94 kW	16.56 kW	30.34 kW	7.70 Ah
M2A2-C5	45.05 kW	16.43 kW	30.56 kW	7.71 Ah
<i>Variation in optimum sizes, %</i>	0.49	0.79	0.72	0.78

Where,

Variation in optimum sizes, %

$$= \frac{\text{Max size}(M2A2 - C1 \text{ to } M2A2 - C5) - \text{Min size}(M2A2 - C1 \text{ to } M2A2 - C5)}{\text{Max size}(M2A2 - C1 \text{ to } M2A2 - C5)} * 100$$

The overall variations in the ICE, generator, motor, and battery sizes for the optimum designs of the M2A2 approach were 0.49, 0.79, 0.72, and 0.78% respectively due to the change in the sequence of driving patterns. These variations were much reduced when compared to that of the traditional methodology (M1) and M2A1 approach, as shown in Table 8.1 and Table 9.2. The variations in component sizes for the M1 methodology, M2 methodology with M2A1 approach, and M2 methodology with M2A2 approach are compared in Table 10.3.

Table 10.3: Variations in component sizes: M1, M2A1, and M2A2

Variation in component sizes, %	M1 methodology	M2 methodology	
		M2A1 approach	M2A2 approach
P_{ICE}	27.64	27.20	0.49
P_G	33.28	34.71	0.79
P_M	21.59	16.31	0.72
C_B	30.38	29.38	0.78

The variations in the ICE, generator, motor, and battery sizes of the M2A2-C1, M2A2-C2, M2A2-C3, M2A2-C4, and M2A2-C5 designs for 10 optimisation trials are shown in Table 10.4. The details of 10 optimisation trials for each optimum design are shown in Appendix C. The variations in the optimum component sizes of each optimum design of the M2A2 approach for 10 optimisation trials were below 1.0%, as shown in Table 10.4. The variations were similar to the variations found in chapter 7 for each optimum design of the M1 methodology for 10 optimisation trials.

Table 10.4: Variation in optimum component sizes for 10 optimisation trials

Design	Variation in optimum sizes for 10 optimisation trials, %			
	P_{ICE}	P_G	P_M	C_B
M2A2-C1	0.60	0.90	0.62	0.91
M2A2-C2	0.62	0.72	0.52	0.91
M2A2-C3	0.55	0.96	0.59	0.91
M2A2-C4	0.58	0.66	0.91	0.78
M2A2-C5	0.49	0.90	0.82	0.91

As the variations of optimum component sizes for the M2A2-C1, M2A2-C2, M2A2-C3, M2A2-C4, and M2A2-C5 designs were also below 1.0% (Table 10.3), it could

be said that the variations were due to stochastic nature of the genetic algorithm. The variations could possibly be reduced further with a higher number of population size and generations.

Hence, neglecting the variations it could be concluded that the M2A2 approach was independent of the sequence of driving patterns. Therefore, the M2A2 approach provided a single optimum design over a range of driving patterns representing different traffic conditions and driving styles simultaneously; this has not been found in the reviewed literature.

The optimum target SOC values of the M2A2-C1, M2A2-C2, M2A2-C3, M2A2-C4, and M2A2-C5 designs during optimisation are shown in Table 10.5. The optimum target SOC values for all the designs over same driving pattern were same. For all the optimum designs, the optimum target SOC values over NEDC, FTP, LA92, HWFET and US06 were 0.57, 0.69, 0.66, 0.55, and 0.56, respectively.

Table 10.5: Optimum target SOC during optimisation: optimum designs of M2A2 approach

Design	Target SOC				
	Sequence of driving pattern				
	First	Second	Third	Fourth	Fifth
M2A2-C1	0.5502 (HWFET)	0.6901 (FTP)	0.6603 (LA92)	0.5601 (US06)	0.5702 (NEDC)
M2A2-C2	0.5703 (NEDC)	0.5503 (HWFET)	0.6601 (LA92)	0.5603 (US06)	0.6904 (FTP)
M2A2-C3	0.5703 (NEDC)	0.5504 (HWFET)	0.6901 (FTP)	0.5602 (US06)	0.6604 (LA92)
M2A2-C4	0.5701 (NEDC)	0.6904 (FTP)	0.6603 (LA92)	0.5602 (US06)	0.5503 (HWFET)
M2A2-C5	0.5704 (NEDC)	0.5501 (HWFET)	0.6903 (FTP)	0.6604 (LA92)	0.5604 (US06)

10.3 Performance of optimum designs: Toyota Prius and M2A2 approach

The performance of the M2A2-C1, M2A2-C2, M2A2-C3, M2A2-C4, and M2A2-C5 designs are shown in Table 10.6. The acceleration time of the M2A2-C1, M2A2-C2, M2A2-C3, M2A2-C4, and M2A2-C5 designs were reduced by 2.5, 2.6, 2.5, 2.2, and 3.0%, respectively compared the Toyota Prius, as shown in Table 10.6. The maximum speed of the M2A2-C1, M2A2-C2, M2A2-C3, M2A2-C4, and M2A1-C5 designs were increased by 1.1, 1.1, 1.1, 1.0, and 1.3%, respectively compared the Toyota Prius, as shown in Table 10.6. The gradeability of the M2A2-C1, M2A2-C2, M2A2-C3, M2A2-C4, and M2A2-C5 designs were increased by 4.0, 4.1, 4.1, 3.8, and 4.6%, respectively compared the Toyota Prius, as shown in Table 10.6.

Table 10.6: Performances of optimum designs: Toyota Prius and M2A2 approach

Performance	Toyota Prius	M2 methodology: M2A2 approach				
		M2A2-C1	M2A2-C2	M2A2-C3	M2A2-C4	M2A2-C5
Acceleration (0~60 mph), seconds	13.4	13.06	13.05	13.07	13.11	13.0
Acceleration (0~60 mph) w.r.t. Prius, %		-2.5	-2.6	-2.5	-2.2	-3.0
Maximum speed, mph	113.3	114.54	114.59	114.59	114.48	114.76
Maximum speed w.r.t. Prius, %		1.1	1.1	1.1	1.0	1.3
Gradeability, %	13.8	14.35	14.37	14.37	14.33	14.44
Gradeability w.r.t. Prius, %		4.0	4.1	4.1	3.8	4.6

The improvements in the performances were due to 3.1, 3.3, 3.3, 3.1, and 3.6% higher combined power of the ICE and motor of the M2A2-C1, M2A2-C2, M2A2-

C3, M2A2-C4, and M2A2-C5 designs, respectively compared to the Toyota Prius, as shown in Table 10.7.

Table 10.7: Combined power: Toyota Prius and M2A2 approach

Combined power	Toyota Prius (base model)	M2 methodology: M2A2 approach				
		M2A1-C1	M2A1-C2	M2A1-C3	M2A1-C4	M2A1-C5
(ICE + Motor), kW	73.0	75.29	75.41	75.39	75.28	75.61
(ICE + Motor) w.r.t. Prius, %		3.1	3.3	3.3	3.1	3.6

10.4 Battery SOC during optimisation: optimum designs of M2A2 approach

The battery SOC of the M2A2-C1, M2A2-C2, M2A2-C3, M2A2-C4, and M2A2-C5 designs during the optimisation over the respective combination of driving patterns are shown in Table 10.8.

The battery SOC after each of the 5 driving patterns was within the desired limits (<0.5% of initial battery SOC) for all the optimum designs, as shown in Table 10.8. For the M2A1 approach, the 4th constraint (Delta SOC < 0.5%) was not satisfied for each driving pattern but satisfied it overall. But for the M2A2 approach, the 4th constraint was satisfied not only overall but also over each driving pattern, as shown in Table 10.8.

Table 10.8: Battery SOC after each driving pattern during optimisation: optimum designs of M2A2 approach

Design	Sequence of driving patterns	Battery SOC after each driving pattern	Delta SOC, %
M2A2-C1	1 st (HWFET)	0.6985	0.21
	2 nd (FTP)	0.702	0.29
	3 rd (LA92)	0.6984	0.23
	4 th (US06)	0.6966	0.49
	5 th (NEDC)	0.7002	0.03
M2A2-C2	1 st (NEDC)	0.6998	0.03
	2 nd (HWFET)	0.6984	0.23
	3 rd (LA92)	0.6985	0.21
	4 th (US06)	0.6972	0.40
	5 th (FTP)	0.7015	0.21
M2A2-C3	1 st (NEDC)	0.7011	0.16
	2 nd (HWFET)	0.6984	0.23
	3 rd (FTP)	0.702	0.29
	4 th (US06)	0.698	0.29
	5 th (LA92)	0.6983	0.24
M2A2-C4	1 st (NEDC)	0.6999	0.01
	2 nd (FTP)	0.7018	0.26
	3 rd (LA92)	0.6986	0.20
	4 th (US06)	0.6978	0.31
	5 th (HWFET)	0.6984	0.23
M2A2-C5	1 st (NEDC)	0.7006	0.09
	2 nd (HWFET)	0.6984	0.23
	3 rd (FTP)	0.7014	0.20
	4 th (LA92)	0.6990	0.14
	5 th (US06)	0.6977	0.33

10.5 FE evaluation over standard driving patterns: optimum designs of M2A2 approach

The M2A2-C1, M2A2-C2, M2A2-C3, M2A2-C4, and M2A2-C5 designs were evaluated for FE over the NEDC, FTP, LA92, HWFET, and US06 separately. The target SOC was varied during the FE evaluation for each design to maintain the

desired final battery SOC (within <0.5% of the initial battery SOC i.e., delta SOC < 0.5%) over individual driving pattern, as discussed in section 6.9 of chapter 6.

10.5.1 Battery SOC during FE evaluation: optimum designs of M2A2 approach

The target SOC and final battery SOC of each optimum design of the M2A2 approach during FE evaluation are shown in Table 10.9 and Table 10.10, respectively. The target SOC values of the optimum designs were same over a driving pattern. This indicates that all the optimum designs of the M2A2 approach were same.

Table 10.9: Target SOC over driving patterns during FE evaluation: M2A2 approach

Driving patterns	Target SOC				
	M2A2-C1	M2A2-C2	M2A2-C3	M2A2-C4	M2A2-C5
NEDC	0.5706	0.5706	0.5706	0.5706	0.5706
FTP	0.6890	0.6902	0.6890	0.6902	0.6902
LA92	0.6569	0.6569	0.6569	0.6569	0.6569
HWFET	0.5500	0.5490	0.5500	0.5500	0.5500
US06	0.5628	0.5628	0.5628	0.5628	0.5628

The final battery SOC of each optimum design of the M2A2 approach during the FE evaluation are shown in Table 10.10. All the designs of the M2A2 approach were able to operate in charge sustaining over all the driving patterns.

Table 10.10: Final battery SOC over driving patterns during FE evaluation: M2A2 approach

Driving pattern	Final battery SOC				
	M2A2-C1	M2A2-C2	M2A2-C3	M2A2-C4	M2A2-C5
NEDC	0.7007	0.6995	0.7008	0.6996	0.7003
FTP	0.7012	0.7021	0.7011	0.7020	0.7018
LA92	0.7001	0.7003	0.7002	0.7001	0.7006
HWFET	0.6985	0.6974	0.6984	0.6984	0.6984
US06	0.6989	0.6997	0.6999	0.7000	0.7002

10.6 FE over standard driving patterns: optimum designs of M2A2 approach

The FE values of the M2A2-C1, M2A2-C2, M2A2-C3, M2A2-C4, and M2A2-C5 designs are shown in Table 10.11.

Table 10.11: FE over standard driving patterns: optimum designs of M2A2 approach

Driving pattern	FE, mpg					FE variation among designs over a driving pattern, %
	M2 methodology: M2A2 approach					
	M2A2-C1	M2A2-C2	M2A2-C3	M2A2-C4	M2A2-C5	
NEDC	81.3	81.3	81.2	81.3	81.0	0.4
FTP	67.4	67.3	67.3	67.4	67.3	0.1
LA92	58.0	58.0	57.9	58.0	57.9	0.2
HWFET	118.8	118.8	118.7	118.7	118.6	0.2
US06	56.9	56.8	56.8	56.9	56.7	0.4
<i>Average FE, mpg</i>	76.5	76.4	76.4	76.5	76.3	0.2
<i>Standard Deviation of FE, mpg</i>	22.9	22.9	22.9	22.9	22.9	
<i>FE variability, %</i>	29.9	30.0	30.0	29.9	30.0	

The average FE values of the M2A2-C1, M2A2-C2, M2A2-C3, M2A2-C4, and M2A2-C5 designs were 76.5, 76.4, 76.4, 76.5, and 76.3 mpg, respectively. The variation in the average FE for all the optimum designs was 0.2%; the variation in FE among the optimum designs over NEDC, FTP, LA92, HWFET, and US06 were 0.4, 0.1, 0.2, 0.2, and 0.4% respectively. The variation was much reduced compared to the variations for the M1 methodology and M2A1 approach, as shown in Table 10.12.

Table 10.12: FE variation among designs over a driving pattern: M1, M2A1, and M2A2

Driving pattern	FE variation among designs over a driving pattern, %		
	M1 methodology	M2 methodology	
		M2A1 approach	M2A2 approach
NEDC	7.5	5.0	0.4
FTP	5.8	5.4	0.1
LA92	8.8	4.9	0.2
HWFET	10.5	11.7	0.2
US06	23.6	24.3	0.4
Average FE	4.0	3.9	0.2

Due to the smaller variations in FE among the designs of the M2A2 approach, it could be concluded that all the designs provided almost similar FE. Hence, the variations in component sizes among the M2A2-C1, M2A2-C2, M2A2-C3, M2A2-C4, and M2A2-C5 designs i.e., 0.49, 0.79, 0.72, and 0.78% variations in the ICE, generator, motor, and battery sizes respectively, as shown in Table 10.2, had little effect on FE.

As the variations in component sizes among the M2A2-C1, M2A2-C2, M2A2-C3, M2A2-C4, and M2A2-C5 designs were small and all the designs provided almost the similar FE, it could be considered that there was effectively no difference among all the designs. In other words, the M2A2 approach provided a single design irrespective of the sequence of driving patterns. Therefore for FE purposes as well as comparative design purposes, the M2A2 approach can be considered deliver a single optimum design.

As the M2A2 approach provided the same design irrespective of the sequence of driving patterns, it eliminated the need of a separate decision making process

required for the traditional methodology and M2A1 approach to find the best design from different optimum designs.

10.7 Optimum designs: Toyota Prius, M1, and M2A2

As all the optimum designs, namely, M2A2-C1, M2A2-C2, M2A2-C3, M2A2-C4, and M2A2-C5 were same, for this study, the optimum ICE, generator, motor, and battery sizes for the M2A2-C1, M2A2-C2, M2A2-C3, M2A2-C4, and M2A2-C5 designs were averaged and the average design was termed as M2A2 design in the subsequent discussions, as shown in Table 10.13. The ICE, generator, motor, and battery sizes of the M2A2 design were 44.94 kW, 16.49 kW, 30.46 kW, and 7.69 Ah, respectively. The average design was considered as the optimum design of the M2A2 approach for the comparison with the traditional methodology (M1) and the base simulation model of the Toyota Prius.

Table 10.13: M2A2 design

Design	Optimum size			
	P_{ICE} , kW	P_G , kW	P_M , kW	C_B , Ah
M2A2-C1	44.83	16.51	30.46	7.65
M2A2-C2	44.92	16.53	30.49	7.71
M2A2-C3	44.95	16.44	30.44	7.66
M2A2-C4	44.94	16.56	30.34	7.70
M2A2-C5	45.05	16.43	30.56	7.71
Average design (M2A2)	44.94	16.49	30.46	7.69

The M2A2 design was compared with the designs of the Toyota Prius and M1 methodology in Table 10.14.

Table 10.14: Component sizes of optimum designs: Toyota Prius, M1, and M2A2

Design parameter	Toyota Prius	Optimum component sizes					
		M1 methodology					M2 methodology: M2A2 approach
		M1-NEDC	M1-FTP	M1-LA92	M1-HWFET	M1-US06	M2A2 design
P_{ICE} , kW	43.0	35.12	37.91	36.33	29.32	40.52	44.94
P_G , kW	15.0	13.21	14.13	13.72	12.23	18.33	16.49
P_M , kW	30.0	39.93	39.52	44.41	44.32	34.82	30.46
C_B , Ah	6.0	6.21	8.92	8.71	7.33	8.74	7.69
P_{IC} w.r.t. M2A2, %	-4.3	-21.9	-15.6	-19.2	-34.8	-9.8	
P_G w.r.t. M2A2, %	-9.0	-19.9	-14.3	-16.8	-25.8	11.2	
P_M w.r.t. M2A2, %	-1.5	31.1	29.7	45.8	45.5	14.3	
C_B w.r.t. M2A2, %	-22.0	-19.2	16.0	13.3	-6.6	13.7	

The optimum ICE, generator, motor, and battery sizes of the M2A2 design were 4.3, 9.0, 1.5, and 22.0%, respectively higher compared to that of the Toyota Prius. Therefore, the M2A2 design was the closest design compared to the Toyota Prius in terms of the maximum power of the ICE, generator, and motor.

The M2A2 design had bigger size of ICE and smaller size of motor compared to all the designs of the M1 methodology. The M2A2 design had 21.9, 15.6, 19.2, 34.8, and 9.8% higher power of ICE compared to the M1-NEDC, M1-FTP, M1-LA92, M1-HWFET, and M1-US06 designs respectively. The M2A2 design had 31.1, 29.7,

45.8, 45.5, and 14.3% lower power of motor compared to the M1-NEDC, M1-FTP, M1-LA92, M1-HWFET, and M1-US06 designs respectively.

The M2A2 design had 19.9, 14.3, 16.8, and 25.8% higher power of generator compared to the M1-NEDC, M1-FTP, M1-LA92, and M1-HWFET designs respectively and 11.2% lower power of generator compared to the M1-US06 design.

The M2A2 design had 19.2 and 4.7% higher capacity of battery compared to the M1-NEDC and M1-HWFET designs respectively and 16.0, 13.3, and 13.7% lower capacity of battery compared to the M1-FTP, M1-LA92, and M1-US06 designs respectively.

The M2A2 design had 4.2% higher combined power (ICE, generator, and motor) compared to the Toyota Prius, as shown in Table 10.15. This potentially leads to higher component cost of the M2A2 design compared to the Toyota Prius.

Table 10.15: Combined power: Toyota Prius, M1, and M2A2

Combined power	Toyota Prius	M1 methodology					M2 methodology: M2A2 approach
		M1-NEDC	M1-FTP	M1-LA92	M1-HWFET	M1-US06	M2A2 design
(ICE + Motor), kW	73.0	75.05	77.43	80.74	73.64	75.34	75.40
(ICE + Motor) w.r.t. M2A2, %	-3.2	-0.5	2.7	7.1	-2.3	-0.1	
(ICE + Motor + Generator), kW	88.0	88.26	91.56	94.46	85.87	93.67	91.89
(ICE + Motor + Generator) w.r.t. M2A2, %	-4.2	-4.0	-0.4	2.8	-6.6	1.9	

The M2A2 design also had 4.0, 0.4, and 6.6% higher combined power (ICE, generator, and motor) compared to the M1-NEDC, M1-FTP, and M1-HWFET designs respectively. But the M2A2 design had 2.8 and 1.9% lower combined power (ICE, generator, and motor) compared to the M1-LA92 and M1-US06 designs respectively.

10.8 Performance of optimum designs: Toyota Prius, M1, and M2A2

The performances of the Toyota Prius, traditional methodology (M1), and M2A2 design are compared in Table 10.16.

Table 10.16: Performances of optimum designs: Toyota Prius, M1, and M2A2

Performance	Toyota Prius	M1 methodology					M2 methodology: M2A2 approach
		M1-NEDC	M1-FTP	M1-LA92	M1-HWFET	M1-US06	M2A2 design
Acceleration (0~60 mph), seconds	13.4	11.8	11.6	10.8	11.6	12.4	13.1
Acceleration (0~60 mph) w.r.t. M2A2, %	2.3	-9.9	-11.5	-17.6	-11.5	-5.3	
Maximum speed, mph	113.3	114.4	115.7	117.5	113.6	114.6	114.6
Maximum speed w.r.t. M2A2, %	-1.1	-0.2	1.0	2.5	-0.9	0.0	
Gradeability, %	13.8	14.3	14.8	15.6	14.0	14.4	14.4
Gradeability w.r.t. M2A2, %	-4.2	-0.7	2.8	8.3	-2.8	0.0	

The M2A2 design had 2.3% lower time of acceleration, 1.1% higher maximum speed, and 4.2% higher gradeability compared to the Toyota Prius. The better

performance of the M2A2 design was due to 3.2% higher combined power of the ICE and motor compared to the Toyota Prius, as shown in Table 10.15.

The M2A2 design had larger acceleration time compared to all the optimum designs of the M1 methodology. The M2A2 design had 9.9, 11.5, 17.6, 11.5, and 5.3% larger acceleration time compared to the M1-NEDC, M1-FTP, M1-LA92, M1-HWFET, and M1-US06 designs, respectively, as shown in Table 10.16. Although the M2A2 design had 21.9, 15.6, 19.2, 34.8, and 9.8% higher ICE power compared to the M1-NEDC, M1-FTP, M1-LA92, M1-HWFET, and M1-US06 designs (Table 10.14), the lower power of the motor of the M2A2 design by 31.1, 29.7, 45.8, 45.5, and 14.3% compared to the M1-NEDC, M1-FTP, M1-LA92, M1-HWFET, and M1-US06 designs (Table 10.14) caused higher acceleration time for the M2A2 design, because at lower speeds only the motor was operated.

The M2A2 design had 0.2, and 0.9% higher maximum speed compared to the M1-NEDC and M1-HWFET designs respectively (Table 10.16), because the M2A2 design had 0.5 and 2.3% higher combined power of the ICE and motor compared to the M1-NEDC and M1-HWFET designs respectively (Table 10.15). The maximum speed depends on the combined power of the ICE and motor. The maximum speed of the M2A2 design was same as that of the M1-US06 design (Table 10.16) due to almost similar combined power of the ICE and motor for the M2A2 and M1-US06 designs (Table 10.15). The M2A2 design had 1.0 and 2.5% lower maximum speed compared to the M1-FTP and M1-LA92 designs respectively (Table 10.16) because the M2A2 design had 2.7 and 7.1% lower combined power of the ICE and motor compared to the M1-FTP and M1-LA92 designs respectively (Table 10.15).

As the gradeability also depends on the combined power of ICE and motor, the M2A2 design had 0.7 and 2.8% lower gradeability compared to the M1-NEDC and M1-HWFET designs respectively, same gradeability with the M1-US06 design and 2.8 and 8.3% lower gradeability compared to the M1-FTP and M1-LA92 designs respectively, as shown in Table 10.16.

10.9 FE evaluation over standard driving patterns: Toyota Prius, M1, and M2A2

The M2A2 design was evaluated for FE over NEDC, FTP, LA92, HWFET, and US06 separately. The target SOC was varied during the FE evaluation over each driving pattern to achieve the desired final battery SOC (within <0.5% of the initial battery SOC i.e., $\Delta \text{SOC} < 0.5\%$), as discussed in section 6.9 of chapter 6.

10.9.1 Battery SOC during FE evaluation: Toyota Prius, M1, and M2A2

The target SOC and final battery SOC of the M2A2 design during the FE evaluation are shown in Table 10.17.

Table 10.17: Target SOC and final battery SOC during FE evaluation: Toyota Prius and M2A2 design

Driving pattern	Toyota Prius		M2 methodology: M2A2 approach	
			M2A2 design	
	Target SOC	Final battery SOC	Target SOC	Final battery SOC
NEDC	0.5401	0.6978	0.5706	0.6995
FTP	0.6803	0.6982	0.6902	0.7021
LA92	0.6604	0.6985	0.6569	0.7003
HWFET	0.5502	0.6995	0.5490	0.6974
US06	0.6204	0.6989	0.5628	0.6997

The M2A2 design required lower target SOC values compared to the Toyota Prius over LA92, HWFET, and US06, whereas the M2A2 design required higher target SOC over NEDC and FTP to achieve the desired final battery SOC. Therefore, the M2A2 design required lower target SOC over aggressive driving patterns compared to the Toyota Prius. The probable reason could be the higher ICE power of the M2A2 design compared to the Toyota Prius.

The M2A2 design was able to operate over all the 5 driving patterns with the desired battery SOC control ($\Delta \text{SOC} < 0.5\%$) i.e., charge sustaining over driving usage.

The battery SOC swing of the M2A2 design during the FE evaluation over NEDC, FTP, LA92, HWFET, and US06 are shown in Table 10.18. The M2A2 design is compared with the designs of the Toyota Prius and the M1 methodology in Table 10.18. The battery SOC swing of the M2A2 design was 28.6, 25.7, 9.2, 17.0, and 52.2% lower over NEDC, FTP, LA92, HWFET, and US06, respectively compared to the Toyota Prius, as shown in Table 10.18. Therefore, the M2A2 design had on average 26.5% lower swing of the battery SOC compared to the Toyota Prius. The lower swing of the battery SOC might lead to higher battery life-cycle for the M2A2 design compared to the Toyota Prius [20], [105].

The M2A2 design had the lowest battery SOC swing over US06 when compared with the Toyota Prius and the designs of the M1 methodology. The M2A2 design had 52.2, 140.5, 32.7, 42.0, 53.1, and 18.9% lower battery SOC swing compared to the Toyota Prius, M1-NEDC, M1-FTP, M1-LA92, M1-HWFET, and M1-US06, respectively over US06, as shown in Table 10.18. The probable reason could be the higher ICE power of the M2A2 design compared to other designs helped the M2A2

design to charge the battery even after delivering desired drive torque over aggressive US06.

Table 10.18: Comparison of battery SOC swing: Toyota Prius, M1, and M2A2

Driving pattern	Parameters	Battery SOC						
		Toyota Prius	M1 methodology					M2 methodology: M2A2 approach
			M1-NEDC	M1-FTP	M1-LA92	M1-HWFET	M1-US06	M2A2 design
NEDC	Maximum SOC	0.7016	0.7000	0.7000	0.7000	0.7030	0.7013	0.7012
	Minimum SOC	0.5117	0.5315	0.5765	0.5788	0.5832	0.5718	0.5535
	<i>SOC swing</i>	0.1899	0.1685	0.1235	0.1212	0.1198	0.1295	0.1477
	<i>Swing w.r.t. M2A2, %</i>	28.6	14.1	-16.4	-17.9	-18.9	-12.3	
FTP	Maximum SOC	0.7421	0.7458	0.7335	0.7355	0.7417	0.7355	0.7386
	Minimum SOC	0.5738	0.5878	0.6187	0.6204	0.6190	0.6175	0.6047
	<i>SOC swing</i>	0.1683	0.1580	0.1148	0.1151	0.1227	0.1180	0.1339
	<i>Swing w.r.t. M2A2, %</i>	25.7	18.0	-14.3	-14.0	-8.4	-11.9	
LA92	Maximum SOC	0.7320	0.7374	0.7286	0.7248	0.7185	0.7334	0.7447
	Minimum SOC	0.6405	0.6281	0.6558	0.6502	0.6274	0.6595	0.6609
	<i>SOC swing</i>	0.0915	0.1093	0.0728	0.0746	0.0911	0.0739	0.0838
	<i>Swing w.r.t. M2A2, %</i>	9.2	30.4	-13.1	-11.0	8.7	-11.8	
HWFET	Maximum SOC	0.7320	0.7298	0.7203	0.7253	0.7354	0.7212	0.7229
	Minimum SOC	0.6405	0.6413	0.6491	0.6522	0.6430	0.6492	0.6447
	<i>SOC swing</i>	0.0915	0.0885	0.0712	0.0731	0.0924	0.0720	0.0782
	<i>Swing w.r.t. M2A2, %</i>	17.0	13.2	-8.9	-6.5	18.2	-7.9	
US06	Maximum SOC	0.7903	0.8342	0.7643	0.7686	0.7000	0.7518	0.7459
	Minimum SOC	0.6046	0.5408	0.6024	0.5954	0.5132	0.6067	0.6239
	<i>SOC swing</i>	0.1857	0.2934	0.1619	0.1732	0.1868	0.1451	0.1220
	<i>Swing w.r.t. M2A2, %</i>	52.2	140.5	32.7	42.0	53.1	18.9	

Among all the designs of the M1 methodology, the M1-NEDC design had always higher battery SOC swing compared to the M2A2 design. The M2A2 design had 14.1, 18.0, 30.4, 13.2, and 140.5% lower battery SOC swing over NEDC, FTP, LA92, HWFET, and US06, respectively compared to the M1-NEDC, as shown in Table 10.18.

The M1-FTP, M1-LA92, M1-US06, and M2A2 designs had lower battery SOC swing compared to the Toyota Prius and the M1-NEDC design over all the driving patterns, as shown in Table 10.18. This indicates that higher battery capacity helped to lower the battery SOC swing, as shown from Figure 10.2 to Figure 10.4. Although the M1-NEDC design had lower battery SOC swing over NEDC and FTP, the M1-NEDC design had higher battery SOC swing over LA92 and US06 compared to the Toyota Prius. As the M1-NEDC design had higher battery capacity and lower ICE power compared to the Toyota Prius, it could be said that the ICE power also influenced the battery SOC swing over aggressive driving patterns. The M1-HWFET design had higher battery SOC swing compared to the M2A2 design and comparable battery SOC swing compared to the Toyota Prius over LA92. As the M1-HWFET design had higher battery capacity and lower ICE power compared to the M2A2 design and Toyota Prius, it also indicates that the ICE power influenced the battery SOC swing over aggressive driving pattern. Therefore, the higher power of the ICE and the higher capacity of the battery could reduce the battery SOC swing and hence, could improve the life of the battery.

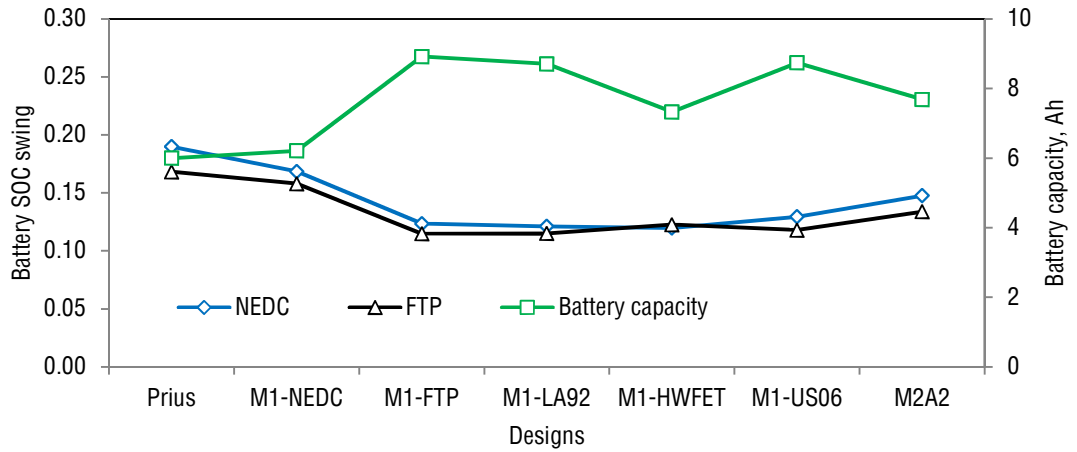


Figure 10.2: Battery SOC swing and battery capacity over NEDC and FTP: Toyota Prius, M1, and M2A2

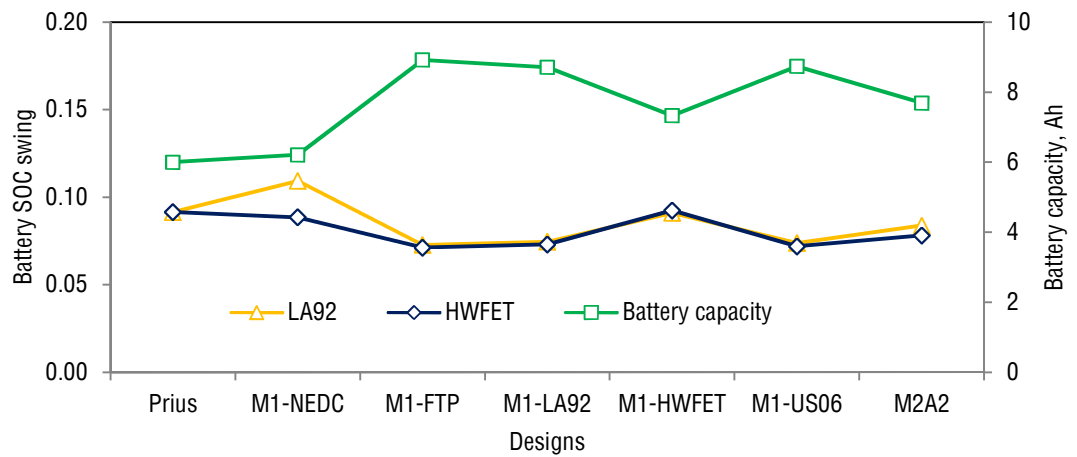


Figure 10.3: Battery SOC swing and battery capacity over LA92 and HWFET: Toyota Prius, M1, and M2A2

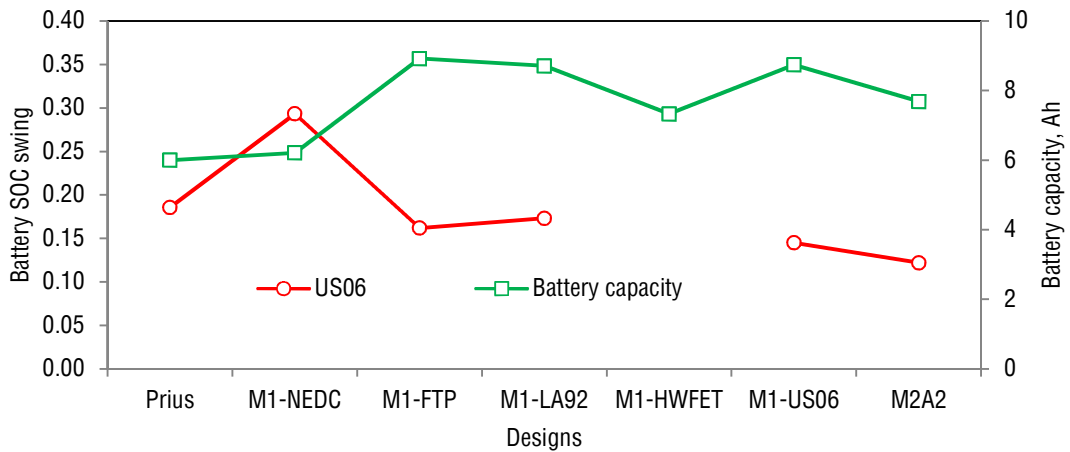


Figure 10.4: Battery SOC swing and battery capacity over US06: Toyota Prius, M1, and M2A2

10.9.2 Battery system efficiency over standard driving patterns: Toyota Prius, M1, and M2A2

The battery system efficiency of the M2A2 design are compared with that of the Toyota Prius, M1-NEDC, M1-FTP, M1-LA92, M1-HWFET, and M1-US06 designs in Figure 10.5 and Figure 10.6. The battery system efficiency of the M2A2 design over NEDC, FTP, HWFET, LA92, and US06 were 90.8, 90.8, 87.2 (Figure 10.5), 86.1, and 63.9% (Figure 10.6), respectively. The battery system efficiency of the Toyota Prius over NEDC, FTP, HWFET, LA92, and US06 were 90.7, 91.2, 86.3 (Figure 10.5), 85.4, and 63.0% (Figure 10.6), respectively. Therefore, the M2A2 design had 0.1, 1.0, 0.8, and 1.4% higher battery system efficiency over NEDC, HWFET, LA92, and US06, respectively compared to the Toyota Prius. But the M2A2 design had 0.4% lower battery system efficiency over FTP compared to the Toyota Prius. Therefore, the M2A2 design had on average 0.6% higher battery system efficiency compared to the Toyota Prius. This indicates the battery of the M2A2 design required less charging over NEDC, HWFET, LA92, and US06 due to

4.3% higher ICE power and 22.0% higher battery capacity of the M2A2 design compared to the Toyota Prius.

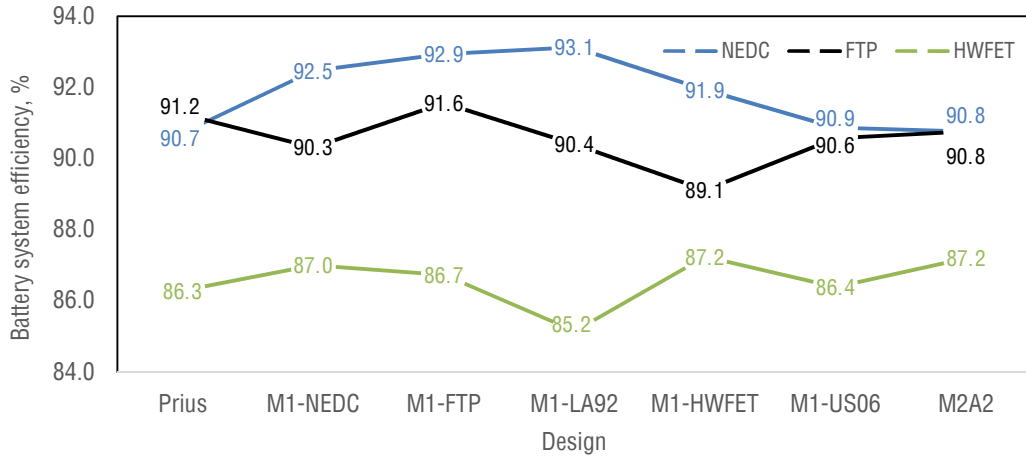


Figure 10.5: Battery system efficiency over NEDC, FTP, and HWFET: Toyota Prius, M1, and M2A2

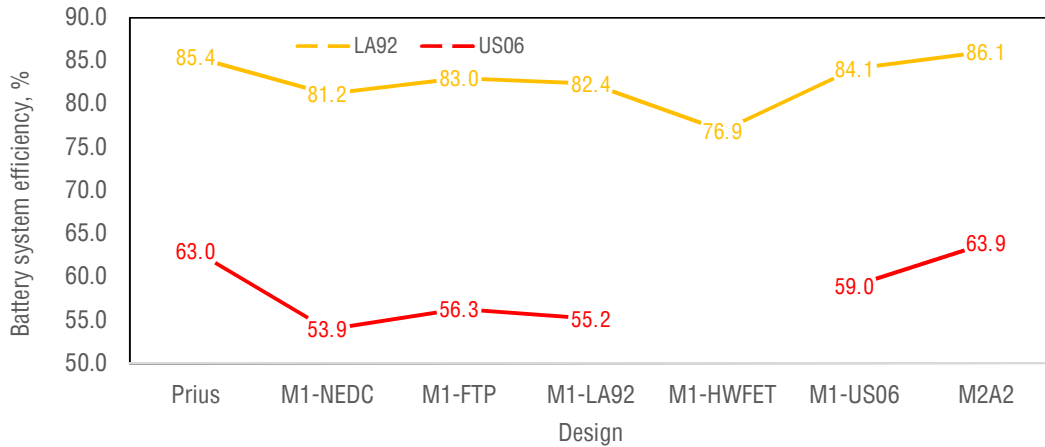


Figure 10.6: Battery system efficiency over LA92 and US06: Toyota Prius, M1, and M2A2

The M2A2 design had the highest battery system efficiency over HWFET, LA92, and US06 when compared with the Toyota Prius, M1-NEDC, M1-FTP, M1-LA92, M1-HWFET, and M1-US06 designs. Therefore, the M2A2 design required less battery charging over aggressive driving patterns due to the highest ICE power of the

M2A2 design compared to the Toyota Prius and all the designs of the M1 methodology.

10.10 FE over standard driving patterns: Toyota Prius, M1, and M2A2

The FE values of the M2A2 design are compared with the Toyota Prius and M1 methodology in Table 10.19. The FE values of the M2A2 design over the NEDC, FTP, LA92, HWFET, and US06 are 81.3, 67.3, 58.0, 118.8, and 56.8 mpg, respectively, as shown in Table 10.19.

The minimum FE of the Toyota Prius, M1-NEDC, M1-FTP, M1-LA92, M1-HWFET, and M1-US06 over all the 5 driving patterns were 55.4, 44.5, 54.2, 50.8, 43.6, and 57.1 mpg respectively over US06, whereas the minimum FE of the M2A2 design was 56.8 mpg over US06. Therefore, the M2A2 design improved the minimum FE by 2.5, 21.7, 4.6, 10.6, and 23.2% compared to the Toyota Prius, M1-NEDC, M1-FTP, M1-LA92, and M1-HWFET designs, respectively. But the M2A2 design had 0.5% lower minimum FE when compared to the M1-US06 design. This is obvious as the M1-US06 design was optimum over US06.

The M2A2 design had 1.2 and 2.5% higher FE over LA92 and US06 respectively, whereas 2.2, 1.0, and 1.2% lower FE over NEDC, FTP, and HWFET respectively, compared to the Toyota Prius. This indicates the suitability of the M2A2 design more towards aggressive driving patterns which might be more common in real world. The M2A2 design provided the lowest FE over FTP and HWFET when compared with the Toyota Prius and designs of the M1 methodology.

The FE variability of the M2A2 design is discussed in section 10.12.

Table 10.19: FE over standard driving patterns: Toyota Prius, M1, and M2A2

Drive cycles	FE, mpg						
	Toyota Prius	M1 methodology					M2 methodology: M2A2 approach
		M1-NEDC	M1-FTP	M1-LA92	M1-HWFET	M1-US06	M2A2 design
NEDC	83.1	86.3	86.2	85.8	79.8	83.4	81.3
FTP	68.0	71.9	72.4	72.2	68.2	70.4	67.3
LA92	57.5	56.9	61.4	61.5	56.1	57.3	58.0
HWFET	120.3	130.5	127.6	129.0	138.4	123.9	118.8
US06	55.4	44.5	54.2	50.8	43.6 (x)	57.1	56.8
<i>Average FE, mpg</i>	76.9	78.0	80.4	79.9	77.2	78.4	76.4
<i>Average FE w.r.t. M2A2, %</i>	0.7	2.1	5.2	4.6	1.0	2.6	
<i>Minimum FE, mpg</i>	55.4	44.5	54.2	50.8	43.6	57.1	56.8
<i>Minimum FE w.r.t. M2A2, %</i>	-2.5	-21.7	-4.6	-10.6	-23.2	0.5	
<i>Standard deviation of FE, mpg</i>	23.8	29.8	26.0	27.2	32.9	24.7	22.9
<i>FE variability, %</i>	31.0	38.2	32.3	34.0	42.6	31.5	30.0
<i>FE variability w.r.t. M2A2, %</i>	3.3	27.3	7.7	13.3	42.0	5.0	
(x): Failed to operate charge sustaining							

10.11 Analysis of FE over US06: Toyota Prius, M1, and M2A2

As all designs had minimum FE over US06 and the M2A2 design had higher FE over US06 compared to the Toyota Prius, M1-NEDC, M1-FTP, M1-LA92, and M1-HWFET designs, but had lower FE compared to the M1-US06 design, US06 driving patterns was chosen to understand the reason for higher FE of the M2A2 design compared to all designs apart from the M1-US06 design. The M1-NEDC design was chosen for comparison with the M2A2 design because the M2A2 design had the maximum improvement of FE (27.6% higher FE) compared to the M1-NEDC design. The M1-US06 design was also compared with the M2A2 design because the M2A2 design had 0.9% lower FE compared to the M1-US06 design. The M2A2 design was also compared with the Toyota Prius because the M2A2 design had 2.5% higher FE compared to the Toyota Prius.

10.11.1 Comparison over US06: M2A2 and M1-NEDC

The FC values of the M2A2 and M1-NEDC designs over US06 are compared in Figure 10.7. The FC of the M2A2 design spread up to around 2.87 g/s but majority of FC occurred up to 1.5 g/s. The FC of the M1-NEDC design spread up to around 2.24 g/s but the spread of majority of FC was between around 0.5 g/s and 2.24 g/s.

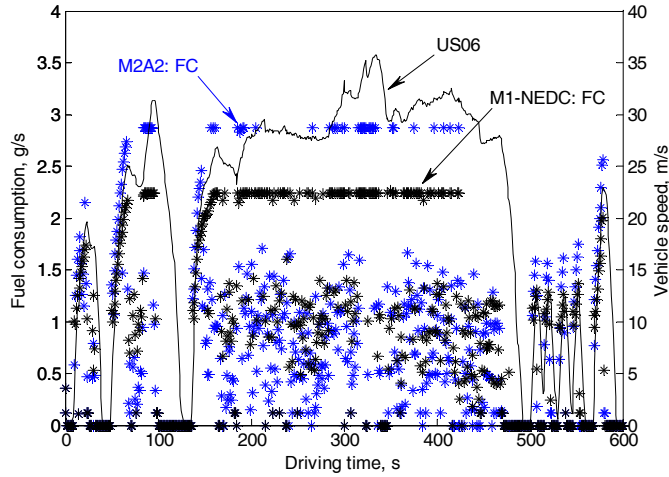


Figure 10.7: Comparison of fuel consumption over US06: M2A2 and M1-NEDC designs

As the FC directly depends on the operation of ICE, the torque and speed of the ICE for the M2A2 and M1-NEDC designs over US06 driving pattern are shown in Figure 10.8 and Figure 10.9, respectively. Figure 10.8 shows that the ICE torque of the M2A2 design spread up to 106.6 Nm but the ICE torque of the M1-NEDC design concentrated more between 60 Nm to 83.2 Nm over US06.

The ICE speed of the M2A2 design concentrated more between 100 rad/s and 300 rad/s, whereas the ICE speed of the M1-NEDC design spread up to around 400 rad/s, as shown in Figure 10.9.

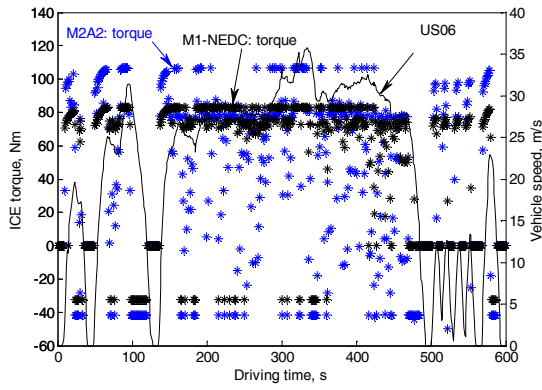


Figure 10.8: Comparison of ICE torque over US06: M2A2 and M1-NEDC designs

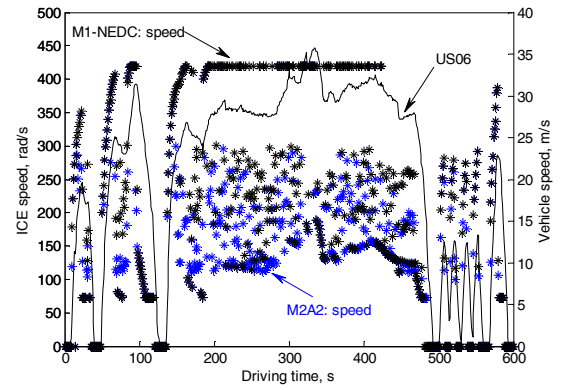


Figure 10.9: Comparison of ICE speed over US06: M2A2 and M1-NEDC designs

As it is difficult to conclude from Figure 10.7, the FC values of both the M2A2 and M1-NEDC designs with respect to torque and speed of ICE are compared in Figure 10.10 and Figure 10.11, respectively. The histograms of the torque and speed of the ICE of the M2A2 and M1-NEDC designs over US06 driving pattern are plotted in Figure 10.12 and Figure 10.13 respectively.

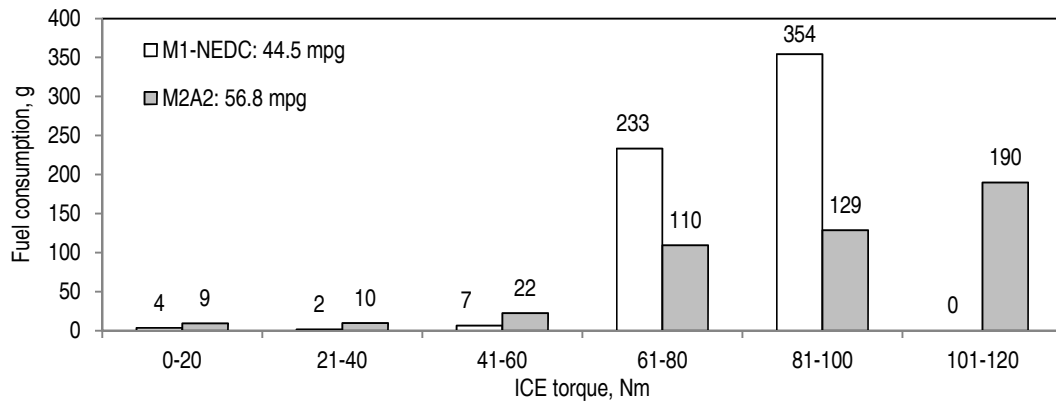


Figure 10.10: Distribution of fuel consumption w.r.t. ICE torque over US06: M2A2 and M1-NEDC designs

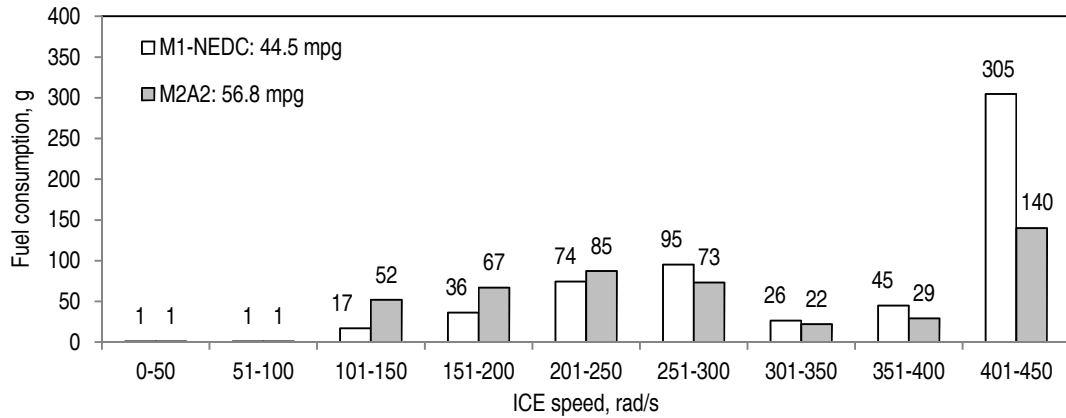


Figure 10.11: Distribution of fuel consumption w.r.t. ICE speed over US06: M2A2 and M1-NEDC designs

The M2A2 and M1-NEDC designs had 91.1 and 98.0% of total FC between 60 Nm and 120 Nm, as shown in Figure 10.10. The M2A2 design had 27.2% lower FC compared to the M1-NEDC between 60 Nm and 120 Nm (Figure 10.10) due to 26.3% lower time of operation of the M2A2 design compared to the M1-NEDC design in this range (Figure 10.12).

The M2A2 and M1-NEDC designs had 74.3 and 90.9% of total FC between 200 and 450 rad/s (Figure 10.11) as the M2A2 and M1-NEDC designs operated 31.6 and 54.2% of total time in this range (Figure 10.13). Hence, the M2A2 design had 41.7% lower time of operation between 200 and 450 rad/s compared to the M1-NEDC design.

Therefore, 26.3% lower time of operation over 60 Nm and 41.7% lower time of operation over 200 rad/s caused 27.6% higher FE in the M2A2 design compared to the M1-NEDC design over US06.

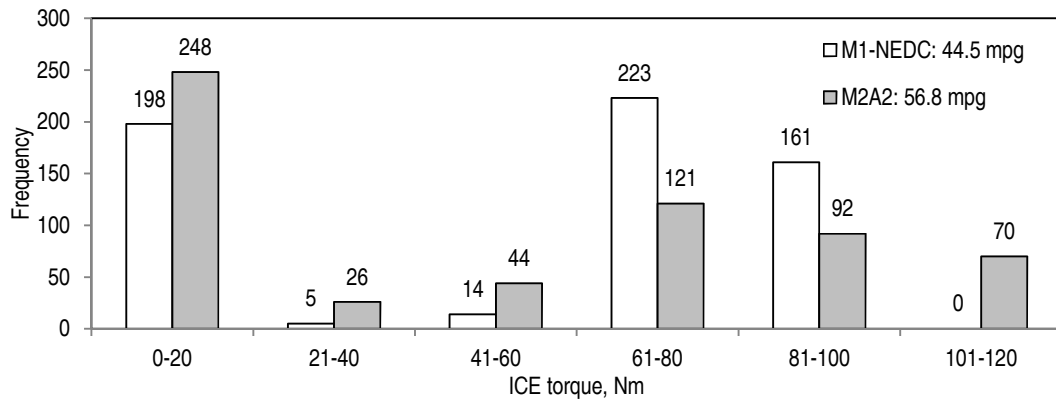


Figure 10.12: Distribution of ICE torque over US06: M2A2 and M1-NEDC designs

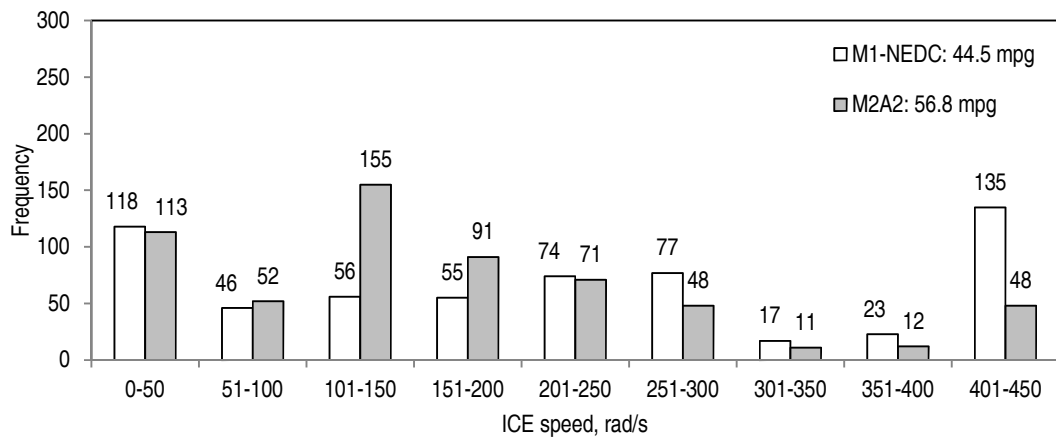


Figure 10.13: Distribution of ICE speed over US06: M2A2 and M1-NEDC designs

Due to the 27.9% lower ICE power and 24.2% lower battery capacity of the M1-NEDC design compared to the M2A2 design, the M1-NEDC design was required to operate more time at higher engine torque and speed to achieve desired final battery SOC, as shown in Figure 10.14. The ICE of the M2A2 design was able to operate at comparatively higher torque compared to the M1-NEDC design during high power demand that assisted to deliver more extra torque to charge battery and this helped to operate lesser time at higher torque region later. The lesser charging was required in

the M2A2 design due to 24.2% higher battery capacity compared to the M1-NEDC design. The 18.6% higher battery system efficiency of the M2A2 design compared to the M1-NEDC design also indicated that the M2A2 design required lesser battery charging compared to the M1-NEDC design. The lesser charging requires lesser ICE operation to support battery charging, ICE operation was required to deliver the driving demand only, therefore more lower torque operation of the ICE.

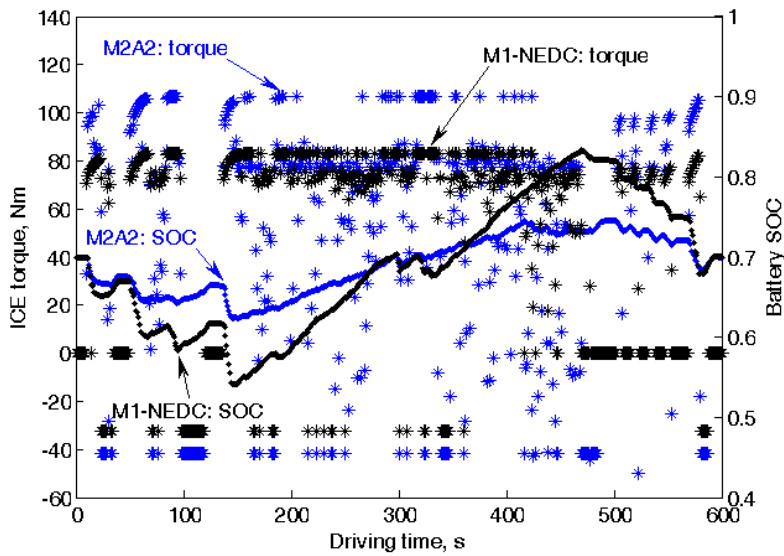


Figure 10.14: Comparison of ICE torque and battery SOC over US06: M2A2 and M1-NEDC designs

10.11.2 Comparison over US06: M2A2 and M1-US06

The FC values of the M2A2 and M1-US06 designs over US06 are compared in Figure 10.15. The FC of the M2A2 and M1-US06 designs spread up to around 2.87 g/s and 2.59 g/s respectively.

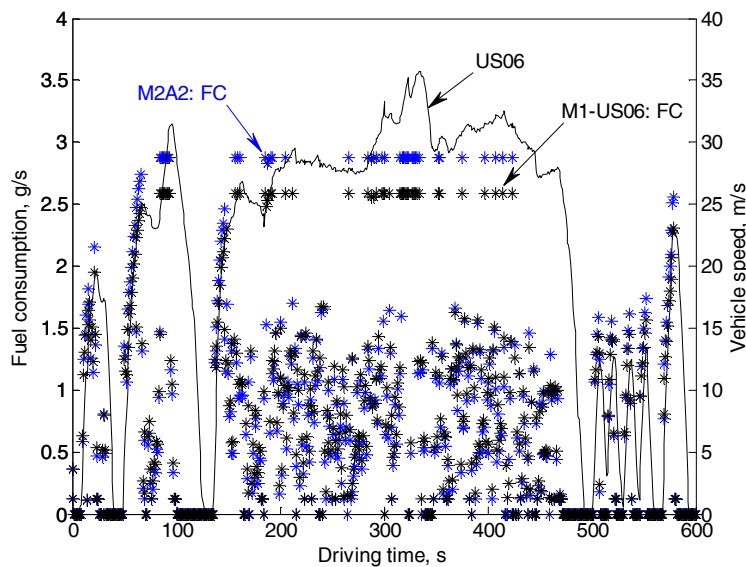


Figure 10.15: Comparison of fuel consumption over US06: M2A2 and M1-US06 designs

As the FC directly depends on the operation of ICE, the torque and speed of the ICE for the M2A2 and M1-US06 designs over US06 driving pattern are shown in Figure 10.16 and Figure 10.17, respectively. Figure 10.16 shows that the ICE torque of the M2A2 and M1-US06 designs spread up to 106.6 Nm and 96.0 Nm respectively. Both the designs operated in similar torque and speed regions, as shown in Figure 10.16 and Figure 10.17 respectively.

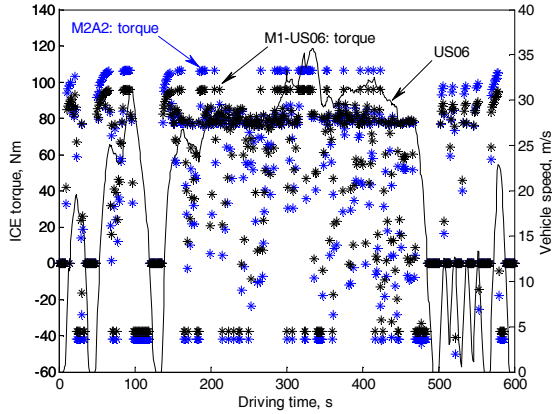


Figure 10.16: Comparison of ICE torque over US06: M2A2 and M1-US06 designs

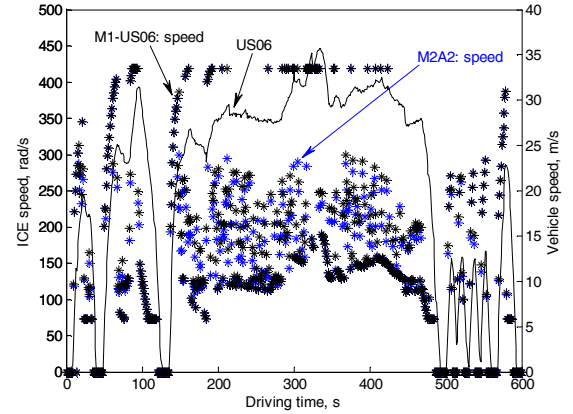


Figure 10.17: Comparison of ICE speed over US06: M2A2 and M1-US06 designs

As it is difficult to conclude from Figure 10.15, the FC values of both the M2A2 and M1-US06 designs with respect to torque and speed of ICE are compared in Figure 10.18 and Figure 10.19, respectively. The histograms of the torque and speed of the ICE of the M2A2 and M1-US06 designs over US06 driving pattern are plotted in Figure 10.20 and Figure 10.21, respectively.

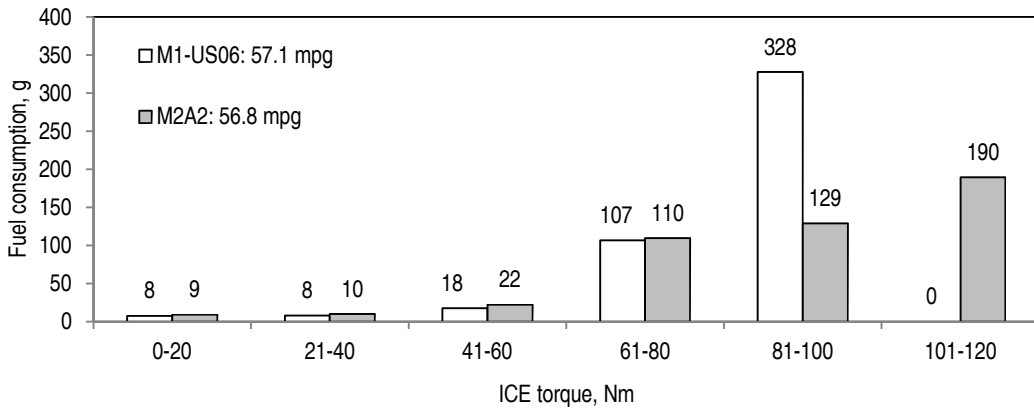


Figure 10.18: Distribution of fuel consumption w.r.t. ICE torque over US06: M2A2 and M1-US06 designs

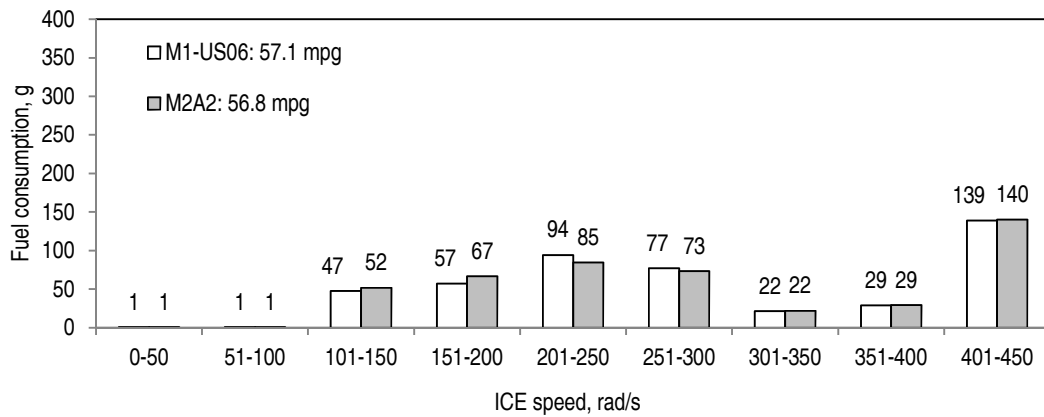


Figure 10.19: Distribution of fuel consumption w.r.t. ICE speed over US06: M2A2 and M1-US06 designs

The M2A2 design had 4.1, 28.1, and 67.8% of total FC below 40 Nm, between 40 Nm and 80 Nm, and above 80 Nm, respectively, as shown in Figure 10.18. The M1-US06 design had 3.3, 26.6, and 70.1% of total FC below 40 Nm, between 40 Nm and 80 Nm, and above 80 Nm, respectively, as shown in Figure 10.18. The M2A2 design had 24.7% higher FC below 40 Nm (Figure 10.18) due to 6.2% higher time of operation in this range compared to the M1-US06 design (Figure 10.20). The M2A2 design had 6.2% higher FC between 40 Nm to 80 Nm (Figure 10.18) due to 3.1% higher time of operation in this range compared to the M1-US06 design (Figure 10.20). The M2A2 design had 2.8% lower FC between 80 Nm to 120 Nm (Figure 10.18) due to 11.5% lower time of operation in this range compared to the M1-US06 design (Figure 10.20). The M2A2 design operated 11.2% lower time above 200 rad/s compared to the M1-US06 design, as shown in Figure 10.21.

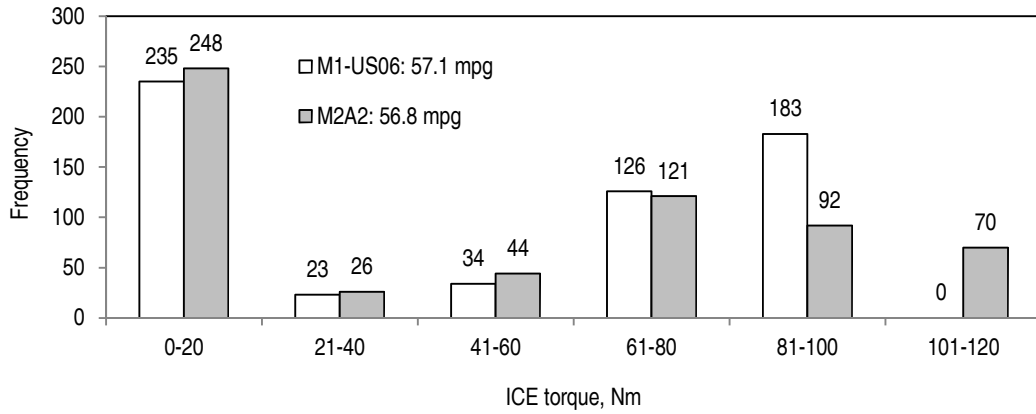


Figure 10.20: Distribution of ICE torque over US06: M2A2 and M1-US06 designs

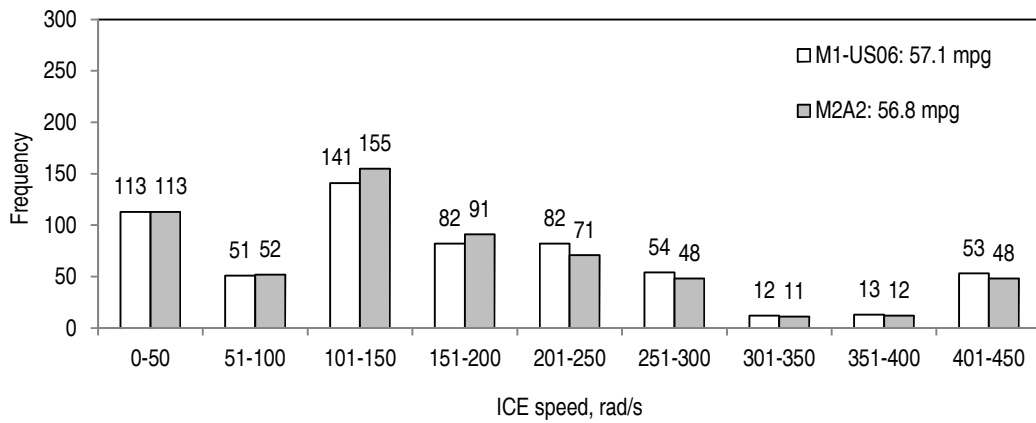


Figure 10.21: Distribution of ICE speed over US06: M2A2 and M1-US06 designs

Figure 10.22 shows that battery SOC of the M1-US06 design was lower compared to the M2A2 design from 90 seconds up to 410 seconds. Therefore, due to 10.9% lower ICE power compared to the M2A2 design, probably the M1-US06 design was required to operate more time above 80 Nm and 200 rad/s to achieve desired final battery SOC.

Although the M2A2 design had lower FC above 80 Nm, the higher FC below 80 Nm caused 0.9% lower FE in M2A2 design.

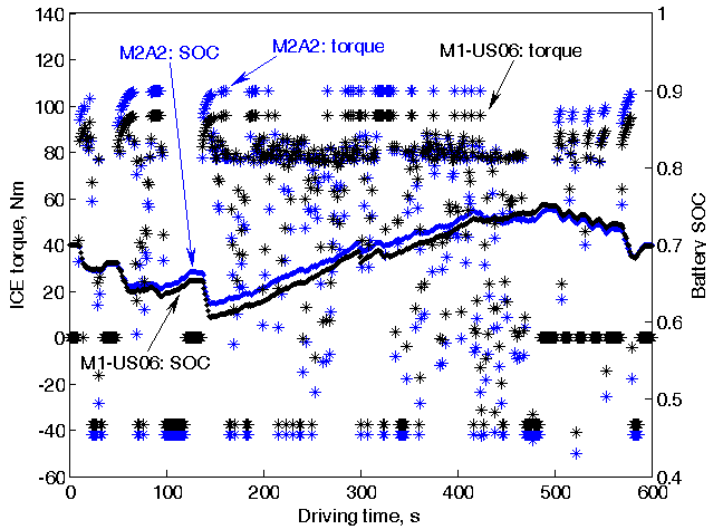


Figure 10.22: Comparison of ICE torque and battery SOC over US06: M2A2 and M1-US06 designs

10.11.3 Comparison over US06: M2A2 and Toyota Prius

The FC values of the M2A2 design and Toyota Prius over US06 are compared in Figure 10.23. The pattern of FC of the M2A2 design and Toyota Prius were similar but the spread of FC of the M2A2 design and Toyota Prius were up to around 2.87 g/s and 2.75 g/s respectively.

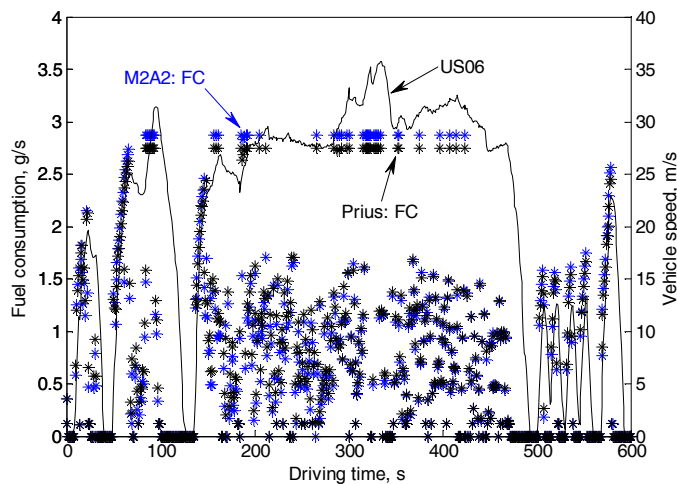


Figure 10.23: Comparison of fuel consumption over US06: M2A2 design and Toyota Prius

As the FC directly depends on the operation of ICE, the torque and speed of the ICE for the M2A2 design and Toyota Prius over US06 driving pattern are shown in Figure 10.24 and Figure 10.25, respectively. Figure 10.24 shows that the operating torque region of ICE for both the designs were similar but ICE torque of the M2A2 design and Toyota Prius spread up to 106.6 Nm and 101.9 Nm respectively. Both the designs operated at similar speed region, as shown in Figure 10.25.

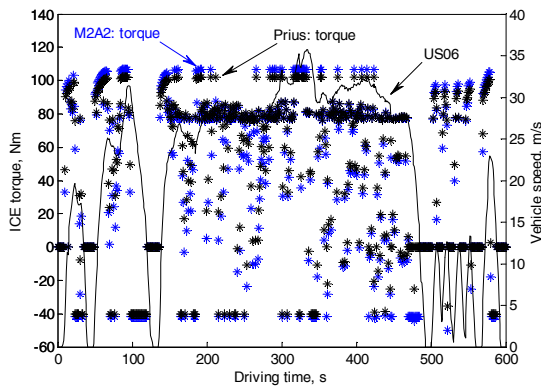


Figure 10.24: Comparison of ICE torque over US06: M2A2 design and Toyota Prius

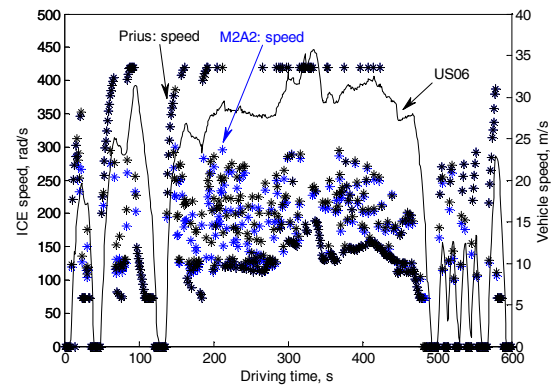


Figure 10.25: Comparison of ICE speed over US06: M2A2 design and Toyota Prius

As it is difficult to conclude from Figure 10.23, the FC values of both the M2A2 design and Toyota Prius with respect to torque and speed of ICE are compared in Figure 10.26 and Figure 10.27, respectively. The histograms of the torque and speed of the ICE of the M2A2 design and Toyota Prius over US06 driving pattern are plotted in Figure 10.28 and Figure 10.29, respectively.

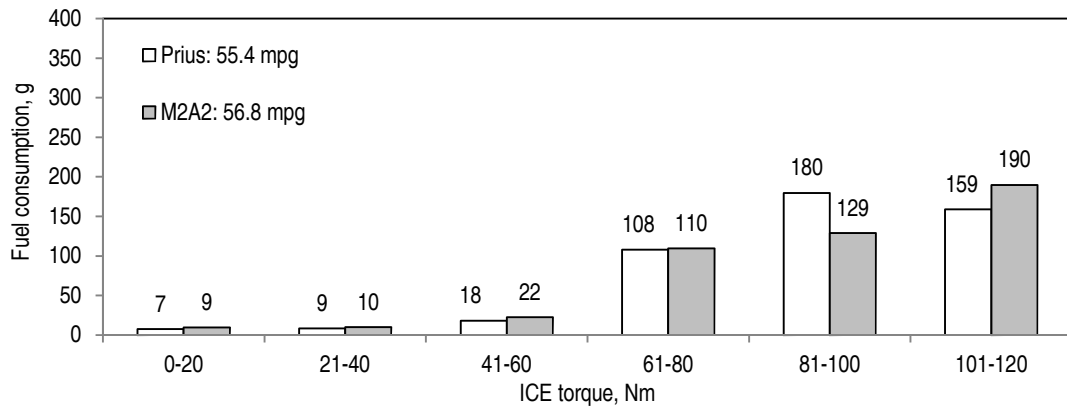


Figure 10.26: Distribution of fuel consumption w.r.t. ICE torque over US06: M2A2 design and Toyota Prius

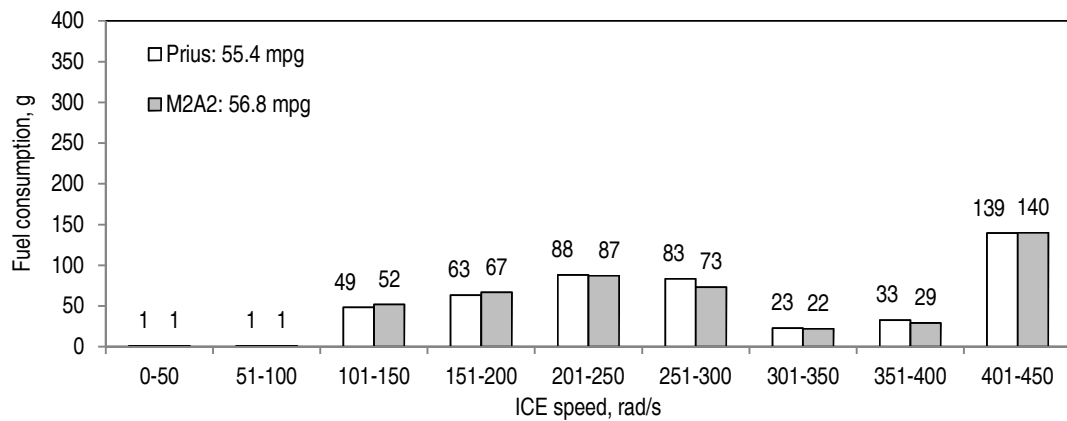


Figure 10.27: Distribution of fuel consumption w.r.t. ICE speed over US06: M2A2 design and Toyota Prius

The M2A2 design and Toyota Prius had 91.3 and 92.9% of total FC between 60 Nm and 120 Nm, as shown in Figure 10.26. The M2A2 design had 4.0% lower FC compared to the Toyota Prius between 60 Nm and 120 Nm (Figure 10.26) due to 7.2% lower time of operation of the M2A2 design compared to the Toyota Prius in this range (Figure 10.28).

The M2A2 design and Toyota Prius had 74.3 and 76.4% of total FC, respectively between 200 and 450 rad/s (Figure 10.26) as the M2A2 design and Toyota Prius

operated 31.6 and 34.3% of total time, respectively in this range (Figure 10.29). The M2A2 design had 4.0% lower FC due to 7.8% lower time of operation between 200 and 450 rad/s compared to the Toyota Prius.

Therefore, 7.2% lower time of operation over 60 Nm and 7.8% lower time of operation over 200 rad/s caused 2.5% higher FE in the M2A2 design compared to the Toyota Prius over US06.

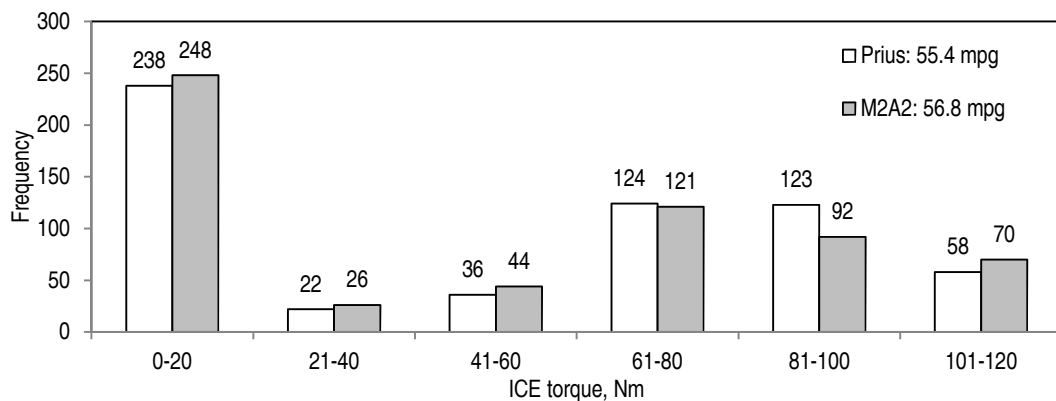


Figure 10.28: Distribution of ICE torque over US06: M2A2 design and Toyota Prius

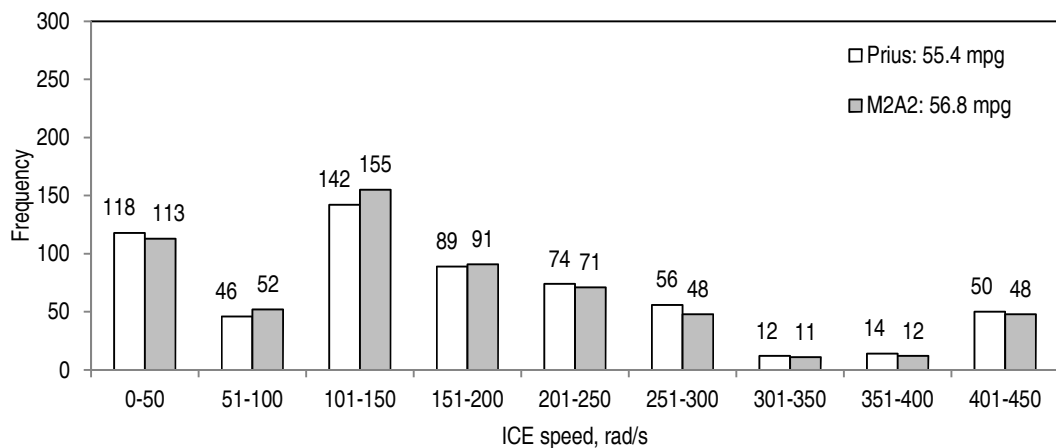


Figure 10.29: Distribution of ICE speed over US06: M2A2 design and Toyota Prius

Due to the 4.3% lower ICE power and 22.0% lower battery capacity of the Toyota Prius compared to the M2A2 design, the Toyota Prius was required to operate more

time at higher ICE torque and speed to achieve desired final battery SOC, as shown in Figure 10.30. Due to the capability to operate at higher ICE torque, the M2A2 design was able to deliver higher extra torque to charge the battery compared to Toyota Prius. The battery of the M2A2 design was required to charge lesser time compared to the Toyota Prius due to the higher battery capacity of the M2A2 design compared to the Toyota Prius. The 1.4% higher battery system efficiency of the M2A2 design compared to the Toyota Prius also indicated that the M2A2 design required lesser battery charging compared to the Toyota Prius.

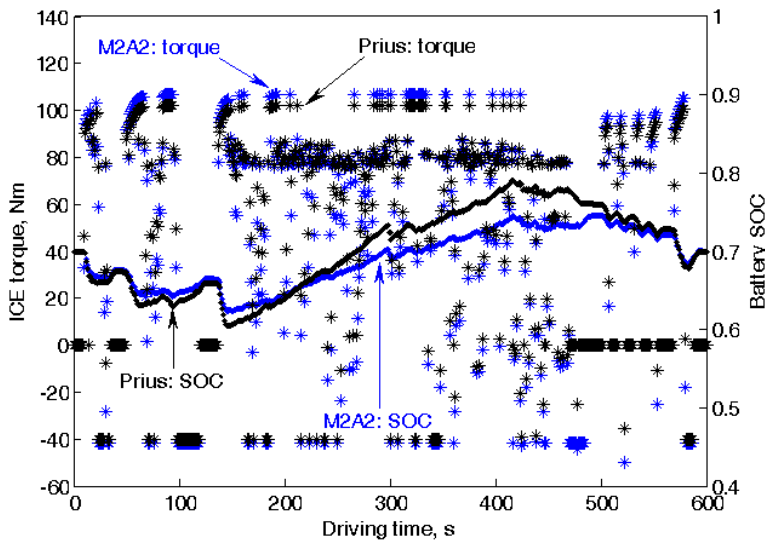


Figure 10.30: Comparison of ICE torque and battery SOC over US06: M2A2 design and Toyota Prius

10.12 FE variability over standard driving patterns: Toyota Prius, M1, and M2A2

The average FE and standard deviation of FE of the Toyota Prius were 76.9 mpg and 23.8 mpg respectively, as shown in Table 10.19. Therefore, FE variability of the Toyota Prius was 31.0%. The average FE of the M1-NEDC, M1-FTP, M1-LA92, M1-HWFET, and M1-US06 designs were 78.0, 80.4, 79.9, 77.2, and 78.4 mpg,

respectively, whereas the standard deviation of the M1-NEDC, M1-FTP, M1-LA92, M1-HWFET, and M1-US06 designs were 29.8, 26.0, 27.2, 32.9, and 24.7 mpg, respectively. Therefore, the FE variability of the M1-NEDC, M1-FTP, M1-LA92, M1-HWFET, and M1-US06 designs were 38.2, 32.3, 34.0, 42.6, and 31.5%, respectively, as shown in Table 10.19.

The average FE of the M2A2 design was 76.4 mpg i.e., the M2A2 design had 0.7, 2.1, 5.2, 4.6, 1.0, and 2.6% lower average FE compared to the Toyota Prius, M1-NEDC, M1-FTP, M1-LA92, M1-HWFET, and M1-US06 designs, respectively, as shown in Table 10.19.

The M2A2 design had FE variability of 30.0%. Therefore, the M2A2 design had 3.3% lower FE variability compared to the Toyota Prius, as shown in Table 10.19. The M2A2 design also had 27.3, 7.7, 13.3, 42.0, and 5.0% lower FE variability compared to the M1-NEDC, M1-FTP, M1-LA92, M1-HWFET, and M1-US06 designs, respectively, as shown in Table 10.19.

The average FE and FE variability of the optimum designs of the M1 methodology and M2A2 design w.r.t. Toyota Prius are shown in Figure 10.31. The average FE and FE variability of the Toyota Prius are shown as the origin of Figure 10.31.

As the M2A2 design marginally reduced (0.7%) average FE as well as reduced FE variability (3.3%) w.r.t. Toyota Prius, the M2A2 design situates in the 3rd quadrant, as shown in Figure 10.31. Although the most desirable region is the 4th quadrant i.e., improvement of the FE along with reduction of the FE variability, the M2A2 design was the only design capable of reducing the FE variability compared to the Toyota Prius.

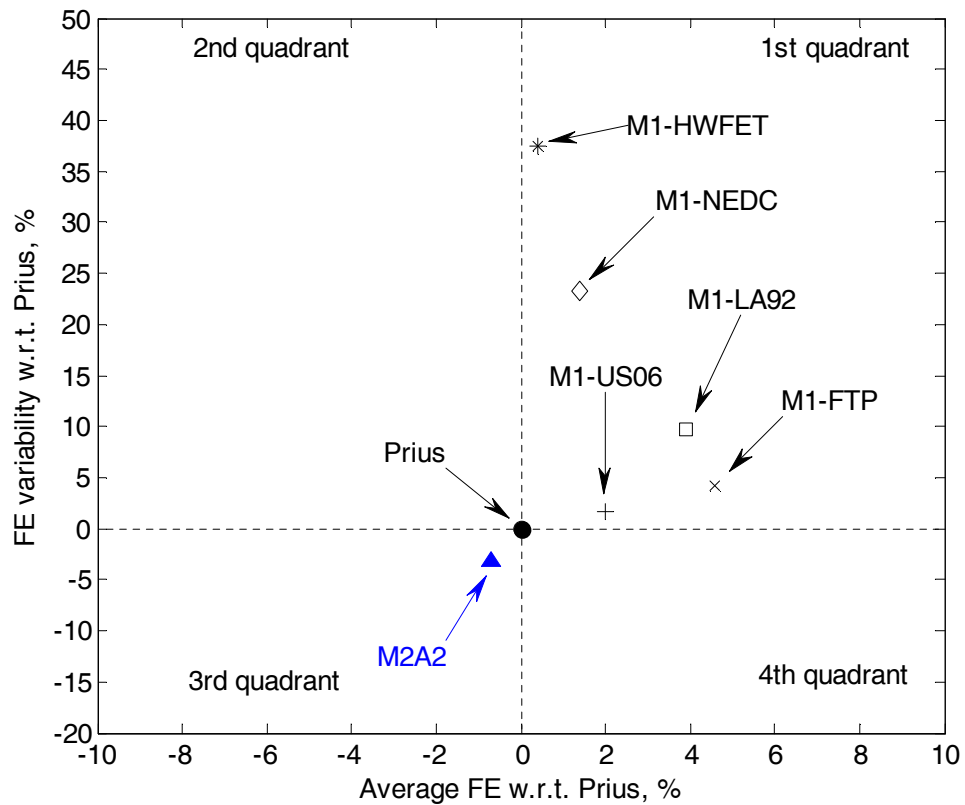


Figure 10.31: Average FE versus FE variability over standard driving patterns: Toyota Prius, M1, and M2A2

As the M2A2 approach provides a single optimum design over different driving patterns irrespective of the sequence of driving patterns, only one optimisation evaluation is required to find an optimum component sizes over different driving patterns and hence, potentially reduces the decision making time required for the M1 methodology and M2A1 approach and also takes the ‘human element’ out of the decisions.

The single optimum design (M2A2 design) produced by the proposed methodology with the second approach (M2A2 approach) was able to operate over all the 5

standard driving patterns and hence, demonstrated the potential for a generalised methodology for the optimisation of powertrain component sizes.

The ability to reduce FE variability, potential for a generalised methodology, and elimination of a separate decision making process to find an optimum design with least FE variability show that the proposed methodology with second approach improves upon the traditional methodology.

10.13 Summary

- The proposed methodology with the second approach (M2A2 approach) provided a single optimum design (M2A2 design) over a range of driving patterns representing different traffic conditions and driving styles simultaneously.
- The single optimum design over different sequence of driving patterns showed that the proposed methodology with second approach (M2A2 approach) was independent of the sequence of driving patterns. This improved up on the proposed methodology with first approach (M2A1 approach) which produced different optimum design with the change in sequence of driving patterns.
- A single optimum design over a range of driving patterns in the M2A2 approach potentially eliminates the decision making process required for the traditional methodology (M1) and M2A1 approach to choose an optimum design with least FE variability over a range of driving patterns.
- The M2A2 design reduced the FE variability by up to 42.0% compared to the optimum designs of the traditional methodology over 5 standard driving patterns.

- The M2A2 design was the only design able to reduce the FE variability (by 3.3%) compared to the Toyota Prius (benchmark vehicle) over 5 standard driving patterns.
- The M2A2 design had 0.7% lower average FE compared to the Toyota Prius.
- The M2A2 design improved the minimum FE by 2.5% compared to the Toyota Prius over standard driving patterns.
- The M2A2 design had on average 26.5% lower battery swing over NEDC, FTP, LA92, HWFET, and US06 respectively compared the Toyota Prius.
- The lower swing of the battery SOC might leads to higher battery life for the M2A2 design compared to the Toyota Prius.
- The M2A2 design had on average 0.6% higher battery system efficiency compared to the Toyota Prius over the standard driving patterns.
- The M2A2 design had better FE over the aggressive driving patterns (LA92 and US06) compared to the Toyota Prius and therefore, the M2A2 design is more suitable for real-world driving as aggressive driving patterns are more common in the real-world.
- The M2A2 design had 1.2 and 2.5% higher FE over the aggressive urban (LA92) and aggressive highway (US06) respectively compared to the Toyota Prius.
- The M2A2 design was able to operate in charge sustaining mode over all the 5 standard driving patterns of different traffic conditions and driving styles.
- The proposed methodology with second approach (M2A2 approach) demonstrated the potential to be a generalised methodology for the optimisation of powertrain component sizes of HEVs.

CHAPTER 11

REAL-WORLD INVESTIGATION OF PROPOSED METHODOLOGY

The traditional (M1) and proposed (M2) methodologies were evaluated over standard driving patterns from chapters 7 to 10. The main purpose of the chapters was to investigate the potential of the traditional and proposed methodologies in terms of FE variability. The proposed methodology with second approach (M2A2 approach) reduced the FE variability compared to the Toyota Prius (benchmark vehicle) and M1 methodology over standard driving patterns which were used for the optimisation. The single optimum design produced by the M2A2 approach needed to be validated over driving patterns that were not used in the optimisation. For complete generality these driving patterns were selected to be real-world driving patterns. The optimum design produced by the proposed methodology needed to be validated in real world driving for more applicability in practical applications. This chapter discusses the investigation of the single optimum design produced by the proposed methodology, as found in chapter 10, for real-world driving patterns over a predefined route consisting of urban as well as highway driving. The optimum designs produced by the traditional methodology, as found in chapter 8, and the simulation model of the Toyota Prius (benchmark vehicle) were also evaluated for FE over the same driving patterns and the results were compared against the proposed methodology. This chapter first discusses the battery SOC during the FE evaluation followed by FE over the real-world driving patterns. Next, the discussion is focused on the analysis to understand the reason for a particular FE over a driving

pattern. Finally, the FE variability of the proposed methodology over the real-world driving patterns is discussed.

11.1 FE evaluation over real-world driving patterns: Toyota Prius, M1, and M2A2

The single optimum design (M2A2 design) produced by the proposed methodology with second approach (M2A2 approach), as found in chapter 10, was evaluated for FE over 10 real-world driving patterns, as mentioned in chapter 6. Similarly, the Toyota Prius and 5 optimum designs of the traditional methodology (M1), namely, M1-NEDC, M1-FTP, M1-LA92, M1-HWFET, and M1-US06 were also evaluated for FE over the same real-world driving patterns.

During the FE evaluation over each driving pattern, the target SOC was varied for each optimum design to maintain the desired final battery SOC (within $<0.5\%$ of the initial battery SOC i.e., $\Delta \text{SOC} < 0.5\%$), as discussed in section 6.9 of chapter 6.

11.1.1 Battery SOC during FE evaluation: Toyota Prius, M1, and M2A2

The target SOC values of each optimum design over the 10 real-world driving patterns are shown in Table 11.1. The target SOC values of the M2A2 design ranged from 0.6745 to 0.7450, as shown in Table 11.1. Therefore, the spread of the target SOC values for the M2A2 design was 0.0705. The target SOC values of the Toyota Prius ranged from 0.6851 to 0.7651. Therefore, the spread of the target SOC values for the Toyota Prius was 0.08. Hence, the M2A2 design had 11.9% lower spread of target SOC values compare to the Toyota Prius. The M2A2 design required lower target SOC values compared to the Toyota Prius over D1 to D10 driving patterns. This was probably due to 4.3% higher power of the ICE of the M2A2 design compared to the Toyota Prius that helped the M2A2 design to provide higher torque

to recharge the battery, and therefore the M2A2 design was able to maintain the desired final battery SOC with lower target SOC values.

Table 11.1: Target SOC during FE evaluation over real-world driving patterns: Toyota Prius, M1, and M2A2

Driving pattern	Target SOC						
	Toyota Prius	M1 methodology					M2 methodology: M2A2 approach
		M1-NEDC	M1-FTP	M1-LA92	M1-HWFET	M1-US06	M2A2 design
D1	0.7201	0.8300	0.7800	0.8200	0.9900 (x)	0.7400	0.7100
D2	0.7503	0.7882	0.7411	0.7627	0.9321	0.7313	0.7319
D3	0.7502	0.8921	0.7921	0.8372	0.9900 (x)	0.7451	0.7260
D4	0.6851	0.7196	0.6823	0.6960	0.8501	0.6764	0.6745
D5	0.7302	0.8235	0.7588	0.7803	0.9900 (x)	0.7333	0.7117
D6	0.7651	0.9750	0.8607	0.9411	0.9900 (x)	0.8019	0.7450
D7	0.7002	0.7313	0.7000	0.7098	0.8452	0.6941	0.6921
D8	0.6853	0.7078	0.6843	0.6921	0.7851	0.6823	0.6784
D9	0.7302	0.8176	0.7333	0.7529	0.9900 (x)	0.7156	0.7019
D10	0.7002	0.7490	0.7117	0.7274	0.9153	0.7039	0.6941
(x): Failed to operate charge sustaining							

The target SOC values of the M2A2 design were lower compared to the M1-NEDC, M1-FTP, M1-LA92, and M1-HWFET designs over D1 to D10. The target SOC values of the M2A2 design were lower compared to the M1-US06 design over all driving patterns except D2, D4, and D7 where both the designs had comparable target SOC values. The lower target SOC values of the M2A2 design probably due

to the higher power of the ICE of the M2A2 design compared to the designs of the M1 methodology.

The final battery SOC values of each optimum design during the FE evaluation over the 10 driving patterns are shown in Table 11.2. The M2A2 design and Toyota Prius were able to operate in charge sustaining mode over all the driving patterns, as shown in Table 11.2. Therefore, the M2A2 design was able to cope with more aggressive real-world driving patterns. Apart from the M1-HWFET design, the M1-NEDC, M1-FTP, M1-LA92, and M1-US06 designs were able to operate in charge sustaining mode over all the 10 driving patterns. The M1-HWFET design failed to operate in charge sustaining over D1, D3, D5, D6 and D9, as shown in Table 11.2. The probable reason for the failure of the M1-HWFET design to operate charge sustaining was due to its smallest power of the ICE and generator compared to all designs. This reason was similar to the reason for the failure to operate over US06, as discussed in chapter 8.

Table 11.2: Final battery SOC during FE evaluation over real-world driving patterns: Toyota Prius, M1, and M2A2

Driving patterns	Final battery SOC						
	Toyota Prius	M1 methodology					M2 methodology: M2A2 approach
		M1-NEDC	M1-FTP	M1-LA92	M1-HWFET	M1-US06	M2A2 design
D1	0.6995	0.6996	0.6996	0.6999	0.5761 (x)	0.7008	0.7013
D2	0.7026	0.7006	0.6988	0.7012	0.6996	0.6998	0.7003
D3	0.6973	0.7013	0.7023	0.7005	0.4610 (x)	0.6982	0.6972
D4	0.6978	0.6996	0.6984	0.6993	0.7006	0.6996	0.6979
D5	0.6980	0.6968	0.7020	0.6979	0.6539 (x)	0.7015	0.6978
D6	0.7012	0.6982	0.6974	0.6984	0.4639 (x)	0.6998	0.6997
D7	0.7023	0.6999	0.7034	0.7008	0.6995	0.7034	0.7021
D8	0.6981	0.6986	0.7013	0.7004	0.7002	0.7026	0.6976
D9	0.6993	0.6990	0.7004	0.6988	0.6935 (x)	0.6998	0.6967
D10	0.6984	0.7016	0.7029	0.6995	0.7002	0.7022	0.6988
(x): Failed to operate charge sustaining							

The battery SOC swing of the Toyota Prius, optimum designs of the M1 methodology, and the M2A2 design over the 10 real-world driving patterns during the FE evaluation are shown in Table 11.3 and Table 11.4.

Table 11.3: Battery SOC swing during FE evaluation over real world driving patterns (D1 to D5): Toyota Prius, M1, and M2A2

Driving patterns	Parameters	Battery SOC						
		Toyota Prius	M1 methodology					M2 methodology : M2A2 approach
			M1-NEDC	M1-FTP	M1-LA92	M1-HWFET	M1-US06	M2A2 design
D1	Maximum SOC	0.8496	0.7515	0.7400	0.7476	0.7696	0.7463	0.8220
	Minimum SOC	0.5044	0.3443	0.4641	0.4454	0.2981	0.4849	0.5522
	<i>SOC swing</i>	0.3452	0.4072	0.2759	0.3022	0.4715	0.2614	0.2698
	<i>Swing w.r.t. M2A2, %</i>	21.8	33.7	2.2	10.7	42.8	-3.2	
D2	Maximum SOC	0.9224	0.8135	0.8002	0.7819	0.7263	0.8288	0.8800
	Minimum SOC	0.6315	0.5709	0.6090	0.6002	0.5336	0.6234	0.6331
	<i>SOC swing</i>	0.2909	0.2426	0.1912	0.1817	0.1927	0.2054	0.2469
	<i>Swing w.r.t. M2A2, %</i>	15.1	-1.8	-29.1	-35.9	-28.1	-20.2	
D3	Maximum SOC	0.8032	0.7713	0.7493	0.7528	0.7332	0.7497	0.7814
	Minimum SOC	0.6233	0.5997	0.6347	0.6225	0.3578	0.6176	0.6212
	<i>SOC swing</i>	0.1799	0.1716	0.1146	0.1303	0.3754	0.1321	0.1602
	<i>Swing w.r.t. M2A2, %</i>	10.9	6.7	-39.8	-23.0	57.3	-21.2	
D4	Maximum SOC	0.9242	0.8522	0.8240	0.8013	0.7267	0.8492	0.8834
	Minimum SOC	0.6141	0.5816	0.6053	0.5983	0.5728	0.6162	0.6153
	<i>SOC swing</i>	0.3101	0.2706	0.2187	0.2030	0.1539	0.2330	0.2681
	<i>Swing w.r.t. M2A2, %</i>	13.6	0.9	-22.6	-32.1	-74.2	-15.1	
D5	Maximum SOC	0.9082	0.7904	0.7819	0.7580	0.7669	0.8127	0.8605
	Minimum SOC	0.6184	0.5573	0.5911	0.5793	0.5369	0.6008	0.6226
	<i>SOC swing</i>	0.2898	0.2331	0.1908	0.1787	0.2300	0.2119	0.2379
	<i>Swing w.r.t. M2A2, %</i>	17.9	-2.0	-24.7	-33.1	-3.4	-12.3	

Table 11.4: Battery SOC swing during FE evaluation over real world driving patterns (D6 to D10): Toyota Prius, M1, and M2A2

Driving patterns	Parameters	Battery SOC						
		Toyota Prius	M1 methodology					M2 methodology : M2A2 approach
			M1-NEDC	M1-FTP	M1-LA92	M1-HWFET	M1-US06	M2A2 design
D6	Maximum SOC	0.7587	0.7557	0.7277	0.7434	0.7000	0.7144	0.7513
	Minimum SOC	0.6234	0.5478	0.6087	0.6019	0.2900	0.6150	0.6273
	<i>SOC swing</i>	0.1353	0.2079	0.1190	0.1415	0.4100	0.0994	0.1240
	<i>Swing w.r.t. M2A2, %</i>	8.4	40.4	-4.1	12.4	69.8	-24.6	
D7	Maximum SOC	0.9082	0.7900	0.7884	0.7585	0.7177	0.8195	0.8626
	Minimum SOC	0.6068	0.5704	0.6043	0.5932	0.5193	0.6122	0.6184
	<i>SOC swing</i>	0.3015	0.2196	0.1841	0.1653	0.1984	0.2073	0.2442
	<i>Swing w.r.t. M2A2, %</i>	19.0	-11.2	-32.7	-47.8	-23.1	-17.8	
D8	Maximum SOC	0.9211	0.8448	0.8263	0.8035	0.7521	0.8502	0.8764
	Minimum SOC	0.6182	0.6046	0.6274	0.6173	0.5656	0.6328	0.6255
	<i>SOC swing</i>	0.3029	0.2402	0.1989	0.1862	0.1865	0.2173	0.2508
	<i>Swing w.r.t. M2A2, %</i>	17.2	-4.4	-26.1	-34.7	-34.5	-15.4	
D9	Maximum SOC	0.9388	0.9311	0.8567	0.8488	0.8396	0.8662	0.8841
	Minimum SOC	0.6402	0.6562	0.6564	0.6602	0.6484	0.6468	0.6309
	<i>SOC swing</i>	0.2987	0.2749	0.2003	0.1886	0.1912	0.2194	0.2532
	<i>Swing w.r.t. M2A2, %</i>	15.2	7.9	-26.4	-34.3	-32.4	-15.4	
D10	Maximum SOC	0.8107	0.7517	0.7502	0.7371	0.7146	0.7647	0.7887
	Minimum SOC	0.5783	0.5772	0.5971	0.5937	0.5934	0.5996	0.5892
	<i>SOC swing</i>	0.2325	0.1746	0.1531	0.1433	0.1212	0.1651	0.1995
	<i>Swing w.r.t. M2A2, %</i>	14.2	-14.3	-30.2	-39.1	-64.6	-20.8	

Where,

$$Swing\ w.r.t.\ M2A2,\ \% = \frac{SOC_{a\ design} - SOC_{M2A2}}{SOC_{M2A2}} * 100$$

The M2A2 design had 21.8, 15.1, 10.9, 13.6, 17.9, 8.4, 19.0, 17.2, 15.2, and 14.2% lower swing of the battery SOC over D1 to D10 respectively compared to the Toyota

Prius. Therefore, the M2A2 design had on average 15.3% lower swing of the battery SOC compared to the Toyota Prius. The probable reason could be due to 4.5% higher power of the ICE and 28.3% higher capacity of the battery of the M2A2 design compared to the Toyota Prius. Due to the lower swing of the battery SOC, the battery of the M2A2 design had higher potential to have improved battery life-cycle compared to the Toyota Prius [20], [105].

The M2A2 design had higher swing of the battery SOC over D2, D5, D7, D8, and D10 compared to all the designs of the M1 methodology, as shown in Table 11.3 and Table 11.4. The M2A2 design had lower swing of the battery SOC over D1 compared to all designs of the M1 methodology, except the M1-US06 design, as shown in Table 11.3. The M2A2 design had lower swing of the battery SOC compared to the M1-NEDC and M1-HWFET designs, but had higher swing of the battery SOC compared to the M1-FTP, M1-LA92, and M1-US06 designs over D3, as shown in Table 11.3. The M2A2 design had higher swing of the battery SOC compared to all designs except the M1-NEDC design over D4 and D9. The M2A2 design had lower swing of the battery SOC compared to the M1-NEDC, M1-LA92, and M1-HWFET designs but higher swing of the battery SOC compared to M1-FTP and M1-US06 over D6. Therefore, the M2A2 design had higher swing of the battery SOC compared to the M1-FTP and M1-US06 designs over all driving patterns. The M2A2 design also had higher swing of the battery SOC compared to the M1-LA92 design over all driving patterns, except D6. The probable reason could be the 13.5, 11.5, and 11.5% lower battery capacity of the M2A2 design compared to that of the M1-FTP, M1-LA92, and M1-US06 designs.

11.1.2 Battery system efficiency over real-world driving patterns: Toyota Prius, M1, and M2A2

The battery system efficiency of the M2A2 design is compared with the Toyota Prius and optimum designs of the M1 methodology over the 10 real-world driving patterns from Figure 11.1 to Figure 11.3.

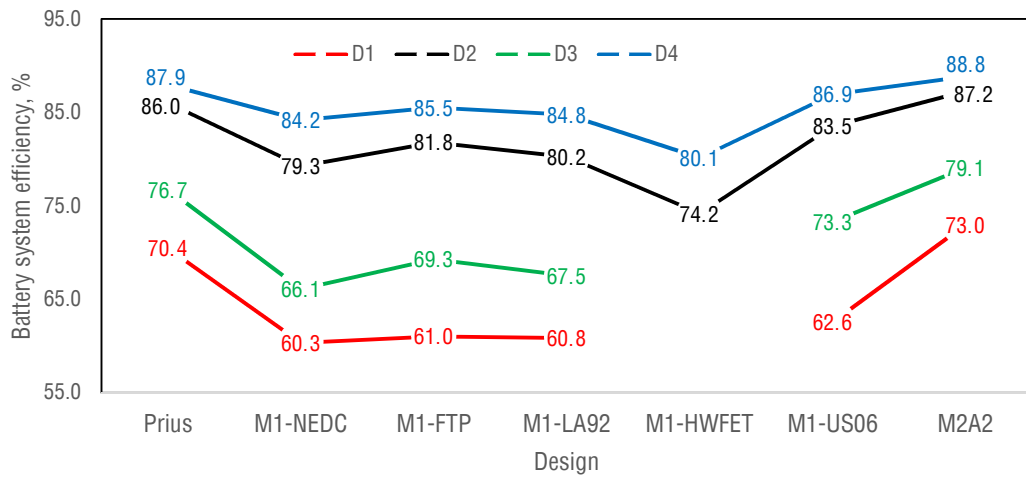


Figure 11.1: Battery system efficiency over D1, D2, D3, and D4: Toyota Prius, M1, and M2A2

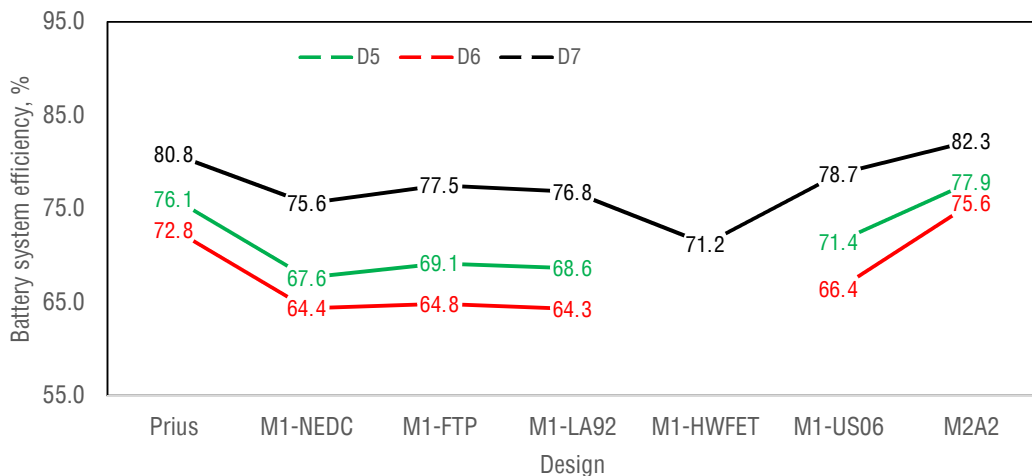


Figure 11.2: Battery system efficiency over D5, D6, and D7: Toyota Prius, M1, and M2A2

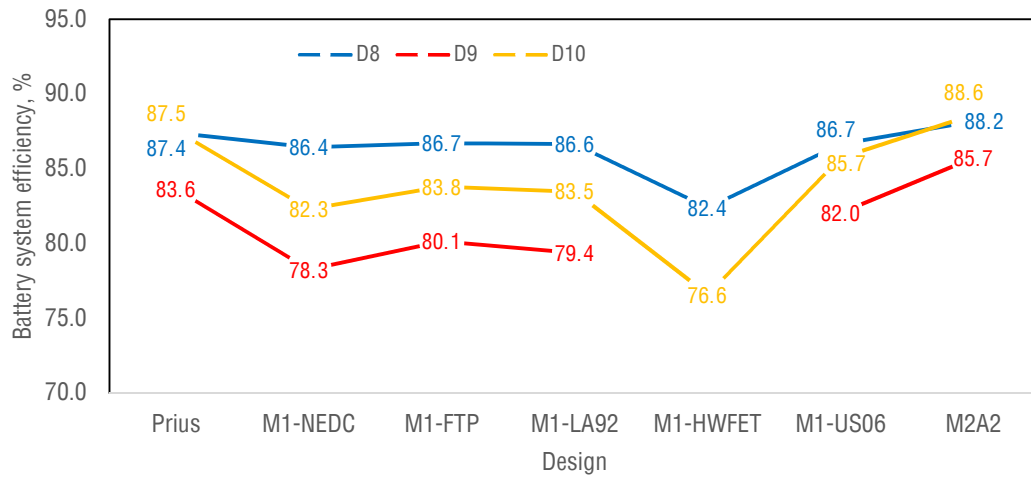


Figure 11.3: Battery system efficiency over D8, D9, and D10: Toyota Prius, M1, and M2A2

The battery system efficiency of the M2A2 design were 73.0, 87.2, 79.1, 88.8% (Figure 11.1), 77.9, 75.6, 82.3 (Figure 11.2), 88.2, 85.7, and 88.6% (Figure 11.3) over D1 to D10 respectively. The battery system efficiency of the Toyota Prius were 70.4, 86.0, 76.7, 87.9 (Figure 11.1), 76.1, 72.8, 80.8 (Figure 11.2), 87.4, 83.6, and 87.5% (Figure 11.3) over D1 to D10 respectively. Therefore, the M2A2 design had 3.6, 1.5, 3.0, 1.0, 2.4, 3.8, 1.8, 0.9, 2.5, and 1.2% higher battery system efficiency over D1 to D10 respectively compared to the Toyota Prius. Hence, the M2A2 design had on average 2.2% higher battery system efficiency compared to the Toyota Prius over 10 real-world driving patterns. The probable reason could be the 4.3% higher power of the ICE and 22.0% higher capacity of the battery of the M2A2 design compared to the Toyota Prius. The M2A2 design has higher potential for better FE compared to the Toyota Prius over real-world driving patterns as higher battery system efficiency helps for better FE [64].

Both the M2A2 design and Toyota Prius had higher battery system efficiency compared to all the optimum designs of the M1 methodology over D1 to D10, as shown from Figure 11.1 to Figure 11.3. The probable reason could be the higher power of the ICE of the M2A2 design and the Toyota Prius compared to all the optimum designs of the M1 methodology.

11.2 FE over real-world driving patterns: Toyota Prius, M1, and M2A2

The FE values of the M2A2 design compared to the Toyota Prius and optimum designs of the M1 methodology over the 10 real-world driving patterns are shown in Table 11.5. The minimum FE value of the M2A2 design over the 10 driving patterns was 51.0 mpg over D6. The minimum FE value of the M1-HWFET design was 47.1 mpg over D1, whereas the minimum FE values of the M1-NEDC, M1-FTP, M1-LA92, and M1-US06 designs were 46.3, 49.2, 47.4, and 49.9 mpg, respectively over D6. The minimum FE of the Toyota Prius was 50.4 mpg over D6. Therefore, apart from the M1-HWFET design, all optimum designs provided the minimum FE over D6.

The maximum FE of the Toyota Prius, M1-NEDC, M1-FTP, M1-LA92, M1-HWFET, M1-US06, and M2A2 designs were 68.1, 70.9, 71.4, 71.5, 66.0, 69.6, and 67.5 mpg, respectively over D8. Therefore, all the optimum designs provided the maximum FE over D8.

The FE variability of the M2A2 design compared to the Toyota Prius and the optimum designs produced by the M1 methodology is discussed in section 11.5.

Table 11.5: FE over real world driving patterns: Toyota Prius, M1, and M2A2

Driving pattern	FE, mpg (miles per gallon)						
	Toyota Prius	M1 methodology					M2 methodology: M2A2 approach
		M1-NEDC	M1-FTP	M1-LA92	M1-HWFET	M1-US06	M2A2 design
D1	54.9	48.6	50.7	49.1	47.1 (x)	52.3	55.4
D2	64.9	64.3	66.7	65.6	57.7	66.1	65.0
D3	50.7	48.7	51.7	50.4	47.5 (x)	52.0	51.1
D4	64.5	66.0	67.2	66.9	60.1	66.1	64.1
D5	57.4	54.5	56.6	55.9	50.1 (x)	57.0	57.4
D6	50.4	46.3	49.2	47.4	47.3 (x)	49.9	51.0
D7	59.3	58.9	60.6	60.4	53.5	59.9	58.8
D8	68.1	70.9	71.4	71.5	66.0	69.6	67.5
D9	60.2	59.9	62.6	62.2	52.9 (x)	61.9	60.9
D10	60.0	61.4	62.5	62.3	55.9	61.1	59.6
<i>Average FE, mpg</i>	59.0	58.0	59.9	59.2	53.8	59.6	59.1
<i>Standard deviation of FE, mpg</i>	5.6	7.8	7.2	7.8	5.9	6.4	5.3
<i>FE variability, %</i>	9.5	13.4	12.0	13.2	11.0	10.7	9.0
<i>FE variability w.r.t. Prius, %</i>		41.1	26.3	38.9	15.8	12.6	-5.3
(x): Failed to operate charge sustaining							

The minimum FE of each optimum design and the minimum FE of each optimum design w.r.t. Toyota Prius over D1 to D10 are shown in Figure 11.4. The minimum FE of the Toyota Prius is shown as the origin of Figure 11.4. The minimum FE values of the M1-NEDC, M1-FTP, M1-LA92, M1-HWFET, and M1-US06 designs were 8.1, 2.4, 6.0, 6.5, and 1.0%, respectively lower compared to that of the Toyota Prius. The M2A2 design had 1.2% higher minimum FE compared to that of the Toyota Prius and improved the minimum FE by 10.2, 3.7, 7.6, 8.3, and 2.2% compared to the M1-NEDC, M1-FTP, M1-LA92, M1-HWFET, and M1-US06 designs respectively.

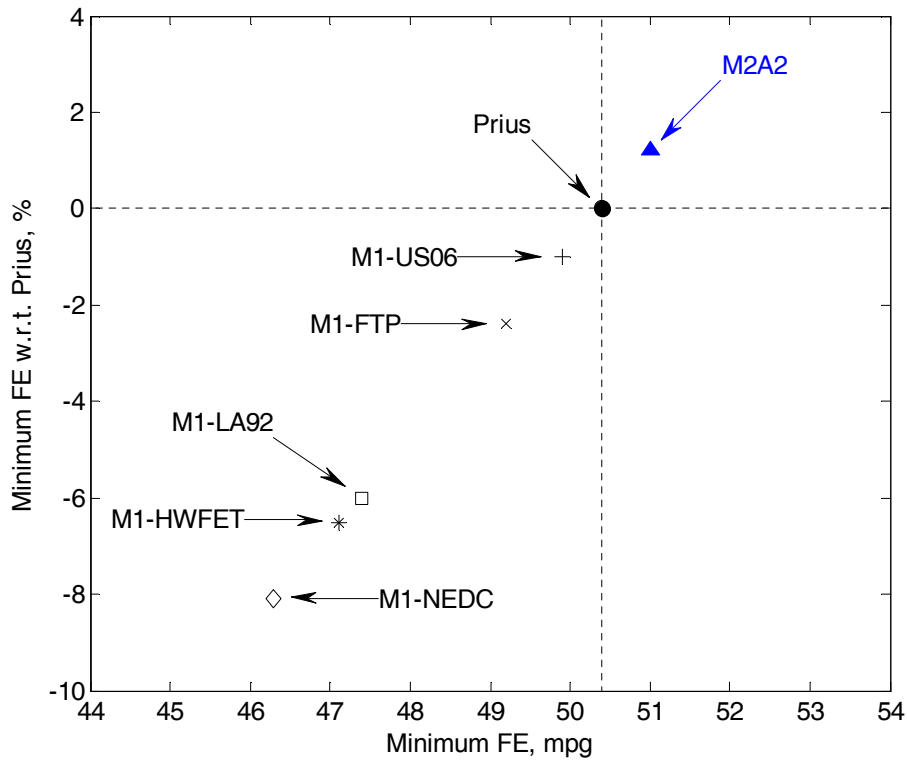


Figure 11.4: Minimum FE versus minimum FE w.r.t. Prius over D1 to D10

The probable reason for the minimum FE over D6 was due to the higher aggressiveness of D6 compared to other driving patterns. D6 had the second highest maximum speed and second highest maximum acceleration, as shown Figure 11.5 and Figure 11.6. D6 had the highest percentage of driving time for acceleration and deceleration among all the driving patterns, as shown in Figure 11.7. D3 also had higher aggressiveness in driving. D3 had the highest maximum speed (Figure 11.5), the third highest maximum acceleration (Figure 11.6), and the second highest percentage of time for acceleration and deceleration (Figure 11.7). For this reason, the Toyota Prius, M2A2, and M1-US06 designs provided the second lowest FE and M1-NEDC, M1-FTP, and M1-LA92 designs provided the third lowest FE over D3.

D8 had the second lowest maximum speed (Figure 11.5) and second lowest maximum acceleration (Figure 11.6). D8 also had the third lowest percentage of time for acceleration and deceleration (Figure 11.7). Therefore, D8 was lesser aggressive compared to other driving patterns and this was probably the reason for the highest FE of all optimum designs over D8.

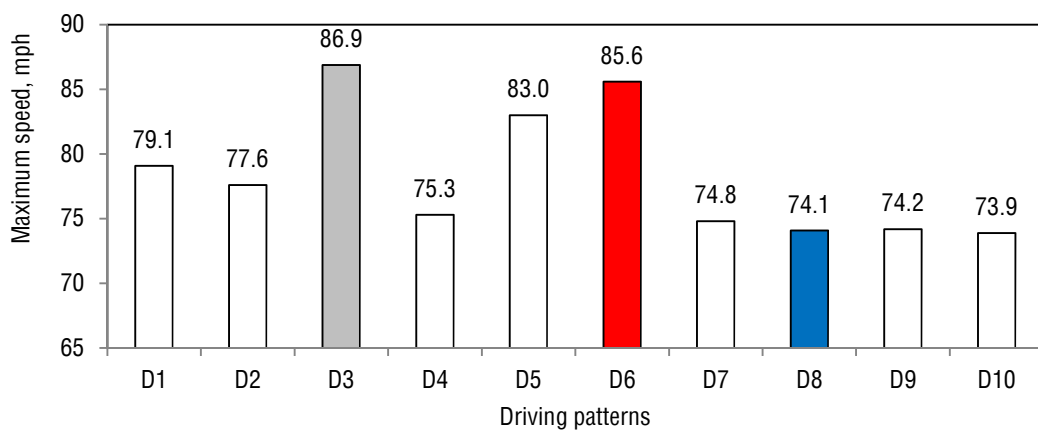


Figure 11.5: Maximum speed: D1 to D10 driving patterns

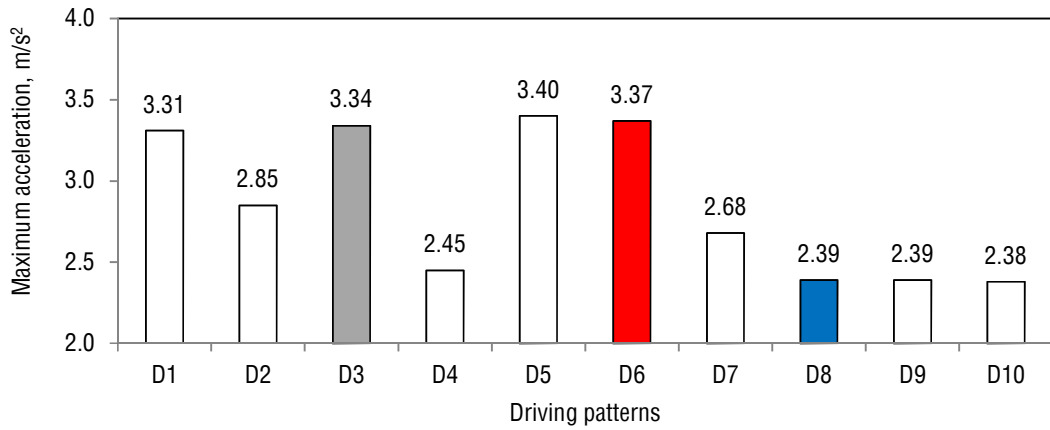


Figure 11.6: Maximum acceleration: D1 to D10 driving patterns

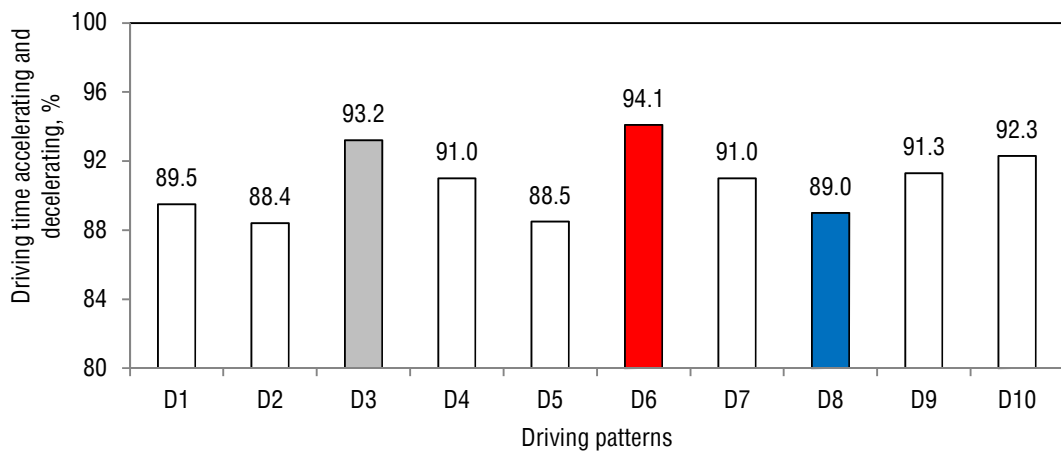


Figure 11.7: Time for acceleration and deceleration: D1 to D10 driving patterns

11.2.1 Comparison of FE: M2A2 and Toyota Prius

The M2A2 design had 0.9, 0.2, 0.8, 1.2, and 1.2% higher FE over D1, D2, D3, D6, and D9, respectively compared to the Toyota Prius. But the M2A2 design had 0.6, 0.8, 0.9, and 0.7% lower FE over D4, D7, D8, and D10 respectively compared to the Toyota Prius. The M2A2 design and Toyota Prius provided same FE over D5. The M2A2 design had higher FE over 5 driving patterns and lower FE over 4 driving

patterns compared to the Toyota Prius. These driving patterns are grouped by comparative performance in Figure 11.8 to Figure 11.11, with driving patterns where the M2A2 design was better than Toyota Prius at the left of the Figures.

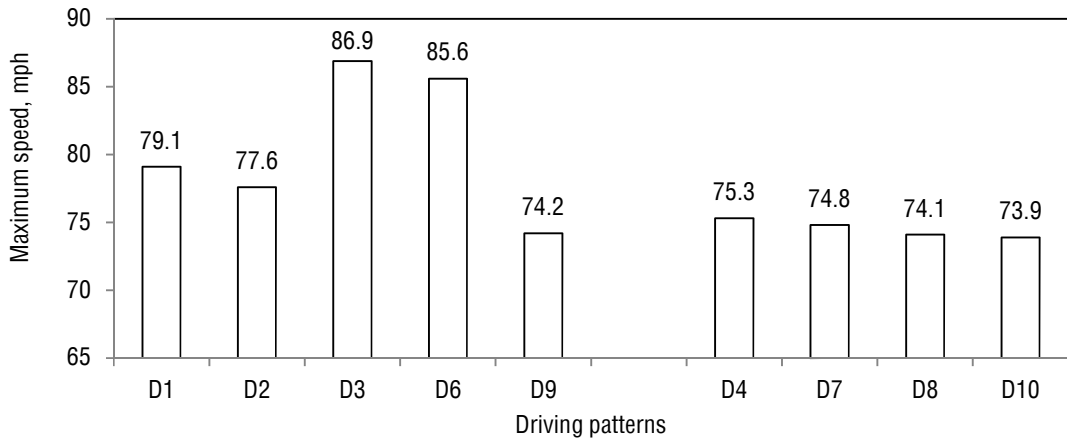


Figure 11.8: Comparison of maximum speeds for the comparison of FE: M2A2 design and Toyota Prius

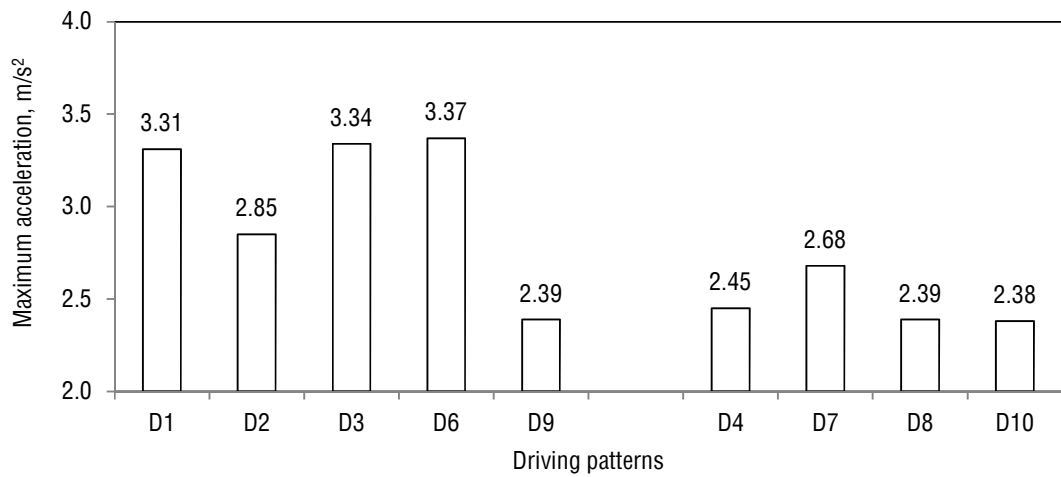


Figure 11.9: Comparison of maximum acceleration for the comparison of FE: M2A2 design and Toyota Prius

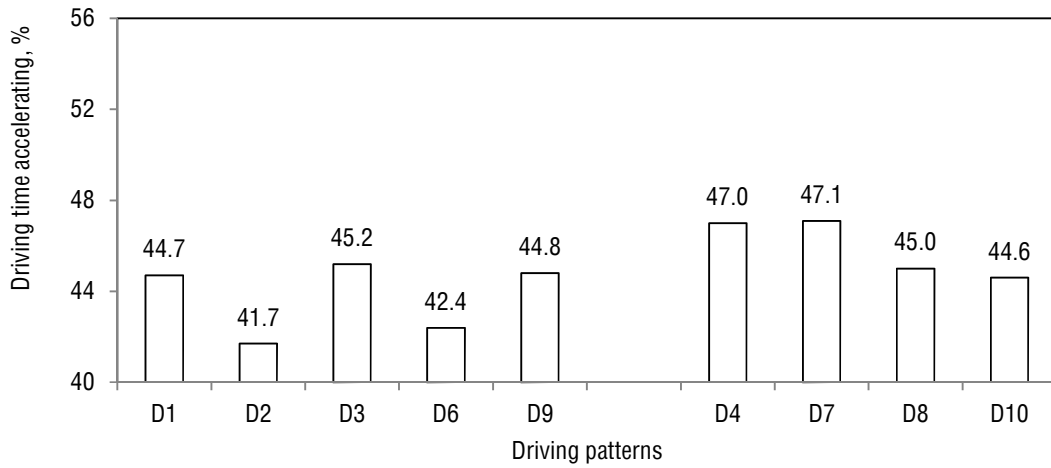


Figure 11.10: Comparison of driving time for acceleration for the comparison of FE: M2A2 design and Toyota Prius

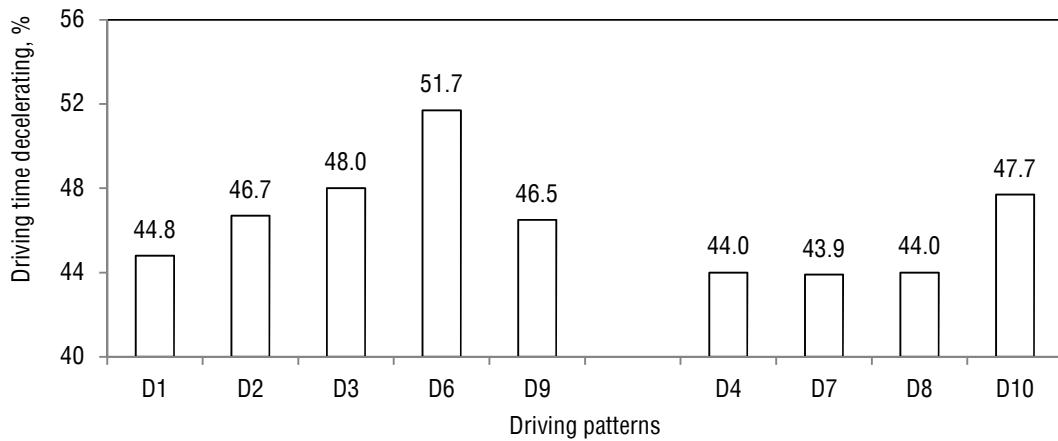


Figure 11.11: Comparison of driving time for deceleration for the comparison of FE: M2A2 design and Toyota Prius

D1, D2, D3, and D6 driving patterns had higher maximum speed and maximum acceleration compared to D4, D7, D8, and D10. D1, D2, D3, D6, and D9 also had more percentage of driving time for deceleration compared to D4, D7, and D8. But D4, D7, D8, and D10 had more percentage of driving time for acceleration compared to D2 and D6. The higher deceleration time in D1, D2, D3, D6, and D9 indicated

potentially higher traffic on the road. The higher driving time for acceleration with lesser time for deceleration in D4, D7, and D8 indicated lesser traffic. Therefore, the M2A2 design had better FE compared to the Toyota Prius, if driving patterns consisted of higher maximum speed, maximum acceleration, and traffic. Hence, the M2A2 design had higher potential for better FE over aggressive driving patterns and more suitable for real-world applications compared to the Toyota Prius.

11.2.2 Comparison of FE: M2A2 and M1

The M2A2 design had 14.0, 1.3, 4.9, 5.3, 10.2, and 1.7% higher FE over D1, D2, D3, D5, D6, and D9, respectively compared to the M1-NEDC design. But the M2A2 design had 2.9, 0.2, 4.8, and 2.9% lower FE over D4, D7, D8, and D10, respectively compared to the M1-NEDC design. The M2A2 design had 9.3, 1.4, and 3.7% higher FE over D1, D5, and D6, respectively compared to the M1-FTP design. But the M2A2 design has 2.5, 1.2, 4.6, 3.0, 5.5, 2.7, and 4.6% lower FE over D2, D3, D4, D7, D8, D9, and D10, respectively compared to the M1-FTP design. The M2A2 design had 12.8, 1.4, 2.7, and 7.6% higher FE over D1, D3, D5, and D6, respectively compared to the M1-LA92 design. But the M2A2 design had 0.9, 4.2, 2.6, 5.6, 2.1, and 4.3% lower FE over D2, D4, D7, D8, D9, and D10, respectively compared to the M1-LA92 design. The M2A2 design had 5.9, 0.7, and 2.2% higher FE over D1, D5, and D6 respectively compared to the M1-US06 design. But the M2A2 design had 1.7, 1.7, 3.0, 1.8, 3.0, 1.6, and 2.5% lower FE over D2, D3, D4, D7, D8, D9, and D10, respectively compared to the M1-US06 design.

The M2A2 design had higher FE over D1, D5, and D6 compared to all the designs of M1 methodology. D1, D5, and D6 had higher maximum speed and maximum acceleration compared to D2, D4, D7, D8, D9, and D10 driving patterns. Therefore,

the M2A2 design had higher chances of better FE compared to the designs of M1 methodology, if driving patterns consisted of higher maximum speed and acceleration. Although D3 also had higher maximum speed and maximum acceleration compared to D2, D4, D7, D8, D9, and D10 driving patterns, the M1-FTP and M1-US06 designs had higher FE compared to the M2A2 design. No conclusion can be drawn in terms of the percentage of time spent for acceleration and deceleration.

11.3 Analysis of FE over D1: Toyota Prius, M1, and M2A2

The M2A2 design had the highest FE over D1 and D6 compared to other designs. The D1 driving pattern was chosen to understand the higher FE of the M2A2 design compared to other designs. The M2A2 design had 14.0, 9.3, 12.8, and 5.9% higher FE over D1 driving pattern compared to the M1-NEDC, M1-FTP, M1-LA92, and M1-US06 designs, respectively. The M1-NEDC and M1-US06 designs were chosen for the comparison with the M2A2 design due to the lowest and highest difference in FE compared to the M2A2 design. The M2A2 design also had 0.9% higher FE compared to the Toyota Prius. The M2A2 design was also compared with the Toyota Prius to analyse the difference in FE.

11.3.1 Comparison over D1: M2A2 and M1-NEDC

The FC values of the M2A2 and M1-NEDC designs over D1 are compared in Figure 11.12. The FC of the M2A2 design at high speed regions (between 2430 and 2730 seconds) spread up to 2.87 g/s but majority of the FC concentrated between 0.5 to 1.7 g/s, whereas the FC of the M1-NEDC design at the same speed range spread up to 2.24 g/s and majority of the FC happened at 2.24 g/s. Apart from the high speed regions (between 2430 and 2730 seconds), the FC of the M1-NEDC design

concentrated more between 0.5 and 1.5 g/s. In the lower speed region, the FC of the M2A2 design spread up to 2.87 g/s but a portion of the FC happened up to 0.5 g/s.

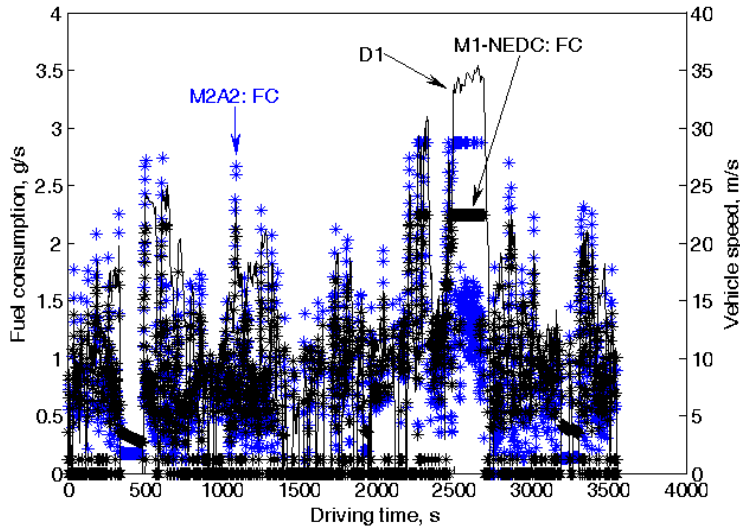


Figure 11.12: Comparison of fuel consumption over D1: M2A2 and M1-NEDC designs

As the fuel consumption (FC) directly depends on the operation of ICE, the torque and speed of the ICE for the M2A2 and M1-NEDC designs over D1 driving pattern are shown in Figure 11.13 and Figure 11.14, respectively. Figure 11.13 shows that the M1-NEDC design operated more time between 60 Nm to 83.2 Nm (maximum torque corresponding to maximum power 35.12 kW), whereas the operation of the M2A2 design spread all over the range between 0 Nm to 106.6 Nm (maximum torque corresponding to maximum power 44.94 kW). The M1-NEDC design operated comparatively higher times at higher speed compared to the M2A2 design, as shown in Figure 11.14.

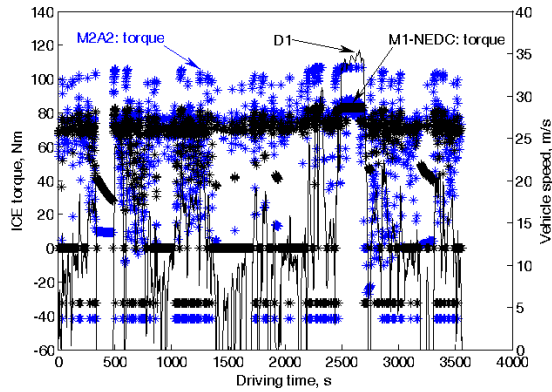


Figure 11.13: Comparison of ICE torque over D1: M2A2 and M1-NEDC designs

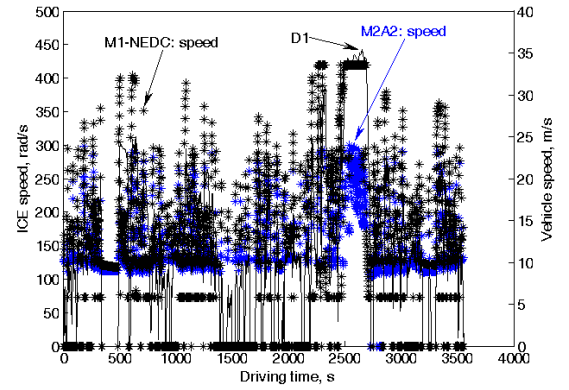


Figure 11.14: Comparison of ICE speed over D1: M2A2 and M1-NEDC designs

Although Figure 11.12 shows the comparison of FC between the M2A2 and M1-NEDC designs, it cannot be concluded directly which design is better in terms of FC? Therefore, the FC of both the designs with respect to torque and speed of ICE are compared in Figure 11.15 and Figure 11.16, respectively. Even though Figure 11.13 and Figure 11.14 show the operation of ICE of the M2A2 and M1-NEDC designs, it is difficult to analyse how many times ICE has been operated at particular speed and torque, which is important to understand the reason behind difference in FE. Therefore, histogram of the torque and speed of the ICE of the M2A2 and M1-NEDC designs over D1 driving pattern are plotted in Figure 11.17 and Figure 11.18 and respectively.

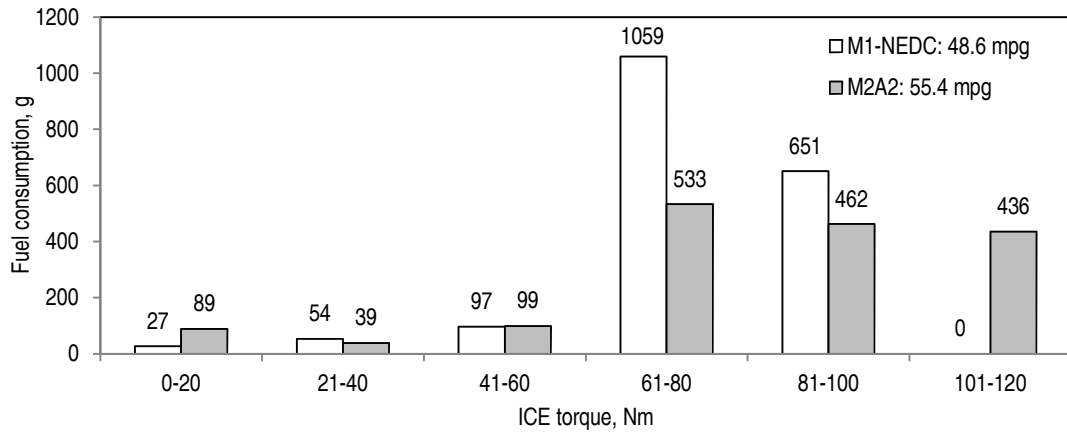


Figure 11.15: Distribution of fuel consumption w.r.t. ICE torque over D1: M2A2 and M1-NEDC designs

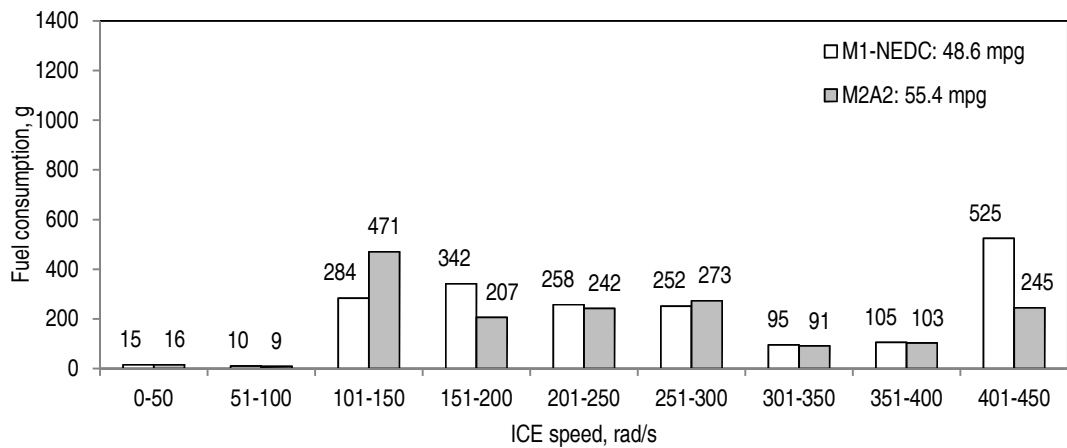


Figure 11.16: Distribution of fuel consumption w.r.t. ICE speed over D1: M2A2 and M1-NEDC designs

The FC over 60 Nm contributed to 86.3 and 90.6% of total FC for the M2A2 and M1-NEDC designs respectively, as shown in Figure 11.15. The M2A2 design had 49.7% less FC between 60 to 80 Nm compared to the M1-NEDC design, as shown in Figure 11.15, due to 41.6% less time of operation between 60 to 80 Nm compared to the M1-NEDC design, as shown in Figure 11.17. Although the M2A2 design operated 8.5% more time between 80 to 100 Nm compared to the M1-NEDC (Figure 11.17) but the M2A2 design had 29.0% less FC between 80 to 100 Nm, as shown in

Figure 11.15, probably due to the operation at higher torque compared to the M1-NEDC design. The M2A2 design had 16.3% lower FC over 60 Nm compared to the M1-NEDC design due to 19.4% lesser time of operation compared to the M1-NEDC design in this range.

The M2A2 design had 39.5 and 53.3% less FC between 150 to 200 rad/s and 400 to 450 rad/s respectively (Figure 11.16) compared to the M1-NEDC design due to 46.8 and 63.7% less time of operation between 150 to 200 rad/s and 400 to 450 rad/s respectively (Figure 11.18). But the M2A2 design had 39.7% more FC between 100 to 150 rad/s compared to the M1-NEDC design due to 40.9% more time of operation in this range. The FC above 200 rad/s contributed to 57.6 and 65.5% of total FC for the M2A2 and M1-NEDC designs, respectively. The M2A2 design had 22.7% lower FC over 200 rad/s due to 31.3% lower time of operation compared to the M1-NEDC design in this range.

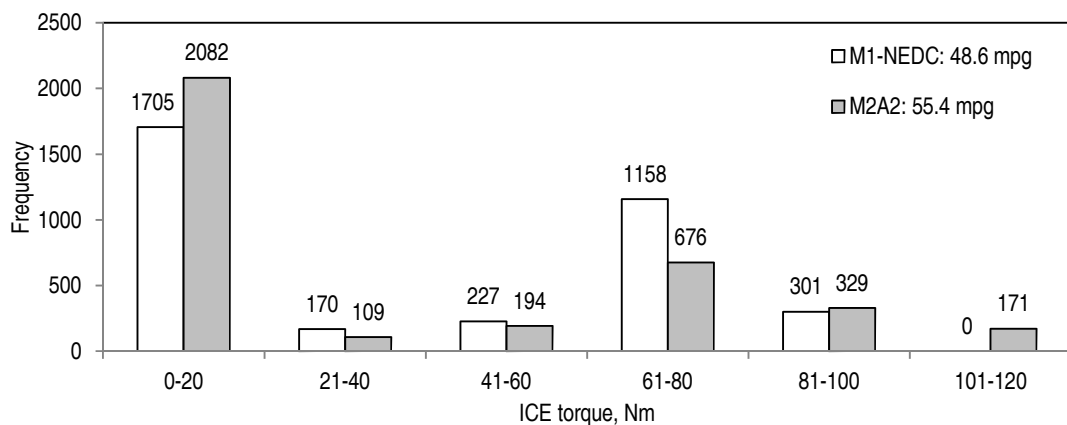


Figure 11.17: Distribution of ICE torque over D1: M2A2 and M1-NEDC designs

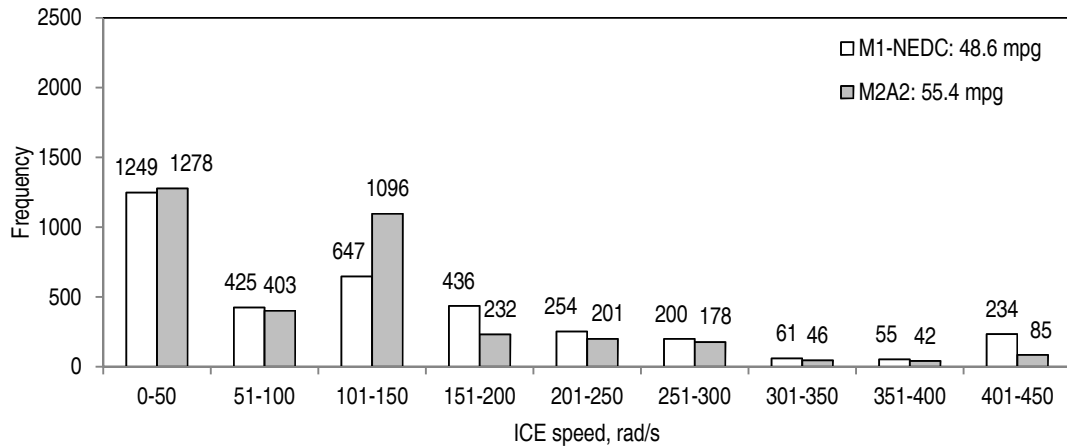


Figure 11.18: Distribution of ICE speed over D1: M2A2 and M1-NEDC designs

Due to 27.9% lower ICE power and 24.2% lower battery capacity of the M1-NEDC design compared to the M2A2 design, the M1-NEDC design was required to operate more time at higher ICE torque (>60 Nm) and speed (>200 rad/s) to achieve the desired final battery SOC. The M1-NEDC design had 17.4% lower battery system efficiency compared to the M2A2 design over D1 driving pattern. This indicated that the battery of the M1-NEDC design was required more time of charging compared to the M2A2 design over D1. Therefore, more time of usage of the ICE in the M1-NEDC design compared to the M2A2 design resulted in lower FE in the M1-NEDC design compared to the M2A2 design.

As the FC over 60 Nm contributed to 86.3 and 90.6% of total FC for the M2A2 and M1-NEDC designs respectively, 16.3% lower FC over 60 Nm due to 19.4% lesser time of operation over 60 Nm along with 31.3% lower time of operation of ICE over 200 rad/s caused 14.0% higher FE in the M2A2 design compared to the M1-NEDC design over D1 driving pattern.

11.3.2 Comparison over D1: M2A2 and M1-US06

The FC values of the M2A2 and M1-US06 designs over D1 are compared in Figure 11.19. The FC of the M2A2 design at high speed regions (between 2430 and 2730 seconds) spread up to 2.87 g/s but majority of FC concentrated between 0.5 to 1.7 g/s, whereas the FC of the M1-US06 design at the same speed range spread up to 2.59 g/s but has less concentration of FC between 0.5 to 1.7 g/s compared to the M2A2 design. In the lower speed regions (apart from the high speed regions between 2430 and 2730 seconds), the spread of FC of the M2A2 and M1-US06 designs were comparable.

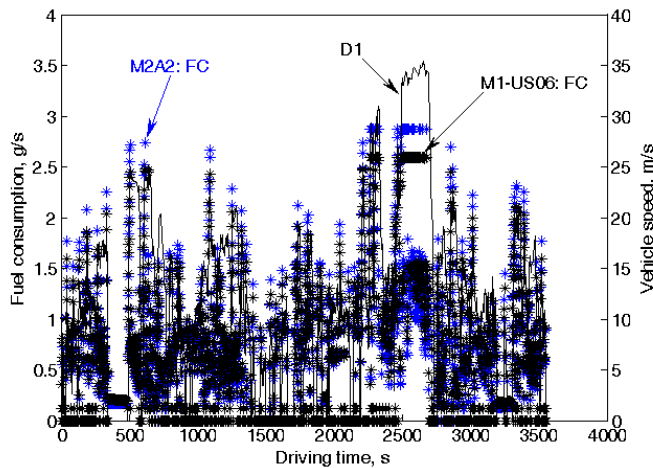


Figure 11.19: Comparison of fuel consumption over D1: M2A2 and M1-US06 designs

The speed and torque of the ICE for the M2A2 and M1-US06 designs over D1 driving pattern are shown in Figure 11.20 and Figure 11.21, respectively. Figure 11.20 shows that the operation of the M1-US06 design spread between 0 Nm to 96.0 Nm (maximum torque corresponding to maximum power 40.52 kW) and the operation of the M2A2 design spread between the range between 0 Nm to 106.6 Nm (maximum torque corresponding to maximum power 44.94 kW). The M1-US06

design operated comparatively higher times at higher speed compared to the M2A2 design, as shown in Figure 11.21.

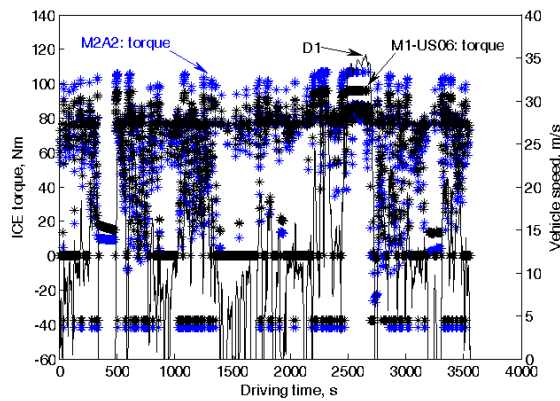


Figure 11.20: Comparison of ICE torque over D1: M2A2 and M1-US06 designs

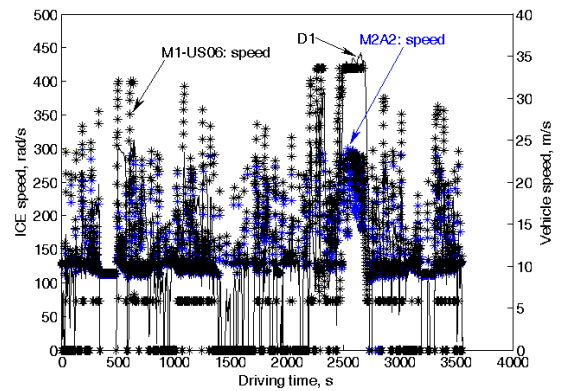


Figure 11.21: Comparison of ICE speed over D1: M2A2 and M1-US06 designs

Although Figure 11.19 shows the comparison of FC between the M2A2 and M1-US06 designs, it cannot be concluded directly which design is better in terms of FC? Therefore, the FC of both the designs with respect to torque and speed of ICE are compared in Figure 11.22 and Figure 11.23, respectively. Even though Figure 11.20 and Figure 11.21 show the operation of ICE of the M2A2 and M1-US06 designs, it is difficult to analyse how many times ICE has been operated at particular speed and torque, which is important to understand the reason behind difference in FE. Therefore, histogram of the torque and speed of the ICE of the M2A2 and M1-US06 designs over D1 driving pattern are plotted in Figure 11.24 and Figure 11.25, respectively.

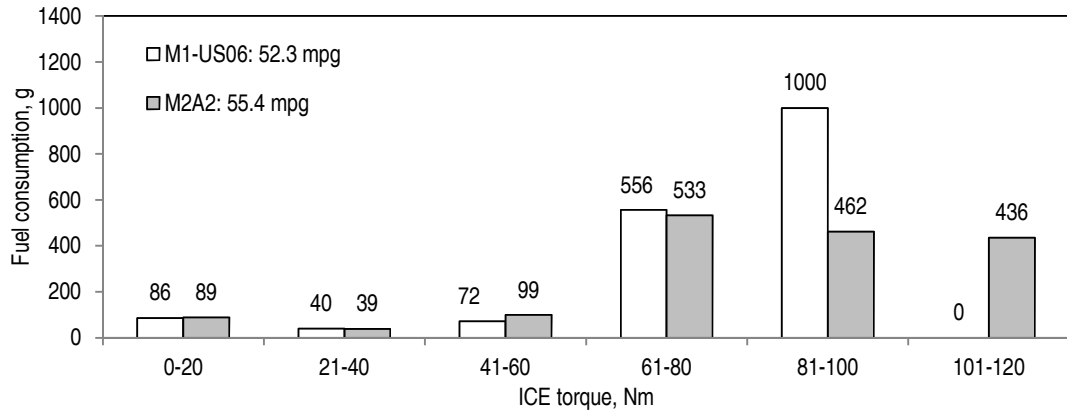


Figure 11.22: Distribution of fuel consumption w.r.t. ICE torque over D1: M2A2 and M1-US06 designs

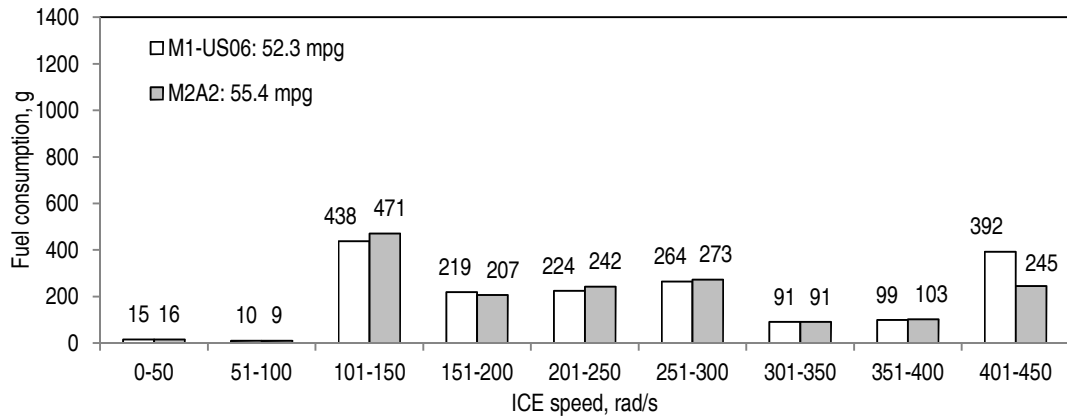


Figure 11.23: Distribution of fuel consumption w.r.t. ICE speed over D1: M2A2 and M1-US06 designs

The FC over 60 Nm contributed to 86.3 and 88.8% of total FC for the M2A2 and M1-US06 designs respectively, as shown in Figure 11.22. The M2A2 design had 4.1% less FC between 60 to 80 Nm compared to the M1-US06 design (Figure 11.22) due to 5.6% less time of operation between 60 to 80 Nm (Figure 11.24). The M2A2 design had 53.8% less FC between 80 to 100 Nm (Figure 11.22) due to 41.3% less time of operation between 80 to 100 Nm compared to the M1-US06 design (Figure 11.24). The M2A2 design had 8.1% lower FC over 60 Nm compared to the M1-

US06 design (Figure 11.22) due to 7.8% lower time of operation compared to the M1-US06 design in this range (Figure 11.24).

The M2A2 design had 5.5 and 37.5% less FC between 150 to 200 rad/s and 400 to 450 rad/s respectively (Figure 11.23) compared to the M1-US06 design due to 9.4 and 43.7% less time of operation between 150 to 200 rad/s and 400 to 450 rad/s respectively (Figure 11.25). But the M2A2 design had 7.0% more FC between 100 to 150 rad/s compared to the M1-US06 design due to 9.0% more time of operation in this range. The FC above 200 rad/s contributed 57.6 and 61.1% of total FC for the M2A2 and M1-US06 designs, respectively. The M2A2 design had 10.9 % lower FC above 200 rad/s compared to the M1-US06 design due to 12.0% lower time of operation in this range compared to the M1-US06 design.

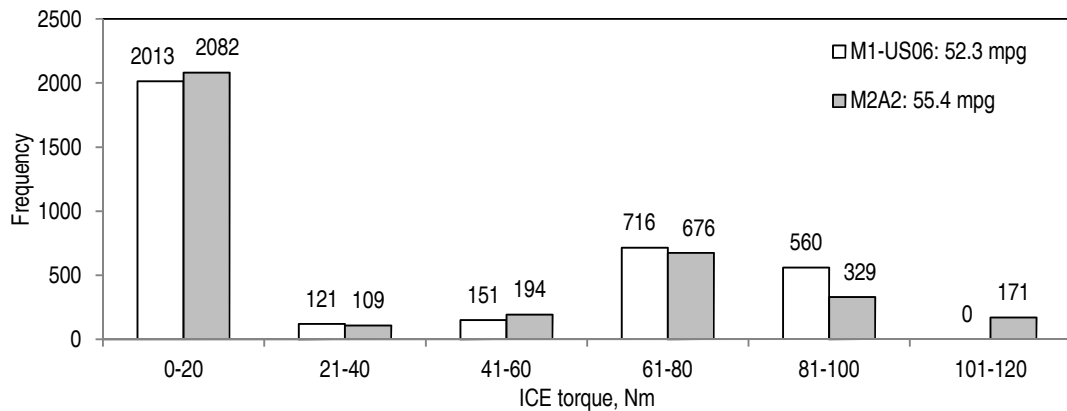


Figure 11.24: Distribution of ICE torque over D1: M2A2 and M1-US06 designs

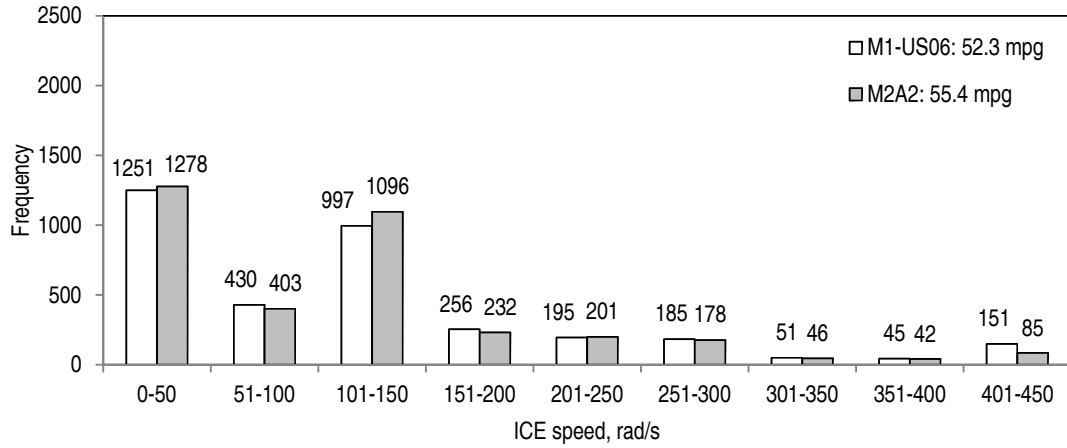


Figure 11.25: Distribution of ICE speed over D1: M2A2 and M1-US06 designs

Although the M1-US06 design had 11.5% higher battery capacity compared to the M2A2 design, the M1-US06 design was required to operate more time at higher ICE torque and speed to achieve desired final battery SOC due to 10.9% lower ICE power of the M1-US06 design compared to the M2A2 design. The M1-US06 design had 14.2% lower battery system efficiency compared to the M2A2 design over D1 driving pattern. This indicated that the battery of the M1-US06 design was required more time of charging compared to the M2A2 design over D1. Therefore, more time of usage of the ICE in the M1-US06 design compared to the M2A2 design resulted in lower FE in the M1-US06 design compared to the M2A2 design.

As the FC over 60 Nm contributed to 86.3 and 88.8% of total FC for the M2A2 and M1-US06 designs respectively, 8.1% lower FC over 60 Nm due to 7.8% lesser time of operation over 60 Nm along with 12.0% lower time of operation of ICE over 200 rad/s caused 5.9% higher FE in the M2A2 design compared to the M1-US06 design over D1 driving pattern.

11.3.3 Comparison over D1: M2A2 and Toyota Prius

The FC values of the M2A2 design and Toyota Prius over D1 are compared in Figure 11.26. The spread of the FC of the M2A2 design and Toyota Prius were comparable.

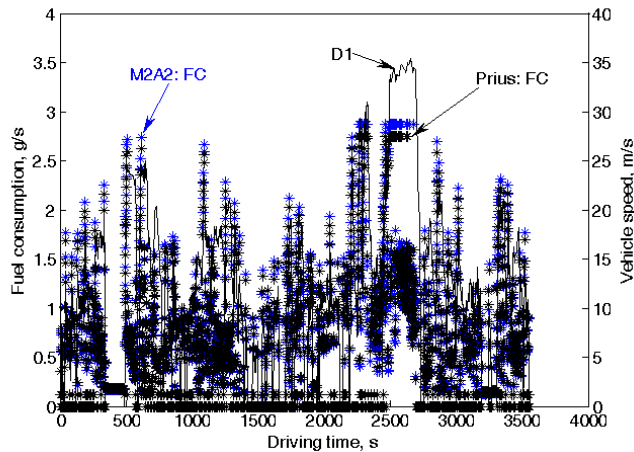


Figure 11.26: Comparison of fuel consumption over D1: M2A2 design and Toyota Prius

The torque and speed of the ICE for the M2A2 design and Toyota Prius over D1 driving pattern are shown in Figure 11.27 and Figure 11.28, respectively. Figure 11.27 shows that the operation of the Toyota Prius spread between 0 Nm to 101.9 Nm (the maximum torque corresponding to the maximum power 43.0 kW) and the operation of the M2A2 design spread between the range between 0 Nm to 106.6 Nm (the maximum torque corresponding to the maximum power 44.94 kW). The M2A2 design and Toyota Prius operated comparatively at similar speed in similar period of times, as shown in Figure 11.28.

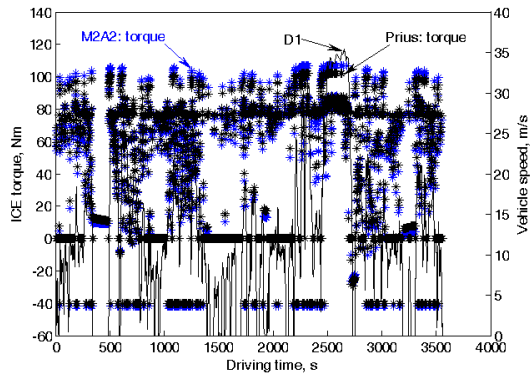


Figure 11.27: Comparison of ICE torque over D1: M2A2 design and Toyota Prius

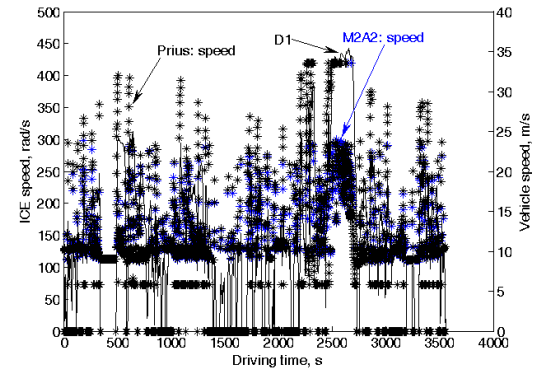


Figure 11.28: Comparison of ICE speed over D1: M2A2 design and Toyota Prius

Although Figure 11.26 shows the comparison of FC between the M2A2 design and Toyota Prius, it cannot be concluded directly which design is better in terms of FC? Therefore, the FC of both the designs with respect to torque and speed of ICE are compared in Figure 11.29 and Figure 11.30, respectively. Even though Figure 11.27 and Figure 11.28 show the operation of ICE of the M2A2 design and Toyota Prius, it is difficult to analyse how many times ICE has been operated at particular speed and torque, which is important to understand the reason behind difference in FE. Therefore, histogram of the torque and speed of the ICE of the M2A2 design and Toyota Prius over D1 driving pattern are plotted in Figure 11.31 and Figure 11.32, respectively.

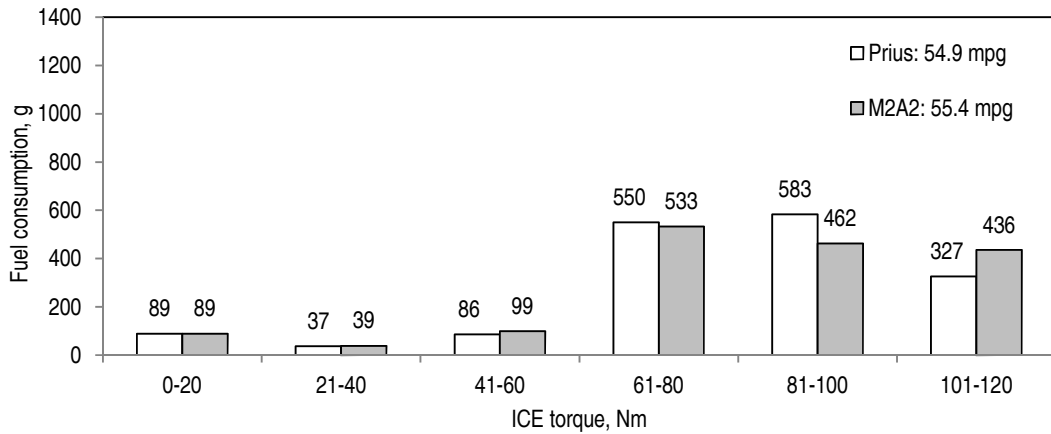


Figure 11.29: Distribution of fuel consumption w.r.t. ICE torque over D1: M2A2 design and Toyota Prius

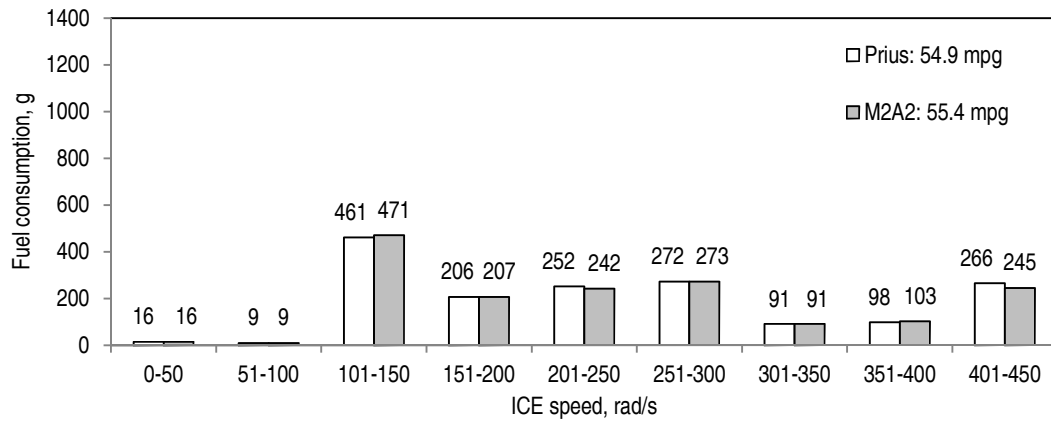


Figure 11.30: Distribution of fuel consumption w.r.t. ICE speed over D1: M2A2 design and Toyota Prius

The FC over 60 Nm contributed to 86.3 and 87.3% of total FC for the M2A2 design and Toyota Prius respectively, as shown in Figure 11.29. The M2A2 design had 3.1% less FC between 60 to 80 Nm compared to the Toyota Prius (Figure 11.29), due to 3.2% less time of operation between 60 to 80 Nm (Figure 11.31). The M2A2 design had 20.8% less FC between 80 to 100 Nm (Figure 11.29) due to 16.7% less time of operation between 80 to 100 Nm compared to the Toyota Prius (Figure 11.31). But

the M2A2 design had 25.9% more FC between 100 to 120 Nm compared to the Toyota Prius due to 29.2% more time of operation compared to the Toyota Prius in this range. The M2A2 design had 2.0% lower FC over 60 Nm compared to the Toyota Prius due to 3.1% lower time of operation in this range compared to the Toyota Prius.

The M2A2 design had 4.0 and 7.9% less FC between 200 to 250 rad/s and 400 to 450 rad/s respectively (Figure 11.30) compared to the Toyota Prius due to 5.6 and 11.5% less time of operation between 200 to 250 rad/s and 400 to 450 rad/s respectively (Figure 11.32). But the M2A2 design had 2.1% more FC between 100 to 150 rad/s compared to the Toyota Prius due to 2.8% more time of operation in this range. Although the M2A2 and Toyota Prius operated similar period of time between 350 to 400 rad/s, the M2A2 design had 4.9% higher FC compared to the Toyota Prius, probably due to higher torque operation in this range. All other speed range both the designs had similar FC due to comparatively similar time of operation of ICE. The FC above 200 rad/s contributed 57.6 and 58.6% of total FC for the M2A2 design and Toyota Prius, respectively. The M2A2 design had 2.5% less FC compared to the Toyota Prius over 200 rad/s due to 5.0% lower time of operation compared to the Toyota Prius over 200 rad/s.

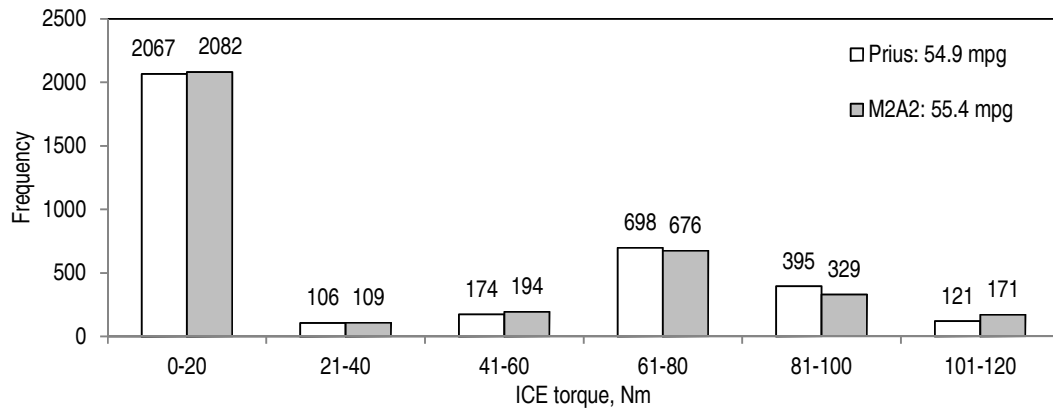


Figure 11.31: Distribution of ICE torque over D1: M2A2 design and Toyota Prius

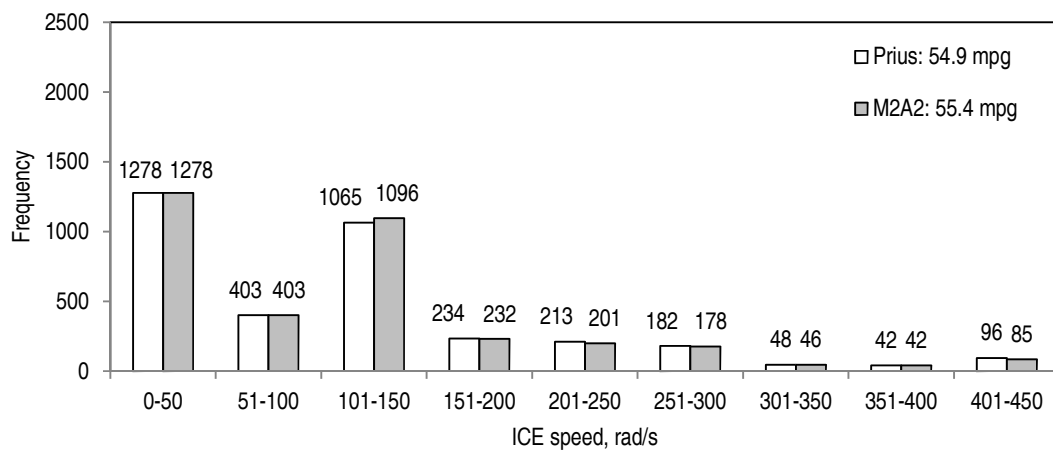


Figure 11.32: Distribution of ICE speed over D1: M2A2 design and Toyota Prius

Due to 4.5% lower power of the ICE and 28.3% lower capacity of the battery of the Toyota Prius compared to the M2A2 design, the Toyota Prius was required to operate more time at higher ICE torque and speed to achieve the desired final battery SOC. The Toyota Prius had 3.6% lower battery system efficiency compared to the M2A2 design over D1 driving pattern. This indicated that the battery of the Toyota Prius was required more time of charging compared to the M2A2 design over D1.

Therefore, more time of usage of the ICE in the Toyota Prius compared to the M2A2 design resulted in lower FE in the Toyota Prius compared to the M2A2 design.

As the FC over 60 Nm contributed to 86.3 and 87.3% of total FC for the M2A2 design and Toyota Prius respectively, 2.0% lower FC over 60 Nm due to 3.1% lesser time of operation over 60 Nm along with 5.0% lower time of operation of ICE over 200 rad/s caused 0.9% higher FE in the M2A2 design compared to the Toyota Prius over D1 driving pattern.

11.4 Distribution of FE: Toyota Prius, M1, and M2A2

The FE values of the Toyota Prius, M1-NEDC, M1-FTP, M1-LA92, M1-HWFET, M1-US06, and M2A2 designs over D1 to D10 driving patterns, as shown in Table 11.5, can be plotted statistically to find the distribution of FE for each design. The statistical distributions of the FE of each design are shown from Figure 11.33 to Figure 11.39.

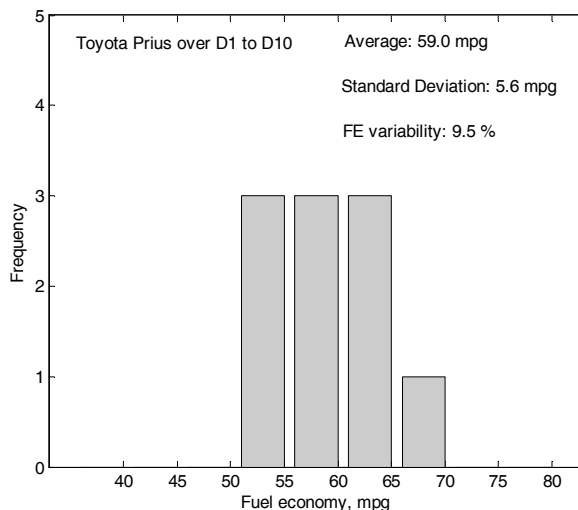


Figure 11.33: Distribution of FE of Toyota Prius over D1 to D10

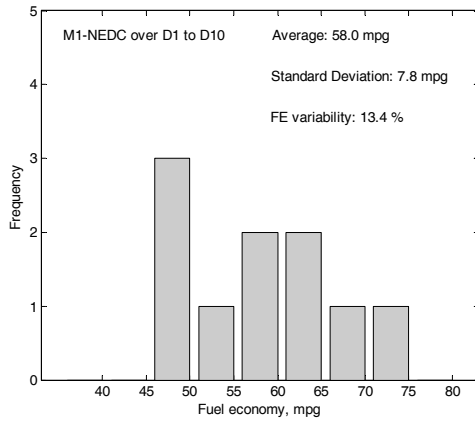


Figure 11.34: Distribution of FE of M1-NEDC design over D1 to D10

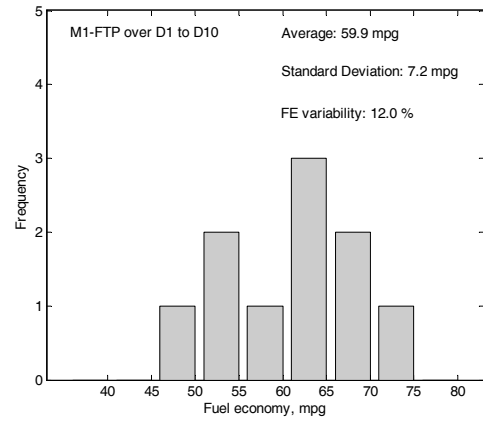


Figure 11.35: Distribution of FE of M1-FTP design over D1 to D10

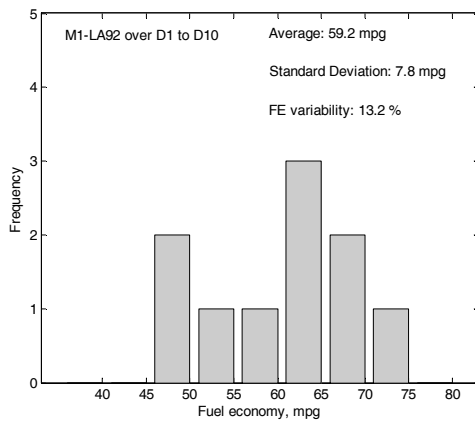


Figure 11.36: Distribution of FE of M1-LA92 design over D1 to D10

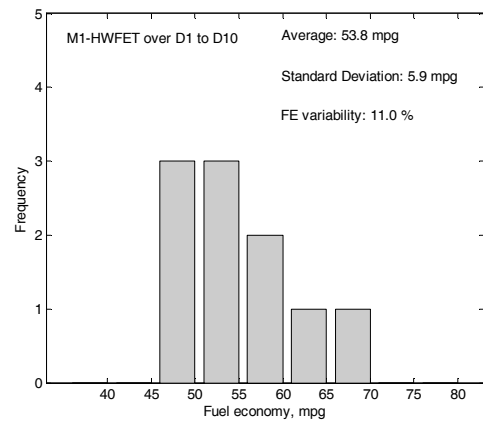


Figure 11.37: Distribution of FE of M1-HWFET design over D1 to D10

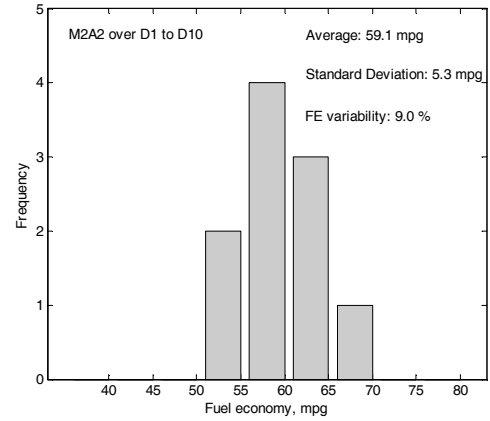
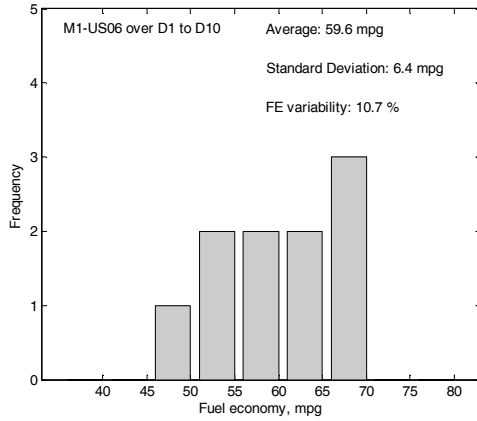


Figure 11.38: Distribution of FE of M1-US06 design over D1 to D10

Figure 11.39: Distribution of FE of M2A2 design over D1 to D10

The FE values of the Toyota Prius and M2A2 design ranged from 50 to 70 mpg, as shown in Figure 11.33 and Figure 11.39. The FE values of the M1-NEDC, M1-FTP, M1-LA92, M1-HWFET, and M1-US06 designs ranged from 45 to 75 mpg, as shown from Figure 11.34 to Figure 11.38 respectively. Therefore, the distributions are shown that each optimum design of the M1 methodology had higher spread in the FE compared to the Toyota Prius and M2A2 design.

Although the Toyota Prius and M2A2 design had similar spread of FE, the M2A2 design shifted the FE from 50 to 55 mpg towards 55 to 60 mpg, as shown in Figure 11.33 and Figure 11.39. Therefore the M2A2 design potentially shifted the FE towards higher values compared to the Toyota Prius. The M2A2 design has moved one of the least efficient drivers in case of the Toyota Prius to a more efficient place.

11.5 FE variability over real-world driving patterns: Toyota Prius, M1, and M2A2

The average FE of the M2A2 design and Toyota Prius were 59.1 and 59.0 mpg respectively, as shown in Table 11.5. Therefore, the M2A2 design had 0.2% higher average FE compared to the Toyota Prius.

The average FE of the M1-NEDC, M1-FTP, M1-LA92, M1-HWFET, and M1-US06 designs were 58.0, 59.9, 59.2, 53.8, and 59.6 mpg, respectively, as shown in Table 11.5. Therefore, the M2A2 design had 1.9% and 9.0% higher average FE compared to the M1-NEDC and M1-HWFET designs, but had 1.4, 0.2, and 0.8% lower average FE compared to the M1-FTP, M1-LA92, and M1-US06 designs, respectively. The M1-FTP, M1-LA92 and M1-US06 designs had 1.5, 0.3, and 1.0% higher average FE, but the M1-NEDC and M1-HWFET designs had 1.7% and 9.7% lower average FE compared to the Toyota Prius.

The standard deviations of FE of the M2A2 design and Toyota Prius were 5.3 and 5.6 mpg respectively, whereas the standard deviations of FE of the M1-NEDC, M1-FTP, M1-LA92, M1-HWFET, and M1-US06 designs were 7.8, 7.2, 7.8, 5.9, and 6.4 mpg, respectively.

The FE variability of the M2A2 design and Toyota Prius were 9.0 and 9.5% respectively. Therefore, the M2A2 design had 5.3% lower FE variability compared to the Toyota Prius.

The FE variability of the M1-NEDC, M1-FTP, M1-LA92, M1-HWFET, and M1-US06 designs were 13.4, 12.0, 13.2, 11.0, and 10.7%, respectively. Therefore, the M2A2 design reduced FE variability by 48.9, 33.3, 46.7, 22.2, and 18.9% compared

to the M1-NEDC, M1-FTP, M1-LA92, M1-HWFET, and M1-US06 designs, respectively. The M1-NEDC, M1-FTP, M1-LA92, M1-HWFET, and M1-US06 had 41.1, 26.3, 38.9, 15.8, and 12.6%, respectively higher FE variability compared to the Toyota Prius.

The average FE and FE variability of the optimum designs of the M1 methodology and M2A2 design w.r.t. Toyota Prius are shown in Figure 11.40. The average FE and FE variability of the Toyota Prius are shown as the origin of Figure 11.40.

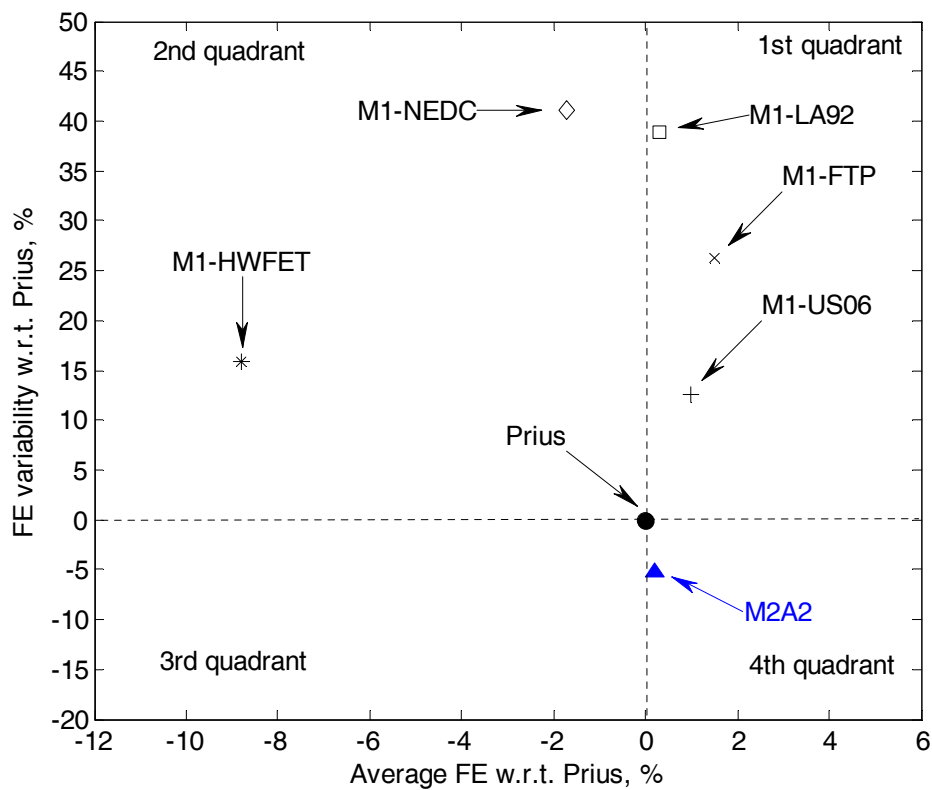


Figure 11.40: Average FE versus FE variability over real-world driving patterns: Toyota Prius, M1, and M2A2

The M1-FTP, M1-LA92, and M1-US06 designs situate in the 1st quadrant because those designs had higher average FE and FE variability compared to the Toyota

Prius. The M1-FTP, M1-LA92, and M1-US06 designs had higher FE compared to the Toyota Prius for average user but some user may experience a lower FE compared to the Toyota Prius as FE variability of the M1-FTP, M1-LA92, and M1-US06 designs were higher compared to the Toyota Prius.

The M1-NEDC and M1-HWFET designs situate in the 2nd quadrant because both the designs had lower average FE and higher FE variability compared to the Toyota Prius. The 2nd quadrant is the most undesired region. The M1-NEDC and M1-HWFET designs were based on NEDC and HWFET driving patterns which are less aggressive driving patterns compared to others (FTP, LA92, and US06). Therefore, the optimum designs based on less aggressive driving patterns might not be suitable for real-world applications.

As the M2A2 design had 0.2% higher average FE and 5.3% lower FE variability compared to the Toyota Prius, the M2A2 design situates in the 4th quadrant in Figure 11.40, which is the target region for any design, as discussed in chapter 3. It is clear from Figure 11.40 that the M2A2 design was the only design able to reduce FE variability without reducing average FE, whereas none of the optimum design of the M1 methodology was able to reduce FE variability compared to the Toyota Prius.

Although the Toyota Prius design was a better compromise in terms of average FE and FE variability compared to the designs of the M1 methodology, the M2A2 design was even better compared to the Toyota Prius in real-world driving. Therefore, the proposed methodology with the second approach (M2A2) showed a new direction to reduce the FE variability without reducing the average FE in real-world driving.

11.6 Summary

- The single optimum design (M2A2 design) produced by the proposed methodology with second approach (M2A2 approach) was the only design able to reduce the FE variability without reducing the average FE compared to the Toyota Prius in real-world driving.
- The M2A2 design had 5.3% lower FE variability and 0.2% higher average FE compared to that of the Toyota Prius (benchmark vehicle) over 10 real-world driving patterns.
- The M2A2 design demonstrated the potential to reduce the FE variability by up to 48.9% compared to the designs produced by the traditional methodology (M1) over 10 real-world driving patterns.
- The traditional methodology failed to reduce the FE variability compared to the benchmark vehicle (Toyota Prius) in real-world driving.
- The optimum designs produced by the traditional methodology had up to 41.1% higher FE variability compared to the Toyota Prius over 10 real-world driving patterns.
- The M2A2 design had 1.2% higher minimum FE compared to that of the Toyota Prius and improved the minimum FE by up to 10.2% compared to the designs produced by the traditional methodology.
- The M2A2 design showed on average 15.3% lower swing of the battery SOC compared to the Toyota Prius over the 10 real-world driving patterns. This might lead to higher battery life in the M2A2 design compared to the Toyota Prius.
- The M2A2 design had on average 2.2% higher battery system efficiency compared to the Toyota Prius over the 10 real-world driving patterns. This

might help in achieving better FE compared to the Toyota Prius in real-world driving.

- The M2A2 design had higher potential for better FE compared to the Toyota Prius over driving patterns consisted of higher maximum speed, acceleration, and traffic.
- The M2A2 design was able to cope with more aggressive real-world driving patterns.
- One design (M1-HWFET) of the traditional methodology failed to operate in charge sustaining over the 10 real-world driving patterns and therefore, the traditional methodology lacks the potential to be a generalised methodology in real-world applications.
- The M2A2 design was able to operate over all the 10 real-world driving patterns and therefore, the proposed methodology with the second approach (M2A2 approach) demonstrated the potential to be a generalised methodology for the optimisation of powertrain component sizes of HEVs in real-world applications.

CHAPTER 12

DISCUSSION AND FUTURE WORK

Chapters 7 to 11 have discussed the investigations of the traditional (M1) and proposed (M2) methodologies over the standard and real-world driving patterns. The discussions in each of the chapters have been mainly focused on the description and analysis of results of that chapter and compared with the most relevant results of the previous chapters. This chapter consolidates the major discussions and interprets the significance of the major results in chapters 7 to 11. The discussion of this chapter starts with the proposed methodology. The learning related to the optimisation of powertrain components for both the proposed and traditional methodologies are discussed. This chapter discusses whether the proposed methodology succeeded in achieving a preferred design for FE and whether the design of the proposed methodology is suitable for real-world applications. The status of the research question i.e., how far the research question has been solved, is discussed in this chapter. The potential of the proposed methodology in addressing customer concerns related to FE is discussed. The life and cost of optimum components of the proposed methodology are discussed. The limitation and applications of the proposed methodology are also discussed. This chapter also discusses possible directions of future work.

12.1 Proposed methodology

Driving patterns are speed-time profiles of vehicles. Driving patterns vary due to variation in traffic conditions and driving styles. Drive cycles or driving cycles (e.g., NEDC, FTP etc.) are standardised driving patterns, which generally used to meet the legislative norms. The standard driving patterns have been developed for different traffic conditions (urban, highway etc.) and driving styles (conservative, aggressive etc.). For example, FTP and LA92 are standard urban driving patterns, HWFET and US06 are standard highway driving patterns, and NEDC and JP 10-15 are standard driving patterns with combinations of urban and highway driving. FTP is more aggressive compared to the urban part of NEDC and US06 is more aggressive compared to HWFET. The driving time of the standard driving patterns are also different from one another. Therefore, a single standard driving pattern is not sufficient to represent the entire variations in real-world driving conditions and hence, design of components considering a single standard driving pattern might not perform optimally over different driving patterns. This is the weakness of the traditional methodology which generally considers a single standard driving pattern for the optimisation of powertrain component sizes. As no ideal driving pattern representing the entire variations in real-world driving conditions is possible, the proposed methodology improves the weakness of the traditional methodology by considering different driving patterns representing different traffic conditions and driving styles simultaneously to represent real-world driving conditions in a realistic way for the optimisation of powertrain component sizes.

Although the reviewed literature [49], [51], [52], [54], [55], [57-59] generally considered a single standard driving pattern, literature [50], [53], [56], [60] were

available where a combination of two standard driving patterns, urban (FTP or UDDS) and highway (HWFET) was considered. Those studies [50], [53], [56], [60] showed that the importance of considering different traffic conditions, but overlooked the importance of different driving styles (e.g., conservative, aggressive etc.). The importance of considering different driving styles has been found in this study. Although both HWFET and US06 are highway driving patterns, FE over US06 was lower compared to HWFET due to higher aggressiveness of US06 compared to HWFET, as seen in chapters 7 to 10. Similarly, though FTP and LA92 are urban driving patterns, FE over LA92 was lower compared to FTP due to higher aggressiveness of LA92 compared to FTP, as seen in chapters 7 to 10. Therefore, the consideration of driving styles is equally important as the traffic conditions. This justifies the consideration of different driving styles along with different traffic conditions in the proposed methodology. It shows that the proposed methodology conceptually improves upon all the reviewed literature [49-60].

12.2 Effect of optimisation variable and design constraint on optimum components

Two important learning related to the optimisation of powertrain component sizes were the effect of target SOC (a parameter of vehicle supervisory control strategy) and delta SOC (a design constraint) on the optimum component sizes. No details have been found in the reviewed literature [49-60] regarding the effect of the target SOC and delta SOC on the optimum powertrain component sizes.

The target SOC needs to be optimised along with the powertrain components to find a global optimum powertrain component sizes. The consideration of the target SOC equal to the final battery SOC might not always helps to achieve the final battery

SOC equal to initial battery SOC over driving patterns (e.g., HWFET) where a HEV operates the majority of driving time at higher speeds. Due to the operation at higher speeds, the ICE of the HEV might recharge the battery continuously and might not get sufficient time to discharge the battery to achieve the desired final battery SOC.

Another important learning related to the proposed methodology is that the control of the delta SOC (<0.5% in this study) after each driving pattern (i.e., M2A2 approach) provides a single optimum design which is optimum over a range of driving patterns with the satisfaction of charge sustainability. The control of the delta SOC after the end of the last driving pattern (i.e., M2A1 approach) leads to different optimum designs over different sequence of driving patterns. The control of delta SOC after the end of the last driving pattern (i.e., M2A1 approach) failed to satisfy a design constraint in this study (delta SOC < 0.5%) i.e., charge sustainability over each driving pattern, and therefore, not satisfied the philosophy of the proposed methodology which suggests that the powertrain components need to be optimum over different driving patterns with the satisfaction of all constraints. The control of the delta SOC after each driving pattern (i.e., M2A2 approach) satisfies all the constraints over all driving patterns, and therefore satisfies the philosophy of the proposed methodology.

12.3 Preferred design for FE

It has been discussed in chapter 3 that HEVs should be in the 4th quadrant marked as the target region where FE is higher with reduced FE variability, as shown in Figure 3.4 (repeated on next page). This is in contrast to the research in the reviewed literature [49-60] which focused only on the improvement of FE overlooking the FE

variability, and therefore potentially higher chances to be situated in the 1st quadrant where both FE and FE variability increase, as shown in Figure 3.4.

The optimum designs produced by the traditional methodology (M1) had on average 26.9% and up to 41.1% higher FE variability compared to the benchmark vehicle (Toyota Prius HEV) over 10 real-world driving patterns, as found in chapter 11. The optimum designs produced by the traditional methodology had up to 1.5% higher and up to 9.7% lower average FE compared to the Toyota Prius, as found in chapter 11. Therefore, the optimum designs produced by the traditional methodology are situated in the 1st and 2nd quadrant in Figure 11.40 (repeated next) compared to the Toyota Prius. Hence, the traditional methodology failed to provide a preferred design of higher FE with lower FE variability, as suspected considering the reviewed literature [49-60].

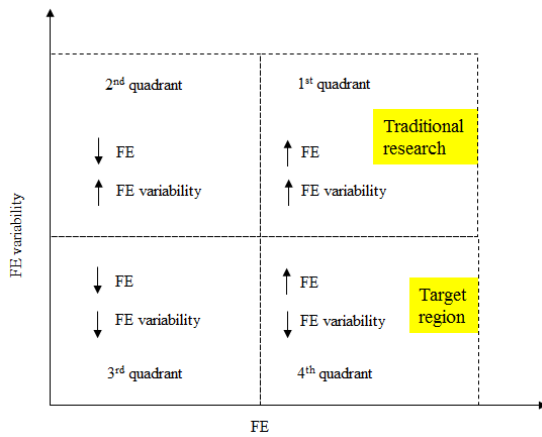


Figure 3.4 (Repeated): FE versus FE variability

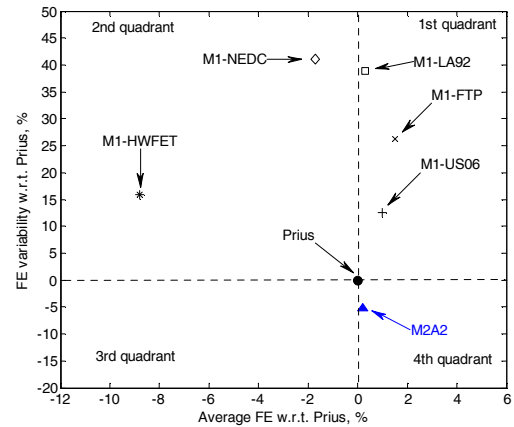


Figure 11.40 (Repeated): Average FE versus FE variability over real-world driving patterns

The optimum design (M2A2 design) produced by the proposed methodology with the second approach (M2A2 approach) had 5.3% lower FE variability with 0.2% higher average FE over 10 real-world driving patterns compared to the benchmark

vehicle (Toyota Prius HEV), as found in chapter 11. Therefore, the M2A2 design is the only design in the target region (4th quadrant) compared to the Toyota Prius over real-world driving patterns, as shown in Figure 11.40. It indicates that the proposed methodology shows a new approach for the optimisation of powertrain component sizes to get the most preferred design of higher FE with lower FE variability in real-world driving.

12.4 Suitability in real-world

The M2A2 design (the optimum design produced by the proposed methodology with second approach) had 5.0% and 18.9% lower FE variability over the standard and real-world driving patterns respectively compared to the M1-US06 design (the best design of the traditional methodology in terms of FE variability). Therefore, the M2A2 design reduced the FE variability by 278.0% over the real-world driving patterns than the standard driving patterns when compared with the M1-US06 design. The M2A2 design also had 3.3% and 5.3% lower FE variability over the standard and real-world driving patterns respectively compared to the benchmark vehicle (Toyota Prius HEV). Therefore, the M2A2 design reduced the FE variability by 60.6% over the real-world driving patterns than the standard driving patterns when compared with the Toyota Prius. Therefore, the FE variability of the M2A2 design reduced further over the real-world driving patterns compared to the standard driving patterns. The lower FE variability of the M2A2 design in the real-world driving patterns compared to the standard driving patterns indicates the higher potential of the proposed methodology in real-world applications.

The FE variability values of the five optimum designs produced by the traditional methodology (M1), namely, M1-NEDC, M1-FTP, M1-LA92, M1-HWFET, and M1-

US06 were higher by 18.8, 4.0, 8.8, 27.2, and 1.6%, respectively over 5 standard driving patterns and higher by 41.1, 26.3, 38.9, 15.8, and 12.6%, respectively over 10 real-world driving patterns compared to the Toyota Prius. Therefore, the FE variability values of the M1-NEDC, M1-FTP, M1-LA92 and M1-US06 designs increased by 118.6, 557.5, 198.9, and 687.5%, respectively over the real-world driving patterns compared to the standard driving patterns. Although it was appeared that the FE variability of the M1-HWFET design was reduced over the real-world driving patterns compared to the standard driving patterns but the comparison would not be fair as the M1-HWFET design failed to operate as charge sustaining over one standard driving pattern (US06) and five real-world driving patterns (D1, D3, D5, D6, and D9). Neglecting the M1-HWFET design, it could be said that the FE variability of the optimum designs produced by the traditional methodology increased further over the real-world driving patterns compared to the standard driving patterns. Therefore, the traditional methodology is more susceptible to higher FE variability in real-world driving.

The M1-US06 design had the lowest FE variability over standard as well over real-world driving patterns among the five optimum designs produced by the traditional methodology. By analysing the results over the standard driving patterns, it might appear that the M1-US06 design could be a close design to the Toyota Prius in terms of FE variability (1.6% higher FE variability than the Toyota Prius), and US06 could be considered as a single representative driving pattern for future use. However this idea runs the risk of neglecting the effect of different driving patterns in the real-world leading to higher FE variability compared to the standard driving patterns. This proved true when the M1-US06 design was evaluated over 10 real-world

driving patterns where the M1-US06 design showed 12.6% higher FE variability compared to the Toyota Prius. Therefore, the M1-US06 design showed 687.5% higher FE variability over the real-world driving patterns compared to the standard driving patterns. This shows that the M1-US06 design is not a close design to the Toyota Prius in terms FE variability over real-world driving. Therefore, US06 could not be considered as a single representative driving pattern for the optimisation of powertrain component sizes of HEVs.

12.5 Solution to the research question

The main objective of this research was to find a solution to the research question which was the reduction of FE variability due to the variation in driving patterns in HEVs through the optimisation of powertrain component sizes. The reviewed literature in chapter 3 has indicated that the traditional research has generally been focused over the years on the improvement of FE, and FE variability has been overlooked. The traditional methodology (M1) for the optimisation of powertrain component sizes followed in the reviewed literature conceptually flawed due to not considering a range of driving patterns during the optimisation of powertrain component sizes. Therefore, it has been predicted in chapter 3 that the traditional methodology followed in the reviewed literature might not be sufficient to address the research question. This research verified that the traditional methodology failed to reduce FE variability when compared with the benchmark vehicle (Toyota Prius HEV).

Only one design out of the five designs of the proposed methodology with the first approach (M2A1 approach) reduced FE variability when compared with the Toyota Prius. The M2A1 approach depends on the sequence of driving patterns and this

requires designer's decision to choose the sequence of driving patterns. Therefore, the M2A1 approach is also lacks the potential for practical applications, similar to the traditional methodology.

The proposed methodology with the second approach (M2A2 approach) demonstrated the potential to reduce FE variability not only when compared to the benchmark vehicle (Toyota Prius HEV) but also compared to all the five designs produced by the traditional methodology. Therefore, it is justified to conclude that the proposed methodology shows a new approach to address the research question.

12.6 Reduction of customer concerns

The maximum and minimum FE values of the M2A2 design over 10 real-world driving patterns were 67.5 and 51.0 mpg respectively, whereas that of the benchmark vehicle (Toyota Prius HEV) were 68.1 and 50.4 mpg respectively. Apart from that, the M2A2 design had 5.3% lower FE variability with comparable average FE (0.2% higher average FE) compared to the Toyota Prius. Due to the reduction of FE variability, reduction of range of FE (difference between the maximum and minimum FE), and comparable average FE, a probable distribution of the M2A2 design compared to the Toyota Prius could be, as shown in Figure 12.1, following the reviewed literature [46] which showed bell-shaped distribution of FE for HEVs when tested over 100 real-world driving patterns in Kansas city conducted by the United States Environment Protection Agency, as shown in Figure 3.3 in chapter 3 (repeated on next page).

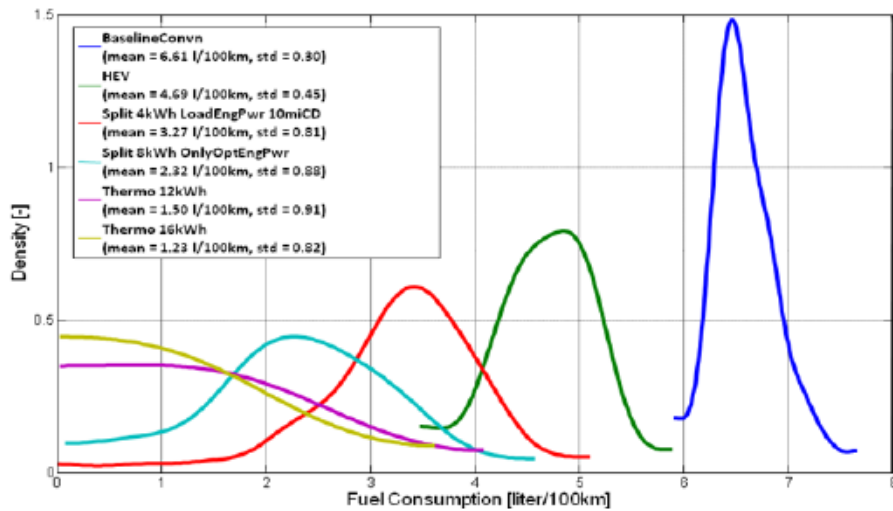


Figure 3.3 (Repeated): FE variability over 100 real-world driving patterns [46]

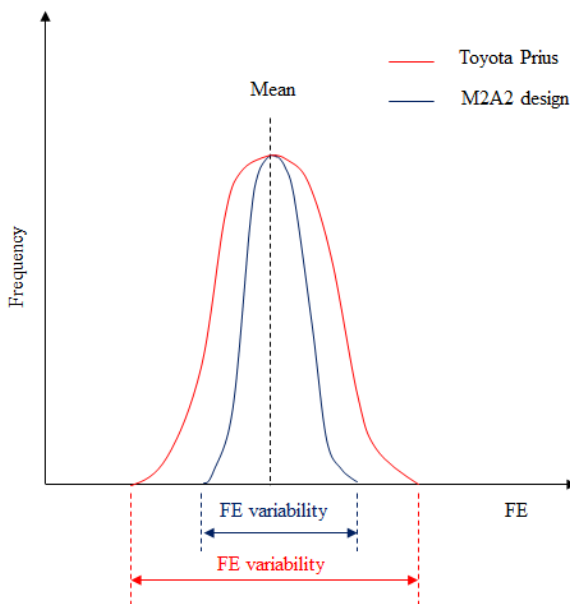


Figure 12.1: Probable distribution of FE: M2A2 and Toyota Prius

Figure 12.1 shows that the M2A2 design could improve the predictability of FE compared to the Toyota Prius. Therefore, better predictability of FE for the M2A2 design has the potential to reduce customer concerns related to the variation in FE between the declared data of manufactures and their real-world FE.

The M2A2 design had up to 1.2% higher FE compared to the Toyota Prius over the driving patterns consisting of higher maximum acceleration, maximum speed, and driving time for acceleration-deceleration, as discussed in chapter 11. Therefore, the M2A2 design is more suitable for aggressive driving patterns compared to the Toyota Prius. As the FE of a vehicle is generally lower over aggressive driving patterns, there is a possibility that the majority of customer complaints for FE are from aggressive drivers. Therefore, the aggressive drivers would complaint less for FE with the M2A2 design compared to the Toyota Prius. Hence, the M2A2 design could potentially reduce the customer concerns related to low FE in real-world driving.

12.7 Elimination of decision making process

The traditional methodology (M1) provided five different optimum designs, one for each driving pattern. Therefore, an optimum design over a driving pattern is not optimum over other driving patterns. This result agrees with the conclusion found in literature [52], [55], [57]. Different optimum designs and FE variability over different driving patterns indicates that the applicability of the M1 methodology is limited by the choice of driving patterns. Similarly, the proposed methodology with the first approach (M2A1) also provided five different optimum designs, one for each sequence of driving patterns. Therefore, the applicability of the M2A1 approach is also limited by the choice of the sequence of driving patterns. As both the M1 methodology and M2A1 approach provide different optimum designs over different driving patterns, they require a separate decision making process to find the best design for the least FE variability. Even though the decision making process is able to find a design with the least FE variability among all the available designs, the

design actually is optimum over a particular driving pattern and there is every possibility that the optimum design would be different than a design which is optimum over all the driving patterns simultaneously.

On the other hand, the proposed methodology with the second approach (M2A2) provided a single optimum design over the five different driving patterns and the design was independent of the sequence of driving patterns. Therefore, the M2A2 approach eliminates the need of a separate decision making process. Hence, the proposed methodology improves up on the traditional methodology. The proposed methodology can therefore be considered as an initial step towards an automated design methodology for the optimisation of powertrain component sizes with the potential to reduce FE variability in real-world conditions.

12.8 Component life and cost

The optimum design (M2A2 design) produced by the proposed methodology had on average 15.3% lower swing of battery SOC and 2.2% higher battery system efficiency compared to the benchmark vehicle (Toyota Prius HEV) over 10 real-world driving patterns. The lower swing of battery SOC and higher battery system efficiency of the M2A2 design might help to improve the battery life-cycle of the M2A2 design compared to the Toyota Prius [20], [105].

The M2A2 design had 9.8, 12.4, and 11.5% smaller generator, motor, and battery sizes, respectively along with 10.9% higher ICE size compared to the M1-US06 design (the best design of the traditional methodology in terms of FE variability). The cost of ICE, generator, and motor are proportional to the maximum power and cost of the battery is proportional to the maximum energy as found from studies by

Electric Power Research Institute (EPRI), USA [52], [62], [63]. The costs of components are as follows.

Cost of ICE \sim $\$12.0 \times (\text{Maximum power of ICE}) + \400

Cost of generator \sim $\$22.0 \times (\text{Maximum power of generator}) + \400

Cost of motor \sim $\$22.0 \times (\text{Maximum power of motor}) + \400

Cost of battery \sim $\$320.0 \times (\text{Maximum energy of battery}) + \700

Although the cost-equations are based on studies conducted in 2001 and at present the cost-equations might change, it is expected that it would only affect the coefficients of the cost-equations. Therefore, the cost-equations can be used to predict the difference in cost not the actual cost. The cost of the powertrain components of the M2A2 design could be lower compared to the M1-US06 design, because the M2A2 design was able to reduce three component sizes (generator, motor, and battery) with the increase in size of one component (ICE) than the M1-US06 design. Considering the above four equations, the M2A2 design could potentially reduce the cost of the powertrain components by around 6.0% compared to the M1-US06 design. Hence, it could be said that the proposed methodology (M2) provided a cost effective design compared to the best design (in terms of FE variability) of the traditional methodology (M1).

The optimum ICE, generator, motor and battery sizes of the M2A2 design were 4.4, 10.0, 1.7, and 28.3%, respectively higher compared to that of the Toyota Prius. Therefore, the overall cost of powertrain components of the M2A2 design would be around 11.0% higher compared to the Toyota Prius using the same above equations. Although the initial cost of the M2A2 design would be higher compared to the Toyota Prius, the initial increase in the cost could be compensated by the lower FE

variability with the increase in the minimum FE and increase in the average FE in long usage. The difference in cost of components between the M2A2 design and Toyota Prius are due the higher battery capacity of the M2A2 design compared to the Toyota Prius. As the M2A2 design had the potential of higher battery life compared to the Toyota Prius, the initial higher cost of the M2A2 design compared to the Toyota Prius might be compensated by the higher battery life-cycle of the M2A2 design in long usage.

Weight of powertrain components could affect the cost of powertrain components as well as the performance of vehicle. But this study did not consider weight of the components because of the lack of data for the relationship between the weight and power of powertrain components. As this research was comparative in nature, the effect of the weight was similar for all the studies and therefore, had little effect on the conclusion of this research. The consideration of weight of powertrain components during optimisation could be a direction of further research.

12.9 Limitation related to the proposed methodology

The proposed methodology recommends the categorisation of driving patterns into different traffic conditions and driving styles. In this study, the standard driving patterns were categorised based on the speed profile and comparison of four parameters, namely, driving time spent for acceleration and deceleration, maximum speed, and maximum acceleration [52], [78], [99], [100]. But this research study has not recommended any general criterion for the categorisation of driving patterns into different driving styles. It means, what are the parameters (maximum speed or acceleration etc.) to be considered for the categorisation of driving styles (e.g., conservative, normal, or aggressive driving) and what would be the limits of each

parameter to qualify for any particular category. No study has been found in the reviewed literature to address the above problem. Therefore, the criteria for the categorisation of driving patterns into different driving styles need to be understood further and could be a direction of research. Although this study has not recommended any criteria for the categorisation of driving styles, which was not the purpose of this study, it does not limit the application of the proposed methodology as designers can include more or less parameters based on their experience to categorise driving patterns into different driving styles.

12.10 Applications

Different optimum designs for different driving patterns, wide range of FE performance of different optimum designs, and failure to operate charge sustaining of an optimum design (M1-HWFET) over different driving patterns (US06, D1, D3, D5, D6 and D9) indicate that the applicability of the traditional methodology is limited by the choice of driving patterns and therefore, the traditional methodology cannot be considered as a generalised methodology. On the other hand, the single optimum design of the proposed methodology with the second approach (M2A2) has demonstrated the ability to operate charge sustaining over real-world driving patterns as well as standard driving patterns representing different traffic conditions and driving styles. Therefore, the proposed methodology has the potential to be a generalised methodology for the optimisation of powertrain component sizes in real-world applications. Hence, the proposed methodology improves up on the traditional methodology.

As this study was carried out for a non-plug-in HEV, the proposed methodology is potentially applicable to non-plug-in HEVs to reduce FE variability in real-world

driving. It could be argued about the applicability of the proposed methodology in plug-in HEVs where final battery SOC needs not be the same as initial battery SOC, as external charging is possible. But the use of the concept in plug-in HEV would also be helpful as higher battery SOC helps to avoid the lack of power at very low battery SOC.

As the proposed methodology demonstrates its applicability for a series-parallel HEV, the proposed methodology is applicable to other major architectures such as series and parallel also because the concept of the proposed methodology is independent of the choice of architecture.

The traditional methodology provides different optimum designs over different driving patterns, and therefore requires a separate decision making process after the optimisation to find the best design with least FE variability. On the other hand, the proposed methodology provides a single optimum design over a range of different driving patterns and hence, eliminates the need for a separate decision making process. Therefore, the elimination of a separate decision making process potentially reduces the development time of the proposed methodology to find an optimum design with least FE variability compared to the traditional methodology i.e., design is fact-based.

The proposed methodology could be applied to any specific region if driving patterns of that region are available. If driving patterns of that region is unavailable then standard driving patterns as considered in this study could be used with the assumption that standard driving patterns are developed considering driving patterns of different regions. Although the proposed methodology requires categorisation of driving patterns, all driving patterns of a specific region, if known, could be

considered without categorisation. The categorisation of driving patterns eliminates the similar type of driving patterns and would reduce computational time for optimisation. But whether there would be any difference in optimum component sizes between the consideration of all driving patterns and categorised driving patterns is not known and requires further investigation. The determination of the minimum number of driving patterns required for the proposed methodology for an optimum design with reduced FE variability also requires further investigation.

The concept of the proposed methodology of using a range of driving patterns for the optimisation of powertrain component sizes can be applied to any automotive vehicle, as all vehicles are subjected to different driving patterns in the real world.

12.11 Future work

- This study considered 5 standard driving patterns representing different traffic conditions and driving styles. The effect of the inclusion of more or fewer driving patterns on the proposed methodology can be investigated to understand the minimum number of driving patterns required to get an optimum design with reduced FE variability.
- In this study, the powertrain components are optimised over 5 standard driving patterns. The powertrain components could be optimised over the 10 real-world driving patterns (aforementioned in this study) in further studies to understand the effect of the use of real-world driving patterns for the optimisation of powertrain component sizes on the proposed methodology.
- This study considered FE variability in real-world driving due to variation in driving patterns. But the variation in atmospheric temperature and operation of air-conditioning also affect the FE variability, as found in the reviewed

literature. Even though the variation in driving patterns are unpredictable and have significant effect on the FE variability, the effect of the variation in atmospheric temperature cannot be avoided. The variation in atmospheric temperature and operation of air-conditioning might be interrelated as more air-conditioning would be required at higher atmospheric temperature. The effect of the operation of air-conditioning could be eliminated by simply turn-off the air-conditioning unit. The variation in atmospheric temperature can be included by incorporating fuel consumption map of internal combustion engine with respect to atmospheric temperature to improve the applicability of the proposed methodology.

- The proposed methodology could be investigated for the series as well as parallel HEVs to investigate the comparative performance of the proposed methodology over all architectures of HEV.
- As the HEVs are not free from exhaust emissions and the cost of HEVs are higher compared to conventional vehicles, the exhaust emissions and cost of components are important parameters along with FE for the selection of optimum powertrain components of HEVs. The exhaust emissions and cost of components can be considered along with FE to improve the proposed methodology for real-world applications. The exhaust emissions and component cost could be considered in two ways, namely, design constraint and objective. This means when emissions and cost will be used as design constraints, the emissions and cost of the optimum design has to be at par with respect to the benchmark vehicle (e.g., Toyota Prius in this study) for optimum FE. When emissions and cost will be used as objectives along with

FE, the design should be optimum for FE, emissions, and cost simultaneously.

- The vehicle supervisory control (VSC) strategy controls the operation of the powertrain components and hence, influences the performance of HEVs. Different parameters of a rule-based VSC strategy can be considered along with the powertrain components for the optimisation to improve the applicability of the proposed methodology for real-world applications. The effect of different VSC strategies on the powertrain component sizes and FE variability can also be considered.
- The variation in results for 10 different optimisation trials was around 1.0%. The effect of other optimisation algorithms (such as particle swarm optimisation and simulated annealing) compared to the optimisation method (genetic algorithm) used in this study could be investigated in relation to the variation in results for different optimisation trials.

CHAPTER 13

CONCLUSIONS

A review of literature highlighted that research has generally been focussed on the improvement of fuel economy (FE) in hybrid electric vehicles (HEVs); FE variability due to variation in driving patterns has generally been overlooked. However the reviewed literature indicated that without reducing FE variability actual improvement of FE of HEVs could not be fully realised in real-world usage. How to reduce FE variability due to variation in driving patterns through the optimisation of powertrain components was considered as the research question.

Although the research overlooked the FE variability, the traditional methodology for the optimisation of powertrain component sizes of HEVs through computer simulation followed in the reviewed literature was assumed unsuitable to address the research question. The assumption was due to the weakness of the traditional methodology which generally considered a single standard driving pattern to represent real-world driving conditions without discussing the reason for choosing the driving pattern for the optimisation.

A new methodology for the optimisation of powertrain component sizes of HEVs to reduce FE variability due to variation in driving patterns has been proposed. The proposed methodology conceptually improves upon the traditional methodology by

considering a range of driving patterns representing different traffic conditions and driving styles simultaneously for the optimisation.

Computer simulation studies over a series-parallel Toyota Prius HEV were conducted to investigate the potential of the proposed methodology to address the research question and to verify the assumption of the inability of the traditional methodology in addressing the research question. The investigations were conducted over standard as well as real-world driving patterns. The Toyota Prius was considered as the benchmark vehicle for comparison.

The traditional methodology failed to reduce the FE variability over standard as well as real-world driving patterns when compared with the benchmark vehicle and therefore, failed to address the research question. This verified the assumption from the literature review. The traditional methodology provided different optimum component sizes over different driving patterns and an optimum design failed to operate charge sustaining over aggressive driving patterns. Therefore, the traditional methodology could not be considered as a generalised methodology because its application is limited by the choice of driving patterns.

The methodology proposed from this research reduced the FE variability compared to the benchmark vehicle and traditional methodology over standard as well as real-world driving patterns, and therefore, shows an approach to solve the research question.

The proposed methodology provided a single optimum design instead of different optimum designs found in the traditional methodology over a range of driving patterns representing different traffic conditions and driving styles. The single

optimum design was also independent of the sequence of driving patterns. The optimum design was able to operate charge sustaining over standard as well as real-world driving patterns. This improved upon the traditional methodology where one optimum design failed to operate charge sustaining over aggressive driving patterns. Therefore, the proposed methodology improves upon the traditional methodology and could be considered as a generalised methodology for the optimisation of powertrain component sizes.

Although the proposed methodology has several potential advantages, one limitation related to the proposed methodology exists. As the proposed methodology recommends categorisation of driving patterns into different traffic conditions and driving styles, this study categorised standard driving patterns in a simple way into two traffic conditions (urban and highway) and each traffic condition into three driving styles (conservative, normal, and aggressive). The categorisation of driving styles was done based on parameters of driving patterns such as the maximum speed, the maximum acceleration, and driving time spent for acceleration-deceleration due to the lack of knowledge available in literature. This study has not suggested which parameters need to be considered and what should be the value of the parameters for the categorisation of driving patterns into different driving styles.

The proposed methodology considers driving patterns representing different traffic conditions and driving styles simultaneously to represent real-world driving conditions in a realistic way for the optimisation of powertrain components. Therefore, the concept of the proposed methodology is applicable to any automotive vehicle as all automotive vehicles are subjected to different driving patterns due to variation in traffic conditions and driving styles.

As the proposed methodology shows an approach to reduce FE variability due to variation in driving patterns and the problem is related to customers of automotive vehicles, the proposed methodology is potentially applicable to address the customer concerns related to FE.

REFERENCES

- [1] Y. S. Chang and S. J. Baek, "Limit to improvement: Myth or reality?: Empirical analysis of historical improvement on three technologies influential in the evolution of civilization," *Technological Forecasting and Social Change*, vol. 77, pp. 712-729, 2010.
- [2] A. E. Atabani, I. A. Badruddin, S. Mekhilef, and A. S. Silitonga, "A review on global fuel economy standards, labels and technologies in the transportation sector," *Renewable and Sustainable Energy Reviews*, vol. 15, pp. 4586-4610, 2011.
- [3] S. Shafiee and E. Topal, "When will fossil fuel reserves be diminished?," *Energy Policy*, vol. 37, pp. 181-189, 2009.
- [4] W. Krewitt, S. Teske, S. Simon, T. Pregger, W. Graus, E. Blomen, S. Schmid, and O. Schäfer, "Energy [R]evolution 2008 - a sustainable world energy perspective," *Energy Policy*, vol. 37, pp. 5764-5775, 2009.
- [5] L. Chapman, "Transport and climate change: a review," *Journal of Transport Geography*, vol. 15, pp. 354-367, 2007.
- [6] J. H. Buckland and J. A. Cook, "Automotive emissions control," in *Proceedings of the American Control Conference*, 2005, pp. 3290-3295
- [7] O. A. Kutlar, H. Arslan, and A. T. Calik, "Methods to improve efficiency of four stroke, spark ignition engines at part load," *Energy Conversion and Management*, vol. 46, pp. 3202-3220, 2005.
- [8] A. M. K. P. Taylor, "Science review of internal combustion engines," *Energy Policy*, vol. 36, pp. 4657-4667, 2008.
- [9] C. Berggren and T. Magnusson, "Reducing automotive emissions—The potentials of combustion engine technologies and the power of policy," *Energy Policy*, vol. 41, pp. 636-643, 2012.
- [10] R. J. Pearson, M. D. Eisaman, J. W. G. Turner, P. P. Edwards, Z. Jiang, V. L. Kuznetsov, K. A. Littau, L. D. Marco, and S. R. G. Taylor, "Energy storage via carbon-neutral fuels made from CO₂, water, and renewable energy," *Proceedings of IEEE*, vol. 100, pp. 440-460, 2012.

- [11] C. E. S. Thomas, "Transportation options in a carbon-constrained world: Hybrids, plug-in hybrids, biofuels, fuel cell electric vehicles, and battery electric vehicles," *International Journal of Hydrogen Energy*, vol. 34, pp. 9279-9296, 2009.
- [12] C. Shen, P. Shan, and T. Gao, "A comprehensive overview of hybrid electric vehicles," *International Journal of Vehicular Technology*, vol. 2011, pp. 1-7, 2011.
- [13] S. Verhelst, "Recent progress in the use of hydrogen as a fuel for internal combustion engines," *International Journal of Hydrogen Energy*, vol. 39, pp. 1071-1085, 2014.
- [14] S. Verhelst and T. Wallner, "Hydrogen-fueled internal combustion engines," *Progress in Energy and Combustion Science*, vol. 35, pp. 490-527, 2009.
- [15] D. J. Durbin and C. Malardier-Jugroot, "Review of hydrogen storage techniques for on board vehicle application," *International Journal of Hydrogen Energy*, vol. 38, pp. 14595-14617, 2013.
- [16] L. Kumar and S. Jain, "Electric propulsion system for electric vehicular technology: A review," *Renewable and Sustainable Energy Reviews*, vol. 29, pp. 924-940, 2014.
- [17] H. Ma, F. Balthasar, N. Tait, X. Riera-Palou, and A. Harrison, "A new comparison between the life cycle greenhouse gas emissions of battery electric vehicles and internal combustion vehicles," *Energy Policy*, vol. 44, pp. 160-173, 2012.
- [18] M. Fischer, M. Werber, and P. V. Schwartz, "Batteries: Higher energy density than gasoline?," *Energy Policy*, vol. 37, pp. 2639-2641, 2009.
- [19] S. Steinhilber, P. Wells, and S. Thankappan, "Socio-technical inertia: Understanding the barriers to electric vehicles," *Energy Policy*, vol. 60, pp. 531-539, 2013.
- [20] S. F. Tie and C. W. Tan, "A review of energy sources and energy management system in electric vehicles," *Renewable and Sustainable Energy Reviews*, vol. 20, pp. 82-102, 2013.
- [21] G. Pistoia, *Electric and hybrid vehicles*. Oxford, UK: Elsevier, 2010.

- [22] M. Catenacci, E. Verdolini, V. Bosetti, and G. Fiorese, "Going electric: Expert survey on the future of battery technologies for electric vehicles," *Energy Policy*, vol. 61, pp. 403-413, 2013.
- [23] M. Ehsani, Y. Gao, and A. Emadi, "Modern electric, hybrid electric and fuel cell vehicles: fundamentals, theory and design," *CRC Press - Technology and Engineering*, 2009.
- [24] C. C. Chan, "The state of the art of electric and hybrid vehicles," *Proceedings of the IEEE*, vol. 90, pp. 247-275, 2002.
- [25] V. Wouk, "Hybrids: Then and Now," *IEEE Spectrum*, vol. 33, pp. 16-21, 1995.
- [26] M. A. Hannan, F. A. Azidin, and A. Mohamed, "Hybrid electric vehicles and their challenges: A review," *Renewable and Sustainable Energy Reviews*, vol. 29, pp. 135-150, 2014.
- [27] T. S. Rurrentine and K. S. Kurani, "Car buyers and fuel economy," *Energy Policy*, vol. 35, pp. 1213-1223, 2007.
- [28] G. Yimin, M. Ehsani, and J. M. Miller, "Hybrid electric vehicle: overview and state of the art," in *Proceedings of the IEEE International Symposium on Industrial Electronics, ISIE 2005*, pp. 307-316.
- [29] K. Ç. Bayindir, M. A. Gözükcükük, and A. Teke, "A comprehensive overview of hybrid electric vehicle: powertrain configurations, powertrain control techniques and electronic control units," *Energy Conversion and Management*, vol. 52, pp. 1305-1313, 2011.
- [30] K. T. Chau and Y. S. Wong, "Overview of power management in hybrid electric vehicles," *Energy Conversion and Management*, vol. 43, pp. 1953-1968, 2002.
- [31] F. Orecchini and A. Santiangeli, "Chapter twenty two - Automakers' powertrain options for hybrid and electric vehicles," in *Electric and Hybrid Vehicles*, ed Amsterdam: Elsevier, 2010, pp. 579-636.
- [32] E. W. C. Lo, "Review on the configurations of hybrid electric vehicles," in *3rd International Conference on Power Electronics Systems and Applications, PESA 2009*, pp. 1-4.

- [33] G. Maggetto and J. V. Mierlo, "Electric and electric hybrid vehicle technology: a survey," in *IEE Seminar on Electric, Hybrid and Fuel Cell Vehicles (Ref. No. 2000/050)* 2000, pp. 1/1-111.
- [34] D. Karner and J. Francfort, "US department of energy hybrid electric vehicle battery and fuel economy testing," *Journal of Power Sources*, vol. 158, pp. 1173-1177, 2006.
- [35] D. Karner and J. Francfort, "Hybrid and plug-in hybrid electric vehicle performance testing by the US Department of Energy Advanced Vehicle Testing Activity," *Journal of Power Sources*, vol. 174, pp. 69-75, 2007.
- [36] R. Alvarez and M. Weilenmann, "Effect of low ambient temperature on fuel consumption and pollutant and CO₂ emissions of hybrid electric vehicles in real-world conditions," *Fuel*, vol. 97, pp. 119-124, 2012.
- [37] R. Carlson, M. Duoba, D. Bocci, and H. Lohse-Busch, "On-road evaluation of advanced hybrid electric vehicles over a wide range of ambient temperatures," in *23rd International Electric Vehicle Symposium and Exposition, EVS23*, California, 2007, pp. 1-15.
- [38] G. Fontaras, P. Pistikopoulos, and Z. Samaras, "Experimental evaluation of hybrid vehicle fuel economy and pollutant emissions over real-world simulation driving cycles," *Atmospheric Environment*, vol. 42, pp. 4023-4035, 2008.
- [39] R. Carlson, H. Lohse-Busch, M. Duoba, and N. Shidore, "Drive cycle fuel consumption variability of plug-in hybrid electric vehicles due to aggressive driving," *SAE Technical Paper 2009-01-1335*, 2009.
- [40] Z. Xiao-hua, S. Da-feng, W. Dong, and W. Qing-nian, "Analysis of car fuel consumption based on driving cycles," in *International Conference on Computer Application and System Modeling, ICCASM*, 2010, pp. 79-84.
- [41] U. S. EPA, "Calculate or share your MPG," *U.S. Environment Protection Agency*. [Online]. Available: <http://www.fueleconomy.gov/mpg/MPG.do?action=browseList2&make=Toyota&model=Prius>.
- [42] E. Ericsson, "Independent driving pattern factors and their influence on fuel-use and exhaust emission factors," *Transportation Research Part D*, vol. 6, pp. 325-345, 2001.

- [43] E. Ericsson, "Variability in urban driving patterns," *Transportation Research Part D*, vol. 5, pp. 337-354, 2000.
- [44] L. Raykin, M. J. Roorda, and H. L. Maclean, "Impact of driving patterns on tank-to-wheel energy use of plug-in hybrid electric vehicle," *Transportation Research Part D*, vol. 17, pp. 243-250, 2012.
- [45] P. Sharer, R. Leydier, and A. Rousseau, "Impact of drive cycle aggressiveness and speed on HEVs fuel consumption sensitivity," *SAE Technical Paper 2007-01-0281*, 2007.
- [46] A. Moawad, G. Singh, S. Hagspiel, M. Fella, and A. Rousseau, "Impact of real world drive cycles on PHEV fuel efficiency and cost for different powertrain and battery characteristics," in *International Battery, Hybrid and Fuel Cell Electric Vehicle Symposium, EVS24, Stavanger, Norway, May 13 - 16, 2009*, pp. 1-10.
- [47] R. Fellini, N. Michelena, P. Papalambros, and M. Sasena, "Optimal design of automotive hybrid powertrain systems," in *Proceedings First International Symposium On Environmentally Conscious Design and Inverse Manufacturing, EcoDesign '99*, Tokyo, Japan, 1999, pp. 400-405.
- [48] A. Klemmt, S. Horn, G. Weigert, and K.-J. Wolter, "Simulation-based optimization vs. mathematical programming - a hybrid approach for optimizing scheduling problems," *Robotics and Computer-Integrated Manufacturing*, vol. 25, pp. 917-925, 2009.
- [49] V. Galdi, L. Ippolito, A. Piccolo, and A. Vaccaro, "A genetic-based methodology for hybrid electric vehicles sizing," *Soft Computing*, vol. 5, pp. 451-457, 2001.
- [50] L. Xudong, W. Yanping, and D. Jianmin, "Optimal sizing of a series hybrid electric vehicle using a hybrid genetic algorithm," in *IEEE International Conference on Automation and Logistics*, Jinan, China, 2007, pp. 1-5.
- [51] E. T. Yildiz, Q. Farooqi, S. Anwar, Y. Chen, and A. Izadian, "Nonlinear constraint component optimization of a plug-in hybrid electric vehicle," in *The 25th World Battery, Hybrid and Fuel Cell Electric Vehicle Symposium & Exhibition, EVS25*, Shenzhen, China, 2010, pp. 1-10.
- [52] X. Wu, B. Cao, X. Li, J. Xu, and X. Ren, "Component sizing optimization of plug-in hybrid electric vehicles," *Applied Energy*, vol. 88, pp. 799-804, 2011.

- [53] W. Gao and S. K. Porandla, "Design optimization of a parallel hybrid electric powertrain," in *IEEE Vehicle Power and Propulsion Conference, VPPC '05*, Chicago, USA, 2005, pp. 530-535.
- [54] C. Desai and S. S. Williamson, "Optimal design of a parallel hybrid electric vehicle using multi-objective genetic algorithms," in *IEEE Vehicle Power and Propulsion Conference, VPPC '09*, Dearborn, Michigan, USA, 2009, pp. 871-876.
- [55] M. Montazeri-Gh and A. Poursamad, "Application of genetic algorithm for simultaneous optimisation of HEV component sizing and control strategy," *International Journal of Alternative Propulsion*, vol. 1, pp. 63-78, 2006.
- [56] Z. Bingzhan, C. Zhihang, C. Mi, and Y. L. Murphey, "Multi-objective parameter optimization of a series hybrid electric vehicle using evolutionary algorithms," in *IEEE Vehicle Power and Propulsion Conference, VPPC '09*, Dearborn, Michigan, USA, 2009, pp. 921-925.
- [57] W. Lianghong, W. Yaonan, Y. Xiaofang, and C. Zhenlong, "Multiobjective optimization of HEV fuel economy and emissions using the self-adaptive differential evolution algorithm," *IEEE Transactions on Vehicular Technology*, vol. 60, pp. 2458-2470, 2011.
- [58] F. Li-Cun and Q. Shi-Yin, "Concurrent optimization for parameters of powertrain and control system of hybrid electric vehicle based on multi-objective genetic algorithms," in *SICE-ICASE International Joint Conference*, Bexico, Busan, Mexico, 2006, pp. 2424-2429.
- [59] J. Wu, C. Zhang, and N. Cui, "PSO algorithm-based parameter optimization for HEV powertrain and its control strategy," *International Journal of Automotive Technology*, vol. 9, pp. 53-59, 2008.
- [60] W. Gao and C. Mi, "Hybrid vehicle design using global optimisation algorithms," *International Journal of Electric and Hybrid Vehicles*, vol. 1, pp. 57-70, 2007.
- [61] J. B. Heywood, *Internal combustion engine fundamentals*. New York: McGraw-Hill Inc., 1988.
- [62] R. Graham, F. Kalhammer, S. Unnasch, E. Kassoy, R. Counts, C. Powars, L. Browning, D. Taylor, J. Smith, A. Frank, R. Schurhoff, M. Duvall, M. Kosowski, R. Bush, D. Santini, A. Vyas, T. Markel, A. Miller, S. Reisen, and

- W. Warf, "Comparing the benefits and impacts of hybrid electric vehicle options," Electric Power Research Institute, Inc., Palo Alto, CA: 1000349, 2001. [Online]. Available: <http://www.epri.com/abstracts/Pages/ProductAbstract.aspx?ProductId=0000000000001000349>.
- [63] M. Duvall, L. Browning, F. Kalhammer, W. Warf, D. Taylor, M. Wehrey, and N. Pinsky, "Advanced batteries for electric-drive vehicles: a technology and cost-effectiveness assessment for battery electric vehicles, power assist hybrid electric vehicles, and plug-in hybrid electric vehicles," Electric Power Research Institute, Inc., Palo Alto, CA: 1009299, 2004. [Online]. Available: <http://www.epri.com/abstracts/Pages/ProductAbstract.aspx?ProductId=0000000000001009299>.
- [64] W. Liu, *Introduction to hybrid vehicle system modeling and control*: Wiley, 2013.
- [65] H. Chen, T. N. Cong, W. Yang, C. Tan, Y. Li, and Y. Ding, "Progress in electrical energy storage system: A critical review," *Progress in Natural Science*, vol. 19, pp. 291-312, 2009.
- [66] C. Desai and S. S. Williamson, "Comparative study of hybrid electric vehicle control strategies for improved drivetrain efficiency analysis," in *IEEE Electrical Power & Energy Conference, EPEC*, 2009, pp. 1-6.
- [67] B. M. Baumann, G. Washington, B. C. Glenn, and G. Rizzoni, "Mechatronic design and control of hybrid electric vehicles," *IEEE/ASME Transactions on Mechatronics*, vol. 5, pp. 58-72, 2000.
- [68] H. Miaohua and Y. Houyu, "Optimal control strategy based on PSO for powertrain of parallel hybrid electric vehicle," in *IEEE International Conference on Vehicular Electronics and Safety, ICVES*, 2006, pp. 352-355.
- [69] F. R. Salmasi, "Control strategies for hybrid electric vehicles: evolution, classification, comparison, and future trends," *IEEE Transactions on Vehicular Technology*, vol. 56, pp. 2393-2404, 2007.
- [70] A. Dhand, B. Cho, A. Walker, A. Muncey, D. Kok, E. Karden, and T. Hochkirchen, "Stop-start micro hybrid: an estimation of automatic engine stop duration in real world usage," *SAE International 2009-01-1336*, 2009.

- [71] M. Matsuura, K. Korematsu, and J. Tanaka, "Fuel consumption improvement of vehicles by idling stop," *SAE International 2004-01-1896*, 2004.
- [72] R. Ripoli, J. Pasquini, J. Liebisch, F. Ferreira, and M. X. Schelp, "Fuel saving intelligence – low fuel consumption components and their benefits running together in an integrated system," *SAE International 2010-36-0362*, 2010.
- [73] Y. Gao, L. Chen, and M. Ehsani, "Investigation of the effectiveness of regenerative braking for EV and HEV," *SAE International 1999-01-2910*, pp. 1-7, 1999.
- [74] S. G. Wirasingha and A. Emadi, "Classification and review of control strategies for plug-in hybrid electric vehicles," in *IEEE Vehicle Power and Propulsion Conference, VPPC '09*, 2009, pp. 907-914.
- [75] M. Ehsani, Y. Gao, S. E. Gay, and A. Emadi, *Modern electric, hybrid electric and fuel cell vehicles: fundamentals, theory and design*: CRC - Press, 2005.
- [76] J. M. Miller, "Propulsion systems for hybrid vehicles," *IEE Power & Energy Series 45, The Institute of Electrical Engineers*, 2004.
- [77] G. J. Offer, D. Howey, M. Contestabile, R. Clague, and N. P. Brandon, "Comparative analysis of battery electric, hydrogen fuel cell and hybrid vehicles in a future sustainable road transport system," *Energy Policy*, vol. 38, pp. 24-29, 2010.
- [78] T. J. Barlow, S. Latham, I. S. McCrae, and P. G. Boulter, "A reference book of driving cycles for use in the measurement of road vehicle emissions," *TRL Limited - Published Project Report PPR354, Version 3, ISBN 978-1-84608-816-2*, 2009. [Online]. Available: https://www.gov.uk/government/uploads/system/uploads/attachment_data/file/4247/ppr-354.pdf.
- [79] A. P. Engelbrecht, *Fundamentals of computational swarm intelligence*: John Wiley & Sons, Ltd, 2005.
- [80] S. Koziel and X.-S. Yang, *Computational optimization, methods and algorithms*. New York: Springer-Verlag Berlin Heidelberg, 2011.
- [81] H. Ma, D. Simon, M. Fei, and Z. Chen, "On the equivalences and differences of evolutionary algorithms," *Engineering Applications of Artificial Intelligence*, vol. 26, pp. 2397-2407, 2013.

-
- [82] J. H. Holland, *Adaptation in natural and artificial system*: Ann Arbor, MI: University of Michigan Press, 1975.
- [83] D. E. Goldberg, *Genetic algorithms in search, optimization and machine learning*: Addison Wesley, 1989.
- [84] Y. J. Cao and Q. H. Wu, "Teaching genetic algorithm using Matlab," *International Journal of Eletrical Engineering Education*, vol. 36, pp. 139-153, 1999.
- [85] J. Kennedy and R. Eberhart, "Particle swarm optimization," in *IEEE International Conference Neural Networks, Piscataway, USA*, 1995, pp. 1942-1948.
- [86] T. C. Moore, "Tools and strategies for hybrid-electric drive system optimization," *SAE Technical Paper Series, 961660*, 1996.
- [87] H. Bufu, W. Zhancheng, and X. Yangsheng, "Multi-objective genetic algorithm for hybrid electric vehicle parameter optimization," in *IEEE/RSJ International Conference on Intelligent Robots and Systems*, 2006, pp. 5177-5182.
- [88] W. Xiaolan, C. Binggang, W. Jianping, and B. Yansheng, "Particle swarm optimization for plug-in hybrid electric vehicle control strategy parameter," in *IEEE Vehicle Power and Propulsion Conference, VPPC '08*, 2008, pp. 1-5.
- [89] A. Piccolo, L. Ippolito, V. zo Galdi, and A. Vaccaro, "Optimisation of energy flow management in hybrid electric vehicles via genetic algorithms," in *IEEE/ASME International Conference on Advanced Intelligent Mechatronics*, 2001, pp. 434-439.
- [90] T. C. Moore and A. B. Lovins, "Vehicle design strategies to meet and exceed PNGV goals," *SAE Technical paper, 951906*, 1995.
- [91] A. Emadi, M. Ehsani, and J. M. Miller, *Vehicular electric power systems: land, sea, air, and space vehicles*: New York: Marcel Dekker, 2003.
- [92] M. Duoba, H. Lohse-Busch, and T. Bohn, "Investigating vehicle fuel economy robustness of conventional and hybrid electric vehicles," in *The 21st World Battery, Hybrid and Fuel Cell Electric Vehicle Symposium and Exhibition, EVS21*, Monaco, 2005.
- [93] B. Ganji, A. Kouzani, and H. Trinh, "Drive cycle analysis of the performance of hybrid electric vehicles," in *Life System Modeling and Intelligent*

- Computing*. vol. 6328, K. Li, M. Fei, L. Jia, and G. Irwin, Eds., ed: Springer Berlin / Heidelberg, 2010, pp. 434-444.
- [94] A. Walker, A. McGordon, G. Hannis, A. Picarelli, J. Breddy, S. Carter, A. Vinsome, P. Jennings, M. Dempsey, and M. Willows, "A novel structure for comprehensive HEV powertrain modelling," in *IEEE Vehicle Power and Propulsion Conference, VPPC '06*, Windsor, United Kingdom, 2006, pp. 1-5.
- [95] J. Lih, "A closed-form method to determine vehicle speed and its maximum value," *International Journal of Vehicle Systems Modelling and Testing*, vol. 3, pp. 1-13, 2008.
- [96] R. Brayer, "Implementation of SAE standard J1666 May 93: Hybrid electric vehicle acceleration, gradeability and deceleration test procedure, ETA-HTP02," *Electric Transportation Applications*, 2004.
- [97] R. S. Wimalendra, L. Udawatta, E. Edirisinghe, and S. Karunarathna, "Determination of Maximum Possible Fuel Economy of HEV for Known Drive Cycle: Genetic Algorithm Based Approach," in *4th International Conference on Information and Automation for Sustainability, ICIAFS, 2008*
- [98] M. Montazeri-Gh, A. Poursamad, and B. Ghalichi, "Application of genetic algorithm for optimization of control strategy in parallel hybrid electric vehicles," *Journal of the Franklin Institute*, vol. 343, pp. 420-435, 2006.
- [99] S. C. Davis, S. W. Diegel, and R. G. Boundy, "Transportation energy data book: Edition 31, ORNL-6987," US Department of Energy, Oak Ridge National Laboratory, Oak Ridge, TN, 2012.
- [100] S. C. Davis, S. W. Diegel, and R. G. Boundy, "Transportation energy data book: Edition 32, ORNL-6989," *US Department of Energy, Oak Ridge National Laboratory, Oak Ridge, TN, 2013. [Online]. Available: http://cta.ornl.gov/data/tedb32/Edition32_Full_Doc.pdf*.
- [101] E. Ericsson, "Independent driving pattern factors and their influence on fuel-use and exhaust emission factors," *Transportation Research Part D*, pp. 325-345, 2001.
- [102] C. Cheng, A. McGordon, J. E. W. Poxon, R. P. Jones, and P. A. Jennings, "A model to investigate the effects of driver behaviour on hybrid vehicle control," in *The 25th World Battery, Hybrid and Fuel Cell Electric Vehicle Symposium & Exhibition, EVS25*, Shenzhen, China, 2010, pp. 1-5.

- [103] A. McGordon, J. Poxon, P. Jennings, and R. P. Jones, "Modeling of real-world driver behaviour for hybrid vehicle control investigations," in *Vehicle Dynamics and Control*, Fitzwilliam College, Cambridge, UK, 2011.
- [104] A. McGordon, J. E. W. Poxon, C. Cheng, R. P. Jones, and P. A. Jennings, "Development of a driver model to study the effects of real-world driver behaviour on the fuel consumption," *Proceedings of the Institution of Mechanical Engineers, Part D: Journal of Automobile Engineering*, vol. 225, pp. 1518-1530, 2011.
- [105] J. Wang, P. Liu, J. Hicks-Garner, E. Sherman, S. Soukiazian, M. Verbrugge, H. Tataria, J. Musser, and P. Finamore, "Cycle-life model for graphite-LiFePO₄ cells," *Journal of Power Sources*, vol. 196, pp. 3942–3948, 2011.

APPENDIX A

A.1 Calculation of acceleration and maximum speed

The acceleration and maximum speed of the Toyota Prius HEV and optimum designs of the traditional and proposed methodologies were calculated as suggested in the reference [95]. The calculation of the time of acceleration and maximum speed are shown in Equations A.1 and A.2.

$$\begin{aligned}
 t = t_0 + \frac{m}{r_1} & \left[\left(\frac{a_2 b_2}{2} - a_3 \right) \frac{2}{\sqrt{4b_3 - b_2^2}} \tan^{-1} \left(\frac{2v + b_2}{\sqrt{4b_3 - b_2^2}} \right) \right. \\
 & - a_1 \log_e [v + b_1] \\
 & - \frac{a_2}{2} \log_e [v^2 + b_2 v + b_3] \\
 & - \left(\frac{a_2 b_2}{2} - a_3 \right) \frac{2}{\sqrt{4b_3 - b_2^2}} \tan^{-1} \left(\frac{2v_0 + b_2}{\sqrt{4b_3 - b_2^2}} \right) \\
 & \left. + a_1 \log_e [v_0 + b_1] + \frac{a_2}{2} \log_e [v_0^2 + b_2 v_0 + b_3] \right] \dots \dots \dots Eq. A. 1
 \end{aligned}$$

$$\begin{aligned}
 v_{Pmax} = \frac{1}{6r_1} & \sqrt[3]{ \left(108r_3 + 12 \sqrt{ \frac{3(4r_2^3 + 27r_3^2 r_1)}{r_1} } \right) r_1^2 } \\
 & - \frac{2r_2}{\sqrt[3]{ \left(108r_3 + 12 \sqrt{ \frac{3(4r_2^3 + 27r_3^2 r_1)}{r_1} } \right) r_1^2 }} \dots \dots \dots Eq. A. 2
 \end{aligned}$$

Where,

$$r_1 = \frac{1}{2} \rho C_d A_f + f_1 W$$

$$r_2 = W(f_0 + \sin \theta)$$

$$r_3 = \eta P_T$$

$$b_2^3 + \frac{r_2}{r_1} b_2 - \frac{r_3}{r_1} = 0$$

$$b_1 = -b_2$$

$$b_3 = b_2^2 + \frac{r_2}{r_1}$$

$$a_1 = \frac{b_2}{3b_2^2 + \frac{r_2}{r_1}}$$

$$a_2 = -a_1$$

$$a_3 = 2a_2 b_2 + 1$$

Where,

a_i, b_i	Coefficients
f_0, f_1	Rolling resistance coefficients = 0.01
g	Acceleration due to gravity = 9.81 m/s ²
m	Vehicle mass = 1368 kg
r_i	Coefficients
t_0	Initial time = 0.0 s
t	Time
v_0	Initial velocity = 0.0 m/s
v	Velocity
A_f	Vehicle frontal area = 2.0 m ²

C_d	Aerodynamic coefficient = 0.29
P_T	Total power = ICE power + motor power
W	Vehicle weight
ρ	Air density = 1.225 kg/m ³
θ	Grade angle = 0°
η	Transmission efficiency = 90%

A.2 Calculation of gradeability

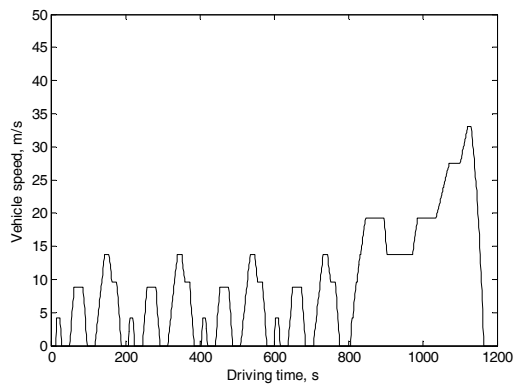
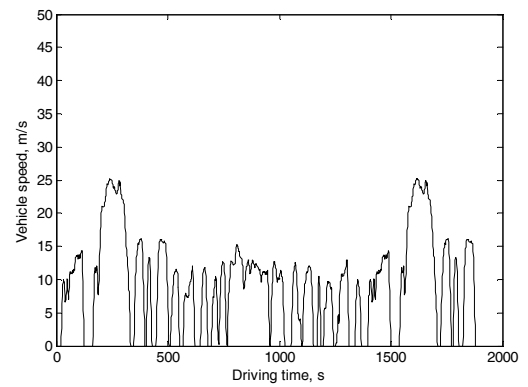
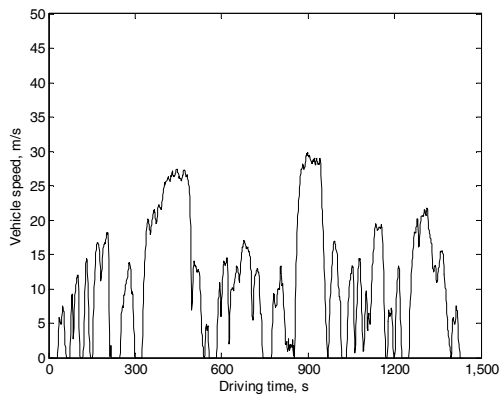
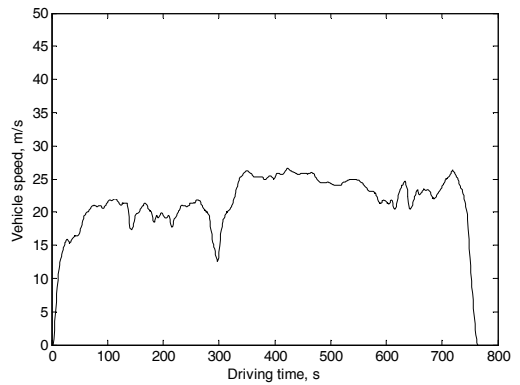
The gradeability of the Toyota Prius HEV and optimum designs of the traditional and proposed methodologies were calculated as suggested in the reference [96] and shown in Equation A.3.

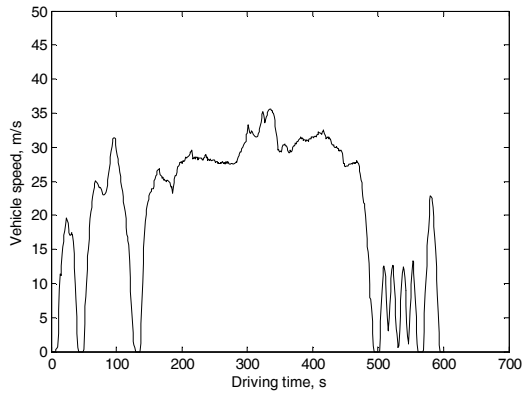
$$\text{Gradeability at a speed} = 100 \tan(\sin^{-1} 0.0455a) \dots\dots\dots \text{Eq. A.3}$$

Where, a = vehicle acceleration at the selected speed, mph/s

APPENDIX B**B.1 Standard driving patterns**

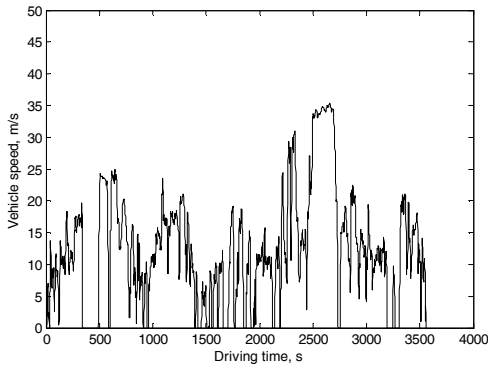
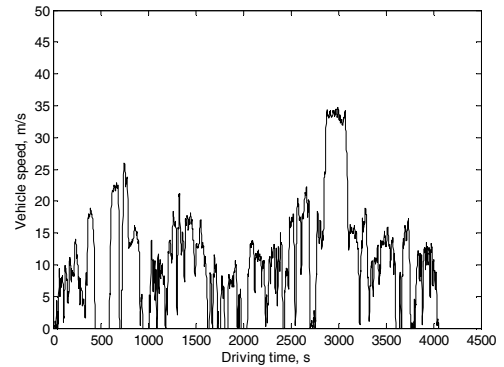
The standard driving patterns used in this thesis are shown in Figures B.1 to B.5.

**Figure B.1: NEDC****Figure B.2: FTP-75****Figure B.3: LA92****Figure B.4: HWFET**

**Figure B.5: US06**

B.2 Real-world driving patterns

The driving patterns over a predefined route consisting of urban and highway driving used as real-world driving patterns for the study in this thesis are shown in Figures B.6 to B.15. The 10 driving patterns are termed as D1 to D10 respectively, as described in chapter 6.

**Figure B.6: D1****Figure B.7: D2**

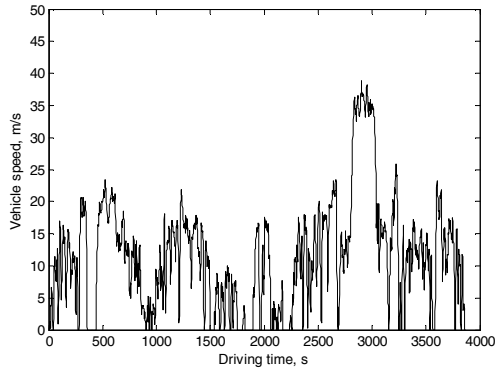


Figure B.8: D3

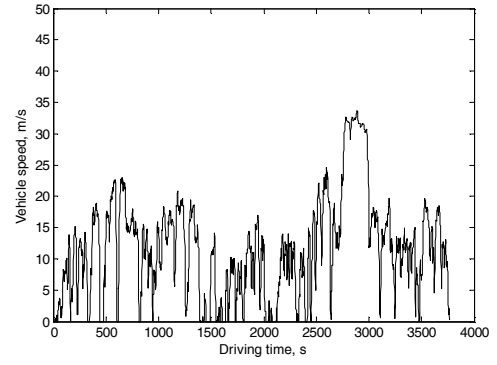


Figure B.9: D4

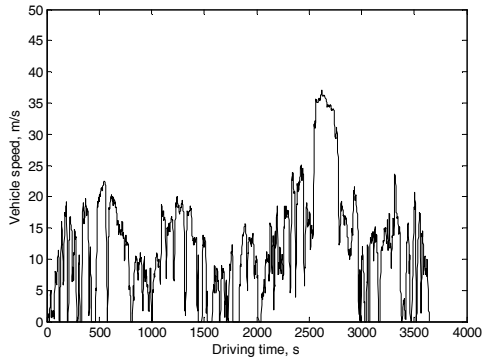


Figure B.10: D5

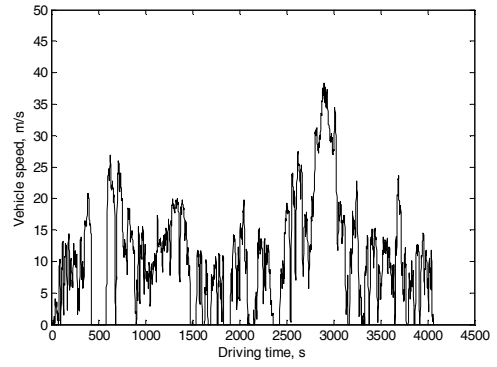


Figure B.11: D6

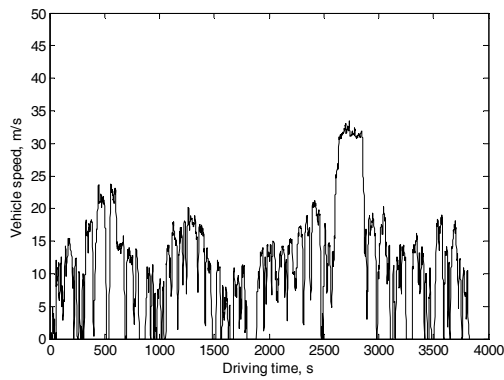


Figure B.12: D7

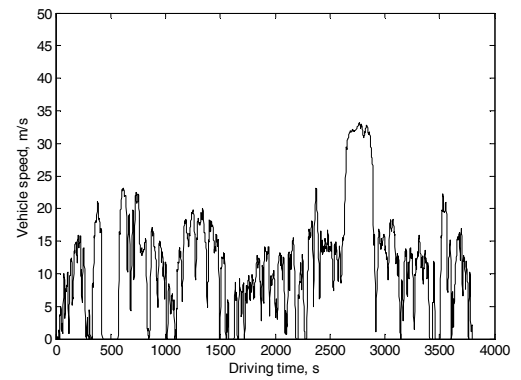


Figure B.13: D8

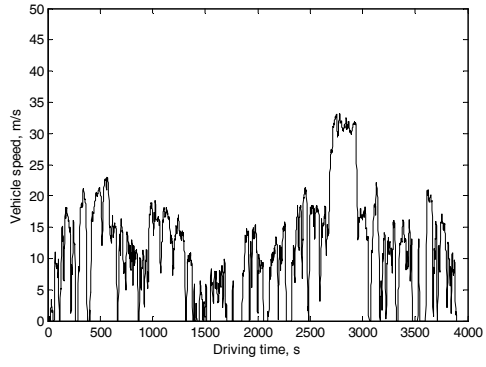


Figure B.14: D9

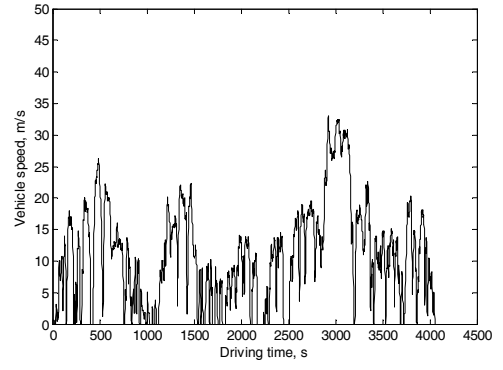


Figure B.15: D10

APPENDIX C

C.1 Variation in optimum component sizes for different optimisation trials:

Traditional methodology

The variation in the optimum ICE, generator, motor, and battery sizes for the M1-NEDC, M1-FTP, M1-LA92, and M1-US06 designs of the traditional methodology (M1) discussed in chapter 7 for 10 optimisation trials are shown in Tables C.1 to C.4, respectively.

Table C.1: Variation in optimum component sizes of the M1-NEDC design for 10 optimisation trials

Trial	M1 methodology				
	M1-NEDC				
	P _{ICE}	P _G	P _M	C _B	FC, l/100km
1	29.91 kW	12.12 kW	43.91 kW	6.98 Ah	3.4757
2	29.95 kW	12.12 kW	43.87 kW	6.98 Ah	3.4860
3	29.97 kW	12.10 kW	43.73 kW	7.01 Ah	3.4783
4	30.00 kW	12.18 kW	43.87 kW	7.02 Ah	3.4797
5	29.94 kW	12.20 kW	43.70 kW	7.01 Ah	3.4766
6	30.00 kW	12.15 kW	43.73 kW	7.03 Ah	3.4793
7	29.91 kW	12.12 kW	43.91 kW	6.98 Ah	3.4757
8	30.00 kW	12.10 kW	43.58 kW	7.05 Ah	3.4785
9	29.98 kW	12.12 kW	43.58 kW	7.01 Ah	3.4784
10	30.00 kW	12.18 kW	43.87 kW	7.02 Ah	3.4797
Variation in optimum sizes, %	0.30	0.82	0.75	0.99	

Where,

Variation in optimum sizes, %

$$= \frac{\text{Max size(Trial 1 to Trial 10)} - \text{Min size(Trial 1 to Trial 10)}}{\text{Max size(Trial 1 to trial 10)}} * 100$$

Table C.2: Variation in optimum component sizes of the M1-FTP design for 10 optimisation trials

Trial	M1 methodology				
	M1-FTP				
	P_{ICE}	P_G	P_M	C_B	FC, l/100km
1	38.01 kW	14.10 kW	39.85 kW	8.82 Ah	3.9072
2	37.92 kW	14.13 kW	39.53 kW	8.88 Ah	3.9027
3	38.05 kW	14.21 kW	39.65 kW	8.85 Ah	3.9084
4	37.92 kW	14.13 kW	39.53 kW	8.88 Ah	3.9027
5	37.98 kW	14.10 kW	39.53 kW	8.86 Ah	3.9046
6	38.05 kW	14.21 kW	39.65 kW	8.85 Ah	3.9084
7	38.10 kW	14.14 kW	39.60 kW	8.86 Ah	3.9108
8	37.96 kW	14.14 kW	39.62 kW	8.80 Ah	3.9039
9	37.92 kW	14.13 kW	39.53 kW	8.88 Ah	3.9027
10	38.03 kW	14.18 kW	39.60 kW	8.87 Ah	3.9058
Variation in optimum sizes, %	0.47	0.77	0.80	0.90	

Table C.3: Variation in optimum component sizes of the M1-LA92 design for 10 optimisation trials

Trial	M1 methodology				
	M1-LA92				
	P_{ICE}	P_G	P_M	C_B	FC, l/100km
1	35.31 kW	15.22 kW	42.73 kW	8.79 Ah	4.6409
2	35.40 kW	15.28 kW	42.90 kW	8.77 Ah	4.6421
3	35.42 kW	15.36 kW	42.65 kW	8.75 Ah	4.6434
4	35.50 kW	15.30 kW	42.85 kW	8.76 Ah	4.6468
5	35.31 kW	15.22 kW	42.73 kW	8.79 Ah	4.6409
6	35.45 kW	15.32 kW	42.60 kW	8.72 Ah	4.6454
7	35.48 kW	15.28 kW	42.65 kW	8.74 Ah	4.6471
8	35.40 kW	15.28 kW	42.90 kW	8.77 Ah	4.6421
9	35.48 kW	15.22 kW	42.60 kW	8.79 Ah	4.6460
10	35.44 kW	15.25 kW	42.85 kW	8.73 Ah	4.6450
Variation in optimum sizes, %	0.54	0.91	0.70	0.80	

Table C.4: Variation in optimum component sizes of the M1-US06 design for 10 optimisation trials

Trial	M1 methodology				
	M1-US06				
	P_{ICE}	P_G	P_M	C_B	FC, l/100km
1	38.48 kW	17.45 kW	39.72 kW	7.89 Ah	5.3437
2	38.53 kW	17.34 kW	39.81 kW	7.89 Ah	5.3416
3	38.53 kW	17.34 kW	39.81 kW	7.89 Ah	5.3416
4	38.48 kW	17.45 kW	39.72 kW	7.89 Ah	5.3437
5	38.50 kW	17.48 kW	39.70 kW	7.82 Ah	5.3419
6	38.49 kW	17.34 kW	39.98 kW	7.88 Ah	5.3428
7	38.53 kW	17.48 kW	39.70 kW	7.86 Ah	5.3453
8	38.49 kW	17.34 kW	39.98 kW	7.88 Ah	5.3428
9	38.53 kW	17.34 kW	39.81 kW	7.89 Ah	5.3416
10	38.50 kW	17.48 kW	39.70 kW	7.82 Ah	5.3419
Variation in optimum sizes, %	0.13	0.80	0.70	0.89	

C.2 Variation in optimum component sizes for different optimisation trials:

Proposed methodology with second approach

The variation in the optimum ICE, generator, motor, and battery sizes for the optimum designs of the proposed methodology (M2) with second approach (M2A2) discussed in chapter 10 for 10 optimisation trials are shown in Tables C.5 to C.9, respectively.

Table C.5: Variation in optimum component sizes of the M2A2-C1 design for 10 optimisation trials

Trial	M2 methodology: M2A2 approach				
	M2A2-C1 design				
	P_{ICE}	P_G	P_M	C_B	FC, l/100km
1	44.83 kW	16.51 kW	30.46 kW	7.65 Ah	19.9086
2	44.83 kW	16.45 kW	30.55 kW	7.60 Ah	19.9146
3	44.95 kW	16.60 kW	30.60 kW	7.66 Ah	19.9248
4	44.92 kW	16.51 kW	30.65 kW	7.67 Ah	19.9226
5	44.95 kW	16.58 kW	30.52 kW	7.61 Ah	19.9268
6	45.10 kW	16.55 kW	30.55 kW	7.65 Ah	19.9528
7	44.94 kW	16.52 kW	30.62 kW	7.64 Ah	19.9314
8	45.06 kW	16.49 kW	30.48 kW	7.63 Ah	19.9438
9	44.98 kW	16.60 kW	30.56 kW	7.64 Ah	19.9337
10	44.83 kW	16.51 kW	30.46 kW	7.65 Ah	19.9086
Variation in optimum sizes, %	0.60	0.90	0.62	0.91	

Table C.6: Variation in optimum component sizes of the M2A2-C2 design for 10 optimisation trials

Trial	M2 methodology: M2A2 approach				
	M2A2-C2 design				
	P_{ICE}	P_G	P_M	C_B	FC, l/100km
1	44.95 kW	16.58 kW	30.52 kW	7.68 Ah	19.9234
2	44.98 kW	16.60 kW	30.56 kW	7.64 Ah	19.9337
3	44.92 kW	16.53 kW	30.49 kW	7.71 Ah	19.9135
4	45.10 kW	16.55 kW	30.55 kW	7.65 Ah	19.9528
5	45.20 kW	16.60 kW	30.60 kW	7.67 Ah	19.9619
6	45.04 kW	16.65 kW	30.65 kW	7.70 Ah	19.9394
7	44.98 kW	16.59 kW	30.60 kW	7.69 Ah	19.9291
8	44.97 kW	16.63 kW	30.60 kW	7.68 Ah	19.9270
9	44.92 kW	16.53 kW	30.49 kW	7.71 Ah	19.9135
10	45.14 kW	16.58 kW	30.65 kW	7.66 Ah	19.9564
Variation in optimum sizes, %	0.62	0.72	0.52	0.91	

Table C.7: Variation in optimum component sizes of the M2A2-C3 design for 10 optimisation trials

Trial	M2 methodology: M2A2 approach				
	M2A2-C3 design				
	P_{ICE}	P_G	P_M	C_B	FC, l/100km
1	44.98 kW	16.50 kW	30.50 kW	7.61 Ah	19.9392
2	45.20 kW	16.60 kW	30.60 kW	7.67 Ah	19.9619
3	45.10 kW	16.58 kW	30.62 kW	7.62 Ah	19.9474
4	45.17 kW	16.50 kW	30.49 kW	7.68 Ah	19.9601
5	44.95 kW	16.44 kW	30.44 kW	7.66 Ah	19.9213
6	44.98 kW	16.49 kW	30.52 kW	7.68 Ah	19.9307
7	44.99 kW	16.46 kW	30.55 kW	7.66 Ah	19.9338
8	45.13 kW	16.56 kW	30.57 kW	7.62 Ah	19.9545
9	45.10 kW	16.57 kW	30.62 kW	7.64 Ah	19.9476
10	45.20 kW	16.60 kW	30.60 kW	7.67 Ah	19.9619
Variation in optimum sizes, %	0.55	0.96	0.59	0.91	

Table C.8: Variation in optimum component sizes of the M2A2-C4 design for 10 optimisation trials

Trial	M2 methodology: M2A2 approach				
	M2A2-C4 design				
	P_{ICE}	P_G	P_M	C_B	FC, l/100km
1	44.98 kW	16.59 kW	30.60 kW	7.69 Ah	19.9291
2	44.94 kW	16.56 kW	30.34 kW	7.70 Ah	19.9240
3	45.10 kW	16.57 kW	30.62 kW	7.64 Ah	19.9476
4	45.00 kW	16.52 kW	30.45 kW	7.70 Ah	19.9268
5	44.97 kW	16.63 kW	30.60 kW	7.68 Ah	19.9270
6	45.15 kW	16.56 kW	30.40 kW	7.70 Ah	19.9500
7	44.94 kW	16.56 kW	30.34 kW	7.70 Ah	19.9240
8	45.00 kW	16.52 kW	30.45 kW	7.70 Ah	19.9268
9	44.94 kW	16.56 kW	30.34 kW	7.70 Ah	19.9240
10	45.20 kW	16.60 kW	30.60 kW	7.67 Ah	19.9619
Variation in optimum sizes, %	0.58	0.66	0.91	0.78	

Table C.9: Variation in optimum component sizes of the M2A2-C5 design for 10 optimisation trials

Trial	M2 methodology: M2A2 approach				
	M2A2-C5 design				
	P_{ICE}	P_G	P_M	C_B	FC, l/100km
1	45.15 kW	16.56 kW	30.40 kW	7.70 Ah	19.9500
2	45.10 kW	16.57 kW	30.62 kW	7.64 Ah	19.9476
3	45.10 kW	16.55 kW	30.55 kW	7.65 Ah	19.9528
4	45.14 kW	16.58 kW	30.65 kW	7.66 Ah	19.9564
5	45.27 kW	16.58 kW	30.50 kW	7.71 Ah	19.9692
6	45.15 kW	16.55 kW	30.62 kW	7.65 Ah	19.9587
7	45.05 kW	16.43 kW	30.56 kW	7.71 Ah	19.9389
8	45.14 kW	16.58 kW	30.65 kW	7.66 Ah	19.9564
9	45.05 kW	16.43 kW	30.56 kW	7.71 Ah	19.9389
10	45.23 kW	16.50 kW	30.65 kW	7.67 Ah	19.9684
Variation in optimum sizes, %	0.49	0.90	0.82	0.91	

APPENDIX D

D.1 MATLAB script to find optimum design with the combination of optimisation algorithm and vehicle simulation software

The MATLAB script to find optimum powertrain component sizes with the combination of the optimisation algorithm (GA) and the vehicle simulation software (WARPSTAR) that was used in chapter 7 is shown below.

```
%% To find optimum design using Genetic Algorithm and
WARPSTAR
%% Hillol Kumar Roy
%% 2011

clc;
clear;
TCollect=[];
d_soc=[];
fc=[];
nval=0;

% Base ICE (Prius) data
eng_tau_max_pt_base = 101.9; % Max torque, Nm
eng_P_max_base = 43000; % Max power, W

% Base Generator (Prius) data
gen_P_max_base=15000; % Max power, W
gen_tau_max_base=55; % Max torque, Nm

% Base Motor (Prius) data
mg_P_max_base=30000; % Max power, W
mg_P_max_gen_base=-30000; % Max power, W
mg_tau_max_base=305; % Max torque, Nm
mg_tau_max_gen_base=-305; % Max torque, Nm

% Base Battery (Prius) data
bat_capacity_max_base=6.0; % Max capacity, Ah

% Range of variables
range_var=0.7;
```

```

% Upper and lower limits of variables (ICE, Gen, Mot, B)
var1min= eng_tau_max_pt_base*(1-range_var);
var1max=eng_tau_max_pt_base*(1+range_var);
var2min=gen_tau_max_base*(1-range_var);
var2max=gen_tau_max_base*(1+range_var);
var3min=mg_tau_max_base*(1-range_var);
var3max=mg_tau_max_base*(1+range_var);
var4min= bat_capacity_max_base*(1-range_var);
var4max= bat_capacity_max_base*(1+range_var);

veh_mass=1368; % Vehicle weight, kg

% Constraints
accl_prius=13.4; % Acceleration (0 ~ 60 mph) of Prius
max_speed_prius=113.3; % Max speed of Prius
%Gradeability of Prius @ 55mph
grade_55_prius=100*tan(asin(0.0455*3.0089));
del_soc=0.005;

bat_SoC_init=0.7; % Initial battery SOC
target_soc=0.7; % Target battery SOC

% I. Setup the GA
npar=4; % number of optimisation variables (ICE, G, M,
B)
%
% II. Stopping criteria
maxit=250; % max number of iterations
%
% III. GA parameters
popsize=50; % set population size
mutrate=0.15; % set mutation rate
selection=0.5; % fraction of population kept
nbits=8; % number of bits in each parameter
Nt=nbits*npar; % total number of bits in a chromosome
keep=floor(selection*popsize); % #population that
survive

%
% Create the initial population
iga=0; % generation counter initialised
pop=round(rand(popsize,Nt)); % random population of 1s
and 0s
x1=pop(:,1:nbits);
y1=pop(:,nbits+1:2*nbits);
z1=pop(:,2*nbits+1:3*nbits);
zz1=pop(:,3*nbits+1:4*nbits);

% Convert binary to continuous values
x=gadecode(x1,var1min,var1max,nbits);

```

```

y=gadecode(y1,var2min,var2max,nbits);
z=gadecode(z1,var3min,var3max,nbits);
zz=gadecode(zz1,var4min,var4max,nbits);
par=[x y z zz];

for ip=1:popsize
    eng_tau_max_pt = x(ip);
    gen_tau_max = y(ip);
    mg_tau_max = z(ip);
    bat_pack_C = zz(ip);

    total_torque = eng_tau_max_pt + mg_tau_max;

    % Call WARPSTAR
    veh_Toyota_Prius_IPS_data_evaluation

    sim('arch_IPS');
    nval=nval+1;
    TCollect=[TCollect,l_100km];
    obj=TCollect(1,nval);

    engine_power =
eng_P_max_base*(eng_tau_max_pt/eng_tau_max_pt_base);
    motor_power =
mg_P_max_base*(mg_tau_max/mg_tau_max_base);
    total_power =
eng_P_max_base*(eng_tau_max_pt/eng_tau_max_pt_base) +
mg_P_max_base*(mg_tau_max/mg_tau_max_base);

    % Acceleration and maximum speed calculation
    accl_max_speed
    accl_time_60 = t(60);
    accl_time_54 = t(54);
    accl_time_55 = t(55);
    max_speed = Vpmax;

    % acceleration at 55 mph
    accl_55 = 1/(accl_time_55-accl_time_54);
    grade_55 = 100*tan(asin(0.0455*accl_55));

    delta_soc=abs((bat_SoC_init-
bat_SoC_final)/(bat_SoC_init));

    if accl_time_60<accl_prius &&
max_speed>max_speed_prius && grade_55>grade_55_prius &&
delta_soc<del_soc
        fc(ip) = obj;
    else
        fc(ip) = obj + 1000;
    end
end
end

```

```

[fc,ind]=sort(fc);
par=par(ind,:);
pop=pop(ind,:);% sorts population with lowest fc first
minc(1,:)=min(fc); % Minimum of population

%-----
% Iterate through generations
while iga<maxit
iga=iga+1           % increments generation counter

%-----
% Pair and mate
M=ceil((popsize-keep)/2);           % number of matings
prob=flipud([1:keep]/sum([1:keep])); % weights
% chromosomes based
% upon position in
% list
odds=[0 cumsum(prob(1:keep))]; % probability
distribution function
pick1=rand(1,M);                    % mate #1
pick2=rand(1,M);                    % mate #2
% ma and pa contain the indices of the chromosomes that
% will mate
ic=1;
while ic<=M
for id=2:keep+1
if pick1(ic)<=odds(id) && pick1(ic)>odds(id-1)
ma(ic)=id-1;
end
if pick2(ic)<=odds(id) && pick2(ic)>odds(id-1)
pa(ic)=id-1;
end
end
ic=ic+1;
end
%-----
% Performs mating using single point crossover
ix=1:2:keep;                        % index of mate #1
xp=ceil(rand(1,M)*(Nt-1));          % crossover point
% 1st offspring
pop(keep+ix,:)= [pop(ma,1:xp) pop(pa,xp+1:Nt)];
% 2nd offspring
pop(keep+ix+1,:)= [pop(pa,1:xp) pop(ma,xp+1:Nt)];
%-----
% Mutate the population
nmut=ceil((popsize-1)*Nt*mutrate); % total number of
mutations
mrow=ceil(rand(1,nmut)*(popsize-1))+1; % row to mutate
mcol=ceil(rand(1,nmut)*Nt);          % column to mutate
for ii=1:nmut

```

```

pop(mrow(ii),mcol(ii))=abs(pop(mrow(ii),mcol(ii))-1);
end
%
% The population is re-evaluated for cost
x1=pop(:,1:nbits);
y1=pop(:,nbits+1:2*nbits);
z1=pop(:,2*nbits+1:3*nbits);
zz1=pop(:,3*nbits+1:4*nbits);

% Convert binary to continuous values
x=gadecode(x1(1:popsize,:),var1min,var1max,nbits);
y=gadecode(y1(1:popsize,:),var2min,var2max,nbits);
z=gadecode(z1(1:popsize,:),var3min,var3max,nbits);
zz=gadecode(zz1(1:popsize,:),var4min,var4max,nbits);
par=[x y z zz];

% FE calculation in WRAPSTAR
for ip=1:popsize
    eng_tau_max_pt = x(ip);
    gen_tau_max = y(ip);
    mg_tau_max = z(ip);
    bat_pack_C= zz(ip);

    total_torque = eng_tau_max_pt + mg_tau_max;

    % Call WARPSTAR
    veh_Toyota_Prius_IPS_data_evaluation

    sim('arch_IPS');
    nval=nval+1;
    TCollect=[TCollect,1_100km];
    obj=TCollect(1,nval);

engine_power=eng_P_max_base*(eng_tau_max_pt/eng_tau_max_pt_base);

motor_power=mg_P_max_base*(mg_tau_max/mg_tau_max_base);
total_power =
eng_P_max_base*(eng_tau_max_pt/eng_tau_max_pt_base) +
mg_P_max_base*(mg_tau_max/mg_tau_max_base);

% Acceleration and maximum speed calculation
accl_max_speed
accl_time_60 = t(60);
accl_time_54 = t(54);
accl_time_55 = t(55);
max_speed = Vpmax;
% acceleration at 55 mph
accl_55 = 1/(accl_time_55-accl_time_54);

```

```

    grade_55 = 100*tan(asin(0.0455*accl_55));

    delta_soc=abs((bat_SoC_init-
bat_SoC_final)/(bat_SoC_init));

    if accl_time_60<accl_prius &&
max_speed>max_speed_prius && grade_55>grade_55_prius &&
delta_soc<del_soc
        fc(ip) = obj;
    else
        fc(ip) = obj + 1000;
    end
end
end
%_____
% Sort the fc and associated parameters

[fc,ind]=sort(fc);
par=par(ind,:);
pop=pop(ind,:);
minc(iga+1)=min(min(fc));

%_____
% Termination criteria
if iga>maxit
break
end
end
end
%_____
clf
for i=1:maxit
    plot(i, minc(i), 'x')
    hold on
end
% Displays the output
disp(['#Generations=' num2str(iga)])
disp(['Lowest FC =' num2str(fc(1))])
disp(['Best solution:'])
disp(['ICE =' num2str(par(1,1))])
disp(['Generator =' num2str(par(1,2))])
disp(['Motor =' num2str(par(1,3))])
disp(['Battery =' num2str(par(1,4))])

```

```
% Conversion of binary to continuous values
% gadecode.m
% f=gadecode(chrom,lo,hi,bits)
% chrom = population
% lo = minimum parameter value
% hi = maximum parameter value
% bits = number of bits/parameter
% Haupt & Haupt
% 2003
function f=gadecode(chrom,lo,hi,bits)
[M,N]=size(chrom);
npar=N/bits;
quant=(0.5.^[1:bits]');
quant=quant/sum(quant);
ct=reshape(chrom',bits,npar*M)';
par=((ct*quant)*(hi-lo)+lo);
f=reshape(par,npar,M)';
```